MICROARRAY ANALYSIS OF GFP-EXPRESSING MOUSE DOPAMINE NEURONS ISOLATED BY LASER CAPTURE MICRODISSECTION

Thesis submitted for the degree of
"*Doctor Philosophiæ*"

S.I.S.S.A. - I.S.A.S.
Neurobiology Sector
7 October 2009

CANDIDATE

Christina Vlachouli

SUPERVISOR

Prof. Stefano Gustincich

Declaration

The work described in this thesis was carried out at the International School for Advanced Studies, Trieste, between November 2004 and August 2008.

Part of the work described in this thesis is included in:

Vlachouli C., Motti D., Lazarevič D., Krmac H., Gustincich S., 2008. Gene-expression profiling of laser capture-microdissected neuronal populations in the mammalian CNS. *MACS&more*, customer report, vol. 12, 2-4; www.miltenyibiotec.com

Milena Pinto*, Marta Biagioli*, Daniela Cesselli, Marta Zaninello, Dejan Lazarevič, Paola Roncaglia, Roberto Simone, **Christina Vlachouli**, Charles Plessy, Nicolas Bertin, Antonio Beltrami, Kazuto Kobayashi, Vittorio Gallo, Claudio Santoro, Isidro Ferrer, Stefano Rivella, Carlo Alberto Beltrami, Piero Carninci, Elio Raviola and Stefano Gustincich. Unexpected expression of α- and β- globin in mesencephalic dopaminergic neurons and glial cells. *Natl Acad Sci, accepted August 2009.*

Charles Plessy*, Roberto Simone*, Nicolas Bertin*, Giovanni Pascarella, Altuna Akalin, Claudia Carrieri, Anne Vassalli, Signe Olivarius, Jessica Severin, Dejan Lazarevič, **Christina Vlachouli**, Silvia Zucchelli, Jun Kawai, Carsten O. Daub, Yoshihide Hayashizaki, Peter Mombaerts, Boris Lenhard, Stefano Gustincich and Piero Carninci. Gene network discovery in mouse olfactory epithelium by nanoCAGE, a new technology for genome-wide identification of transcription start sites from tiny amounts of fixed tissue, *submitted to Neuron.*

Dejan Lazarevič*, Roberto Simone*, Nicholas Bertin*, **Christina Vlachouli***, Charles Plessy, Altuna Akalin, Geoffrey J. Faulkner, Paola Roncaglia, Milena Pinto, Marta Biagioli, Helena Krmac, Sean M. Grimmond, Jun Kawai, Yoshihide Hayashizaki, Carsten O. Daub, Boris Lenhard, Piero Carninci and Stefano Gustincich. The transcriptional landscape of dopaminergic neurons of the Substantia Nigra, *in preparation*.

Authors with an * have contributed equally to the work.

TABLE OF CONTENTS

ABBREVIATIONS

5-HT: serotonin

AADC: Aromatic Aminoacid Decarboxylase

aRNA: antisense RNA

CA: Catecholaminergic

CA1: Cornu Ammonis

CAGE: Cap Analysis of Gene Expression

cDNA: complementary DNA

CNS: Central Nervous System

DA: Dopaminergic

ds cDNA: double strand complementary DNA

DAT: Dopamine Transporter

DEPC: Diethyl Pyrocarbonate

DSP: Dithio-bis (succinimidyl proprionate)

EtOH: Ethanol

FACS: Fluorescent Activated Cell Sorter

GABA: Gamma-aminobutyric acid

GAPDH: Glyceraldehyde-3-Phosphate Dehydrogenase

GBA: Glucocerebrosidase

GFAP: Glial Fibrillary Acidic Protein

GFP: Green Fluorescent Protein

HCN: Hyperpolarization-activated Cyclic-Nucleotide gated

IC: Inferior Colliculus

I_h: hyperpolarization cation current

ISH: In Situ Hybridization

KO: Knockdown

LBs: Lewy Bodies

LC: Locus Coeruleus

LCM: Laser Capture Microdissection

LGE: Lateral Ganglionic Eminence

LMPC: Laser Microdissection Pressure Catapulting

LPA: Lipophosphatidic Acid

MAP-2: Microtubule Associated Protein-2

mDA: mesencephalic Dopaminergic

mRNA: messenger RNA

MPTP: 1-methyl-4-phenyl-1,2,3,6-tetrahydropyridine

MPP^+: 1-methyl-4-phenylpyridinium

MS: Multiple Sclerosis

NA: Noradrenergic

NM: Neuromelanin

NMDA: N-methyl-D-aspartic acid

PCR: Polymerase Chain Reaction

PD: Parkinson's Disease

PEN: Poly-Ethylene-Naphthalene

PET: Polyethylene Tetraphthalate

PFA: Paraformaldehyde

PLAP: Placental Alkaline Phosphatase

qPCR: quantitative Polymerase Chain Reaction

ROS: Reactive Oxygen Species

RR: Retrorubral field

RT: Reverse Transcription

SAGE: Serial Analysis of Gene Expression

SC: Superior Colliculus

SK: Small-conductance calcium-activated K^+ channels

SN: Substantia nigra

SNc: Substantia nigra, *pars compacta*

SNl: Substantia nigra *pars lateralis*

SNr: Substantia Nigra *pars reticulata*

TdT: Terminal deoxy Transferase

TTX: Tetrodotoxin

TF: Transcription Factor

TFRC: Transferrin Receptor

TH: Tyrosine Hydroxylase

TSS: Trascription Starting Site

UV: Ultraviolet Light

VM: Ventral Midbrain

VMAT2: Vesicular Monoamine Transporter 2

VTA: Ventral Tegmental Area

WT: Wild Type

Note: The abbreviations LCM and LMPC are used interchangeably in the text.

ABSTRACT

The Central Nervous System (CNS) contains an enormous variety of cell types which organize in complex networks. The lack of adequate markers to discern unequivocally among this cellular heterogeneity make the task of dissecting out such neural networks and the cells that comprise them very challenging. The present study represents a "bottom-up" approach that entails a description of A9 and A10 nuclei, which are components of the mesencephalic dopaminergic system, and the identification of their molecular make-up through microarray analysis of their gene expression profiles.

These mesencephalic dopaminergic nuclei give rise to the mesocortical and mesostriatal projections and are well known for their roles in initiation of movement, reward behaviour and neurobiology of addiction. Moreover, in *post mortem* brains of Parkinson Disease patients a specific topographic pattern of degeneration of these neurons, also recapitulated in experimental animal models, is noted, with A9 neurons presenting with a higher vulnerability to degeneration with respect to A10 cells among which, neuron loss is almost negligible. Molecular differences may be at the basis of this different susceptibility.

In this study we have optimized a protocol for laser-assisted microdissection of fluorescent-expressing cells and have taken advantage of a line of transgenic mice TH-GFP/21-31, which express GFP under the TH promoter in all CA cells, to guide laser capture microdissection of A9 and A10 mDA neurons for differential informative cDNA microarray profiling.

Results show that our optimized method retains the GFP-fluorescence of DA cells and achieves good tissue morphology visualization. Moreover, RNA of high quality and good reproducibility of hybridizations support the validity of the protocol. Many of the genes that resulted differentially expressed from this analysis were found to be genes previously known to specifically define the different identities of the two DA neuronal nuclei. Transcripts were verified for expression, in DA neurons, using the collection of in situ hybridization in the Allen Brain Atlas. We have identified 592 differentially expressed transcripts

(less than 8%) of which 242 showing higher expression in A9 and 350 showing higher expression in A10. Categorical analysis showed that transcripts associated with mitochondria and energy production were enriched in A9, while transcripts involved in redox homeostasis and stress response resulted enriched in A10. Of all the differentially expressed genes, eight transcripts (Mif, Hnt, Ndufa10, Aurka, Cs, enriched in A9 neurons and Pdia5, Whrn, and Gpx3 enriched in A10 neurons), verified with the Allen Brain Atlas and not noted or confirmed as differentially expressed before, emerged from this analysis. These and other selected genes are discussed.

INTRODUCTION

1. 1 NEURONAL CELL TYPES

1.1.1 A historical perspective

The mammalian brain is the most intricated biological structure known and still the scale of its complexity is grossly underestimated. It is composed of tens to hundreds of areas, each containing a comparable number of distinct cell types, about a trillion nerve cells in addition to astrocytes, oligodendrocytes and microglia. Identification and classification of these different cell types that constitute the elementary building blocks of the brain is at the basis of understanding brain circuitry and function. In fact, one of the key questions of brain microcircuitry studies is the degree to which a single canonical circuit comprised of a set of canonical cell types can be recognized across cortical areas (Monyer et al., 2004). Many neural cell types have been known for over a century, but the coverage has been spotty and far from complete.

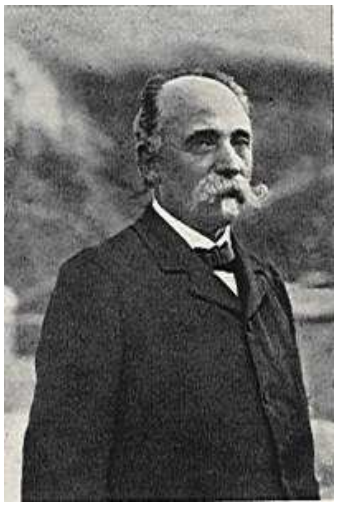

Figure 1. Camillo Golgi (1843-1926)

Systematic analysis of neuronal diversity started over 125 years ago with the publication of a technique for silver staining (black reaction or reazione nera) by Camillo Golgi that revolutionized histological studies of the nervous system. The Golgi method consisted in submerging small pieces of nervous tissue in an osmium – bichromic solution for several days, following which the pieces of tissue were left in a fresh

solution of silver nitrate for a few more days (Valverde, 1970). As a result some cells became filled with a fine-silver chromate precipitate that made them visible in their entirety against a translucent yellow background (Figure 2). Because this technique allowed the reaction of only a few, widely separated cells in a sample of cell-dense neural tissue, Golgi was able to observe for the first time an incredible morphological diversity amongst neurons. He could examine many of the fundamental cell types from various regions of the central nervous system such as the olfactory bulb, cerebral cortex, spinal cord and the cerebellum (including the sole output neurons of the cerebellar cortex, the Purkinje cells). At about the same time Ramon y Cajal used a modified Golgi method for his survey of the retina and

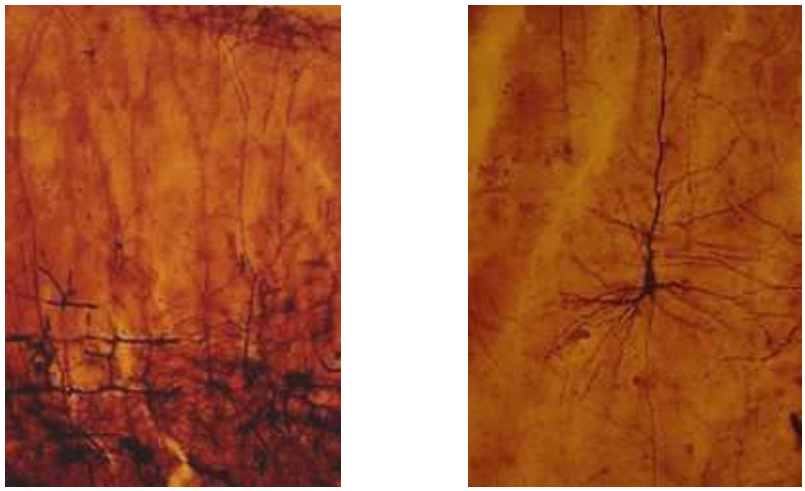

Figure 2. Photomicrographs from Cajal's preparations (housed in the museo Cajal at the Cajal Institute, Madrid, Spain) of the cerebral cortex of a newborn infant, showing neurons impregnated by the Golgi stain. "Cajal on the cerebral cortex", Oxford University Press, New York, 1988.

Figure 3. Ramon y Cajal (1852-1934)

the cerebellum. In his analysis of flow of impulses in these regions, he confirmed the cell types that Golgi had described in the cerebellum, and added a detailed description of the two types of afferent fibers to the cerebellar cortex, the "mossy" and "climbing" fibers. He recognized that Golgi's large basket cells of the cerebellar cortex were distinct functional entities and could only

exert an effect upon the white matter through their axon terminations on the cell bodies of Purkinje cells (Cajal 1888). This observation led him to the idea of the "connections by contact" and his "connectionist view of the nervous system", which demolished the old network theory, supported by Golgi, and resulted in the formulation of the Neuron Doctrine by Waldeyer (1891) in the form that we know it today. His illustrations of the retina, with the description the of major cell types that constitute it, was restricted horizontally and extended vertically, reflecting his view for a unidirectional flow of nerve signals.

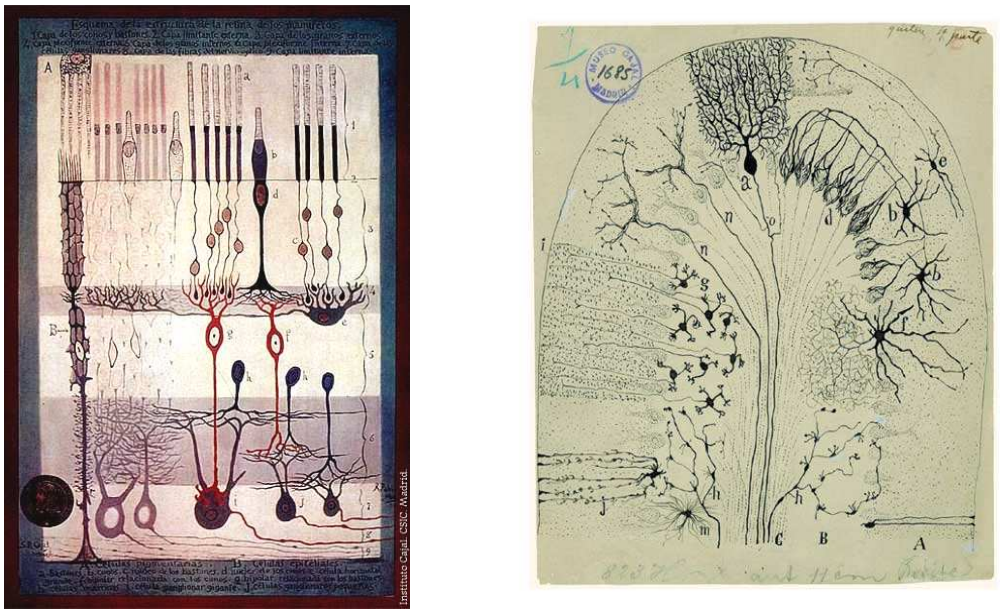

Figure 4. Drawings made by Ramon y Cajal of the retina and the cerebellar cortex, respectively. The variety of cell types recognized and the interwiring of the neurons into polarized circuits, allowing for a unidirectional flow of nerve signals, is evident.

The recognition that neurons were distinct functional entities coming in a variety of types that interconnected in specific ways to form circuits, underlying specific brain functions, laid the modern basic principles of neuroscience and started off a systematic analysis of neuronal types.

1.1.2 How many different neuronal cell types exist ?

Traditionally, cell types have been defined on the basis of a wide variety of characteristics including anatomical location, morphology, intrinsic firing

patterns, synaptic physiology, expression of particular neurotransmitters and receptors, presence or absence of particular marker genes, such as those encoding neuropeptides and calcium binding proteins. In fact, different structure - intending here by structure both morphology and the expression of functionally important proteins - indicates different function. The commonest way to distinguish between different neuronal types has been the shape of a cell, as the shape is a direct reflection of its synaptic connections. The methods that typically have been used to reveal the morphology of a cell fall in three main categories: 1) staining methods such as the Golgi technique, methylene blue or the reduced silver stain, 2) filling the cell with a dye, such as biocytin, through a microelectrode, and 3) other histochemical methods that rely on biochemical markers present in single neuronal types. Increasingly and with the development of immunohistochemistry in the 1960s and 1970s, cells have been distinguished by the expression of genes/proteins. Occasionally, cells have been first distinguished by patterns of electric activity.

In recent years, the development of sensitive and reproducible mRNA in situ hybridization techniques have permitted the systematic analysis of gene expression in neurons. Furthermore, transgenic (promoter-based and BAC-based) and knock in approaches have made it possible to visualize the pattern of expression of particular genes using genetically encoded reporters driven from the gene locus in transgenic mouse lines.

Gene expression profiling needs consecutively neuroanatomical verification and integration with connectional data to lead to meaningful interpretation of cerebral brain functions. Thus, in parallel to gene expression analysis, intensive connectivity studies were set off by the development of a technological innovation on tracing techniques in the late 1960s that saw a rapid development in the decade of the 1970s. These tracing techniques utilize anterograde and retrograde naturally occurring cellular transport for fiber tracing purposes and have been fundamental in providing the solid neuroanatomical background for many concepts of brain function. Recently, the development of genetically encoded tracers that are transported across synapses and of genetic encoded reporters of electrical activity (for example changes in intracellular

calcium concentration), have allowed patterns of connectivity and neuronal functions to be defined.

In the past decade, different laboratories have undertaken studies in an attempt to quantify neuronal diversity in a single class of neurons, reaching the conclusion that indeed neuronal diversity is higher than previously thought. In this perspective, MacNeil and Masland (1998) conducted a study on the amacrine cell population of the retina, which is fundamental to the processing of visual information. Because the retina is a highly ordered laminar structure, the shape and extent of an amacrine's cell dendritic arbor determines its connections with other neurons, bipolar (the output cells) and ganglion cells, modulating their responses. By describing the dendritic shape and stratification of 261 randomly chosen amacrine cells by a new method termed photofilling, MacNeil and Masland were able to classify 26 different types of neurons, including the four major types already known (Figure 5).

One year earlier, in 1997, DeVries et al., exploited the multielectrode array which permitted simultaneous recordings from a large number (in the order of 100) of neighboring ganglion cells in the rabbit retina, distinguished 11 distinct physiological classes. In the same year, Parra et al. attempted to quantitate the number of different interneurons present in the CA1 area of the hippocampal cortex. These neurons were first classified on the basis of morphology (somatic location, dendritic orientation, regions of innervation), then physiology (action potential firing properties) and finally sensitivity to modulatory neurotransmitters. They were able to distinguish 16 distinct morphological phenotypes and 3 different modes of discharge. Most cells responded to 2 to 3 agonists and 25 different response combinations were detected. To their surprise each cell was unique across these criteria. They concluded that the number of different types in the CA1 region of the hippocampus must be between two dozen and four dozen.

Still, the question of how many different neuronal cell types might there be in the brain has not found a definite answer. An assumption can be made based on spacing, cell number and dendritic cell diameter.

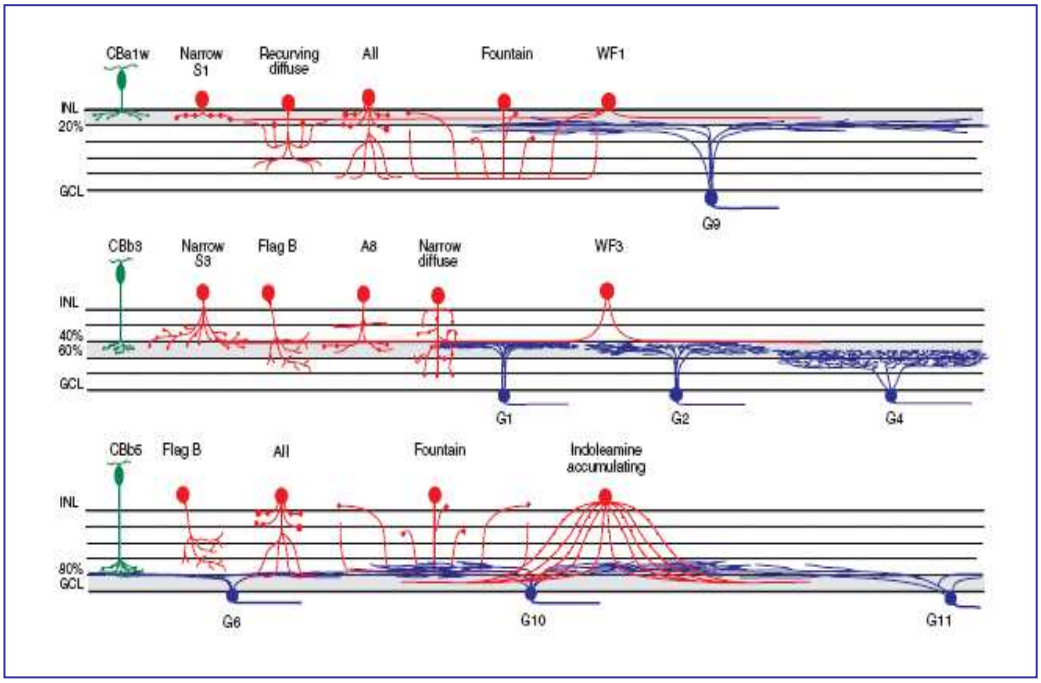

Figure 5. Patterns of connectivity in the retina, illustrated for 3 levels of the inner plexiform layer. Cell bodies are indicated by ovals, with dendrites extending below. Note the dendritic extension to different cell levels (horizontal cell lines) for different cell types and the difference in arborization patterns, the level of stratification of the different cell types defines which cells can contact each other (from Masland et al., 2004).

Initial observations that some particular ganglion cell types just cover the retina with their dendritic fields (Wässle et al., 1981 and DeVries and Taylor, 1997) demonstrated the generality of what has come to be known as the "tiling" principle. According to this principle it is reasonable to assume that the receptive field belonging to any particular type of neuron overlap only moderately with other cells of the same type. Since each neuron type contributes to information processing in a distinct way, all other neuronal types should have similar access to at least one member of each distinct class, by filling in a brain region with minimal redundancy. Another aspect to take into consideration when trying to envision the scale of neural diversity is that some brain areas more than others might afford redundancy, or, in other words, might have multiple copies of a neuron. In fact, this would ensure, on one hand, the function of the circuit if a few neurons died and, on the other, the possibility to average information over multiple copies of a single neuron. It is well known that mammalian brains can still function after relatively heavy neuronal loss (Stevens et al., 1998). So, for example, to estimate neuronal diversity in the neocortex one could argue that

underneath 1 mm^2 of most regions of the primate cortical surface there are about 10^5 neurons, each of which with a dendritic spread of 0.05 mm^2. This means that 20 neurons would be needed to cover a square millimeter of cortex if we assume they tile the region. The upper limit on number of cell types should then be $10^{5/}$/20 or 5000 cells. Considering a generous redundancy factor of 10 (10 times more neurons of each type than required to cover the cortex), then the total number of individual neuronal types in the neocortex alone is calculated to be around 500 (Stevens et al., 1998).

With over a third of the genome expressed in the brain, a large number of different neuronal types should not perhaps come as a surprise. The scale of neuronal diversity probably also indicates the existence of an unsuspected variety of microcircuits or networks, still far from being understood, and each devoted to a specialized computational task. One could then argue that a good way to discriminate a neuronal type is by characterizing its unique function or task within a circuit.

1.2 METHODS FOR CELL-TYPE-SPECIFIC EXPRESSION PROFILING

1.2.1 Overview

It is reasonable to assume that the role of a neuron within a circuit is highly correlated and dependent on its transcriptome. For this reason, it has been suggested that global gene expression profiling could provide a useful alternative strategy for the identification and classification of neuronal types (Mott et al., 2003 and Makram et al., 2004). In the last years, mRNA profiling has become feasible through the introduction of cDNA (Schena et al., 1995) and oligonucleotide microarrays (Lockhart et al., 1996) as well as modern sequencing techniques on full length cDNA libraries and tag sequences (Velulescu et al., 1995; Shiraki et al., 2003), which allow simultaneous analysis of thousands of genes. Initial gene expression profiling studies have been carried out on tissue homogenates from entire brain regions or subregions where cell-specific gene expression is “lost” in favor of more abundant cells within the tissue (Mirnics et

al. 2000, Sandberg et al., 2000, Xie et al. 2002, Zhao et al., 2001, Zirlinger et al., 2003). The results of such studies are difficult to interpret without localization of individual transcripts at the cellular level and can lead to biased conclusions. In fact, in a pioneering study, Barlow and colleagues detected more cerebellum-expressed transcripts than neocortical transcripts (Sandberg et al., 2000), although the underlying complexity of mRNA is likely to be inverse (Geschwind 2000). Despite the drawbacks of this approach, such studies have been useful, for example, in suggesting functional gene classes involved in schizophrenia (Mirnics et al., 2000) and identifying neuronal markers in the amygdala (Zirlinger et al., 2003), holding promise for the use of this technology in the classification of neuronal types.

The problems arising from the heterogeneity of tissue samples and the difficulty of isolating homogeneous neural types for expression profiling have a dual nature. In the first place, as mentioned earlier, a significant fold change in the expression of a particular gene can be diluted considerably if the cell type expressing a particular gene represents only a fraction of the overall population being studied. Moreover, it is possible that up-regulation in the expression of a gene in one cell population can be masked by down-regulation of the same gene in a neighboring cell population in the tissue sample under study, resulting in loss of information of expression changes. A second problem lies with the nature itself of the genes under scrutiny. It has been reported that gene products fundamental for neuronal function such as neurotransmitters, receptors and their regulatory factors, are expressed at very low levels compared to other cellular constituents like structural proteins (Jiang et al., 2000; Wurmbach et al., 2002). Moreover, it seems that physiological and clinical features in neuropsychiatric diseases are due to moderate changes in gene expression rather than the often two-fold or higher gene expression changes noted for cancer tissues (Soverchia et al., 2005). If the population looked at is complex, then discriminating real expression from experimental noise becomes rather difficult.

As a consequence, various cell selection techniques have been developed to enhance homogeneity of cell samples and achieve purity of neuronal populations. The strategy used can be generally outlined as follows.

i) A functionally distinct cell type must be rendered recognizable. This can be achieved with the use of an antibody by immunocytochemical labeling against a known marker. The fact that few neural cell types bear specific markers has made sampling of specific cells very difficult until recently. Cells can also be labeled by stereotaxic injection of fluorescent tracers into their projection target or a cell population can be engineered to express a fluorescent protein such as green fluorescent protein (GFP) under a specific promoter or enhancer. Finally, it is possible to select cells based solely on their topographic position, morphology or electrophysiology, without the need for specific labeling.

ii) The population bearing the specific label must be purified from the rest of the tissue.

iii) The mRNA must be extracted.

iv) The mRNA must be amplified to yield a sample that can be probed on a microarray platform.

Many laboratories have put considerable effort in optimizing and integrating all of these steps with very promising results.

1.2.2 Techniques for enriching specific cell populations

1.2.2.a Fluorescent Activated Cell Sorting (FACS)

Labeling of defined cell types *in vivo* has been used for Fluorescent Activated Cell Sorting. The first to utilize this sampling strategy to analyze genome wide gene expression was Zhang and his co-workers in 2002. He expressed green fluorescent protein (GFP) in the six touch-receptor neurons of the nematode *C. elegans*, then purified these cells from thousands of dissociated embryos on automated fluorescent activated cell sorter (FACS), after culturing them overnight to increase GFP expression, and finally extracted and amplified mRNA for microarray analysis. This method was subsequently implemented in other C. *elegans* studies (Colosimo et al., 2004; Fox et al., 2005; Cinar et al., 2005) and soon after in cell-type-specific expression profiling in the mammalian nervous system (Buchstaller et al., 2004; Arlotta et al., 2005). Arlotta and co-

workers used a tracer labeling strategy to mark the cells to be FACS sorted and profiled, i.e. cortical projection neurons were retrogradely labeled by injection of tracer intro controlateral cortex and spinal cord. The major limitations of this approach are the applicability to adult and aged brain tissue, and eventually, the effect that the *ex vivo* prolonged tissue processing may have on gene expression. On the other hand, contamination with glia, which may have their own distinct role especially if studying response to neurodegeneration, and neuronal fibers is negligible and RNA is preserved well as it is not subjected to freezing or fixation procedures.

1.2.2.b Manual Cell Sorting

A similar way to purify labeled neuronal populations is by manual sorting. A glass pipette is used to collect and purify dissociated cells under a fluorescent dissecting microscope (Sugino et al., 2006). Compared to the automated FACS sorting, this method, being a very gentle procedure, allows purification of adult neurons, leads to even higher population purity and it can be used even on cells expressing low fluorescent intensity. The samples that can be collected are though limited in size (usually between 30 and 100 cells).

Single cell aspiration has been used mainly on single cell expression studies. It is a microinjection technique by which a patch electrode filled with first strand cDNA synthesis components is injected into a single cell. The cell is loaded with the reaction mix, followed by suction of the entire cell content into the electrode for further processing (Cao et al., 1996; Crino et al., 1996; Gustincich et al., 2004).

1.2.2.c Immunomagnetic positive selection

This technique uses magnetic beads conjugated to an antibody directed against a specific antigen present on the membrane of the cell population to be sorted (Lyons et al., 2007).

1.2.2.d Laser assisted microdissection (LCM)

In recent years, several investigators have used laser-assisted microdissection to isolate small areas of tissue or single cells out of histological sections to achieve nearly pure cell samples for subsequent expression profiling studies. This technology allows the excision by laser of cells of interest from a thin tissue section, chosen by the operator on the basis of specific topographic, morphologic or staining characteristics, and their collection in a tube for subsequent analysis. Compared to fluorescent-activated cell sorting or magnetic bead sorting, this method does not require tissues to be exposed to collagenase digestion before cell isolation. As these cells are directly collected *in situ* from the tissue, they conserve their RNA profile in a true *in vivo* state. In fact, the metabolism of neurons *in vivo* is coupled to that of glial cells, which means that the study of transcriptional profiles of dissociated neurons *in vitro* is likely to lead to artificial results (Pellerin and Magistretti, 1994; Kasischke et al., 2003). Limitations lie in the fact that the tissue needs to be frozen or fixed with cross-linking agents (e.g. formaldehyde) or precipitating agents (e.g. ethanol) and very often to be stained by immunohistochemical and immunofluorescent assays. All the aforementioned interventions do not allow isolation of high-quality RNA, which affects the subsequent microarray analysis (Karsten et al., 2002; Van Deerlin et al., 2002). Moreover, the absence of a coverslip and the complete dehydration of the tissue section required by the procedure lead to poor visualization of cell morphology. The fact that only small amounts of nucleic acids can be isolated with this method calls for further DNA or RNA amplification of the collected material with all the difficulties that amplification may bring. Finally, contamination by surrounding cells cannot be completely controlled for.

The first instrument for laser-assisted microdissection was developed in 1996 at the National Cancer Institute (Emmert-Buck et al., 1996) for the analysis of tumor cells. Only recently has it been applied to the study of the CNS (Luo et al., 1999). It was commercialized and released on the market by NCI and Arcturus Engineering, California, USA, as the PixCell system, 12 months after publication.

Soon after the first commercial LCM microscope was released, various companies developed microdissection systems with similar characteristics (Table 1).

Company	*Instrument*	*Laser*	*Excision*	*Collection*
Arcturus Engineering	PixCell II	IR	Laser hitting of desired cells by cap thermoplastic melting	CapSure cap (EVA polymer film)
Arcturus Engineering	Arcturus^{XT} (open and modular)	UV and IR	LCM and Laser Cutting	CapSure cap (EVA polymer film)
Arcturus Engineering	Veritas (enclosed and automated)	UV and IR	LCM and Laser Cutting	CapSure cap (EVA polymer film)
PALM Microlaser Technologies	PALM Microbeam	UV	Laser cutting around tissue of interest	Laser pressure catapulting
Leica Microsystems	Leica AS LMD	UV	Laser cutting around tissue of interest	Excised tissue falls down by gravity
Molecular Machines and Industries	Mmi Cellcut	UV	Laser cutting around tissue of interest	Adhesive collection cap

IR, infrared; UV, ultraviolet

Table 1. List of commercially available laser-based tissue microdissection systems, their excision and collection methods.

Nowadays, the LCM system (Laser Capture Microdissection, Arcturus Engineering) and the LMPC (Laser Microdissection Pressure Catapulting) system from PALM Microlaser Technologies are the most widely used laser-based microdissection systems (Figure 6). The Arcturus system is based on a technology referred to as *Laser Capture Microdissection* (LCM). In this procedure a cap, coated with a special thermoplastic film, is placed on the tissue section and an infrared (IR) laser is directed through the cap to melt the film onto the cells of interest. The cap is then lifted with the selected cells attached to it and automatically placed onto 0.5 ml microcentrifuge tube for subsequent molecular analysis. The PALM Microlaser system based on LPC, uses an Ultraviolet A (UV-A) laser beam to collect cells of interest through an inverted microscope after these have been marked for dissection by the operator. The laser beam impacts the tissue sample and, at the focal point, the energy transfer is sufficient to break molecular bonds resulting in fragmentation of the radiated matter, a phenomenon that is called “cold ablation” or “ablative photodecomposition” (Srinivasan, 1986;

Vogel and Venugopalan, 2003). The tissue sample results cut while a defocused laser beam gives the pulse that lifts up and catapults the sample into the collection tube overlying the tissue with the advantage of isolating material in a non-contact manner, thus minimizing the risk of contamination (Schutze et al., 1998).

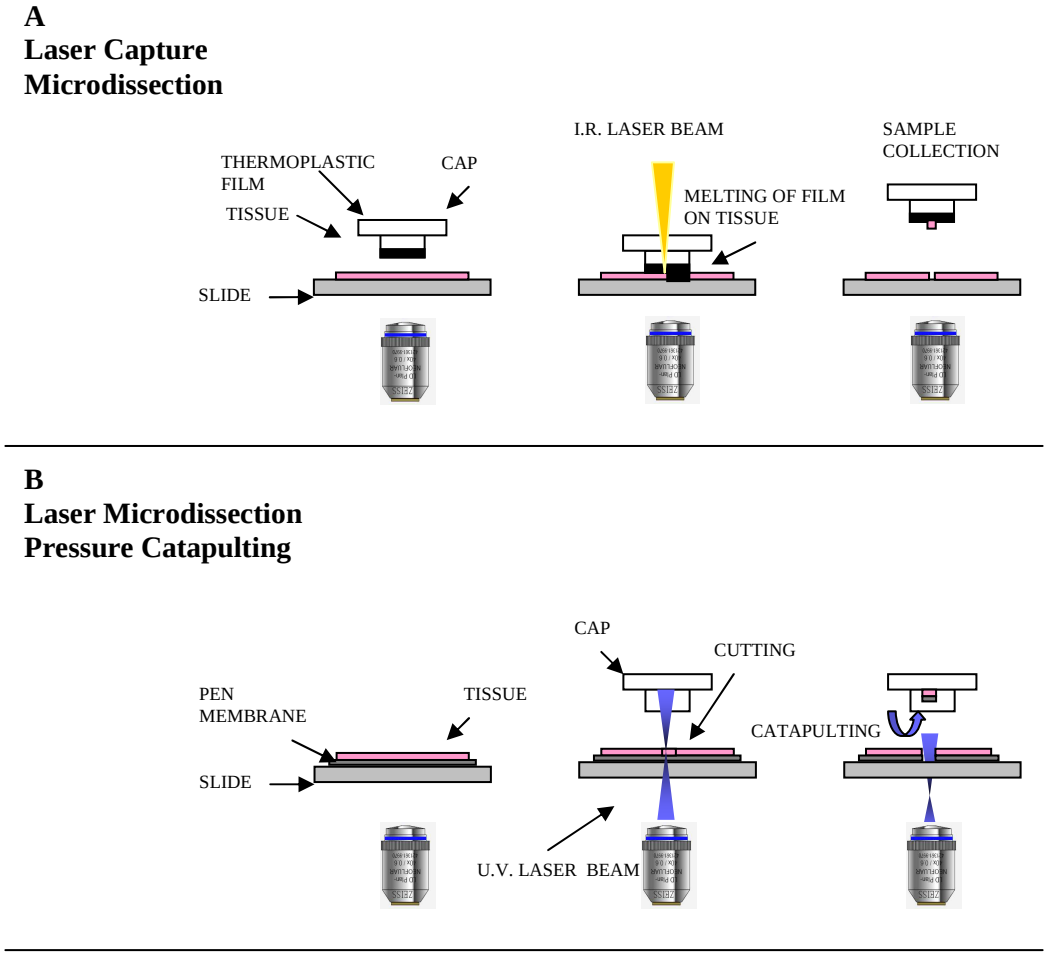

Figure 6. Principles of laser-assisted microdissection techniques. Tissue slides are viewed through and inverted microscope in both A and B versions of the technique. A) LCM. A film-coated cap is lowered on top of the specimen. An infrared laser beam is directed against the region of interest, determining, with its passage through the cap, the melt down of the thermoplastic film on the selected region of the tissue. Finally, the cap is removed achieving the detachment of the selected cells from the tissue section. B) LMPC. The tissue specimen is mounted on a PEN membrane-coated slide (or directly on a glass slide). An ultraviolet A (U.V.-A) laser beam is pulsed through the objective of the inverted microscope, and at the focal point through a process known as “cold ablation” cuts the tissue sample around the demarked region. Subsequently, the excised area is catapulted, through a defocused U.V.-A pulse, out of the tissue and into the collection cap overlying the tissue specimen. Collection is achieved against gravity protecting the collected sample from contaminants.

Since the microscope is inverted, tissue sections can be mounted either on glass slides or on poly-ethylene-naphthalene (PEN)-coated glass slides. The latter allow for the collection of the tissue sample of interest in its integrity, since it is excised and catapulted on a piece of membrane which permits the preservation of its morphology.

The success of molecular analysis after laser-assisted capture microdissection depends on the careful optimization of every step involved in the process, that is, tissue sample preparation and handling, RNA extraction, amplification, microarray hybridization, data analysis and interpretation and, finally validation of results.

1.2.3 Tissue sample preparation for LCM

Collected specimen can be either snap-frozen or fixed in various ways to prepare tissue sections for LCM collection. Snap-frozen tissues minimize RNA degradation and provide excellent RNA and DNA quality. The gold standard for brain tissue preparation consists in the immersion of the sample in liquid nitrogen-cooled isopentane (at -60˚C). Not all tissues can be snap-frozen as the possibility of ice-crystal formation within the tissue can destroy morphological detail, rendering histological examination cumbersome, especially when some sort of staining for cell recognition is required. Therefore, fixation and tissue embedding need to be used for microdissection when retention of rich morphological detail is a prerequisite for cell collection.

A number of different fixatives have been used to prepare tissue sections for LCM. Aldehyde-based fixatives (such as formalin or paraformaldehyde) function as chemical cross-linking agents giving excellent morphological visualization whereas simple organic coagulants like ethanol, methanol, acetone or zinc salts have precipitating effects. Several researchers have found it (Brownstein et al., 2004; Lewis et al., 2001) impossible to extract good quality RNA from formalin-fixed tissues. In fact, in a study conducted by Karsten et al., (2002), cDNA microarray experiments performed using RNA samples from frozen tissue resulted in very reproducible expression data while results generated

from RNA coming from fixed tissue, either formalin or ethanol, were characterized by lower correlation coefficients and irreproducibility. Formalin-fixed tissue was more severely affected than ethanol-fixed tissue. Time and temperature seem to have a determinating effect during formalin fixation (Foss et al., 1994; Van Deerlin et al., 2002) as prolonged fixation in formalin (longer than 12-18 hours) results in shorter amplifiable targets, while fixation under high temperature does not preserve RNA integrity. There is some controversy surrounding the use of ethanol as a fixative for LCM procedures as it has been reported to result in bad quality RNA by some researchers (Fend et al., 1999; Huang et al., 2002; Gillespie et al., 2002; Brownstein et al., 2004), but to yield intact or good RNA by others (Luo et al., 1999; Mikulowska-Mennis et al., 2002; Luzzi et al., 2003; Wang et al., 2009). Acetone has resulted in good RNA preservation in several studies (Goldsworthy et al., 1999; Salunga et al., 1999; Burbach et al., 2004; Torres-Muñoz et al., 2004). Methanol seems to efficiently recover RNA with preserved integrity, comparable to that of acetone fixation (Goldsworthy et al., 1999; Schleidl et al., 2002). A zinc-based fixative, acting as a precipitating agent, has proven successful in terms of both preservation of tissue morphology and RNA quality (Johansson et al., 2000; Schleidl et al., 2002). Fixation in zinc salts can be performed prior to cryosectioning, allowing thus subsequent cryopreservation in glucose solution, which further aids retention of tissue morphology in successive steps. Another interesting fixative compound that has been reported to assure good tissue morphology and RNA integrity is dithio – bis (succinimidyl proprionate) (DSP), a cross-linker, also known as Lomant's reagent (Brownstein et al., 2004).

Tissue embedding in paraffin or in OCT for snap-frozen samples is generally used to improve tissue morphology, but it can also affect RNA tissue integrity. Schleidl et al., 2002, showed that the effect of OCT embedding on nucleic acid preservation was negligible while paraffin embedded samples resulted in the production of lower amounts of cDNA. Histological stains, immunohistochemistry, immunofluorescence, and in situ hybridization also have deleterious effects on RNA quality. Various methods have been developed to limit the adverse effects of staining on RNA quality. Usually shortening of incubation

times for histological staining (Goldsworthy et al., 1990; Ginsberg and Che, 2004; Torres-Muñoz et al., 2004], for immunohistochemical protocols (Fend et al., 1999; Burbach et al., 2004), and for immunofluorescent protocols (Mojsilovic – Petrovic et al., 2004; Chung et al., 2005) appear to result in improved RNA quality since the shortened protocols protect from the activation of tissue RNases. For the same reason, special compounds such as RNase inhibitors have been added to the various incubation solutions especially in immunohistochemical protocols with positive results in terms of RNA preservation (Grimm et al., 2004; Greene et al., 2005).

Once tissues are prepared, they are sectioned with a microtome or, if frozen in a cryostat, in sections of such thickness that will allow good microscopic resolution but not at the expense of the quantity of material that can be harvested. Usually, 5-8 μm sections are considered as a monolayer of small cells while for larger cells tissue thickness can vary from 10 to 20 μm, despite this makes morphological visualization more difficult. It is important that sections have no wrinkles and scratches and that they adhere to the slide, so that a uniform contact between the thermoplastic film and the tissue (for LCM) (Mora et al., 2002) or a constant focusing plane for cutting (for LMPC) can be achieved.

In this work we have evaluated various fixatives in terms of tissue morphology, cell marker retention, and RNA integrity and we have set up each step of the method accordingly.

1.2.4 Harvesting the cells of interest amongst heterogeneity

One of the main disadvantages of laser-assisted tissue microdissection is the poor morphology of tissue sections from which cells are excised. This is due primarily to the fact that sections cannot go through the canonical histological procedures which would be incompatible with downstream analysis; secondly, sections need to be air-dried and uncovered for the technology to be applied; finally, microscopes used with laser dissecting systems are generally not very powerful. To improve microscopic visualization several strategies have been devised amongst which the use of a diffuser filter (provided with the PALM

LMPC system). This filter diffracts light passing through the cap giving a better image of the tissue. In this case, cells must be selected first and they can only be harvested later without the diffuser (Simone et al., 1998). Alternatively, drops of xylene or ethanol have been used in various occasions for this purpose. Again, morphology is improved temporarily, allowing just the time for cells to be selected by the investigator, before the tissue is dry and excision can start. PALM offers a resin (LiquidCover N) as a mounting medium that improves tissue morphology and does not interfere with UV laser cutting efficiency, catapulting or downstream molecular applications. It is not suited though for fluorescent expressing tissues, since being alcohol-based, quenches fluorescence as xylene and ethanol do.

In our laboratory, in order to improve visualization of GFP – expressing dopaminergic cells from our TH-GFP/21-31 transgenic mouse lineage we have used a drop of Zincfix (zinc-based fixative) on the region of interest to be harvested. We have evaluated the effects on UV cutting and RNA quality.

1.2.5 RNA extraction procedures

Numerous RNA extraction procedures have been developed in conjunction with the advent of LCM technology that are appropriate for small samples (Parlato et al., 2002; Burgemeister et al., 2003; Niyaz et al., 2005), all of which should be optimized by each user to best suit their own application. For this reason, but also to avoid loss of material in samples so small as the ones obtained by LCM and to speed up the process of extraction, many investigators have chosen to use kit-based methods especially developed for this type of samples, i.e. Strategene Absolutely Microprep kit, Qiagen RNeasy Minikit, Arcturus Pico-Pure RNA Isolation kit. These kits are column-based and this allows a greater yield than methods that rely on multiple organic extractions since each extraction step equals some loss of RNA. Moreover, these kits: 1) use elution volumes in the order of 10 μl, and 2) allow treatment with DNase directly on the column, thus avoiding further RNA purification and precipitation steps.

For paraffin-embedded, formalin-fixed tissues various procedures have been suggested (Godfrey et al., 2000; Specht et al., 2001), but the most common method is based on Proteinase K digestion of the fixed or embedded tissue (Lewis et al., 2001), which facilitates subsequent RNA extraction. Most companies today provide kits especially optimized for RNA extraction for paraffin-embedded microdissected tissues, i.e. Strategene Absolutely RNA FFPE kit; Ambion RNAqeous microkit, Arcturus Paradise reagent system.

1.2.6 RNA amplification

Standard protocols for microarray hybridization technology require a large amount of RNA. In fact, the total RNA quantity required for use in microarray experiments was reported to be 50-200 μg in a number of review papers (Duggan et al., 1999). Considering that a cell contains 5-10 pg total RNA, the number of cells required to achieve 50-200 μg ranges from 1.6×10^6 to 2×10^7, amount that corresponds to several milligrams of tissue (~ 100 mg).

RNA extracted from small tissue samples like those obtained by LCM is not enough for microarray hybridization as such; instead amplification of some sort is required.

Two main approaches have been developed to overcome limitations deriving from the use of small samples, signal amplification and global poly (A)+ RNA amplification.

The first strategy functions by increasing the fluorescence signal emitted per transcript. This is achieved by technologies such as dendrimer (Stears et al., 2000) or tyramide signal amplification (TSA) (Karsten et al., 2002), which claim avoidance of dye bias and improved signal to background ratio. Commercial products have achieved considerable improvements of these technologies with a minimum number of cells required to achieve good quality arrays amounting to 2.5×10^4 (denrdimer technology by Genisphere). Still this number is too high for LCM captured samples.

The second strategy, that allows RNA amplification from limited quantities down to the single cell, entails global amplification of the sample based

either on exponential PCR amplification (Lukyanov et al., 1997) or isothermal linear RNA polymerase amplification (Van Gelder et al., 1990).

The classic T7 RNA polymerase amplification method, commonly referred to as the Eberwine method (Van Gelder et al., 1990), has provided the basis of the procedures and commercial kits routinely used today (Figure 7). This method utilizes a synthetic oligod(T) primer annealed to a phage T7 RNA polymerase promoter to prime synthesis of first strand cDNA by reverse transcription of the poly(A)+ RNA pool of total RNA. Second strand cDNA is synthesized with RNase H by degrading the RNA strand followed by second strand synthesis with E.Coli DNA polymerase I. Amplified antisense RNA (aRNA) is synthesized by *in vitro* transcription of the double-stranded cDNA (ds cDNA) template using T7 RNA polymerase (Figure 7). Since its appearance, this method has been subjected to numerous variations and optimizations. Amongst those the exploitation of the template switching effect of the 5' end of the mRNA to ensure the synthesis of full length ds cDNA, which is not ensured with the classical method, is to be noted (Chenchik et al., 1998; Wang et al., 2000). This template-switching effect is based on the terminal transferase activity of the reverse transcriptase that adds additional, non-template residues, primarily cytosines, to the 3' end of the cDNA. The reverse transcript buffer mixture also contains a primer containing an oligo(G) sequence at its 3' end which will base pair with the newly synthesized dCTP stretch. Reverse transcriptase then switches templates and continues replicating the defined sequence of the annealed primer. This method can amplify the starting poly(A)+ RNA by up to 200 fold and a double T7 amplification round can take this figure up between 1000 and 100,000.

Linear amplification methods have been preferred over exponential amplification methods for use in combination with microarray technology as they have been reported by several studies to better preserve relative transcript copy numbers. In fact, the efficacy of the Eberwine based methods has been evaluated in several studies by comparing profiles between amplified and non-amplified material (Puskas et al., 2002), Northern analysis (Eberwine et al., 1992), dot blot differential screening (Poirier et al., 1997), use of internal standard (Madison and Robinson, 1998), hierarchical clustering analysis to compare consistency of

outlier genes upon amplification (Wang et al., 2000), validation by RT-PCR (Puskas et al., 2002), and comparisons of the ratio/intensity distribution of the total gene set (Schleidl et al., 2002). The disadvantage of this methodology is that it is very laborious, requiring multiple steps and hence it is time consuming and cost effective.

As an alternative to T7-based linear methods, PCR-based approaches have been introduced. These methods introduce PCR-priming sites at both ends of each reverse cDNA transcribed molecule, followed by global amplification of cDNA by PCR cycles (Hertzberg et al., 2001, Iscove el., 2002). There are many variations of this method. One approach involves reverse transcription of first strand cDNA primed by oligo(dT), addition of an oligo(dA) tail with terminal transferase and exponential amplification with an oligo(dT) containing primer (Iscove et al., 2002). Three-prime-end amplification (TPEA) is a method that results in global amplification of 3'- ends of all mRNAs present in the sample (Dixon et al., 1998; Freeman et al., 1999). In this approach, PCR amplification occurs between primers incorporated into the first strand cDNA during reverse transcription and a primer used to initiate second strand synthesis. The second strand primers have a partially degenerate 3' end and are designed to anneal approximately once every 1 kb. This results in similarly amplified amplicons therefore all mRNA species should amplify equally well regardless of the initial size of the transcript. The amplification factor using a PCR-based method has been reported to be between 10^7 and $3x10^{11}$ (Iscove et al., 2002).

Approaches that combine linear with exponential methods (Aoyagi et al., 2003; Ji et al., 2004) have also been used in some studies to achieve amplification from limited amounts of starting material with an amplification factor between 10^6 and 10^7 (Ohtuka et al., 2004). Gustincich et al., in 2004 used a combination of SMART PCR based on the template switching principle (Chenchik et al., 1998) and T7 linear amplification, called SMART7 to profile single dopaminergic neurons of the retina. With this method the first strand DNA is synthesized in the presence of the SMART template Switching Oligonucleotide and PCR amplified for a limited number of cycles. The amplification product becomes in turn the new

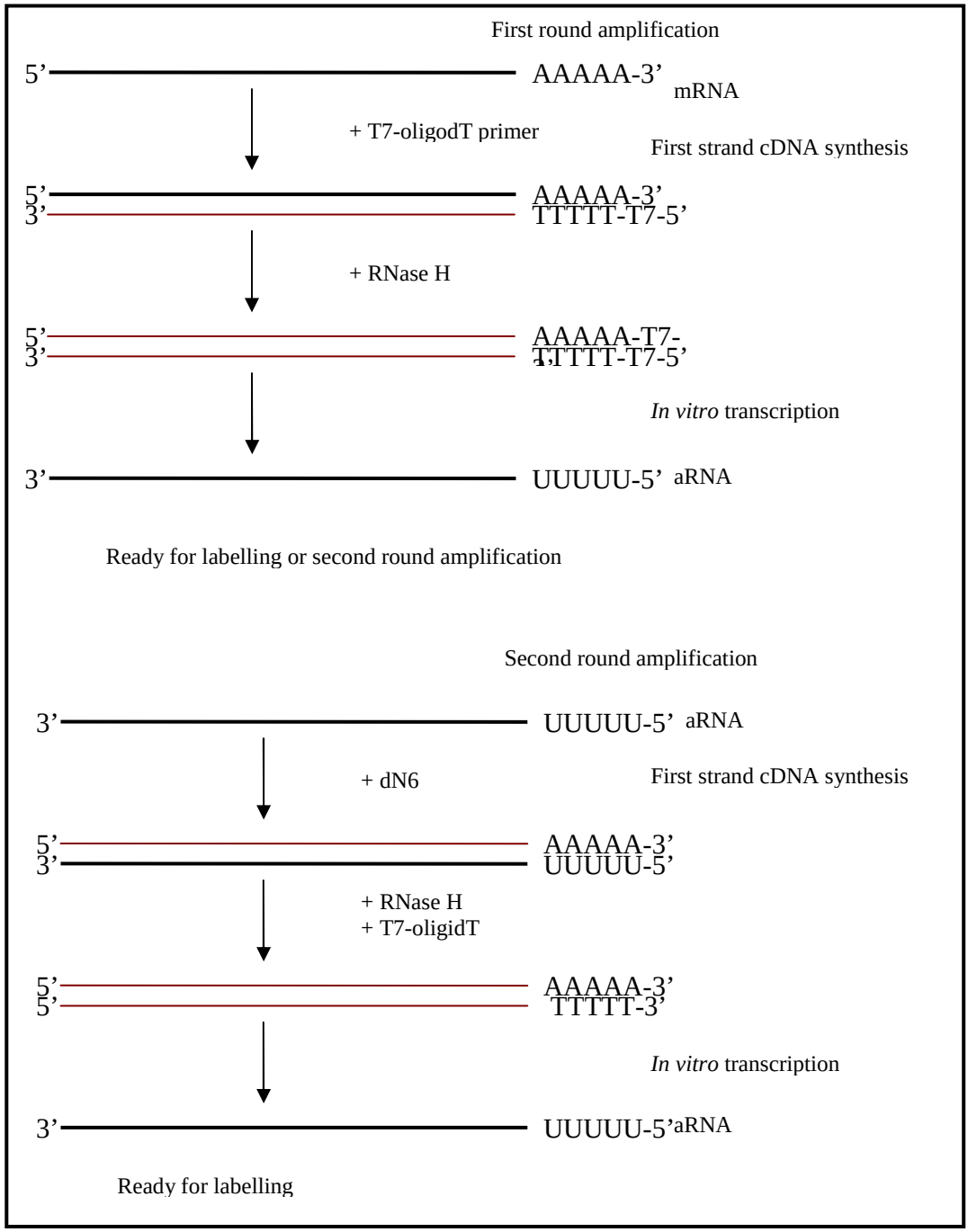

Figure 7. Diagram of a global linear mRNA amplification procedure generating antisense RNA (aRNA). An oligo (dT) primer containing a T7 Polymerase binding site is used to prime the first strand cDNA synthesis. Digestion of mRNA strand in the mRNA-cDNA hybrid by RNase H leaves small fragments of RNA, which are used to prime second strand cDNA synthesis. Antisense RNA is then transcribed by T7 RNA polymerase. Second and subsequent rounds of amplification are initiated by random priming (Figure based on method presented by Van Gelder et al., 1990).

template for two rounds of linear T7 aRNA synthesis. The combination of exponential and linear amplifications keeps the number of PCR cycles low (less than 20) and avoids the strong competition from template-independent amplification that occurs when T7 RNA polymerase is used with very low amounts of starting material (less than 1 ng total RNA). Other recently published studies on expression profiling of single cells have preferred PCR-based techniques for amplification rather than the classic linear approaches (Chiang et al., 2003; Nakagawa et al., 2004).

PCR-based amplification methods do have some advantages over linear amplification methods. First of all, they are simpler to perform. They can be used on lower input amount material, down to the single cell, since amplification yields exceed by far those of linear amplification techniques, achieving amplification rates up to 10^7 fold and over. The double stranded products are more stable than RNA products. The main disadvantage of this method is that it has been reported by several studies to lead to a bias in the transcriptome abundance relationships. These concerns arise from properties, inherent in the DNA polymerase enzyme, like misincorporation of bases, bias towards shorter transcripts and differential amplification efficiencies of different templates based on GC composition. Various studies have documented the degree of fidelity of PCR-based methods by real time PCR and by comparing profiles between amplified and non amplified material (Seth et al., 2003; Petalidis et al., 2003). In the first of these studies, conducted by Iscove et al., 2002, fidelity of PCR-based amplification was evaluated by comparing the outliers between exponentially amplified, linearly amplified and non-amplified targets. Their conclusion was that their exponential method was superior to one round linear amplification. In fact, recently there has been a turn to the use of exponential over linear amplifications methods.

1.2.7 Reproducibility

An important aspect of RNA amplification is its degree of reproducibility that can be evaluated at the end of the process itself and at subsequent hybridizations. In general, it has been reported to be high. Zhao et al., (2002)

observed significantly higher correlations (0.97) for samples amplified on the same day compared to samples amplified on different days (0.90). It is of note that the reproducibility of replicate hybridizations of amplified material is higher than for experiments using total non-amplified RNA (Nygaard et al., 2003; Stoyanova et al., 2004), which demonstrates consistency and indicates that amplification is reproducible even for genes whose relative transcript levels are not maintained. The amplification process is also affected by the amount of input total RNA. In fact, it has been reported that correlation values are reduced as the input RNA diminishes (Soverchia et al., 2005; Kenzelmann et al., 2002), showing that reproducibility increases with RNA starting quantity.

Results regarding reproducibility amongst linear and PCR-based amplification procedures are incongruent. Puskas et al., (2002) showed that reproducibility was very high for linear amplification and slightly lower for a SMART-PCR based amplification. In contrast, Klur et al., (2004) showed that their PCR-based protocol was slightly more reproducible than the linear approach.

1.2.8 Further considerations on amplification

As discussed in the above paragraph, faithful preservation of abundance levels of gene transcripts is the most important issue regarding the use of any amplification procedure in combination with quantitative microarray studies. The widest used method to control that quantitative relationships of input RNA are maintained has been by comparing profiles between amplified and non amplified material, while the most common statistical algorithm applied, when comparing profiles, has been the calculation of Pearson correlation coefficient. Other methods, such as calculation of gene-specific t-scores or calculation of the correlation value between a subgroup of amplified data against real time RT-PCR data, have also made their way into assessing the degree of fidelity of amplification on differential gene expression. To this extent, recently, researchers have focused their attention on genes co-regulated in pathways or signatures rather than single, differentially expressed genes, as this approach seems to result in more reliable interpretations (Nygaard and Hovig, 2006), especially when

dealing with minute samples. In fact, the lower the abundance of any template, the smaller the probability its true abundance will be maintained in the amplified product (Stenman et al., 2003). The reason for this lies in sampling variation that can be affected by the stochastic distribution of low abundance mRNAs and in the inherent stochastic nature of the amplification process at low template concentrations (Nygaard and Hovig, 2006).

Some general conclusions that can be drawn from these studies are summarized in the following points.

1) Amplified material gives in general a better signal to noise ratio.

2) The number of genes detected by fluorescent signaling using amplified material is significantly higher compared to non amplified targets (Nygaard et al., 2003; Stoyanova et al., 2004; Puskas et al., 2002). This increased sensitivity seems to interest low abundance transcripts more.

3) It has been reported (Nygaard et al., 2003) that some genes with low expression are scored as differentially expressed in the amplified target contrary to the reference, non-amplified target. The reason for this is that the amount of amplified aRNA used for labeling is 3-10 times higher than the corresponding mRNA content in the total RNA targets, which means that in reality the amplified products are closer to the true expression as these transcripts become detectable only when amplified from an optimal amount of RNA (Nygaard and Hovig, 2006). It follows that it is not so straightforward to infer which differentially expressed genes between the amplified material and the total RNA are the result of poor amplification or of the undetectability of low copy number transcripts obtained from the total RNA arrays. To obviate this situation, replicate arrays are used to explore consistency or variability of results.

Comparison against results from other high-throughput methods and use of quantitative real time RT-PCR for verification of gene expression or ratio levels are also valid alternative strategies for validation of microarray procedures. Finally, it is important to set a lower threshold for sample size with respect to reliable gene expression measurements.

1.2.9 Amplification – our approach

In this work we have used and tested a new kit-based method that permits one step mRNA isolation and cDNA synthesis followed by exponential amplification, called μMACS SuperAmp. This kit has been developed by Miltenyi Biotec (Bergisch Gladbach, Germany) for amplification of small samples (Figure 8 for an overview of the procedure). In brief, the sample is lyzed in a solution containing proteinase K and subsequently incubated with magnetic microbeads bearing an oligo(dT)-tag, followed by application of the lysate on a μMACS column which retains all the Poly(A)+ RNA.

cDNA synthesis by reverse transcription and cDNA tailing with Terminal Deoxynucleotidyl Transferase takes place on the same column in which the mRNA was retained. In column mRNA capture and first strand synthesis allow high sensitivity, avoid loss of precious material and speed up the process. Global PCR (a total of 40 cycles) through the use of one common primer that anneals on multiple sites of comparable length along the cDNA template permits sample amplification avoiding PCR bias due to different transcript length and due to different primer annealing conditions. The PCR product represents also a stable resource that can be used to repeat experiments.

All reactions are performed in a very small volume to gain sensitivity and the Klenow fragment assures a good rate of dye incorporation. The kit has been specifically developed to be compatible with FACS, immunomagnetic and microdissection sorted cells. The manufacturers guarantee good reproducibility of gene expression profiles for a number of cells between 100 and 1000, and detectability of differentially expressed genes down to the single cell.

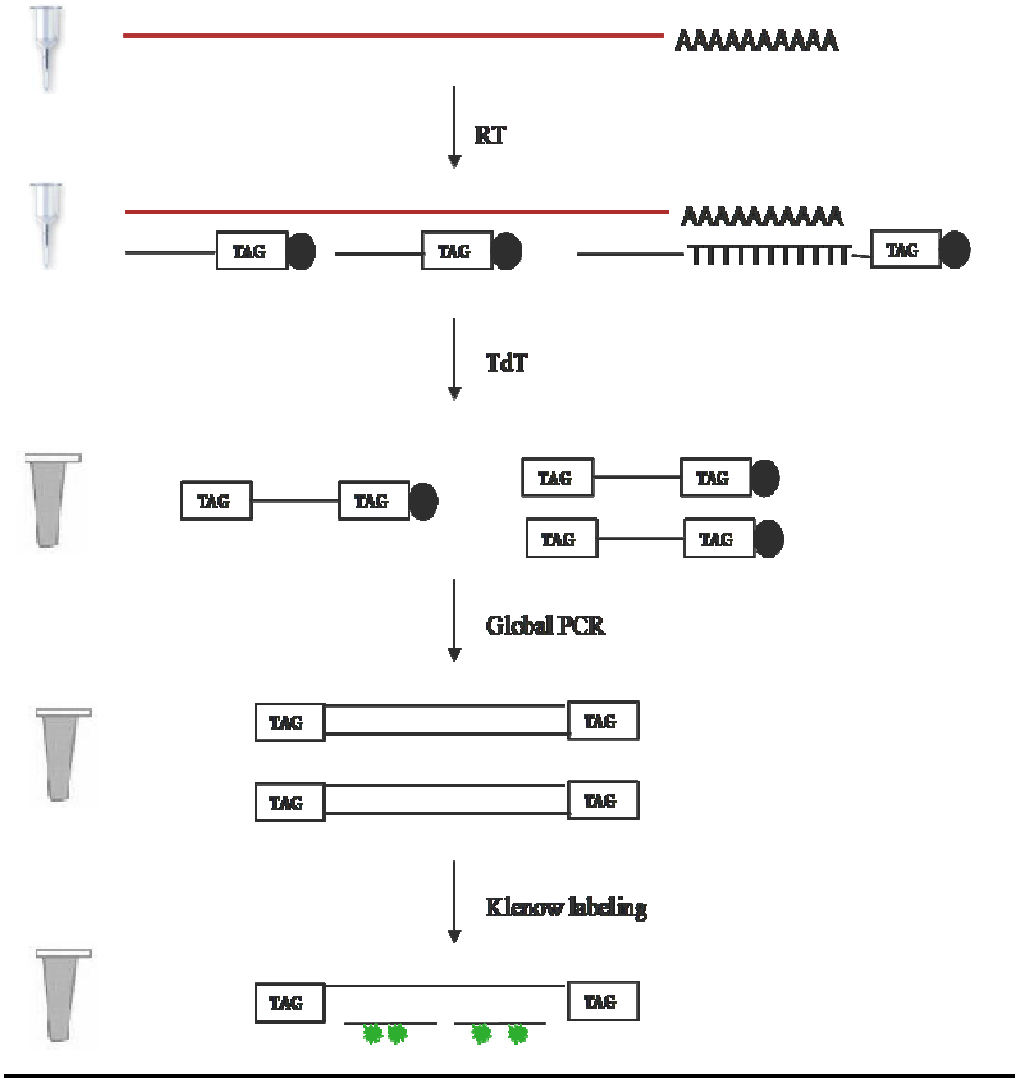

Figure 8. The sample is lyzed in the lysis buffer that contains Proteinase K and an RNA carrier and subsequently is incubated with magnetic beads that have an oligo(dT) - tag attached to them, before being added to a μMACS column applied to a magnet, which allows separation of all Poly(A)$^+$ RNA. cDNA syntesis and cDNA tailing are performed on the same column assuring high sensitivity of the reaction. The eluate is subsequently amplified with a PCR reaction through the use of one single primer that has been designed so as to that prime multiple cDNA sites of comparable length allowing good amplification of the sample without the PCR bias due to different transcript length and different priming annealing contitions. Last step involves labelling of the amplified dsDNA with Klenow fragment direct dye incorporation.

1.3 HIGH THROUGHPUT GENE EXPRESSION PROFILING

1.3.1 Overview

The introduction of automated large scale sequencing, supported by adequate computational and bioinformatic tools, has greatly increased our knowledge of the genomic sequences of humans and other organisms as well as that of the genes that they encode. This wealth of data has triggered the development of techniques, based both on hybridization and sequencing methods, that allow surveys of expression patterns for thousands of genes in a single assay. These techniques include the widely used serial analysis of gene expression (SAGE) (Velculescu et al., 1995), cDNA microarrays (Schena et al., 1995), oligonucleotide arrays (Lockhart et al., 1996), full length cDNA cloning. To those we can add tiling arrays, which permit identification of novel transcribed elements and internal structure of transcripts, cap-analysis of gene expression tag sequencing (CAGE) (Shiraki et al., 2003), which allows identification of transcription starting sites (TSS), and quantitative profiling of relative promoter usage across tissues and cell types (linking gene expression with controlling promoter elements) further increasing our understanding of the transcriptome architecture. Recently, we have developed nanoCAGE (submitted manuscript) which is a modified version of CAGE that allows identification of TSS from minute samples from fixed tissue. The current estimate of transcripts in the mammalian genome, based on analysis of cDNA clones and tags, is of at least 181,000 (Katayama et al., 2005), one order of magnitude larger than the previously estimated 22,000 protein mammalian coding genes. More than half of those transcripts are non-coding. As these latter technologies are out of the scope of this work, I shall focus on microarray technology and particularly on cDNA arrays.

1.3.2 Microarray technology

By reversing the Northern blot principle, the labeled moiety, referred to as the “target” and derived from the mRNA sample, is hybridized in parallel to a large number of DNA sequences known as “probes”, immobilized on a solid surface in an ordered array. These filter-based gene expression analysis have enabled simultaneous determination of expression levels of thousands of genes in one experiment. Furthermore, advancements made in attaching nucleic acids to a glass support through the development of slide surface chemistries and robotics able to miniaturize the size of the reactions have made possible the passage from nylon membranes to glass slides and the development of microarray technology as known today.

Amongst the many different microarray systems that have been developed, the ones of most common use can be divided into two groups, according to the arrayed material: complementary DNA (cDNA) and oligonucleotide microarrays. Probes for cDNA arrays are usually products of the polymerase chain reaction (PCR) generated from cDNA libraries or clone collections, using either vector-specific or gene-specific primers, and are printed onto glass slides or nylon membranes as spots at defined locations in a total area of few squared centimetres. Spots are typically less than 200 μm in size and are spaced about the same distance apart. The cDNA probes are immobilized onto the glass solid surface by one of the various deposition methods developed (contact or non-contact printing) and exposed to a set of targets derived from experimental or clinical samples either separately or in a mixture. This method, “traditionally” called DNA microarray, is commonly considered as developed at Standford University. This technique is widely used by research scientists around the world to produce "in-house" printed microarrays from their own labs. For oligonucleotide arrays, short 20-25mer (Affymetrix) or 60mer probes (Agilent) are synthesized *in situ*, either by photolithography onto silicon wafers (high density oligonucleotide arrays from Affymetrix (Wodicka et al., 1997) or by ink-jet technology (developed by Rosetta Inpharmatics and licensed to Agilent technologies). In oligonucleotide microarrays, the probes are short sequences designed to match parts of the

sequence of known or predicted open reading frames. Pre-synthesized oligonucleotide probes can also be printed onto glass slides like cDNA probes.

Methods based on synthetic oligonucleotides offer the advantage that probes can be designed to represent the most unique part of a given transcript, making the detection of closely related genes or splice variants possible. Spotted arrays, on the other hand, offer a greater degree of flexibility in the choice of arrayed elements. As the sequences for *de novo* synthesized arrays are stored electronically rather than physically in frozen DNA libraries, the costs and the potential for errors in amplification, storage, and retrieval are eliminated.

Here we have used home-spotted arrays based on the FANTOM 2 collection of mouse transcripts (Okazaki, Furuno et al., 2002; FANTOM International Consortium). Genes were represented in triplicate and the whole collection was printed on two slides.

1.3.3 Target preparation

Several methodologies are now routinely used for labelling targets and many of these systems are supplied as commercially available kits. *In situ* synthesized high-density oligonucleotide arrays (Affymetrix) and spotted arrays present differences also in target preparation. In both cases, mRNA from cells or tissues is extracted, converted to DNA and labelled, hybridized to the DNA elements on the array surface, and detected by phospho-imaging or fluorescent scanning. The high reproducibility of in situ synthesis of oligonucleotide chips, though, adopts the one-channel method as it allows accurate comparisons of signals generated by samples hybridized on different arrays. In the classic cDNA microarray experiment, targets are prepared from mRNA extracted from two different cell populations or tissues, one labelled using cyanine 3 (Cy3) and the other using cyanine 5 (Cy5). The two labelled samples are then pooled and hybridized together on the same array, which results in competitive binding of the target to the arrayed sequences. After hybridization and washing, the slide is scanned using two different wavelengths, corresponding to the dyes used, and the intensity of the same spot in both channels is compared. This results in the

measurement of the ratio of transcripts level for each gene represented on the array. It is worth to mention at this point that cDNA arrays only allow the detection of relative abundance of target samples, but not their absolute quantities. In fact, incorporation of labelled nucleotides depends on the length of the DNA sequence, which means that a bright fluorescent spot does not necessarily imply a high expression of a gene. It may just be an indication of a low expression, but structurally long transcript.

1.3.4 Design and analysis of microarray cDNA experiments

The development of computational and statistical tools to analyze the amount of data produced by microarray experiments constitute a great challenge, especially when we consider that, typically, microarray studies implicate the integration of data from multiple experiments. For this reason, a brief description of experimental design issues and of computational analysis of cDNA microarrays is introduced in the next few paragraphs.

1.3.4.a Direct versus indirect comparisons

The key issue in designing a cDNA microarray experiment is to decide whether to use direct or indirect comparisons, or, in other words, whether to make the comparisons within or in between slides. The efficiency of comparisons between two samples is determined by the length and number of paths connecting them (Kerr et al., 2001; Yang et al., 2002). The most efficient approach is to make the comparisons of greatest interest directly on the same array. Let us suppose we want to carry out two hybridazations: a direct comparison is carried out when sample A, labeled with Cy5 and sample B, labeled with Cy3, are hybridized together (A-B) on both slides. For any gene, two independent estimates of the log ratio (A/B) would be obtained. If the variance for one such measurement is σ^2, then the variance of the average of the two independent measurements is $\sigma^2/2$. If we do an indirect comparison and make use of a common reference R, then the two hybridizations would be A-R, and B-R. In this case, the log ratio log (A/B),

for any gene is the difference of two independent log ratios from the equation log (A/B)=log (A/R) – log (B/R). As above, if the variance of a single log ratio is σ^2 , it follows that that the variance of the difference of the two independent log ratios is $2\sigma^2$. In summary, with two hybridizations, we obtain a measure of the log-ratio of a gene with variance $\sigma^2/2$ by doing two direct hybridizations, and the log-ratio of a gene with variance $2\sigma^2$ by doing two indirect comparisons (Yang et al., 2002). Direct comparisons give more immediate and less variable results with respect to indirect comparisons. For this reason we have chosen to perform direct comparisons in this work.

.

1.3.4.b Dye swap experiments

If samples are compared directly, then it is good practice to introduce a correction for eventual dye imbalances. Since the efficiency of incorporation of nucleotides labeled with different fluorescent dyes during target-sample preparation may not be equal, reciprocal labeling with swapped colors is recommended with direct cDNA experiments. This means that two arrays are used to compare two samples. On one array, sample A is assigned to the red dye, and sample B is assigned to the green dye. On the other array, the dye assignments are reversed. This arrangement can be repeated by using four or six or more arrays to compare the same two biological samples. This repeated dye-swap experiment reduces technical variation due to labeling imbalances.

1.3.4.c Reference sample

When using a common reference to compare more samples, dye orientation used is always the same. As a result dye effects are confounded with inherent biological difference of the samples (Kerr et al., 2001; Yang et al., 2002). The choice of the reference sample, in this case, becomes the most important issue. It should present (can be either constructed or bought) particular characteristics such as homogeneity, stability over time, and finally it should “light up” most spots on the array. The reference sample should also be as close to

the experimental samples as possible. Typically, a pooled reference is formed from the samples that will be assayed in the experiment. This ensures that every transcript present in the test samples will be represented in the reference sample and that the relative amounts of each RNA species will be similar. Samples that have similar concentrations are easier to compare and handle during data analysis (Quackenbush et al., 2001). A commercial RNA reference will not have these advantages and it will not represent all genes of the test samples, but it can be useful for continuous projects and data collections.

Choice between these two design modes depends on the aim of the experiment. For instance, if we would decide to compare several healthy tissue samples with many disease samples, then a good experimental design would be to compare each disease sample with a common reference constructed by pooling all healthy tissue samples. On the other hand, if we would like to compare healthy tissue versus disease tissue samples obtained from the same patient then direct comparison would be the best option. Very often a combination of direct and indirect comparisons is the best practical solution to a design problem.

1.3.4.d Variability and replication

One way to monitor and improve the overall quality of the outcome of a microarray experiment is by putting replicates of the same spot (cDNA probe) on each slide (Black et al., 2002). This increases precision (Lee et al., 2000) of the measurements if the spot intensities are averaged. It can also minimize problems due to scratches or dust present on the microarray surface. It is advisable, however, to have repeated spots well spaced over the microarray surface and not adjacent, as this would give a better reflection of the variability across the slide. Often, internal control spots, such as missing spots, spiked spots, and housekeeping genes, are used to produce good data quality.

The form of replication described in the previous paragraph allows quality control of the data to some extent, but because nearly all aspects of the experiment (printing, general hybridization, and scanning conditions) will be shared by spot replicates, these will lack the independence that greatly reduces their value for

broader statistical inference. Different hybridizations of identically prepared material, or, even better, of differently prepared material, have been shown to increase precision of measurements and to give more reliable results. In fact, replicate hybridizations reduce variability in summary statistics and data obtained from replicate slides can be analyzed by using formal statistical methods. In essence, replication allows averaging, and averages are less variable than their component terms. For this reason, replication allows extrapolation of results from the investigated sample to the whole population from which the sample originates. There are two types of replicates that can be performed to render more robust microarray data analysis, technical and biological replicates.

a) Technical replicates

Technical replicates between slides refer to replication in which the target mRNA comes from the same pool, that is from the same extraction. This means that these replicates generally involve a smaller degree of variation in measurements than the biological replicates. Technical replicates serve the scope of reducing the variability between slides.

b) Biological replicates

Biological replicates usually refer to hybridizations that involve mRNA from different extractions – for example, from different samples of a particular cell line or tissue. This approach leads us close to the use of independent variables. The term can also refer to target mRNA that comes from different individuals or versions of a cell line. This approach may bring with it some noise, such as hormonal and immune systems of individuals being in different states or tissues being in different states of inflammation. This variation may make harder to discern the real expression differences between the samples. For experiments that have the aim of generalizing their conclusions to an entire inbred strain of mice for example, this is the appropriate form of replication. Biological replicates serve the purpose of obtaining averages of independent data, hence strengthening statistical analysis. This allows a generalization of conclusions.

Choice of type and number of replicates for a particular experiment needs careful consideration. Here, we have used a direct experimental design, with three

biological replicates. For every biological replicate 3 technical replicates were prepared and for each one of those a dye swap, for a total of 18 hybridizations.

1.3.4.e Data Analysis

After hybridization, microarray slides are scanned with two different wavelengths, corresponding to the dyes used, and the relative fluorescent intensity of spots in both channels is measured. These fluorescent intensities need to be subjected to normalization, which adjusts for differences in labelling and detection efficiencies of the fluorescent labels and for differences in the quantity of initial RNA from the two samples examined in the assay, so as to avoid shifts in the average ratio of Cy3 to Cy5. The most widely used normalization algorithms assume that all genes in the array have an average expression ratio equal to one. A normalization factor is then calculated and used to rescale the intensities before the experiment is analyzed (for review, see Quackenbush, 2001). Normalized data for each gene are typically reported as an 'expression ratio' or as the logarithm of the expression ratio. The expression ratio is simply the normalized value of the expression level of a particular gene in the query sample divided by the normalized value of the control. At this point, a list of differentially expressed genes can be produced. Often a two fold increase or decrease in measured level is used to define differential expression, although there is no firm theoretical basis for selecting this level as significant.

The true power of microarrays though lies in the mining of data aimed at identifying common patterns of gene expression. We can assume that genes that are contained in particular pathways, or that respond to a common exogenous challenge, are co-regulated, and consequently, should show similar patterns of expression. Statistical methods, generally referred to as 'cluster analysis', have been devised to identify genes that show similar patterns of expression. Amongst those the most popular tools are hierarchical clustering (Eisen et al., 1998) and self-organising map (SOM) clustering (Tamayo et al., 1999).

In hierarchical clustering, the distances between genes are calculated for all the genes based on their expression pattern and the closer genes are merged to

produce a cluster. The distances between these small clusters are calculated to produce a new cluster. Self-organizing map (SOM) clustering assigns genes to a series of groups on the basis of expression pattern similarities. Random vectors are constructed for each group and a gene is assigned to the closest vector (for review, see Quackenbush, 2001).

1.3.4.f Considerations on brain gene expression profiling studies

Many investigators have reported that manipulation of animals may often result in dramatic changes in gene expression in the brain (Soverchia et al., 2005). For example, studies analyzing early onset gene expression (c-Fos, c-Jun) have revealed that changes in their transcript levels may occur within a few minutes of animal handling (Herdegen and Leah, 1998). Exposure to stressful events such as the laboratory environment, presentation of odors like, for example, blood from other animals can result in gene expression changes (Herdegen and Leah, 1998). Moreover, since expression of many genes is heavily influenced by 'biological clock' genes, which in turn depend on the dark-light cycle, the time of day in which the experiments are conducted should also be kept into serious consideration (Soverchia et al., 2005). Animals should be followed by the same people and the killing procedure should be reproducible for what regards the environment, the method and the time of day.

1.3.5 Applications of LCM paired with microarray technology on brain tissue samples

Integration of LCM technology with microarray platforms has been intensively used in cancer studies for identification of tumor markers, but also to produce tumor expression profile signatures that can distinguish between clinical subtypes, leading to refined diagnosis and treatment with tailored therapies. This approach holds also promise for the understanding of the underlying molecular biology of cancer disease. The positive results obtained in this field have pushed investigators to use this technology in studies on neurodegenerative diseases,

neural classification and brain circuitry identification, where brain tissue heterogeneity calls for cell sampling. A combination of LCM with microarray analysis has been applied to define specific subclasses of neurons by Luo et al., 1999, who analyzed differential gene expression between large and small LCM-captured neurons from dorsal root ganglia. Since then the application of this approach to define gene expression of specific neuronal types either for their characterization or their implication in neurodegenerative diseases has increased. Bi et al., 2002, have profiled NMDA receptor subunits using real time PCR in NOS (Nitric Oxide Synthase)-immunopositive neurons dissected from flash frozen brain sections. Bonaventure et al., 2002, used LCM to collect 100 Nissl-stained cells from seven different brain nuclei. Amplified RNA was then applied to a custom cDNA microarray platform and the transcriptomes of the different nuclei were compared. For each nucleus, expression of one or two known signatures genes was enriched. Further validation of their results contemplated qRT-PCR and in situ hybridization. In fact, the expression levels of four randomly selected genes validated by qRT-PCR seemed to confirm microarray results.

Other studies have used LCM and gene profiling to analyze gene expression in Nissl-stained single cells with promising results (Kamme et al., 2003; Tietjen et al., 2003). In particular, Kamme showed the diversity of expression profiles that characterizes cells of the CA1 region of the hippocampus, which, up to that moment, were considered as a broad neuronal subclass.

A number of studies have concentrated on the dopaminergic neurons because of their clinical relevance in neurodegenerative disorders such as Parkinson's disease, schizophrenia and addiction, but also for the ease with which these cells can be identified in brain though quick labeling by antibodies against tyrosine hydroxylase (TH), the rate limiting enzyme in the synthesis of dopamine. Chung et al., 2005 and Green et al., 2005 compared dopaminergic cells from neighboring midbrain regions, the ventral tegmental area (VTA) and the substantia nigra (SN), to identify genes that might contribute to the higher susceptibility of the latter population to neurodegeneration in Parkinson's disease. Both studies identified numerous genes that had statistically significant differential expression. Yao et al., 2005 compared VTA dopaminergic neurons

with corticostriatal pyramidal cells retrogradely labeled by striatal injection of fluorogold. Several genes were identified as differentially expressed by the microarray analysis but only some of them were actually confirmed to show expression differences when analyzed with qRT-PCR. Results from the microarray showed the occurrence of some contamination with oligodendrocytes and thus the importance of independent validation of results when using this methodology.

Grimm et al., 2004 have presented the global gene expression profiles that define the four major classes of dopaminergic (DA) and noradrenergic (NA) neurons in the brain. Hypothalamic DA neurons and noradrenergic neurons in the locus coeruleus (LC) were found to display distinct group-specific signatures of transporters, channels, transcription, plasticity, axon guidance, and survival factors. In contrast, the transcriptomes of midbrain DA neurons of the substantia nigra and the ventral tegmental area presented closely related with less than 1% of differentially expressed genes. Transcripts implicated in neural plasticity and survival were enriched in ventral tegmental area neurons consistent with their role in schizophrenia and addiction and their decreased vulnerability in Parkinson's disease.

All the aforementioned studies demonstrate that LCM in combination with microarray technology achieve sufficient cell type purity and RNA integrity. The importance of validating microarray results by independent methods such as qRT-PCR or in situ hybridization also becomes evident.

In this work, we also address the issue of defining the mesencephalic dopaminergic identities of the SNc and the VTA populations by producing and analyzing their gene expression profiles.

1.4 THE DOPAMINERGIC SYSTEM

1.4.1 Overview

Some of the most interesting and most intensively studied neuronal systems in the CNS are those comprising the catecholamine-neuronal systems

and, in particular, the dopaminergic cells. This is due to their involvement in several mental and neurological disorders and to the ease with which we can visualize and map anatomically their circuit components, the DA cells. In fact, the dopamine (DA), noradrenaline (NA) and serotonin (5-HT) systems in the brain were the first transmitter systems to be mapped with accuracy (Dahlström and Fuxe, 1964). In the early 1960s, the newly introduced formaldehyde histofluorescence method (Falck et al., 1962), based on the visualization of fluorescent monoamines following formaldehyde treatment, allowed Carlsson, Falck, and Hillarp (Carlsson et al., 1962) to identify the two primary CAs, noradrenaline (NA) and dopamine (DA), in discrete neural systems in the brain. Two years later, in 1964, Dahlström and Fuxe published a detailed account of the distribution of CA and serotonin-containing neurons in the rat brain, with a description of twelve groups of CA cells (appointed letter A and a number, A1-A12) distributed from the medulla oblongata to the hypothalamus. Subsequent advances in histochemical techniques led to the detection of groups A13-A17 located in the diencephalon, olfactory bulb and retina, and to the three adrenaline-containing cell groups, C1-C3 (Hökfelt T. et al., 1984, from *Handbook of Chemical Neuronatomy*, Vol 2). The nomenclature underlying this basic organization is still accepted today.

1.4.2 Origin and development

The growth of midbrain neurons follows a specific, genetically regulated, developmental program initiated early during brain formation, as happens for most neuronal types. Mesencephalic dopamine-containing cells arise from a single embryological cell group that originates in the floor plate and base plate (adjacent to the floor plate on both sides of the neural tube) at the ventral midline, around the cephalic flexure, at around E10.5 in mouse. Secreted signaling proteins, sonic hedgehog (SHH) and fibroblast growth factor 8 (FGF8), derived from the ventral midline cells and the isthmic organizer (Hynes and Rosenthal, 1999) at the mid/hindbrain border respectively, specify the identity of early proliferating dopaminergic progenitors. In fact, the combination of SHH and FGF8 are

necessary and sufficient for the generation of ectopic mDA neurons in embryonic explant cultures derived from the rat brain (Ye et al., 1998).

When these dopaminergic progenitors become postmitotic, they start to express TH and migrate along radial glia towards their final location (Di Porzio et al., 1990). Cells immunoreactive for TH are distributed throughout the entire length of the ventral mesencephalic wall at E12, and by E14 TH cells are located laterally, along the ventral pial surface, to form the primordia of the substantia nigra (Kawano et al., 1995). When the SN neurons have reached their position in the midbrain, they form axons that project towards the Lateral Ganglionic Eminence (LGE), which develops into mature striatum. It takes weeks for the dopamine innervation to be completed.

Early DA progenitors express the LIM homedomain proteins Lmx1a and Lmx1b, but the two proteins seem to have distinct roles in the development of these cells. Lmx1a has been recently shown to be selectively expressed in midbrain progenitor cells in ventral midbrain and to be involved in the process of DA cell-fate specification (Andersson et al., 2006). It is maintained in postmitotic DA neurons and functions as a specific activator of downstream genes, including the transcription factor Nurr1. In contrast to Lmx1a, Lmx1b is not specifically expressed in DA progenitor cells, it is not maintained over the period of DA generation and it seems likely to have a more profound role in differentiating post-mitotic DA neurons (i.e. it is necessary for Ptx3 expression – Smidt et al., 2000; Andersson et al., 2006 –). Important TFs for subsequent differentiation and maintenance of DA cells include Nurr1, critical for the transcriptional activation of genes required for dopamine biosynthesis and neurotransmitter expression (Zetterstrom et al., 1997), the transcription factors En1/En2 which are essential for the generation and survival of mDA neurons (Simon H. et al., 2001, Thurret et al., 2004, Sgado P., et al., 2006), and the *bicoid*-related homeodomain containing transcription factor Pitx3. Pitx3 is expressed exclusively in mesencephalic dopaminergic neurons and is involved in their development and maintenance (Smidt et al., 1997; Nunes et al., 2003). It promotes, in co-operation with Nurr1, the terminal maturation of mammalian embryonic stem cells into mDA neurons with the expression of the full repertoire of DA markers (i.e. coexpression of TH,

Nurr1, Lmx1a, Lmx1b, En1/En2, and DAT) (Martinat et al., 2006) (for reviews, see Sillitoe and Vogel, 2008 and Marten P. et al., 2007).

Coupling information from signaling molecules, morphogens and transcription factors in control of DA cell differentiation with the molecular codes identifying the different cell subpopulations present among adult mDA neurons could lead to the development of new drugs to treat mDA neuron-associated neurological disorders such as schizophrenia or depression and enable new strategies in the field of stem cell engineering. Dopaminergic neurons of the desired specificity could, for example, be induced from stem cells *in vitro* to be utilized in cell replacement therapies in Parkinson's disease patients.

1.4.3 Mesencephalic dopaminergic neurons and their projections

The largest assembly of DA neurons is found in the ventral midbrain (VM). A distinction is usually made between nigral (A9) and non-nigral (A8 and A10) DA neurons, although there is no clear definable boundary between them and these groups can be seen as a continous cell system (Björklund and Lindvall, 1984, from *Handbook of Chemical Neuroanatomy*). Nigral neurons are confined to the *pars compacta and pars lateralis of the substantia nigra*. Few A9 cells are scattered ventrally in the *pars reticulata*. The A10 cell group is largely confined to the *ventral tegmental area* (VTA) and is positioned medially to the substantia nigra proper. The DA neurons of the A8 cell group located in the *retrorubral field* (RR), caudally to the substantia nigra proper, can be considered as a caudal extension of the A9 cell group as they too project to the striatum (Nauta et al., 1978). The designation of subpopulations of dopamine neurons according to their topographic location conforms to some extent to their projection targets (Bjorklund and Lindvall, 1984). VTA A10 cells give rise to the mesolimbic and mesocortical pathways that innervate the nucleus accumbens, olfactory tubercle, septum, amygdala and the prefrontal, cingulate and perirhinal cortex, respectively. The overlap between the VTA neurons that project to these various targets is considerable and for this reason the two systems are often collectively referred to as the mesocorticolimbic system (Wise et al., 2004). The dopaminergic cells of

the A10 group are implicated in the control of emotional balance, reward-associated and addictive behaviour, attention and memory. The A9 cells in the SNc give rise to the nigrostriatal pathway which innervates the caudate-putamen (dorsal striatum) and plays an essential role in the control of postural reflexes and initiation of voluntary movement. SNl dopaminergic cells project to the striatum and amygdala (Moriizumi et al., 1992). Finally, the A8 dopamine neurons that reside in the RR project primarily to the dorsal striatum and the pontomedullary reticular formation and are thought to influence orofacial movements (Figure 8).

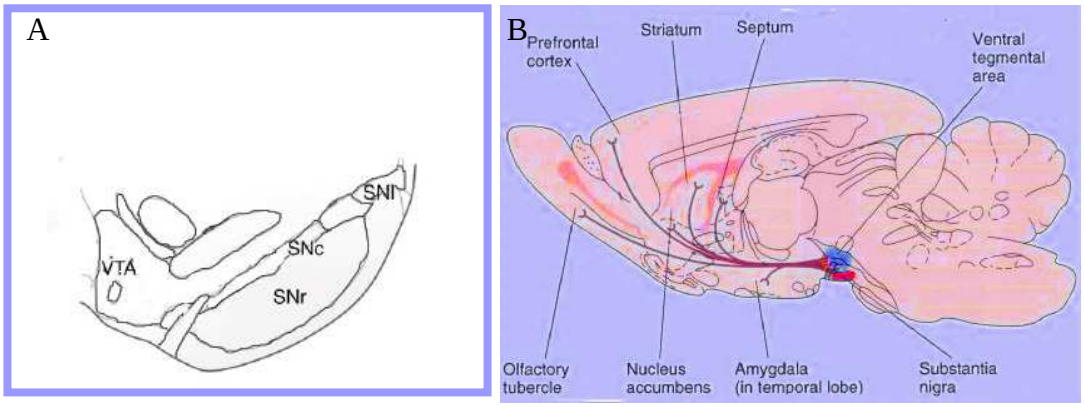

Figure 8. A) Schematic diagram of a coronal view of the topographic location of SN and VTA. B) Drawing showing the principal projections of DA cells groups.

In rodents, the total number of TH-positive cells in all three cell groups bilaterally is ~ 20,000 - 30,000 in mice and 40,000 - 45,000 in rats with about half of the cells located in SN (German and Manaye 1993; Nelson et al., 1996). The totality of mDA cells does hardly reach the figure of 1% of total midbrain. A striking increase of DA neurons occurs in primates with 165,000 mDA cells in the macaca monkey and up to 450,000 cells in the young human (German and Manaye, 1993). This increase is due to an expansion of the DA innervation territory, particularly in the neocortex, in primates and human. In rodents, the cortical innervation is largely confined to areas of the frontal, cingulate and entorhinal cortex, whereas, in primates, DA innervation spreads over the entire cortical mantle (Lewis et al., 1998). This cortical innervation derives from the dorsal regions of all parts of the mesencephalic neural complex, that is A8, A9, and A10 cells (Williams et al., 1998).

Differences in the morphology of neuronal dendrites, the expression of the calcium-binding protein calbindin, and the projections to either the patch or the matrix striatal compartments (Gerfen et al., 1987 a and b) of mDA cells have led researchers to an alternative topographical classification of these neurons into a dorsal and a ventral tier. The dorsal tier comprises cells located in the dorsal VTA and SN and cells from the RR and innervates the ventral striatal, limbic and cortical areas and the matrix of the dorsal striatum. These cells extend their dendrites in the *pars compacta*, they are calbindin-positive, and express low levels of the DAT transporter (Prensa et al., 2001; Gerfen et al., from Paxinos 2004). The ventral tier cells, located in the ventral SN and VTA, extend their dendrites ventrally, in the *pars reticulata*, appear more densely packed, are negative for calbindin immunoreactivity, express higher levels of DAT, and are generally immunopositive for the ion channel protein GIRK2. These cells project to the striatal patch compartment (Prensa et al., 2001; Gerfen et al., from Paxinos 2004).

It has become evident with time that the mDA neurons are not a simple system but they are organized in a complex circuit that comprises subpopulations of neurons exhibiting differences in their morphology, but also in several molecular markers and patterns of forebrain projections. Although the projections of the three DA pathways (nigrostriatal, mesolimbic and mesocortical) are both anatomically and functionally distinct and confined to their projection targets with a very limited degree of collateralization, their cells of origin are more intermixed than originally thought. In fact, the striatal DA innervation derives from the SNc (both the dorsal and ventral tiers) but also from the lateral VTA and the RR. More specifically, SN cells project to the sensorimotor striatum through the "nigrostriatal" pathway, in the strict sense of the term. Lateral VTA (A10) and RR (A8) project to the limbic part of the striatum, which includes the nucleus accumbens rostrally and the central nucleus of the amygdala and adjacent parts of the caudal striatum. It follows that the term mesostriatal DA pathway may be more appropriate to describe all components of the midrain DA system projecting to the striatum. Therefore, often the three DA projections arising from mDA are described with the terms mesostriatal and mesocorticolimbic pathways.

The dual functional and chemical organization that saw dopaminergic neurons lying in SNc, VTA, RR and GABAergic neurons being localized mainly in the SN *pars reticulata*, forming one of the most important output pathways of the basal ganglia projecting to the thalamus, colliculi and tegmentum (Di Chiara et al., 1979; Redgrave et al., 1992), has been challenged by the finding of a non-dopaminergic nigrostriatal pathway. In fact, the different projections of the mesostriatal and mesocorticolimbic systems comprise dopaminergic and non-dopaminergic neurons for which γ-aminobutyric acid has been identified as the neurotransmitter (Maler et al., 1973; van der Kooy et al., 1981; Swanson et al., 1982; Gerfen et al., 1987; Hattori et al., 1991). In contrast to the VTA, where dopaminergic and non-dopaminergic cells projecting to a certain terminal area seem to be essentially intermixed (Björklund and Lindvall, 1984, from *Handbook of Chemical Neuroanatomy*), in the SNl, the non-DA containing neurons, which project to the inferior colliculus (IC), are confined to its dorsoventral part (Moriizumi et al., 1992). Surprisingly, the use of immunohistochemistry has reported the existence of a small subpopulation of SNl neurons projecting to the Superior Colliculus (SC) that co-express tyrosine hydroxylase and glutamic acid decarboxylase (GAD) (Campbell et al., 1991). Co-expression has also been reported in a 10% of mesostriatal neurons mostly lying in the medial region of the SNc and neighbouring A10 region (Gonzàlez-Hernàndez et al., 2001). These findings reveal the existence of a third nigrostriatal pathway formed by dopaminergic/gabaergic neurons. Interestingly, other DA groups in the basal hypothalamus, the olfactory bulb, and the retina, have been found to co-express DA and γ-aminobutyric acid, and might thus operate with more than one transmitter (Bjorklund and Dunnet, 2007; Hirasawa et al., 2009).

1.4.4 DA projections to downstream striatal targets

The external and internal segments of the globus pallidus (entopeduncular nucleus in rodents), parts of the ventral pallidum and the subthalamic nucleus (Hassani et al., 1997; Lindvall and Björklund, 1979) receive innervation from mDA neurons.

Moreover, in the SN itself, DA is known to be released from a plexus of long slender dendrites that run ventrally from the ventral tier of the SNc, to ramify in the SNr (Björklund and Lindvall, 1984). In this context, the DA neurons can regulate the activity not only of the DA neurons themselves, but also modulate the release of GABA from striatonigral afferent fibers and perhaps also from GABAergic interneurons within the SNr and part of its efferent neurons (Björklund and Lindvall, 1984). In other words, midbrain dopamine neurons can exert their action not only at the level of the caudate nucleus and putamen, but can also modulate the activity of basal ganglia output neurons at the pallidal, subthalamic and nigral levels.

1.4.5 Electrophysiological properties of DA neurons

Functional analysis of midbrain DA neurons started in the early eighties and have led to important findings regarding their firing patterns and the channels involved in their production. A brief description follows.

In their landmark studies, Grace and Bunney showed that DA midbrain neurons *in vivo* discharge in two distinct modes of electrical activity in the anesthetized rodent brain: either in a slow irregular single-spike pattern with a very narrow frequency band (between 1 and 8 Hz) characterized by a broad action potential followed by a pronounced hyperpolarization (Grace and Bunney, 1984b) or alternatively in short bursts of action potentials at higher frequencies (Grace and Bunney, 1984a) (see Figure 9).

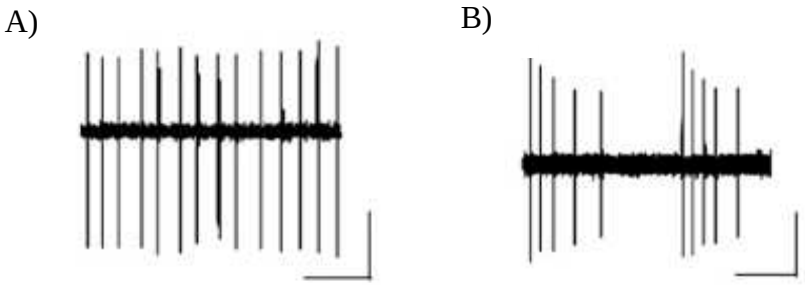

Figure 9. Examples of activity patterns of two individual dopaminergic midbrain neurons from adult mouse: A) *in vivo* (extracellular recording, sampling rate 12.5 kHz) pacemaker activity, B) *in vivo* burst activity. Scale bars: 1s, 0.5mV. (Modified from Liss et al., 2008).

This spontaneous pacemaker activity seems to rely on a different ionic mechanism than most other cells in the CNS. In fact, it has been reported that blocking of the hyperpolarization cation current I_h (mediated by hyperpolarization-activated cyclic-nucleotide cation – HCN – channels) has no effect on pacemaking in most midbrain dopamine neurons (Mercuri et al., 1995), except for a subpopulation of SN neurons, where pacemaking is slowed but not stopped (Neuhoff et al., 2002), whereas replacement of calcium by cadmium or cobalt completely silences pacemaking (Fujimura and Matsuda 1989; Grace and Onn, 1989; Harris et al., 1989). This pacemaker activity has been shown to depend principally on the subthreshold membrane potential oscillations created by voltage-gated L-type channels (Puoppolo et al., 2007). In SN neurons, Cav1.3 channels (which are activated at more negative potentials compared to other L-type calcium channels, also expressed in SNC) carry the bulk of calcium inward currents during the interspike interval, although multiple calcium channel types have been suggested to contribute to pacemaking of midbrain DA neurons (Puoppolo et al., 2007). A significant contribution to the same function has been reported to be given by subthreshold TTX (tetrodotoxin)-sensitive sodium current (Puoppolo et al., 2007). This calcium component is far more dominant in SN DA neurons compared to those of other pacemaker neurons in brain (i.e. Purkinje neurons, suprachiasmatic nucleus neurons), which mainly rely on interspike sodium influx by TTX-sensitive sodium channels or HCN channels (Bean, 2007).

However, HCN channels, comprising slow gating HCN2, HCN3, and HCN4 channel variants (Franz et al., 2000), show large differences in density among different DA subpopulations (Neuhoff, 2002) and in part contribute to the subthreshold membrane potential oscillations. It has been shown that only a subpopulation of DA neurons within the SN actively uses HCN channels for pacemaker frequency control (Neuhoff et al., 2002), while there exists a population of DA cells in the medial posterior VTA that possesses almost no functional HCN channels. Although these channels have been extensively used to identify DA subpopulations, their variability in expression among DA cells and in response to homeostatic mechanisms does not make them good candidates for DA neuron identification.

In SN neurons, this interspike depolarization towards threshold, driven by calcium, sodium and HCN channels is opposed by fast inactivating A-type potassium channels, which are composed by the pore-forming alpha subunits Kv4.3L (long splice variant) and the auxiliary beta-subunits Kchip3.1 (Liss et al., 2001).

The switch from pace-making activity to bursting has not generally been observed to occur spontaneously in midbrain DA neurons in reduced *in vitro* preparations (Grace et al., 2007) indicating a possible dependence of the burst-firing mode of DA neurons on the interplay of patterned synaptic input and intrinscic conductances. Moreover, spontaneous burst discharges in midbrain DA neurons have been reported to be completely silenced by apamine-sensitive small-conductance calcium-activated potassium (SK) channels (Ji and Shepperd 2006) implicating the latter in stabilization of distinct thresholds for burst-firing in the presence of variable synaptic inputs (Liss and Roeper, 2008). It is very interesting that the same neurons in the medial VTA that almost lack HCN conductances also show the smallest SK channel-mediated after-hyperpolarizations (Liss and Roeper, 2008).

Recently, Lammel et al., 2008, have suggested that the dopamine midbrain system consists of two distinct types of DA midbrain neurons with very different functional properties. In addition to the well-studied conventional dopaminergic midbrain dopamine neurons described in the above paragraphs, they have described an atypical fast-firing subtype of dopaminergic neurons. These mesocorticolimbic DA neurons project selectively to medial prefrontal cortex, basolateral amygdala, and the core of the medial shell of the nucleus accumbens and are able to fire action potentials at significant higher frequencies in a sustained fashion compared to the “conventional” DA neurons (<10 Hz). Among these DA fast-firing neurons, those projecting to the prefrontal cortex are unique in that they neither possess functional D2 dopamine receptors nor their downstream targets, the GIRK2 channels. This mode of discharge at higher frequencies has been suggested to contribute to the more sustained DA release pattern recognized *in vivo* in the amygdala and the prefrontal cortex (Garris and Wightman, 1994), which could also be assisted by the absence of D2 mediated

inhibition. Interestingly, these mesocortical DA neurons can be identified by their low D2 and GIRK2 expression levels combined with their low DAT/TH and DAT/VMAT2 mRNA ratios (Lammel et al., 2008) in addition to their expected low abundances for SK3 (Wolfart et al., 2001) and HCN (Neuhoff et al., 2002). The DAT/TH and DAT/VMAT2 ratios indicate a lower re-uptake capacity relative to TH-mediated synthesis and VMAT2-mediated vesicular packaging of dopamine, which corroborates well with a slower decay of extracellular dopamine concentrations in cortical areas compared to dorsal striatum (Yavich et al., 2007). This is an illustration of how combination of functional and molecular data can lead to shaping functional identity of neurons, in this case for instance in mediating sustained forms of behaviorally relevant release of DA in several brain regions *in vivo*, involving this VTA subpopulation for example in working memory (Seamans and Yang, 2004).

Up to date, two channel-based mechanisms have been advanced to explain the different vulnerability that DA neurons show to degeneration in Parkinson's disease or in animal toxic models. Liss et al., 2005, report that electrical activity of less vulnerable VTA neurons is not affected by toxin concentrations in contrast to the electrical activity of more vulnerable SN neurons where the effects are dramatic. They show that, in response to PD toxins, there is selective activation of ATP-sensitive potassium (K-ATP) channels in DA neurons (build by Kir6.2 and SUR1 subunits), which hyperpolarize the membrane potential and completely prevent action potential generation, *in vitro*, in adult mice. Furthermore, studies in K-ATP channel knockout (KO) mice and wild type (WT) mice, under chronic MPTP treatment demonstrate that high vulnerable SN neurons are selectively rescued in K-ATP KO mice, while the mild loss in VTA neurons is not affected (Liss et al., 2005). A second, channel-based, proposed mechanism for differential vulnerability of SN neurons is proposed by Chan et al., 2007 with their Cav1.3 KO mouse. Based on the finding that SN DA neurons continue to generate spontaneous pacemaker activity in these mice, due to a switch from calcium to sodium-based pacemaking, they demonstrate that a corresponding drug-induced pacemaker-switching of SN DA neurons by selective blockade of L-type calcium

channels, significantly reduces their vulnerability in a model of chronic MPTP treatment (Chan et al., 2007).

Puopollo et al., 2007, propose that the massive entry of calcium during both the slow spontaneous depolarization and also during the spike, involved in pacemaking activity of DA neurons, and the mechanisms to clear such a calcium load could be involved in differential vulnerability of DA neurons. In support to this hypothesis, VTA DA neurons that depend less on calcium entry for their pacemaker drive than SN neurons, as discussed previously, are less vulnerable to neurodegeneration. Moreover, different synaptic inputs may also contribute to different vulnerability of DA neurons. For example glutamatergic input loads the cells with calcium; neurons presenting with higher density of HCN channels directly involved in pacemaker frequency control, are likely to be more sensitive to neuromodulatory input by for instance serotonin (Kitai et al., 1999) due to their modulation by cyclic nucleotide levels in neurons. Finally, it has been proposed by Neuhoff et al. 2002, that differences in I_h channel density in DA neurons may be important for the integration of GABAergic signaling which represents more than 70% of synaptic input to midbrain DA neurons. DA autocrine control of spontaneous firing by GABA release, as it was recently hypothesized for retinal dopaminergic neurons (Hirasawa et al., 2009) could be yet another mode of action contributing to pacemaker control.

1.4.6 DA and associated pathologies

1.4.6.a Overview

Consistent with their varied functions DA neurons are associated with multiple neurodegenerative and psychiatric disorders. Selective degeneration of DA neurons in the SN, but not in the VTA, leads to Parkinson's Disease (Hirsch et al., 1988; Purba et al., 1994; Varastet et al., 1994), whereas abnormal function of VTA DA neurons has been linked to schizophrenia, drug addiction and attention-deficit-hyperactivity disorder (ADHD) (Bonci et al., 2003; Viggiano et al., 2003; Meyer-Lindenberg et al., 2002; Nestler et al., 2006). Other conditions

that affect the *pars compacta* with a pattern of cell loss similar to PD include striatonigral degeneration (or multiple systems atrophy), progressive supranucear palsy and corticobasoganglionic degeneration (Rehman et al., 2000).

1.4.6.b Parkinson's disease

The major neurodegenerative disorder associated with dopaminergic loss is PD. PD was first described by James Parkinson in 1817 as a neurological disorder associated with specific neuropathological lesions. It is the second most common progressive neurodegenerative disorder, affecting 1-2% of all individuals above the age of 65. The main pathological hallmark of PD is progressive loss of neuromelanin-containing dopaminergic neurons in the SNc of the ventral midbrain and the presence of eosinophilic intraneuronal inclusions, called Lewy bodies (LBs), composed of specific cytoplasmic proteins like alpha-synuclein, parkin, synphilin, ubiquitin, and oxidized neurofilaments (Goldman et al., 1983). LBs were first described by Lewy in 1913 in degenerating neurons in the basal forebrain.

In PD the loss of nigral neurons follows a specific pattern of degeneration with the A9 and in a lesser extent the A8 cell groups presenting with a higher vulnerability with respect to the A10 cells, among which neuron loss is almost negligible. Significant differences are also seen within the A9 cell group with lesions being more prominent at caudal, ventral and lateral positions in contrast to more rostral, dorsal and medial regions. This pattern of cell loss is also seen in animal model systems (Betarbet et al., 2000). MPTP treatment in rodents and primates, 6-hydroxydopamine infusion in rodents, and rotenone infusion in rats all produce dopamine neuron death following this specific pattern (Rodriguez et al., 2001; Burns et al., 1983; Dawson et al., 2002). Moreover, this susceptibility, higher in SN neurons with respect to VTA cells, is also seen after proteosomal inhibition in the rat or spontaneously in the weaver mouse (Graybriel et al., 1990; McNaught et al., 2004). The result of this cell loss is severe dopamine depletion in the striatum, responsible for the motor symptoms associated with PD, especially bradykinesia, tremor at rest, rigidity, and loss of postural control

(Bernheimer et al., 1973; Ehringer and Hornykiewicz, 1960; Selby, 1984). The cardinal symptoms first appear when about 50% of the dopamine neurons in the SN are lost and levels of dopamine in the striatum are reduced by 80% (Agid, 1991). Other lesions are observed in the noradrenergic locus coeruleus and the ascending cholinergic pathway from the nucleus basalis of Meynert (Ehringer and Hornykiewicz, 1960; Candy et al., 1983). These non-nigral lesions lead to cognitive and psychological impairments such as dementia which is estimated to occur in around 30% of all PD patients (Aarlsland et al., 1996). The loss of neurons in the LC is actually more prominent than the loss in SN (Ehringer and Hornykiewitz, 1960; German et al., 1992). The observations that cell loss in the nucleus coeruleus results in increased vulnerability of mDA neurons to various insults such as 1-methyl-4 phenyl1-1,2,3,6-tetrahydropyridine (MPTP) (Srinivasan and Smith, 2004) and that oxidative stress is reduced on VM cultures by noradrenaline application (Troadec et al., 2001) have led to the hypothesis that the cause of Parkinson's disease is due to the degeneration of neurons in the LC. Moreover, a recent study has suggested that loss of locus coeruleus neurons contributes to motor dysfunction in PD (Rommelfanger et al., 2007). According to this hypothesis, LC neurons precede and might initiate DA loss.

1.4.6.c Other etiologies for Parkinson's disease

Epidemiological and genetic studies have suggested multiple etiological factors for Parkinson's disease that is more appropriately described as a syndrome rather than one disease (Calne et al., 2001). Some of the features found to be implicated in the destruction of dopaminergic neurons are age, genetic and environmental factors, neuroinflammation and oxidative stress.

DA neurons are thought to be particularly prone to oxidative stress due to their high rate of oxygen metabolism, low levels of antioxidants, and high iron content. Lower glutathione (GSH) content has been reported in the brains of parkinsonian patients which show a reduced capacity to clear hydrogen peroxide (Lang et al., 2001). Laboratory experimental evidence in support of the oxidative stress hypothesis comprises the external administration of anti-oxidants such as

cysteine to reduce 6-hydroxydopamine's neurotoxic action (Méndez-Ámlvarez et al., 2001).

Dopamine itself is capable of producing toxic reactive oxygen species (ROS) via both its enzymatic and non-enzymatic catabolism (Halliwell, 1992). Specifically, dopamine oxidation can occur either spontaneously in the presence of transition metal ions or via an enzyme-catalyzed reaction involving monoamine oxidase (MAO). Oxidation of dopamine via MAO generates a spectrum of toxic species including H_2O_2, oxygen radicals, semiquinones and quinones (Graham et al., 1978). An increased brain concentration or utilization of dopamine could lead to an increase in the formation of active metabolites especially under conditions in which the ratio of available dopamine to antioxidant capacity is high (Hastings et al., 1994).

Exposure to environmental toxins and pesticides (rotenone or paraquat), i.e. in agriculture, and various heavy metals have been associated with disease insurgence (Baldereschi *et al*., 2003; Betarbet *et al*., 2000). Neutotoxins, such as MPTP, a side product during heroin production, have been related to PD when it was noted in 1980s that its accidental use by young heroin addicts in California resulted in their exhibiting parkinsonian features (Langston *et al*., 1983). It is this substance and the elucidation of the mechanism by which it causes Parkinsonism in animal models, that have led to the implication of mitochondrial dysfunction in the pathogenesis of PD. MPTP is highly lipophilic, and it crosses the blood brain barrier within minutes (Markey *et al.*, 1984). In the brain, MPTP is oxidized to 1-methyl-4 phenyl-2,3-dihydropyridinium ($MPDP^+$) by monoamine oxidase B (MAO B) in glia and serotonergic neurons and then is spontaneously oxidized to MPP^+. Due to its high affinity for the DA Transporter (DAT), it is selectively accumulated in dopaminergic neurons, where it causes toxicity and neuronal death by impairing mitochondrial respiration through inhibition of complex I of the electron transport chain (Javitch et al., 1985; Blum et al., 2001). Complex 1 deficiency specific to the substantia nigra has been reported in human PD brains (Shapira et al., 1990). The common herbicide 1,1'-dimethyl-4,4'-5 bipyridinium (paraquat) and rotenone exert their toxic effects on complex I in a similar fashion.

There is strong debate over the mechanism by which an external event eventually leads to the disease, with a traditional and conventional model of etiopathogenesis, which envisions a continual process affecting all susceptible cells in the SN, in contrast to the so called “event hypothesis”, by which a transient environmental factor would cause sublethal damage that eventually would result in the premature death of neurons, at variable periods after the insult has occurred (Calne, 1994). In support of the latter theory come the following models: a) Von Economo’s encephalitis (Calne et al., 1988), which often led to the appearance of parkinsonism several years after the infection, b) the selective nigral damage caused by MPTP, that has been shown to lead to immediate death of cell dopaminergic neurons and then, many years later, to active cell destruction with progression of the disease (Vingerhoets et al., 1994; Langston et al., 1999), and, finally, c) reports of traumatic brain injuries, that have led to parkinsonism with disease progression after cessation of the traumatic event (Vingerhoets et al., 1994; Langston et al., 1999).

Neuroinflammation has been suggested to participate in the degeneration of dopamine neurons in Parkinson’s disease. Activated microglia are found to correlate in areas within the SN with extracellular neuromelanin (a product of catecholamine metabolism), and anti-inflammatory drugs have been associated with reduced risks to develop PD (Beach et al., 2007; Chen et al., 2003). Within CNS, microglia can act as macrophages by removing cell debris and fighting infections by the production of pro-inflammatory cytokines like interleukin-1ß (IL-1ß) and TNFa. Microglia is also associated with increased expression of iNOS and NADPH oxidase, enzymes that generate free radicals such as nitric oxide and superoxide (Langston et al., 1999). NM is released by dying neurons, which are phagocytosed by microglia, and such a microglial activation would elicit a vicious cycle of NM release followed by inflammation. Misfolded or aggregated proteins from diseased SN neurons could similarly activate a local immune response.

About 5-10% of all cases of Parkinson’s disease are familial (Olanov and Tattom, 1999). Up to this moment two autosomal-dominant genes, (α-synuclein and LRRK2) and three autosomal recessive genes (parkin, DJ-1 and PINK1) have been definitely associated with inherited PD (Polymeropoulos et al., 1997: Kitada

et al., 1998; Bonifati et al., 2003; Valente et al., 2004; Paisán-Rui'z et al., 2004; Zimprich et al., 2004). UCHL-1 (Leroy et al., 1998; Healy et al., 2006), Nurr1/NR4A2 (Le et al., 2003; Healy et al., 2006), synphillin-1 (Marx et al., 2003) and Htra2/Omi (Strauss et al., 2005; Simón-Sánchez et al., 2008) have also been described to be associated with PD, but these reports have neither been replicated nor they have shown any linkage or association to disease (Hardy et al., 2007). α-synuclein was the first gene in which a mutation was found to cause an autosomal-dominant form of Parkinsonism (Polymeropoulos et al., 1997). Furthermore, it was found to be the principal constituent of Lewy bodies (Spillantini et al., 1997). Its function is currently not known. It has been shown though to be involved in fatty acid metabolism since α-synuclein knockout mice have a defect in brain fatty acid metabolism (Govolko et al., 2005). LRRK2, whose function is also unknown, is a complex kinase for which it has been proposed that a simple gain of kinase function could lead to toxicity (Greggio et al., 2006). Parkin is an E3 ligase, whose functions in the cell may include preparing proteins for proteosomal degradation, but its key function emerges now to be related to the mitochondrion (Golovko et al., 2005). DJ-1 is an atypical peroxidase that protects from oxidative stress. PINK 1 is a mitochondrial kinase, but neither its direct activators nor repressors are known. UCHL-1 has been shown to have ubiquitin ligase activity as well as hydrolase activity that could result in proteosomal degradation of proteins (Liu et al., 2002; Osaka et al., 2003). Its mutation has been reported to result in selective degeneration of DA neurons in a familiar case of PD (Liu et al., 2002). NR4A2 is a transcription factor required for the differentiation of midbrain neurons and there are indications that synphilin-1 may interact with alpha-synuclein and parkin (Zarranz et al., 2004). It has also been found as a component of LBs in brains of sporadic PD patients.

Autozygous mutations linked to PD have been reported also for ATP13A2 (Ramirez et al., 2006), which is a lysosomal pump (likely to be involved in a lysosomal storage disorder.), and for FBXO7, part of an E3 ubiquitin ligase (Laman et al., 2006). Mutations in the glucocerebrosidase gene (GBA), which in homozygous modality causes Gaucher's disease, a lysosomal storage disorder, in its heterozygous mutated state has been proposed as an risk factor for PD (Goker-

Alpan, 2004; Clark et al., 2007). GBA catalyzes the breakdown of the glucosecerebrosides to ceramide and glucose. Lysosomal build up of glucosecerebroside in the liver is the acute cause for its clinical manifestation.

In this context, oxidative stress and mitochondrial dysfunction have been proposed as one pathway leading to mitochondrial cell death. For this, evidence exists, that PINK1 and parkin are on the same mitochondrial pathway with PINK1 acting upstream of parkin (Park et al., 2006) and, although there is no direct evidence linking DJ-1 to parkin and PINK1, it has been suggested that this gene also might be part of the same pathway (Fitzgerald et al., 2008). Aberrations in the ubiquitin-proteasome pathway might relate to alpha-synuclein, UCHL-1 and parkin. Malfunctioning of this system could lead to an accumulation and deposition of proteins.

Finally, Hardy et al., 2009 include the following three diseases, in their critical review of the genetics of Parkinson's syndromes, for their clinical and neuropathological (presence of Lewy bodies) associations with parkinsonian syndromes: the Niemman-Pick type C (NPC) caused by mutations in the NPC1 gene, the Hallervoden-Spatz disease (also known as Neurodegeneration with Brain Iron Type 1/NBIA-1) caused by mutations in the PANK2 gene (Zhou et al., 2001) and the Neurodegeneration with Brain Iron Type 2 (NBIA-2) caused by mutations in the PLAG2G6 gene (Morgan et al., 2006). As these proteins GBA, PLA2G6, PANK2, and NPC1 all map directly on to lysosomal ceramide metabolism (Bras et al., 2008), they propose this pathway as an interesting possibility to take into consideration for future explorations. Work in yeast has also suggested a relationship between alpha-sunuclein and lysosomal recycling (Gitler et al., 2009) (for review on genetics of Parkinson's syndromes, see Hardy et al., 2009).

1.4.6.d Treatment of PD

There is no current cure for the disease. Treatment is largely symptomatic. The most commonly prescribed drug for PD is L-dopa. L-dopa is the natural precursor for the metabolism of dopamine (Cotzias et al., 1967), and since it is not

charged like dopamine, it can cross the blood brain barrier. It is given with decarboxylase inhibitors to decrease its peripheral metabolism. The intake of L-dopa proves to be efficient in reducing parkinsonian symptoms, but it is also accompanied by severe side effects such as nausea, vomiting, and altered blood pressure. Moreover, after some years of treatments, the effects of L-dopa decline and patients develop dyskinesias (Lang and Lonzano, 1998 a & b). Dopamine agonists are also used therapeutically to replace dopamine function, but, up to now, none has proved as efficient as L-dopa. Other treatments include inhibition of the catecol-O-methyl transferase (COMT) and monoamine oxidase B. Experimental methods used at this time include deep brain stimulation and stem cell implantation. Deep brain stimulation consists in implanting high frequency electrodes in the brain to stimulate the thalamus reducing tremor (Putzke et al., 2003). Stimulation of the subthalamic nucleus or the globus pallidus interna diminishes bradykinesia, rigidity, and reduces L-dopa induced dyskinesia (Kumar et al 1998a, Kumar et al., 1998b). Transplantation of neural stem cells from fetal tissue into the striatum is still in its infancy although it has proved promising up to this moment as it appears that neural stem cells survive within the host and replace the function of the damaged dopaminergic neurons (Storch et al., 2004). The outcome of recent clinical trials however revealed poor cell survival of transplanted grafts with only portions of the host brain becoming re-innervated by subpopulations of these grafted cells Furthermore, it was noted that some transplanted patients develop dyskinesias (Bjorklund et al., 2003; Olanow et al., 2003). Other problems with grafting fetal tissue derive by its limited availability and the ethical issues that come with it. Alternative sources should be approached, such as the use of multipotent stem cells from the patient's own body and research effort put in developing appropriate protocols for the induction of the desired dopaminergic phenotype that could then be used to replace midbrain dopaminergic neurons lost during the disease process.

1.4.7 Transcriptional anatomy of DA cells

Three recent gene expression profile experiments, already mentioned in section 1.3.5, (Grimm et al., 2004; Chung et al., 2005; and Greene et al., 2005) have looked at differences between SN and VTA and have confirmed previous results obtained traditionally by looking at one candidate at a time. These studies have produced new data, a number of which have been validated and used for the formulation of testable hypothesis. These data have been examined either by looking at differentially expressed genes individually or by searching for concerted differences in gene expression, which are more likely at the base of functional differences between populations. A brief review of genes identified by all three studies follows.

MARCKS (myristoylated, alanine-rich, C-kinase substrate), ADCYAP1 or PACAP (pituitary adenylate cyclase activating polypeptide) and LPL (lipoprotein lipase) are three genes that have been found to show higher expression in the VTA, whereas a higher expression of GSYN (gamma synuclein) and NMDAR2C (N-methyl-D-aspartate receptor subunit 2C) has been noted for SN neurons. MARCKS has been implicated in learning and long term potentiation and the pathophysiology of mood disorders (Matus, 2005). PACAP has a known neurotrophic role during development and in cultures of ventral mesencephalic dopamine neurons. A neuroprotective function against MPP+ induced toxicity has also been noted (Vaudry et al., 2000; Takei et al., 1998; Reglodi et al., 2004). LPL is a candidate for protecting cells from damage caused by oxidized lipoproteins (Paradis et al., 2003). These gene functions seem to comply well with the diminished susceptibility of VTA DA cells to neurodegeneration. Gamma-synuclein has been reported to be involved in the regulation of the cell cycle (Inaba et al., 2005) and NMDAR2C in excitatory neurotoxicity of SN neurons (Kress et al., 2005).

Examination of gene categories of microarray expression studies has highlighted two major distinctions between VTA and SN neurons. All three studies converge to the idea that the most prominent difference concerns genes encoding energy-related metabolism, electron-transport and mitochondrial

proteins, which appear to be more expressed in SN rather than VTA neurons. This corroborates well with the fact that mitochondrial dysfunction is considered one of the aetiologies of PD (Greenamyre et al., 2001). SN neurons appear to be more metabolically active than VTA neurons and accordingly more energy (ATP)-dependent. As a consequence they may be more susceptible to toxins such as MPP+, rotenone (Betarbet et al., 2000), to mutant forms of alpha-synuclein or parkin that have been proposed as interfering with normal mitochondrial function (Hsu et al., 2000; Palacino et al., 2004). Genes related to lipid metabolism categories (Willingham et al., 2003) and vesicle-mediated transport are also found to be more expressed in A9 neurons with respect to A10 neurons and interestingly several RAB three genes (implicated in vesicle mediated transport) were found within genomic linkage regions for PD (Hauser et al., 2003). It has been proposed that vesicle-mediated transport may be more active in A9 neurons rendering them more vulnerable to eventual genetic or environmental factors that interfere with this pathway functioning. Large differences have been noted in neuropeptide and neurotrophic factors, more highly expressed in VTA rather than SN neurons (Chung et al., 2005; Greene et al., 2005). This could explain the preservation of VTA neurons in PD patients and in animal models that recapitulate the neuropathology of the disease.

Up to now, a total of six studies have analyzed the expression profile of ventral midbrain cells or mDA neurons specifically, resulting in a list of several hundred genes. The three studies that have just been dealt with have identified the global expression profile of the subpopulations of mDA neurons in rats amd mice using microarrays. The other three studies (Stewart et al., 1997; Barret et al., 2001; Thuret et al., 2004), based on differential display, have examined the expression profile of the midbrain tissue in mice. In a retrospective study, Alavian and Simon (2009), have combined the resulting datasets from all six studies and have produced a database of the genes expressed in the mDA cell population. They have then verified the expression of each gene in dopaminergic neurons, using the collection of in situ hybridization in the Allen Brian Atlas. What they have found is that the efficiency of each screen in identifying mDA-specific genes was 25% for Chung et al., 29% for Barrett et al., 28% for Stewart et al., 37% for

Greene et al., 24% for Thuret et al., and 24% for Grimm et al., which is an indication for the complementary and non-redundant nature of such studies.

The importance of being able to identify unequivocally DA cell subpopulations and having a full ID of each subtype emerges if we take into consideration the centrality of these nuclei in brain function and dysfunction. It clearly is important for defining which neurons are marked for death and in which pattern in the various neurodegenerative diseases that affect the mesencephalic DA neurons. It is also crucial for the development of selective drug targets and therapies. This because the drugs do not distinguish between classes of neurons and the desired effects in one condition become the adverse effects in another. For example, hallucinations and paranoia are common side effects of PD drug therapy, while schizophrenia drug therapy is characterized by unwanted PD-like extrapyramidal motor disturbances (Grimm et al., 2004).

Very importantly still, although the presence of TH enzyme is the most sensitive and consistent single marker available to us for the identification of dopaminergic cells and while it works very well for mDA cells, it has proven not to be always a reliable or necessary condition for determining the DA identity of a neuron. The reason for this is that TH at immunohistochemically detectable levels can change over time and vary in response to changes in functional demands and hormonal status. For instance, there is an age-related decline in dopaminergic function in the nigrostriatal system which is linked to a downregulation of the TH enzyme. This decline is also seen in dysfunctional but surviving neurons in PD. On the other hand, TH positive cells, undetectable with the histofluorescence technique, occur in rodents in the hypothalamus and in primates and humans also in the basal forebrain, striatum and cortical areas. These neurons do not contain any detectable CA and lack AADC, as well as VMAT-2 (Ikemoto et al., 1999, Weihe et al., 2006) and the majority of them exhibit morphological features of GABA interneurons (for review, see Björklund et al., 2007). From here follows the importance of finding additional markers to identify cells as functional DA-producing neurons in other areas of the nervous system. Identification of specific markers in combination with molecular profiles will also support stem cell

engineering in targeting the production of specific DA subpopulations for cell replacement therapies.

Finally, full expression profiles of A9 and A10 cells may shed light on the biological basis that dictate the differences in susceptibility seen in the two mDA subpopulations. Unraveling eventually such differences in expression at baseline and prior to any experimental manipulation may help to elucidate this selective vulnerability and the specific function of these neurons.

1.5 AIMS OF THIS WORK

- To develop a suitable method for producing high quality RNA from GFP-expressing mDA cells isolated by LMPC
- To apply the extracted and suitably amplified material on cDNA microarrays for gene expression profiling of A9 and A10 mDA subpopulations
- To validate most interesting results by cross-referencing them with literature data from previous expression profiling studies and with in situ hybridization data from the Allen Brain Atlas, in order to identify potential markers that may discriminate between A9 and A10 cells and interesting genes that could be at the basis of the differential vulnerability of the two subpopulations in Parkinson's and other neurodegenerative diseases.

MATERIALS AND METHODS

2.1 ANIMALS

2.1.1 TH - GFP transgenic mice

Two to three months old female TH-GFP transgenic mice that express GFP protein in the majority of midbrain DA neurons under the control of the 9-kb upstream region of the rat TH gene were used for all expression profile experiments involving DA cells. The TH-GFP/21-31 strain was kindly provided to us by Prof Kazuto Kobayashi (Department of Molecular Genetics, Institute of Biomedical Sciences, Fukushima Medical University, School of Medicine, Fukushima, Japan). The transgenic line was maintained by breeding to C57BL/6J inbred mice in our Animal House Facility (Settore Stabulario, Università di Trieste, via Valerio 28, Trieste). Homozygous mice are lethal possibly because of disruption of some gene functions by transgene integration. Transgenic mice were identified by PCR of tail DNA using the GFP sequence.

2.1.1.a Generation of transgenic mice carrying a TH-GFP fusion gene

Briefly, the transgene construct contained the 9.0-kb 5'-flanking region of rat TH gene, the second intron of the rabbit β-globin gene, cDNA encoding EGFP (Clontech, Palo Alto, CA, USA), and polyadenylation signals of the rabbit b-globin and simian virus 40 early genes (Sawamoto et al., 2001). The construct was microinjected into fertilized (C57BL/6J x DBA/2J) F2 mouse eggs, which were then implanted into pseudo pregnant females. Ten copies of the transgene were integrated per haploid genome in this strain. The typical expression frequency of the GFP protein in the TH-GFP/21-31 line was 94.1% in the SNc and 85% in the VTA whereas the ectopic expression frequency, defined as the percentage of expression of the number of GFP+ only cells in the total number of TH+/GFP+ cells, was 7.5% in the SNc and 8.3% in the VTA (Matsushita et al., 2002).

2.1.2 C57BL/6J

For all other applications unless otherwise stated C57BL/6J mice were used.

2.2 DISSOCIATION OF DOPAMINERGIC NEURONS

Dissociation trials were performed on wild type C57BL/6J aged P20. Animals were killed by cervical dislocation and brains were removed. Ventral mesencephalon was dissected out in ice-cold dissociation solution (Earle's Balanced Salt Solution 10X EEBS, Sigma, St Louis, MO, USA; 7.5% NaHCO3; 1M HEPES, Sigma, St Louis, MO, USA; pH adjusted to 7.4 with 1N HCl) and minced in small pieces with a scalpel blade. These pieces were subsequently put in a Falcon tube containing 5 ml of the dissociation solution with 20 u/ml of papain (Worthington Biochemicals Co., Freehold, NJ, USA). Papain was pre-activated by incubation at 37˚C for 30 minutes in the presence of 1 mM L-cysteine and 0.5 mM EDTA. After papain, 250 µl DNAse I (Worthington Biochemical Co. Freehold) were added to the digestion solution and the tube was gently agitated at 37˚C for 40 minutes. The digestion medium was then removed and the contents washed briefly in EBSS. An additional wash (5 min at 4˚C) was then performed with 5 ml of EEBS containing 500 µl of 1% ovomucoid inhibitor (Worthington Biochemical Co. Freehold) and 1% BSA (Sigma, St Louis, MO, USA). To stop the enzymatic digestion, the supernatant was discarded and 2 ml of albumin/ovomucoid inhibitory mix were added to the tube. The mesencephalic pieces were mechanically triturated with a fire-polished glass Pasteur pipette and the cloudy cell suspension transferred to a new tube with fresh ovomucoid inhibitory solution and triturated further with a glass Pasteur-pipette fire-polished to a smaller diameter. The supernatant was then pooled and centrifuged at 900 rpm for 5 minutes. Pelleted cells were resuspended immediately in DMEM + 10% FBS + Pen/Strept. Resuspended cells were seeded on glass coverslips, previously treated with Concanavalin A (Sigma), and washed with PBS (2x) and culture DMEM (1x). Cells were left to adhere for 30 to 60 minutes and fixed in PFA 4% for 10 minutes.

Immunofluorescence with a mouse monoclonal anti-TH primary antibody (DiaSorin, Stillwater, MN, USA) was coupled with an Alexa Fluor 594 immunofluorescent secondary antibody. Fixed dissociated cells were washed twice in PBS, incubated at RT for 4 minutes with 0.1% Triton solution (in PBS), followed by two further PBS washes. Cells were incubated with the primary antibody in a 1:1000 PBS solution (0.1% BSA + 0.02% NGS + 0.1% TritonX-100) for 90 minutes. After two five minute washes with PBS, the secondary antibody was applied in a 1:250 dilution in a PBS solution (0.1% BSA). Cells underwent two more five minute washes with PBS. Finally, cells were counterstained with the immunofluorescent nuclear 4', 6-diamidino-2-phenylindole (DAPI; Invitrogen Molecular Probes) in a 1:2000 dilution made in PBS, washed three times in PBS and one final time in H_2O, before being mounted with Vectashield for microscopic inspection.

2.3 DEVELOPMENT OF PROTOCOL FOR USE WITH LMPC

2.3.1 RNase – free experimental environment

All procedures were performed in an RNase-free environment. Working surfaces and plasticware were treated with RNase decontamination solution (RNase Zap, Ambion, Austin, TX, USA) and rinsed with Diethyl Pyrocarbonate (DEPC, Sigma) treated water. Glassware was baked at a minimum of 220˚C for 4 hours to inactivate RNases. All solutions were prepared either with DEPC-treated water or from purchased certified RNase- free water.

DEPC-treated H_2O: 1 ml of DEPC was added to 1L of bidistilled H_2O and the solution was stirred for 6-8 hours at RT and left uncovered overnight under a fume hood. The day after residual DEPC was removed by autoclaving. To avoid interference of residual traces of DEPC with subsequent enzymatic reactions such as nucleic acid amplifications, the solution was autoclaved twice and stored at RT. All chemical substances containing amino groups like TRIS, MOPS, EDTA, HEPES etc were prepared in DEPC-treated H2O and never directly treated with DEPC.

2.3.2 Comparison of fixatives and staining in relation to tissue morphology and RNA quality retention

Adult C57BL/6J mice and TH-GFP/21-31 were killed by cervical dislocation in the laboratory environment always at 6 p.m. The brains were rapidly removed with the help of forceps, briefly washed in ice-cold PBS, and the regions of interest dissected and included in section medium Neg-50 (Richard Allan Scientific, Kalamazoo, MI, USA) in cryomolds in the desired position and orientation. Blocks of tissue were then snap-frozen on an isopentane layer (Sigma, St Louis, MO, USA) previously hardened in liquid nitrogen. Brains to be used immediately were left to equilibrate in a cryostat chamber (Microm International, Walldorf, Germany) at -21ºC for 1 hour. Fourteen micrometer (14 μm) cryosections were cut at the cryostat and thaw-mounted onto plus-charged Superfrost glass slides (Superfrost plus, Menzel-Gläser, Menzel GmbH & co KG, Braunschweig, Germany). Six sections were mounted on each slide. Slides were kept in the cryochamber at -21ºC during the whole procedure. Cutting and mounting were performed as quickly as possible (approximately 15 minutes).

To compare and evaluate the effects of fixatives and staining on tissue morphology of wild type mice sections and the effect of fixatives on the retention of the GFP fluorescence of TH-GFP/21-31 mice sections as well as the effects on RNA recovery and quality, slides were air-dried for at least 2 minutes and fixed in the following compounds:

A) Ice-cold ethanol (EtOH) 95% for 1 minute.

B) Ice-cold acetone 99% for 2 minutes.

C) DSP (Pierce, Rockfold, IL, USA) at a final concentration of 1mg/ml for 5 minutes. 50x stock solutions of DSP in anhydrous DMSO (Sigma) were prepared and stored at -80 ºC. To prepare a working concentration the stock solution was diluted with 1xPBS immediately before use. DMSO stock was added to PBS dropwise while the solution was on a stirrer so as to avoid the formation of white precipitate (Xiang et al., 2004).

D) Paraformaldehyde (PFA) 4% for 5 minutes.

E) Zinc-based fixative (Zincfix). Immediately after brain dissection, a piece of tissue was placed in 1X ice-cold Zincfix (BD Biosciences, Franklin Lakes, NJ, USA) for 6 - 8 hours followed by an overnight immersion in a solution of 1X Zincfix + 30% sucrose at 4 ºC, until the specimen sunk at the bottom of the Falcon tube. The ratio, fixative volume to specimen volume, was >10. The cryoprotected brain portion was subsequently embedded in Neg-50, snap frozen on liquid nitrogen cooled 2-methylbutane (isopentane), and sectioned at 14 μm intervals at the cryostat, at -21 ºC.

F) Fresh brain sections prepared at the cryostat from snap-frozen brain were used as control.

Following fixation, half of the slides were used for morphological evaluation and half for estimation of RNA recovery and integrity. Wild type mice sections were washed with nuclease-free water (10 seconds) with the exception of ethanol-fixed sections which also underwent a 70% ethanol rinse before the water wash, and Zincfic-fixed sections which underwent a five-minute immersion in ice-cold Zincfix to get rid of the Neg-50 tissue embedding medium. Subsequently, they were stained into a 1% cresyl violet solution (1gr Cresyl Violet Acetate, Sigma, in 100 nuclease-free H_2O) for 2 minutes, rinsed in nuclease-free H_2O, and finally dehydrated through a decreasing series of EtOH solutions, 75% for 30 seconds, 95% for 30 seconds, and 100% for 30 seconds (2x). Xylene was used for 1 minute only if stain was too deep.

The slides were left to air dry on the bench and stained tissue sections were examined together with fixed unstained sections from TH-GFP/21-31 mice with regards to morphology and retention of the fluorescent marker respectively, with a Zeiss PALM LMPC microscope (Carl Zeiss Inc., Germany). Some Zincfic-fixed sections were subjected to a shorter modified Nissl stain for which, they too, were evaluated in terms of tissue morphology and RNA integrity. The short cresyl violet staining consisted in a one minute 70% EtOH wash, followed by staining in a 1% cresyl violet solution prepared in 70% EtOH in place of H_2O for 2 minutes, and a final wash in 100% EtOH.

In parallel, to study RNA recovery and quality, similarly prepared sections (6 from each slide) were scraped off the slides and into Eppendorf tubes with the help of a scalpel and collected at the bottom of the tubes with a centrifuge at 13000g for 5 minutes. The procedure was repeated five times. RNA was extracted, quantified, and its quality assessed as described in paragraph 2.5, "RNA extraction and quality assessment".

2.3.3 Improving tissue visualization

Morphology of tissue sections when dry and not mounted and coverslipped is far from ideal. Recognition of structures of interest becomes difficult, especially when looked at though an LMPC objective, which does not offer high optical resolution. This is particularly true for fluorescent-expressing cells and tissues, for when these dry, fluorescent structures tend to blend with the background which shows a diffuse fluorescence itself.

In order to improve visualization of tissue morphology and discern cells of interest, in this case the TH-GFP expressing DA cells of the midbrain, we applied to our sections a series of compounds, in drops, before looking at them at the LMPC: i) the LiquidCover Glass N (PALM, Microlaser Technolgies GmbH, Benried, Germany), which is a resin that can be thinned with EtOH, ii) EtOH 100%, and iii) Zincfix. Sections were evaluated for their morphology and RNA quality was assessed only for the compound which gave the best results, in this case Zincfix, as described in the paragraph on “RNA extraction and quality assessement”. This application was called the “postfixation” step. Concomitantly RNA quality was analyzed for a) a piece of fresh cerebellum, b) a piece of cerebellum fixed in Zincfix, c) Zincfic-fixed cerebellar sections, and d) postfixed, Zincfic-fixed cerebellar sections subjected to the laser-microdissection procedure, in order to grossly evaluate the loss of RNA quality at each step of the process. For RNA extraction and quality assessment see paragraph 2.5.

2.3.4 Storage of sections

LPC sessions often last for many hours and if more than 1000 cells are to be collected one by one, then the harvest can continue the day after. For this reason it was necessary to test and select the best storage conditions for the tissue sections intended for LMPC use.

Sections from TH-GFP/21-31 transgenic mice were prepared as aforementioned (paragraph 2.4.2) and fixed with Zincfix. One batch of slides was stored in dry conditions, in a box with silica beads, in a vacuum, for two months; a second batch was stored in a box, with dessicant, at -80◦C for the same time period. These sections were consequently evaluated for tissue morphology after a dropwise addition of Zincfix on their surface and RNA recovery and quality as in paragraph 2.5.

2.4 TISSUE PREPARATION FOR LMPC

For laser capture microdissection, regions of midbrain, cerebellum and hippocampus, respectively from TH-GFP/21-31 mice and wild type mice were dissected and incubated in 1X Zincfix solution for 6 hours. They were then cryoprotected in a 1X Zincfix + 30% sucrose solution at 4˚C overnight, embedded in Neg-50 section medium, snap-frozen and left to equilibrate in a cryostat chamber at -21˚C for 1 hour before sectioning, as described earlier. Coronal 14 μm sections were prepared from cerebella and hippocampi of wild type mice and thaw-mounted on PEN membrane-coated slides (PALM), which were then Nissl stained as described earlier. Midbrain sections from TH-GFP/21-31 were thaw-mounted on thinner PET membrane slides (PALM), which gave lower background fluorescence and hence allowed better visualization of the DA GFP-expressing cells. For all microarray experiments TH-GFP midbrain sections were thaw-mounted on Superfrost plus glass slides (Mezzle-Glasser) as brain sections adhered better on them rather than on membrane-coated slides which were confounding because of their inherent fluorescence. Sections were left to air dry for 30 minutes and postfixed with LiquidCover N and Zincfix just prior to the

moment of cell selection. Sections were left to dry for few minutes. Up to three slides were placed each time on the slide holder of the PALM Robot-MicroBeam system (PALM Microlaser Technology AG, Benried, Germany).

With the help of a mouse, a line was drawn around each cell to be collected and once all cells of a specific section were chosen, on activation, the UV laser beam made an excision along the previously drawn cell borders. Subsequently, a brief laser pulse was shot against the desired cell which was catapulted upwards, against gravity, in a small tube cap, situated directly above the processed section. Membrane slides allowed for a brief laser pulse to be used for catapulting as the laser beam excised both the tissue and membrane and the cell could be collected in its entirety. For sections on glass slides, tissue was dissected by the laser beam along the perimeter of the cell but more laser pulses were needed to catapult upwards the whole structure, achieving this, only by fragmenting the cell in pieces. All cells were harvested under a 40x magnification. Two types of caps were used to collect the cells. Trials for the development of the protocol were conducted with 0.2 ml eppendorf tubes carrying transparent caps coated with a small amount of mineral oil so as to provide a sticky surface for the cells. All hybridization trials and experiments were performed with 0.2 ml microfuge tubes provided with a white cap (PALM adhesive caps), filled with an inert sticky substance, which immobilized catapulted samples instantly. At the end of each LMPC session, cell collection was verified by inspecting the tube cap. Microdissected sections were monitored and controlled throughout the procedure to make sure that cell selection and collection were optimal. Never were more than 1000 cells collected in one cap. Microcentrifuge tubes were left at RT until the end of the LMPC session before RNA isolation or stored at RT, in a box with silica beads, inside a vacuum for up to a week if more samples were to be collected and pooled for a single RNA extraction.

2.5 RNA EXTRACTION AND QUALITY ASSESSMENT

Total RNA was extracted from pieces of fresh brain and Zincfic-fixed brain with 500 μl TRIzol (Invitrogen Molecular Probes, Carlsbad, CA, USA)

according to the manufacturer's instructions. Scraped sections were lyzed in 100 μl TRIzol and RNA was extracted with the RNA Miniprep kit (Stratagene, La Jolla, CA, USA) in a final elution volume of 30 μl. DNAse treatment was performed if appropriate and according to the protocol used. The quality of purified RNA was assessed using an Agilent 2001 Bioanalyzer (Agilent, Palo Alto, CA, USA) and quantified with an ND-1000 spectrophotometer (Nanodrop technologies, Wilmington, DE, USA).

To extract total RNA from LMPC collected cells, 10 μl of lysis buffer were added directly onto the cells in each microcentrifuge cap and the solution was pippetted up and down a few times. Tubes were left on ice upside down for 5 minutes to allow time for cell lysis and centrifuged briefly at max speed so that they could be collected at the bottom of the tube. If more samples were to be extracted together, centrifuged material from more caps was pooled in one tube and processed as one sample. Total RNA extraction was performed with the RNA Nanoprep kit (Stratagene, LA Jolla, CA, USA) according to manufacturer's recommendations in an elution volume of 12 μl. RNA quality and yield were analyzed with RNA 6000 Pico Lab Chips (Agilent).

Samples that were not extracted immediately were kept homogenized in TRIzol at -80ºC until later processing.

2.6 RNA ASSESSMENT OF MICRODISSECTED CELLS BY RT-PCR AND QPCR

RNA obtained from microdissected cells was further evaluated for integrity with RT-PCR and qPCR. Moreover, the sensitivity of the procedure was assessed by evaluating RNA extracted from 100 and 10 microdissected cells.

2.6.1 RT-PCR

Global amplification with the use of an oligod(T)-tailed primer, followed by specific PCR for the DJ1 cDNA was conducted on fresh brain, Zincfic-fixed brain, Nissl-stained Zincfic-fixed sections, and 1000 LMPC Nissl-stained granule cells microdissected by their morphology and topography from the hippocampus.

Extracted RNA (see paragraph 2.5) was subjected to 2 units Rnase-free DNase (2 units/µl; Ambion) at 37˚C for 20 minutes to get rid of any genomic material still present. Reverse transcription (RT) was conducted in a 15 µl volume, with 5µl RNA, 0.5 µl (500 ng/µl) of primer SMART724 (Clontech), 0.5 µl RIBOSMART and DEPC-treated H_2O up to 10 µl. After five minutes at 68˚C and quick chill on ice, the following reagents were added to the reaction: 2 µl of First-strand 5x buffer, 1 µl of 1 mM DTT, 1 µl of 10 mM dNTPs, 0.5 µl of 200 u/µl of Superscript II (Invitrogen), 0.5 µl of 40 u/µl of RNase Inhibitor (Ambion). The reaction was carried out at 37˚ for 90 minutes. For each sample, a mock reaction without reverse transcriptase was performed. Unreacted primer was specifically removed by adding to the tube 1 µl of 20 u/µl exonuclease I (New England Biolab) while 0.5 µl of 1 u/µl phosphatase SAP (Shrimp Alkaline Phosphatase) (Roche) were used to inactivate free nucleotides. The reaction was incubated at 37˚C for 30 minutes and at 80˚C for 10 minutes to inactivate the enzymes. Tailing was performed on a total volume of 30 µl with 3 µl of 10X tailing buffer, 3 µl of 1 mM dATPs, 1 µl of terminal deoxy transferase (TdT) (Roche) and DEPC-treated H_2O at 37˚C for 30 minutes. Finally, the reaction was stopped by incubation at 70˚C for 10 minutes. A global conventional 35-cycle PCR was performed with 2.5 µl of the newly formed cDNA, 0.5 µl of (500 ng/µl) SMART724 primers, in a total volume of 50 µl to dilute previously used reagents, employing La Taq Takara (Takara Bio Inc.), in a thermal cycler, at the following conditions: 94 ˚C for 3 minutes to destroy RNA strand and inactivate previously used enzymes, 37˚C for 5 minutes, and 72˚C for 20 minutes to complete first strand synthesis. Next, a 35-PCR cycle followed, with denaturation at 94˚C for 30 seconds, annealing at 55˚C for 30 seconds, extention at 72˚C for 5 minutes, with a final extention step at 72˚C for 10 minutes. 1 µt from this PCR was used to perform a conventional 30-PCR cycle with specific primers for DJ1, with the employment of La Taq Takara and an annealing T of 50 ˚C.

Specific amplification for SUMO 1 was performed from RNA extracted (see paragraph 2.5) from 100, 10 microdissected cells and plain microdissected membrane to assess the sensitivity of the procedure and control for contamination from debris due to the laser cutting. 3 µt of the RT-PCR products, with an RT

reaction performed as described previously, were tested with a conventional 35-PCR cycle for the presence of SUMO 1 with no prior global amplification. Controls were prepared as before.

Specific gene amplifications were also performed from 1000 hippocampal and 1000 dopaminergic neurons microdissected from TH-GFP/21-31 mice sections in groups of 3 or 4. We looked for the presence of gene transcripts characteristic for the isolated cells and for eventual contamination by surrounding cells by using TH (present in DA neurons), MAP-2 (present in all neuronal cells), GFAP (present in astrocytes), and the housekeeping gene GAPDH (See table 1 for full gene names and primers). The primers used for these amplifications, with the exception of GAPDH, were designed to be intron-spanning to avoid amplification of unwanted genomic material, also in view of the amplification protocol used. 10 μt of a lysis solution (containing: 0.2 mM guanidinium thiocynate, 10 mM DTT, 0.5% NP-40 and 100 ng/μl twentymer of inosine in DEPC-treated water, at final concentrations) were directly added to the cap collector containing the LMPC isolated cells, which were pipetted up and down so as to allow rupture. Each sample was split it two tubes in order to perform a normal and a mock RT reaction. After addition of 1.0 μt 10 mM dNTPs, 0.5 μt of random primers, the tubes were warmed at 70˚C for 2 minutes and immediately put on ice. Reverse transcription was performed with 2.0 μt of First-strand buffer, 1 μt of Superscript II (Invitrogen), 0.5 μt RNase Inhibitor (Ambion) on a total volume of 10 μt at 37˚C, for two hours. Conventional 35-cycle PCR amplifications with specific primers for the above cDNAs were performed using 1 μt from the RT-PCR products and La Taq Takara (for primers, see table 1).

We assessed RNA quality from two samples, each of 300 dopaminergic GFP-fluorescent cells, microdissected one at a time from sections mounted on Superfrost Plus glass slides and microdissected in small groups of 3 to 4 from membrane-coated slides respectively, by gene specific amplification of the GFP cDNA fragment. In the same two samples the degree of astrocytic contamination was evaluated by amplification of the GFAP fragment (see table 1 for primers).

Specific PCR primers		
Name	**Sequence**	**Amplicon size**
Dopamine Transporter (DAT)	Fw: CGGCTAAAGAGCCCAATGCTGTGG Rv: CATCAATGCCACGACTCTGATGG	643 bp
Microtubule-associated protein 2 (MAP-2)	Fw: CTGGCTCAGGCATTCAGAAACAGC Rv: TACCATTGCTGAAACTCCAGCGCA	521 bp
Tyrosine Hydroxylase (TH)	Fw: TCTGACGATGTGCGCAGTGCCAGAG Rv: CGCAGCTGGAAGCCAGTCCGTTCC	413 bp
Green Fluorescent Protein (GFP)	FW: CTTTTCACTGGAGTTGTCCCAA Rv: TGGTCTGCTAGTTGAACGCTTCC	530 bp
Glial Fibrillary Acidic Protein (GFAP)	Fw: GGATGTGGCCAAGCCAGACCTCAC Rv: CTTAATGACCTCACCATCCCGCA	594 bp
Glyceraldehyde-3-phosphate dehydrogenase (GAPDH)*	Fw: CCACTAACATCAAATGGGGTG Rv: ACGTCAGATCCACGACGGACAC	496 bp
DJ1*	Fw: GATGGAGACAGTGATTCCTGTGG RV: ACATACTACTGCTGAGGTTCC	610 bp
Small ubiquitin-like modifier (SUMO 1)	Fw: AGTCATTGGACAGGATAGCAGTGAG Rv: TCACATCTTCTTCTTCCATTCCC	196 bp
*All primers except for GAPDH and DJ1 were intron-spanning		

Table 1. Primer sequences used in this study

2.6.2 Real time assessment of RNA integrity

We also used qPCR to look at astrocytic contamination of LMPC isolated samples, by GFAP amplification, from 500 A9 and 500 A10 neurons. DAT and TH were used as dopaminergic specific genes (see table 2). RNA was extracted from LMPC-collected cells with Absolutely RNA Nanoprep kit (Strategene). Single strand cDNA was obtained from purified RNA using the iSCRIPT^{TM} cDNA Synthesis kit (Bio-Rad Laboratories, Hercules, CA, USA) according to manifacturer's instructions. Quantitative RT-PCR was performed using SYBER-Green PCR Master Mix and iQ5 Real-Time PCR Detection System (Bio-Rad). Quantitative RT-PCR was performed with an iCycler IQ (Bio-Rad); the housekeeping gene β-actin was used as an endogenous control to normalize the expression level of target genes. Primers were designed with the Beacon Designer^{TM} 6.0 (PREMIER Biosoft International, Palo Alto, CA, USA). Results were normalized to β-actin and the initial amount of the template of each sample

was determined as relative expression versus the sample chosen as reference. In this case, RNA extracted from mouse TH-GFP/21-31 total mesencephalon.

Finally, qPCR was used to evaluate RNA integrity in a sample of 500 A9 and a sample of 500 A10 microdissected cells by looking at the 3'/5' ratio of a qPCR-amplified, widely expressed gene, as the tranferrin receptor (TFRC).

Real Time Primers	
Gene Name	**Primer Sequence**
Dopamine Transporter (DAT)	Fw: GTGCTGGTCATTGTTCTG Rv: TCACAGAGACGGTAGAAG
Tyrosine Hydroxylase 5' (TH 5')	Fw: CCGTCTCAGAGCAGGATACC Rv: CGAATACCACAGCCTCCAATG
β-actin	Fw: CACACCCGCCACCAGTTC Rv: CCCATTCCCACCATCACACC
Glial Fibrillary Protein (GFAP)*	Fw: CAAGGCTCAATCAGTGCTAAG Rv: AACAACAAGGATGAAGGAAGTG
Tranferrin Receptor 5' (TRFR 5')	Fw: GGCTGAAACGGAGGAGA Rv: ACGAGGAGTGTATGTATTCTGG
Transferrin Receptor 3' (TRFR 3'	Fw: AGGCATTGACTCAGAAAG Rv: GTAGACTTAGACCCATATCC
* All primers were intron-spanning except for GFAP	

Table 2. qPCR primers used in this study

2.7 LMPC WITH MICROARRAYS

Three hundred A9 and 300 A10 neurons were LCM-isolated by their GFP identity and topographic location from the whole expanse of the VM of the same mouse, for each experiment (biological replicate). Three biological replicates and three technical replicates, each of which with two dye orientations, were used for hybridization on a total of 18 slides. The SISSA 2 slide, home-spotted with 7 246 from the ~60 000 FANTOM 2 collection of mouse transcipts (Okazaki et al., 2002), was used for our experiments.

2.7.1 RNA extraction and probe synthesis

Isolation of mRNA, millionfold amplification and labeling of the resulting cDNA with Cy3-dCTP and Cy5-dCTP (PerkinElmer) was performed using the

μMACS SuperAmp Kit (Miltenyi Biotec) and a thermoMACS Separator, according to the recommended protocol. A brief description follows:

mRNA isolation. 5.4 μl of incubation buffer were added directly to the microdissected cells previously collected in an adhesive cap (PALM), incubated on ice upside down for a couple of minutes, vortexed, and briefly centrifuged. The incubation buffer (for 1 to 5 reactions) was prepared by adding in a 1.5 ml RNase-free tube the following reagents in the indicated order: 25 μl of Lysis/Binding Buffer, 2 μl tRNA Solution, 1 μl of Proteinase K (5 μg/μl, Roche). The tube was placed in a thermal cycler and incubated for 10 minutes at 45ºC, then for 1 minute at 75ºC. The lysate was incubated with 5 μl magnetic microbeads (SuperAmp Microbeads) and then applied to a μMACS column, previously prepared by rinse with a 100 μl of Lysis/Binding Buffer and placed in the magnetic field of a thermoMACS separator, which retained all the Poly $(A)^+$ RNA. Finally, the column was washed with 4x100 μl Wash Buffer to remove proteins, DNA and rRNA.

cDNA synthesis in the column and cDNA tailing. Samples were reverse transcribed for 45 minutes at 42ºC on the same column. 1 μl of RNase Inhibitor (10 units/ μl, Protector, Roche) was added to the resuspended First-strand cDNA mix, which was eluted to follow a cDNA tailing reaction for another hour at 37ºC with Terminal Deoxynucleotidyl Transferase (TdT) (GE Healthcare).

Global PCR. For the PCR reaction the Expand Long Template PCR system (Roche) was used. This protocol utilizing only one primer, allowed similar annealing conditions. The cDNA was primed at multiple sites of comparable length avoiding bias due to different transcript lengths. The amplification reactions were run with 41 cycles as indicated in the following profile:

Step 1		78ºC	30 s
Step 2	20 cycles	94ºC	15 s
		65ºC	30 s
		68ºC	2 min
Step 3	21 cycles	94ºC	15 s
		65ºC	30 s
		68ºC	2.5 min + 10 s/cycle
Step 4		68ºC	10 min
HOLD		4ºC	

PCR products were purified with High Pure PCR Product Purification kit (Roche). Purified DNA was quantified by spectrophotometric measurement (Nanodrop ND1000). At this point the cDNA could be stored at -20ºC for later labelling. Klenow labelling. 200 nanograms of anyone of the purified PCR products were labelled with direct incorporation of Cy3-dCTP and Cy5-dCTP (PerkinElmer) with 2 µl of Klenow Fragment (10 units/µl, MBI Fermentas). The reactions were incubated for 2 hours at 37 ºC in the dark. The Klenow fragment labeling reaction yielded a 5-30 fold amplification of the template DNA. Labeled DNAs were purified with CyScribe GFX Purification Kit (GE Healthcare) according to manufacturer's protocol 1 (65 ºC elution buffer) with an additional incubation of 4 minutes at room temperature before elution. Cy3 and Cy5-labeled samples to be co-hybridized were pooled and purified in one column. The final product was quantified spectrophotometrically (Nanodrop).

Klenow labeling using the RadPrime kit (Invitrogen). The PCR yield of most amplification reactions was high enough to permit the repetition of the labeling of a given sample when needed. This labeling reaction was prepared on a total of 50 µl, mixing the following reagents: 20 µl of Buffer 2.5X, H_2O (up to a total of 50 µl), 200 ng from the amplified DNA (PCR reaction). It was then incubated at 100ºC for 5 minutes and immediately placed on ice. The following reagents were further added to the tube: 1 µl of dNTPs (50x, 5mM dGTP, 5mM dATP, 5mM dTTP + 3mM dCTP), 2 µl of fluorescent-conjugated 1mM dCTP, 2 µl (40 U) of Klenow Fragment. The reaction was incubated in the dark for 2 hours at 37ºC and at 70ºC for 5 minutes to inactivate the enzyme. It was finally purified with CyScribe (GE Healthcare) according to the manufacturer's protocol. Samples intended for co-hybridization were pooled and purified as one. Dye incorporation efficiency and quantity of labeled probes were measured spectrophotometrically (Nanodrop).

2.7.2 Microarray hybridization

Before hybridization, microarray slides were incubated for 1 hr at 55˚C in 0.2X SSC (Ambion), buffers filtered through a 0.22 μm filter, washed in distilled water and centrifuged at 2000 rpm for 5 minutes. For hybridization on two microarray slides, labeled DNA from the two probes to be co-hybridized (a total of 3.0 μg per slide) were mixed together with 1.3 μl of 3.5 mg/ml Salmon Sperm (Sigma, St Louis, MO, USA), 1.3 μg/ml Cot-1 mouse (Invitrogen, Carlsbad, CA, USA), 6.6 μl of PolyA and 6.6 μl of 11.8 mg/ml tRNA (Sigma, St Louis, MO, USA). Sample volume was brought to 150 μl with distilled H_2O, before adding 150 μl of 2X formamide-based hybridization buffer (Genisphere, Hatsfield, PA, USA) pre-heated to 65˚C for 10 minutes. Slides were mounted on a GeneMachine Hyb4 Microarray Station (Genomic Solutions, MI, USA) and after having pre-heated at 80˚C for 10 minutes, 150 μl of sample were pippetted onto each slide. Hybridization was performed with the following protocol: 65˚C for 2 hr, 55˚C for 2 hr and 44˚C for 12 hr. Slides were washed 5 times with 2X SSC + 0.2 SDS at 65˚C, 5 times with 2X SC at 55˚C, and 5 times with 0.2 SSC at 42˚C. Each wash included 10s of flowing solution, and 30s at holding temperature. Before scanning, slides were centrifuged at 2000 rpm for 10 minutes in the dark.

2.7.3 Analysis of expression profile data

Slides were scanned with GenePix Personal 4100A microarray scanner (Molecular Devices Corporation, CA, USA) and the GenePix version 6.0 software. Normalization and statistical analysis were performed in the R computing environment (www.r-project.org/, version R 2.8.0 for Windows) using the LIMMA package (Smyth 2004) from the BioConductor software project (www.bioconductor.org/). Normalization of intensity values within arrays was done with the function “normalizeWithinArrays” based on the LOWESS algorithm: normalizeWithinArrays(RG,method=”loess”,bc.method=”normexp”, offset=50)”. Normalization between arrays was done with the function “normalizeBetweenArrays” based on the quantile method:

“normalizeBetweenArrays(MA,method=”quantile”)”. Subsequently, a linear model was fit to the normalized data. P-values were adjusted for multiple testing using Benjamini and Hochberg’s method to control the false discovery rate (Hochberg and Benjamini, 1990). Genes with adjusted P-values below 0.01 were considered differentially expressed.

Gene Ontology (GO) analysis was performed using tools for annotating gene lists available at DAVID Bioinformatic Resources at david.abcc.ncifcrf.gov/ (Dennis et al., 2003; Huang et al., 2009). Clustering association analysis was performed after application of a threshold p-value ≤0.05 and high stringency classification. Enrichment p-values were corrected, to control for family-wide false discovery rate, with the Benjamini correction technique.

2.8 VERIFICATION OF MICROARRAY DATA ON THE ALLEN BRAIN ATLAS

Genes resulted differentially expressed between SN and VTA from the mmicroarray analysis were verified one by one with the aid of expression data in the Allen Brain Atlas (ABA), which collects the gene expression patterns of over 21,000 genes, derived from high throughput, semi-automated in situ hybridization (ISH) on mouse brain sections. Only coronal digital sections from the publicly available Allen’s Brain Atlas ISH database at www.brain-map.org/ were used to verify the results as it was difficult to discriminate between the two subpopulations on saggital sections.

RESULTS

3.1 DEVELOPMENT OF PROTOCOL FOR LASER CAPTURE MICRODISSECTION OF MESENCEPHALIC DOPAMINERGIC CELLS

3.1.1 Dissociation of DA mesencephalic neurons

The original idea was to collect our cells of interest either manually, by the patch clamp technique (Gustincich et al., 2004), or by fluorescence activated cell sorting (FACS) (Herzenberg, Sweet et al., 1976). In fact, the original plan was to make use of a line of a transgenic mice as a source for DA cells, where a reporter gene, human placental alkaline phosphatase (PLAP), is expressed in all catecholaminergic neurons of the central nervous system under the control of the promoter for tyrosine hydroxylase, the rate limiting enzyme for dopamine biosynthesis (Gustincich et al., 1997). Mesencephalic dissociations followed by quick immunofluorescence on living dissociated cells with an antibody against the PLAP membrane marker would allow cell collection specifically of mDA cells.

First attempts consisted in dissociating the mesencephalon using papain to digest the tissue and in plating cells on concavalin A-coated glass coverslips placed in multi-well plates to assess the effects of the dissociation procedure on cell size and shape and the percentage of DA cells that could be detected. In these trials, PFA-fixed cells were labeled with a primary mouse anti-Tyrosine Hydroxylase monoclonal antibody (Chemicon, Temecula, CA) and a fluorescent Alexa Fluor 488 labeled secondary rabbit anti-mouse antibody (MoBiTec, Göttingen, Germany). Microscopic observation of the plated cells revealed the presence of DA cells in a degree of 2% to 3% and a decent preserved morphology (Figure 1).

The low percentage of dopaminergic cells obtained with this method up to that moment and the concomitant arrival of the Zeiss PALM LCM system (Carl Zeiss Inc., Germany) in our laboratory, pushed us towards the use of a different methodology to obtain DA cells. As it follows from above, we turned to Laser

Capture Microscopy to isolate mesencephalic dopaminergic cells for gene expression profiling and hence to the development of a suitable protocol for this purpose.

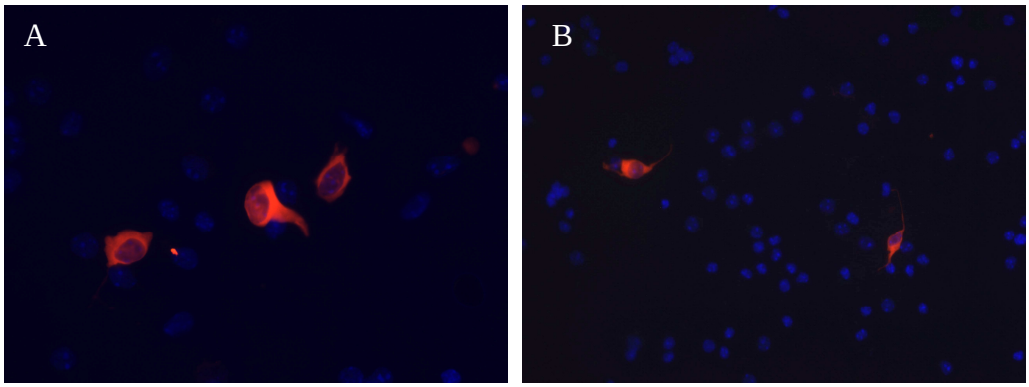

Figure 1. Plated dissociated mesencephalic cells. A) 40x magnification, B) 10x magnification. Fixed cells labeled with anti-TH antibody in red and nuclei counterstained with DAPI in blue. Shape and size of TH-positive cells look sufficiently preserved.

3.1.2 Evaluation of fixatives

Specific laser-assisted cell capture for subsequent expression profiling requires good visualization of structures and cells in tissue sections and recovery of good quality RNA. With the aim of developing a suitable protocol for this method of cell acquisition, we tested several fixatives followed by a standard Nissl stain on mice cerebellar or hippocampal sections with regards to preservation of tissue morphology and recovery of quality RNA.

Cerebellum coronal Nissl-stained sections fixed in paraformaldehyde and Zincfix rendered very good staining results with no significant difference in tissue architecture, cellular morphology, or tinctorial reaction. Following acetone, ethanol and DSP fixation Nissl staining was weaker; still tissue morphology was satisfactory and comparable among the three fixatives. Images were taken with the Zeiss PALM microscope (Carl Zeiss Inc., Germany) (Figure 2, A to F). Tissue sections were not cover-slipped, but reflect what one sees when laser dissections are performed.

The fixation methods used differently affected our ability to extract RNA. To determine the efficiency of RNA recovery from fixed and stained tissues, six sections were scraped off of slides for each fixative and their RNA extracted and

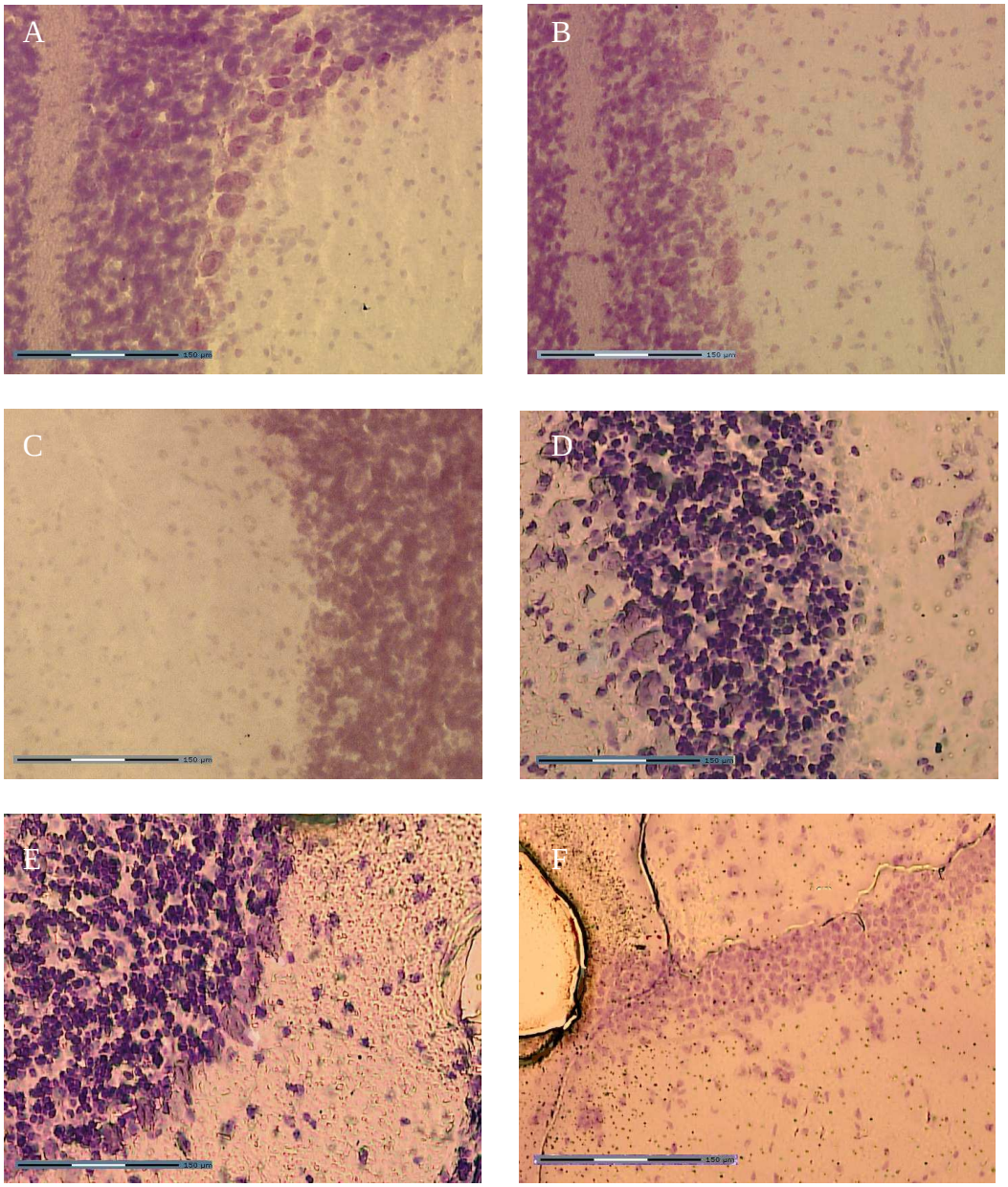

Figure 2. Morpholgical evaluation of Nissl-stained sections of mouse cerebellum fixed with the following agents: A) Acetone, B) Ethanol, C) DSP, D) PFA 4%, E) Zincfix, F) Zincfix (short modified Nissl stain). Images reflect what one sees during the LMPC procedure.

quantified by UV-spectrophotometric analysis with the Nanodrop spectrophotometer (Nanodrop Technologies Inc.,Wilmington, DE, USA). Measurements were repeated five times. Recovery rates are presented as the

percentage of the mean quantity of RNA extracted from the differently fixed tissue sections with respect to the mean RNA content recuperated from the same number of unfixed (fresh) sections (Figure 3). It was impossible to extract RNA from paraformaldehyde-fixed tissues, in agreement with the literature (Fend et al., 1999; Goldsworthy et al., 1999; Vincek et al., 2003), and we found difficult to extract RNA from DSP-fixed tissues although Xiang et al., 2004 have reported ease in extracting RNA of excellent quality with this fixative. Our failure in extracting RNA from DSP-treated tissues could be due to two factors: a) the difficulty in preparing a good and clear working solution of DSP – it often presented with precipitates –, and b) the omission of a reducing agent such as DTT before RNA extraction. One possibility is that RNA was never released during the extraction procedure, but was instead held in place by the crosslinking fixative. Precipitating agents such as Zincfix, acetone and ethanol resulted in efficient RNA recovery with Zincfix performing best and acetone and ethanol being less efficient but still permitting decent and comparable recovery rates (Mikulowska-Mennis et al., 2002; Schleidl et al., 2002) (Figure 3).

Generally, the fixatives with good recovery rates also preserved RNA integrity, which was evaluated by capillary electrophoresis using the Agilent 2100 bioanalyzer (Agilent Technologies, Waldbronn, Germany). The Agilent bioanalyzer allows quality RNA assessment by both computing the 28S/18S ratios and a parameter called the RNA Integrity Number (RIN), which takes into account the entire electrophoretic trace. RIN is based on evaluation of total eukaryotic RNA, including ribosomal RNA, using a numbering system from 1 to 10, with 1 being the most degraded profile and 10 the most intact. The quality of RNA for sections fixed with Zincfix, acetone and ethanol was very good with readily detectable 18S and 28S ribosomal peaks and with RINs ranging from 6.1 to 8.5. There appears to be controversy with regards to the integrity of RNA that can be extracted by ethanol-fixed tissues. Some reports (Goldsworthy et al., 1999; Mikulowska – Mennis et al., 2002; Schleidl et al., 2002, Wang et al., 2009) are in agreement with our results but others (Fend et al.,1999; Xiang et al., 2004; Huang et al., 2002; Gillespie et al., 2002) reported degraded RNA. Zincfix-fixed sections yielded RNA of integrity (RINs between 7.0 and 8.2) nearly as good as that of

unfixed (fresh) tissue which generally scored RINs between 7.7 and 9.5 (Figure 4).

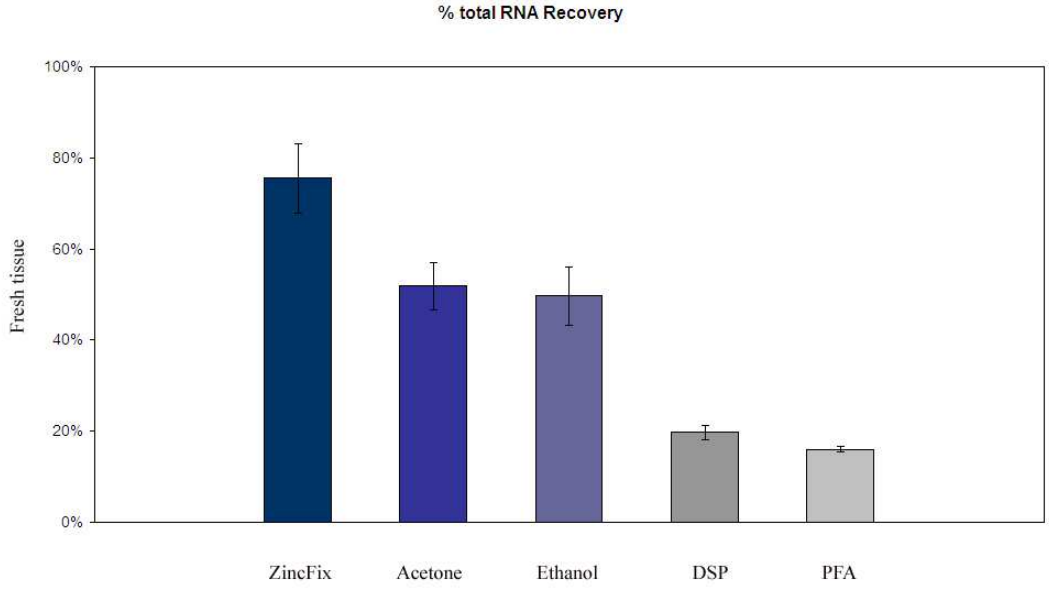

Figure 3. Several fixatives were evaluated for total RNA recovery. RNA content was quantified spectrophotometrically with the Nanodrop spectrophotometer and recovery rates are presented as the percentage of RNA recovered from fixed tissue with respect to RNA recovered from the same amount of fresh tissue.

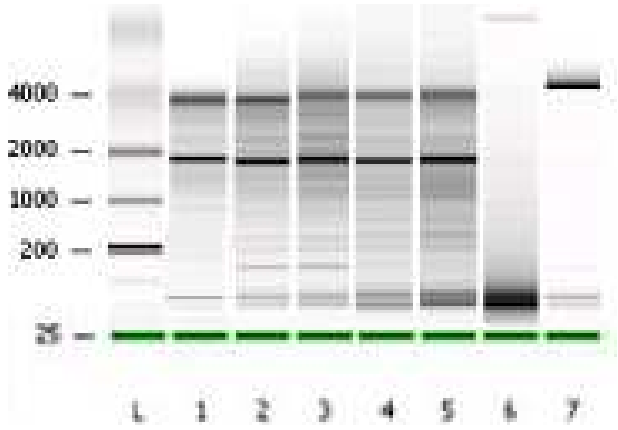

Figure 4. Quality of RNA from Nissl-stained mice cerebellar sections. Following extraction of RNA from unfixed (fresh) tissues (Lane **1**), or samples fixed in ethanol (**Lane 2**), acetone (**Lane 3**), Zincfix (**Lanes 4 & 5**), DSP (**Lane 6**), PFA 4% (**Lane 7**), the quality of the products were assessed with an Agilent Bioanalyzer. No RNA was recovered in tissues fixed with DSP (**Lane 6**) or PFA (**Lane 7**). Quality of RNA for the other samples was comparable and acceptable for use in expression profiling experiments. Zincfix-fixed sections showed overall RNA of higher quality. Sections in Lane 4 underwent a modified, quick, Nissl stain compared to tissue sections in Lane 5.

Some reports (Johansson et al., 2000; Schleidl et al. 2002; and Lykidis et al., 2007) describe Zincfix as an excellent fixative for preserving RNA integrity for downstream expression profiling experiments.

Two different Nissl staining protocols were used to stain sections for LMPC use. In the standard protocol, Zincfix-fixed mouse cerebellar sections were washed briefly in PBS, in 1% cresyl violet for 2 minutes, rinsed in DEPC-treated water and then dehydrated in a series of increasing ethanol gradients. In the quick cresyl violet staining protocol, Zincfix-fixed sections were taken through a 1 minute wash into a 70% EtOH solution and subsequently dipped for 2 minutes into a 1% cresyl violet solution prepared with 70% EtOH. Finally, sections were briefly washed in 100% EtOH and left to dry. The second protocol was short, comprised few simple steps and presented no need for washes in aqueous solutions, which should minimize RNA degradation (Burbach et al., 2003; Fink and Bohle, 2002). On the other hand, Nissl staining resulted much weaker compared to that of the standard protocol although tissue morphology was of similar quality (Figure 2). Further assessment of RNA integrity of the two staining methods performed with the Agilent Bioanalyzer showed high RNA quality for both methods with the quick protocol often being associated with higher RINs (Figure 4). The short protocol, because of its resulting in a faint staining, is useful when the cells to be isolated are easily distinguishable (Figure 2).

We have tested sections from transgenic TH-GFP/21-31 mice, that selectively express green fluorescent protein (GFP) in catecholaminergic cells under the control of tyrosine hydroxylase (TH) gene promoter (Sawamoto et al., 2001 and Matsushita et al., 2002), The only fixatives that preserved fluorescence of DA cells were PFA, DSP and Zincfix (Figure 5). Ethanol and acetone resulted in quenching of the green-fluorescent GFP signal.

To summarize, Zincfix efficiently recovered and preserved the integrity of RNA, mantained tissue morphology very nicely, allowed histochemical stainings such as Nissl stain or Fast Red (results not shown), and protected the fluorescence of GFP-expressing tissues, presenting as the optimal candidate for downstream LCM applications (Table 1).

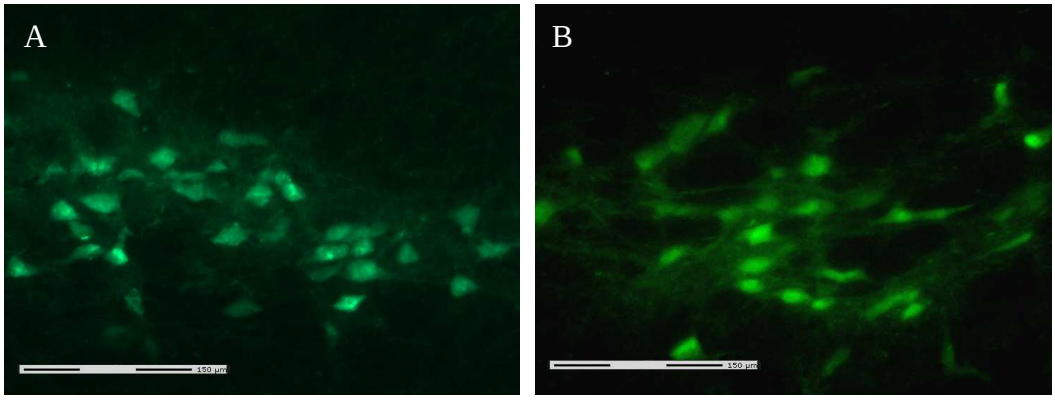

Figure 5. Mouse TH-GFP/21-31 mesencephalic sections fixed with A) PFA 4%, and B) Zincfix. Morphology and fluorescent signal of mDA cells are comparable.

Test	Fixative					
	Fresh	Acetone	Ethanol	Zincfix	DSP	PFA
RNA recovery	+++++	+++	++	++++	+	-
Nissl stain	-	+++	+++	++++	+++	+++++
GFP expressing tissues		-	-	++++	+++	++++

Table 1. Scores from mouse brain fixed in acetone, ethanol, Zincfix, DSP, PFA and fresh tissue.

Furthermore, Zincfix fixation can be performed prior to cryosectioning, contrary to precipitating agents adding value to the convenience and ease of use of this fixative. Zincfix became the fixative of choice for all subsequent experiments.

3.1.3 Zincfix as the fixative of choice: evaluation of the experimental procedure

3.1.3.a Improvement of tissue visualization

As mentioned in the previous paragraphs, for LMPC applications it is of utmost importance to have the possibility to discriminate cells and tissues, in order to be able to select with precision the structures of interest. This methodology though does not lend itself to that end. In fact, it is the opposite. In addition to the difficulties in finding a fixative that maintains decent morphology without interfering with downstream recovery of RNA and DNA, what adds to the loss of optical resolution is the omission of the coverslip and the use of the optics

of the LCM machine, which naturally are not those of a good fluorescent microscope.

We have met difficulties in discerning with precision all GFP-expressing DA cells in the mesencephalic sections of the TH-GFP/21-31 strain of mice. Adding a drop of ethanol on the sections as suggested by Grimm et al., 2004 was not helpful in our case as the GFP fluorescence quenched. The same happened when we embedded the tissue section with the polymeric and low viscose PALM LiquidCover Glass N, which, on the other hand, worked very nicely on Nissl-stained sections, significantly ameliorating morphological inspection. We subsequently tried to view DA GFP-fluorescent cells by adding a drop of Zincfix on the sections. A drop of Zincfix made cells visible. In fact, we could see cells that were not apparent before the addition of the Zincfix drop while achieving quenching of non specific fluorescent signals (autofluorescence of the tissue) (Figure 6).

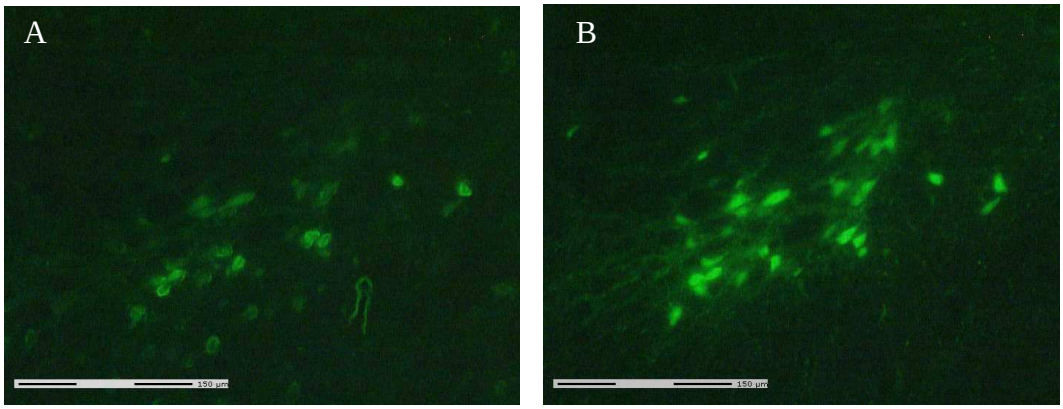

Figure 6. TH-GFP mesencephalic mouse sections fixed in Zincfix for LMPC. A) Dry, with no post-fixing, B) with the application of a Zincfix drop which allows better optical resolution.

We called the addition of Zinfix drops intended for DA cell observation the “post-fixing step”. We checked whether this operation could in anyway affect RNA integrity by extracting RNA from scraped sections. Results indicated that RNA quality of Zinfix-fixed sections and sections undergone the post-fixation step was comparable and often with the latter even showing better RNA preservation. This step was added to our microdissection protocol which comprises the following phases: fixation, OCT embedding (can be omitted), cryoprotection, cryosectioning, postfixation, LMPC, and finally RNA extraction.

3.1.3.b Storage of sections

Collecting specific cells from a complex tissue like the brain by LMPC is time-consuming especially if cells have to be collected one by one. We could collect DA cells from one or two slides, containing 4 to 6 mesencephalic sections, in one day at most. Remaining slides had to be stored for use in the following days. It was important to have the possibility to store sections for some time with no further RNA degradation and maintenance of tissue morphology.

We stored cerebellar sections from TH-GFP/21-31 mice under two different conditions for two months: a) in a box with dessicant at -80ºC, and b) in a box with silica gel balls, in a vacuum, in dry conditions. We then controlled whether cells were still recognizable for LMPC collection and whether RNA had been preserved at a good quality standard. Results were positive. Both storage modalities resulted in good preservation of the fluorescent GFP marker of DA cells. Fluorescent DA neurons became visible only after the addition of one drop of Zincfix on the region of interest in both dry and frozen stored sections (Figure 7). There was no significant deterioration of RNA integrity even after two months storage for any of the above storage conditions (Figure 8).

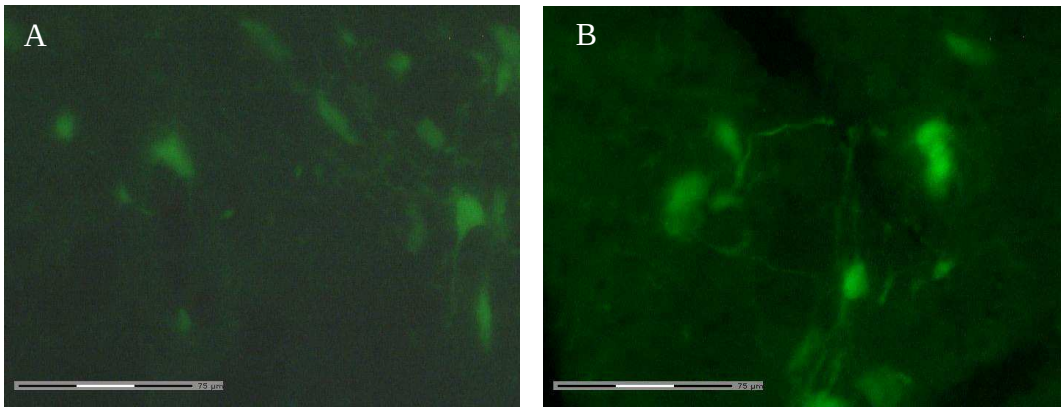

Figure 7. Inspection of TH-GFP/21-31 mesencephalic mouse sections fixed in Zincfix, after: A) two months storage in dry conditions, B) two months storage at -80ºC. A drop of Zincfix allows identification of cells and permits their collection by LMPC.

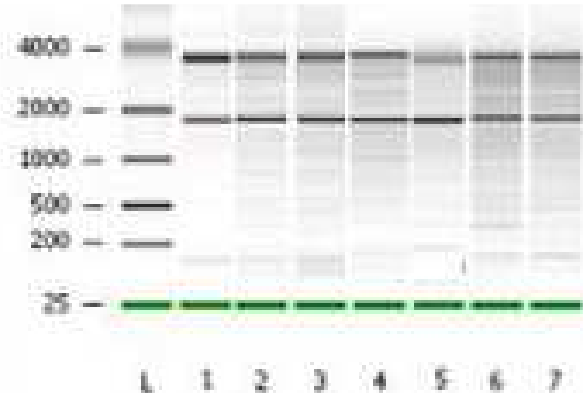

Figura 8. RNA from mouse brain subjected to quality analysis on an Agilent Bioanalyzer. Piece of fresh cerebellum (**Lane 1**), piece of cerebellum fixed in Zincfix (**Lane 2**), Zincfix cerebellar sections (**Lane 3**), Zincfix cerebellar sections with postfixation (**Lane 4**), Zincfix cerebellar sections with postfixation and subjected to laser-microdissection (**Lane 5**), 2 months old Zincfix cerebellar sections stored in dry conditions (**Lane 6**), 2 months old Zincfix cerebellar sections stored at -80ºC (**Lane 7**). Clear 18S and 28S RNA bands and no significant shift of RNA fragments to shorter migration times showed good RNA quality. RINs were between 6.6 and 8.6.

3.1.3.c LMPC collection

All the sections we prepared for LMPC were fixed in Zincfix as described in "Materials and Methods" and a drop of Zincfix was added on the region of interest to aid observation of the cells of interest. Cells to be collected were marked for dissection when still visible through the inverted microscope covered by the Zincfix drop and only cut with a UV-A laser and catapulted into a collecting device overlying the specimen with a precisely aimed laser shot in a second moment when the Zincfix drop evaporated and sections were completely dry. For our microarray experiments we used the PALM adhesive caps (caps coated with a white adhesive inert surface) as the collector device, but preliminary experiments were made by coating the caps with mineral oil (Sigma-Aldrich Chemie GmbH) to provide a sticky surface for the catapulted cells. Cell collection was verified by inspection of the cap at the end of every LMPC session (Figure 9). To optimize cell recovery the cap collector was brought as close to the specimen as possible. This shortened distance also permitted to use reduced LPC energy which protects from non specific carry-over of neighboring cell material (Burbach et al., 2003).

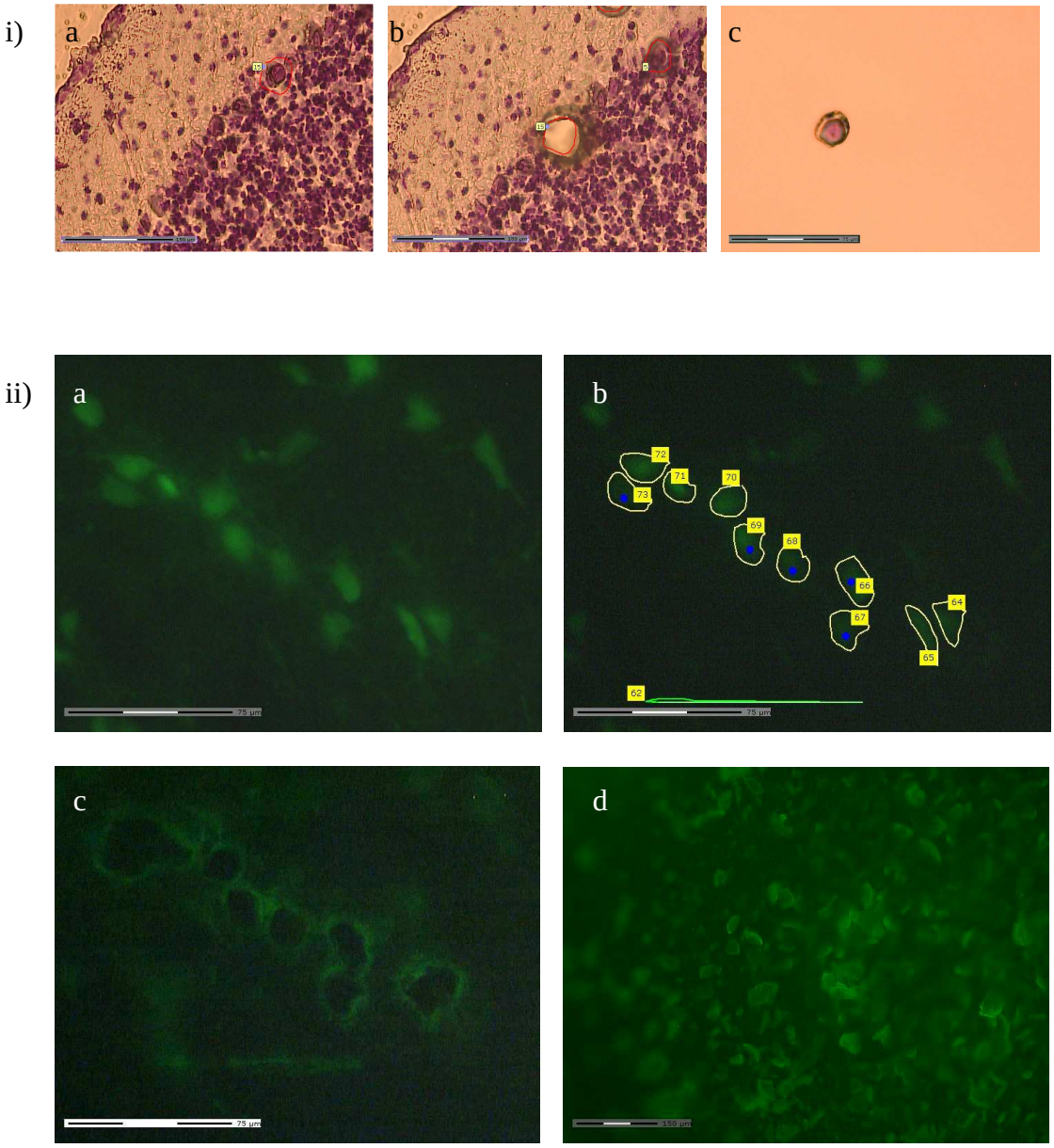

Figure 9. i) Zincfix-fixed, Nissl-stained mouse cerebellum. One Purkinje cell is selected (a), excised (b) and catapulted into a PALM adhesive cap (c). ii) Zincfix fixed TH-GFP/21-31 mesencephalic sections. Several TH-GFP expressing DA cells (a) are marked for collection (b), cut by the laser and catapulted (c) into the cap collector for microscopic inspection (d).

The application of a drop of Zincfix (post-fixation) on the demounted sections (see paragraph 3.1.3a) did not interfere with the process of LMPC.

All experiments regarding the evaluation of fixatives were performed using sections mounted on poly-ethylene-naphthalene (PEN) slides (PALM). These membrane-coated slides worked nicely with histochemical stains like cresyl violet and nuclear fast red. For the preliminary microarray experiments, sections

with TH/GFP-expressing DA cells were mounted on thinner PET-coated slides instead, which allowed better morphological evaluation and lower fluorescent background levels. Membrane-coated slides optimized tissue capture. When excised by the UV laser and catapulted on the cap collector, membranes transfered with them the overlying cells with just one laser shot, speeding the procedure and minimizing contamination from tissue debris created during the tissue cutting of the laser. Moreover, these inert membranes did not interfere with subsequent DNA or RNA applications. All microarray experiments on the contrary were performed using sections mounted on “Superfrost plus charged” (Menzel-Glaser) glass slides. We found that brain sections adhered better on glass rather than membrane. Glass slides also allowed best appreciation of the green fluorescent signal of the TH-GFP expressing cells while the + charged surface did not interfere with the process of cataplulting.

3.1.4 Zincfix fixation and amplification of specific cDNA fragments – Evaluation of RNA quality

To further test the compatibility of our LMPC-derived RNA for downstream applications such as hybridizations to cDNA microarrays, several specific gene transcripts amplifications were performed. For these experiments, PEN membrane-coated slides and PALM adhesive caps were used. Cells were collected from Zincfix, Nissl-stained mouse brain sections. DJ1 cDNAs with a length of ~600 bp were successfully amplified from fresh brain, Zincfix-fixed brain, Nissl-stained Zincfix sections, and 1000 LMPC Nissl-stained granule cells collected by their morphology and topography from the hippocampus. A first global amplification was followed by a specific PCR for the DJ-1 fragment. Extracted RNA was subjected to DNase treatment to get rid of any genomic material still present. No signal was observed after amplification of the negative RT control without addition of reverse transcriptase, nor was it noted for the H_20 control with reverse transcriptase but without cDNA (Figure 10).

Zincfix allowed the amplification of a fragment of cDNA of medium length. We next sought to see how low we could go with our starting material to achieve gene specific amplifications. After DNase treatment of extracted RNA,

gene specific PCRs for the SUMO-1 cDNA (fragment lenght: 196 bp) with no prior global amplification from 100 and 10 LMPC collected granule cells resulted in amplification of the fragment with a 50% success rate. As a control, few shots of membrane collected from a region of the slide adjacent to the LMPC processed tissue underwent the same experimental steps as cell samples to control for possible contamination with debris during the laser cutting. As expected, there was no amplification of the specific transcript neither for this type of control, nor for the H_20 control (Figure 11).

Intron-spanning primers were designed to circumvent the problem of unwanted genomic amplification, since many of the amplification experiments were performed with no prior RNA isolation or DNase treatment (see "Materials and Methods") to avert the difficulties met by a large elution volume (Fink and Bohle, 2002). Specific gene amplifications were so performed from 1000 hippocampal neurons and 1000 dopaminergic neurons microdissected from TH-GFP/21-31 mice sections. We looked for the presence of gene transcripts characteristic for the cells collected such as TH (present in DA neurons), MAP-2 (present in all neuronal cells), GFAP (present in astrocytes), and the housekeeping gene GAPDH. TH amplification produced a positive band in an agarose electrophoretic run with ethidium bromide for DA neurons and a thinner band for granule neurons from the hippocampal dentate gyrus. In fact, this should have been expected because of the innervation of this lamina by NA terminals originating in the Locus Coeruleus (Lindvall and Bjorklund, 1974; Loy et al., 1980; Oleskevich et al., 1989). MAP-2 was expressed equally well in both neuronal types. As cells were collected in small groups of three or four, contamination with astrocytes would have been unavoidable and that would explain the amplification of the GFAP transcript for both cell groups. GAPDH resulted to be present in both cell types as expected, but being an intronless gene, we could not discriminate whether the fragment was amplified from RNA or genomic material. The no RT control in this case resulted positive because of amplification being performed from a non purified RNA sample containing genomic material (see "Material and Methods").

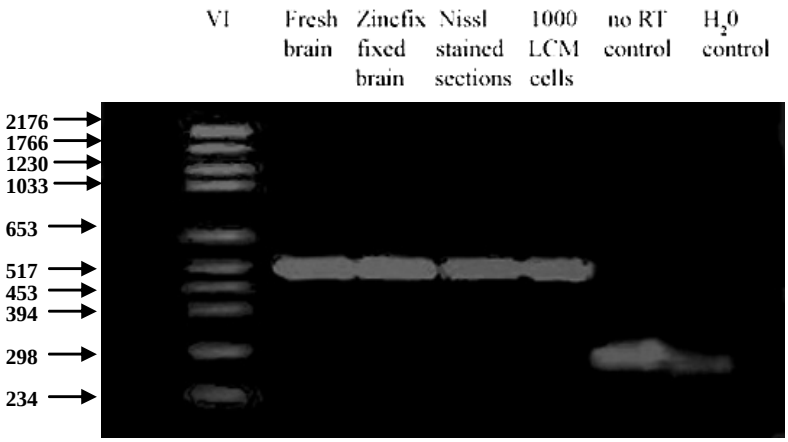

Figure 10. RT, global cDNA amplification, and one cycle of PCR for DJ1 (610 bp) cDNA from material originating from: 1) Fresh brain sections, 2) Zincfix-fixed brain sections, 3) Zincfix-fixed, Nissl-stained sections, 4) 1000 LMPCcollected cells, 5) RT mock control, 6) H_20 control**.**

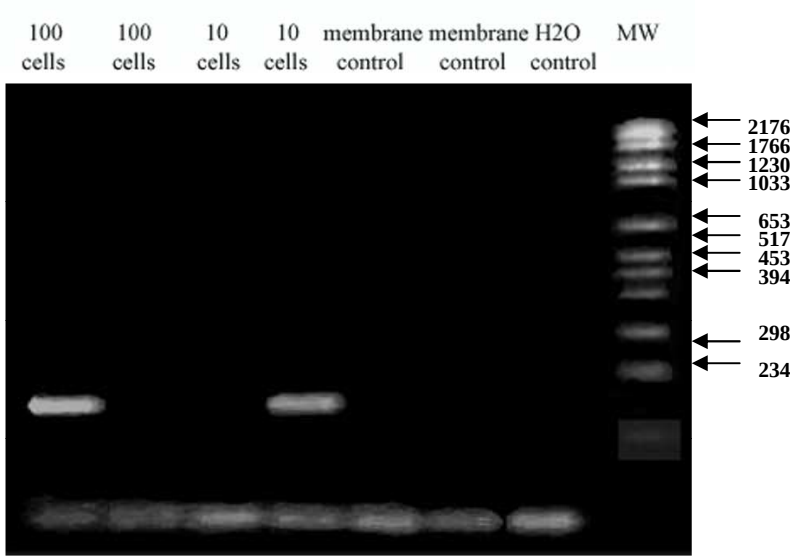

Figure 11. RT and specific PCR amplification for SUMO 1 (196 bp) fragment from 100 and 10 hippocampal microdissected cells. Controls: Membrane control, pieces of membrane excised and catapulted into a collector cap from membrane-coated slides and processed as cells samples. H_20 control: sample with H_20 instead of cDNA.

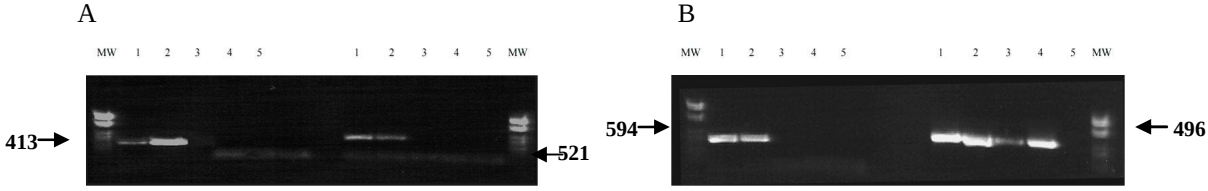

Figure 12. Reverse Transcription and specific PCR amplification for fragments: A) TH and MAP2, and B) GFAP, GAPDH. Samples: (1) 1000 granule cells from the hippocampus, (2) 1000 mesencephalic TH-GFP expressing DA cells, (3) no RT control for sample 1, (4) no RT control for sample 2, (5) H_2O control. RT control for the GAPDH fragment appeared positive since the gene is intronless and amplification was performed with no prior RNA purification or DNase treatment. All other primers were designed to be intron-spanning.

We looked at potential differences in the RNA quality derived from cells collected by LMPC from sections mounted on Superfrost plus charged glass slides and membrane-coated slides.

We noted no appreciable difference in RNA characteristics in terms of specific gene amplification (GFP cDNA amplification) between the two collection modalities, nor could we see any considerable difference in the degree of contamination from surrounding glial cells (GFAP cDNA amplification) (Figure 13). In other words, cells collected one by one from the glass slides showed similar degree of contamination with cells collected in small groups from membrane-coated slides. When we looked in the collected samples for contamination with astrocytes by quantitative real time PCR, we found it to be smaller when DA neurons were collected one by one. Real time PCR comparing A9 cells and A10 cells for the dopaminergic specific genes TH, DAT, and the astrocytic gene GFAP, indicated that TH and DAT were highly expressed in the A9 and A10 cell groups as expected, while GFAP resulted to be present, but in low quantities and with its expression being a little higher in A10 cells rather than A9 cells (Figure 13).

This could be due to the fact that A10 cells are typically smaller compared to A9 cells and hence more difficult to be selected for and dissected from the tissue section without carrying along contaminating astrocytes and other cell types. Moreover, for the same number of collected cells, the RNA quantity for a sample of A10 neurons should be, at best, half the RNA quantity of a sample of A9 neurons. As a result, contaminating RNA is less diluted in the A10 cell samples and becomes a stronger competitor in the amplification reaction. Real time curves were constructed with four dilution points and were normalized to the housekeeping gene actin and to a control sample derived from a TH-GFP/21-31 ventral mesencephalic dissection. In literature, Yao et al., 2005 and others, have noted a contamination of their SN samples with oligodendrocytes.

We also looked at the 3’/5’ ratio of a qPCR-amplified, widely expressed gene as the tranferrin receptor (TFRC), in a sample of A9, a sample of A10 LMPC collected cells and a cell sample from dissected total mesencephalon. Intronless primers (to circumvent problems deriving from genomic

contamination) were designed near the 5' and 3' ends of the aforementioned mRNA sequence. The ratios were close to 1 for all three samples indicating the balanced presence of the two ends of the 5.2 kb long transcript (Figure 14). This last control constituted further indication that cDNAs produced by reverse transcription at the end of our microdissection protocol were representative of the whole length of the transcripts.

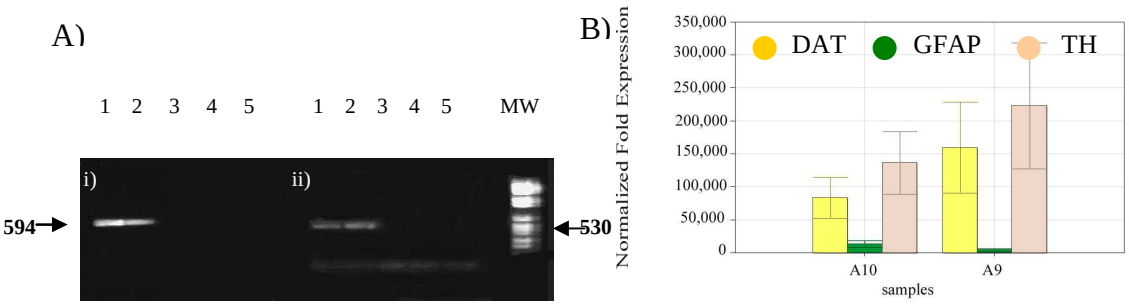

Figure 13. A) Reverse Transcription and specific amplification from 1000 TH-GFP expressing DA cells for i) GFAP fragments, and ii) GFP fragments, collected from: (1) membrane-coated slides in groups of two or three, and (2) glass slides one by one, (3) no RT control for sample 1, (4) no RT control for sample 2, (5) H_2O control.. There is not an appreciable difference in the RNA quality between the two collection modalities in terms of specific fragment amplification. B) Normalized expression of DAT, GFAP, and TH fragments in A10 and A9 cell populations as resulting from real time PCR. Both samples are contaminated with astrocytic material.

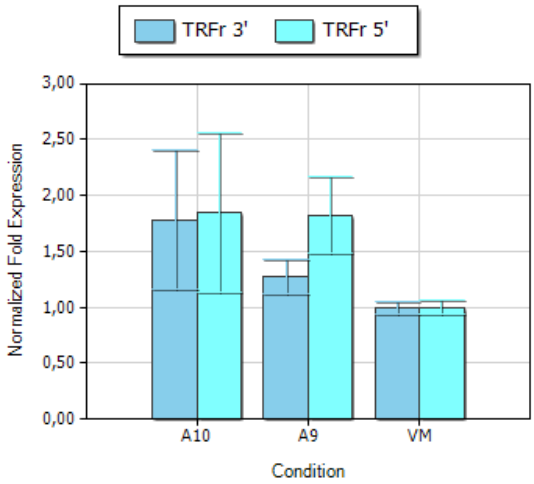

Figure 14. Expression of TRFr 3' and TRFr 5' ends in A10 and A9 and VM cell populations as resulting from quantitative real time PCR. The balanced amplification of the two ends of the transcript further supports the good RNA quality at the end of the microdissection protocol. VM: ventral mesencephalon, control sample.

Finally, we quantified the amount of RNA that we could obtain from 1000 singularly microdissected mDA cells and evaluated RNA quality with the Agilent Bioanalyzer. Typically, RNA recovered from 1000 cells collected by LMPC ranged between 2 ng and 3 ng, which is in agreement with published data (Schleidl et al., 2002) with characteristic RNA quality ranging between 6.1 and 7.5 (Figure 15).

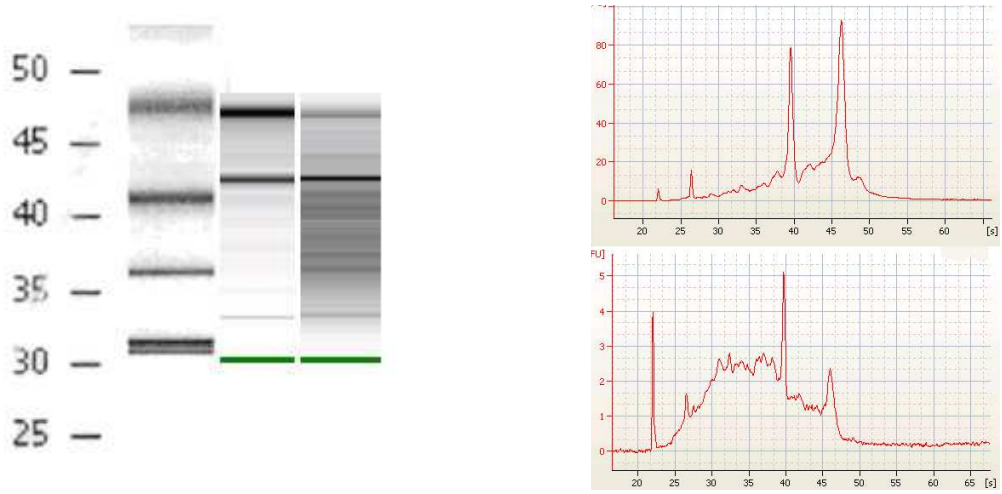

Figure 15. (1) RNA quality from a control sample (1) from fresh brain, and (2) from 1000 TH-GFP expressing dopaminergic cells selected and excised one by one from mesencephalic sections. A) 28S/18S ratios, and B) eletropherograms.

Loss of RNA quality occured during fixation (Figure 4) and further so during the microdissection process itself (Figure 8) and RNA extraction. The estimated loss in RNA content during the experimental procedure was calculated to be 40% to 50%, considering a theoretical total RNA content of 5 pg per cell, but the quality was good for downstream applications (Figure 16).

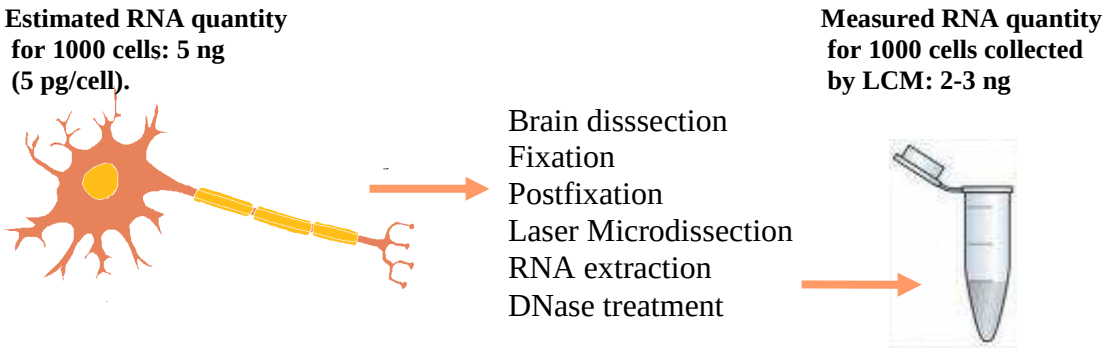

Figure 16. Schematic representation of the steps of the microdissection methodology with an estimate of RNA loss from the intact cell to the purified sample to be amplified and hybridized.

In light of the above results, to microdissect mDA cells from TH-GFP/21-31 mice brain sections, we used Superfrost plus charged glass slides and Zincfix as fixative and post-fixative to improve morphological visualization. The optimized protocol for gene expression analysis of laser-microdissected GFP-expressing cells is described in the box that follows.

Leave in 1X Zincfix/30% glucose solution to cryoprotect tissue overnight at 4˚C

↓

Embed in –Neg50 or O.C.T. compound (can be omitted)

↓

Snap freeze brain tissue in liquid nitrogen cooled isopentane

↓

Cut 14 µm sections and mount on plus charged Superfrost glass slides

↓

If not used immediately, sections can be stored either dry in a vacuum or at -80˚C or up to two months

↓

LMPC and harvest cells by visualizing them with drops of Zincfix

↓

Cells collected in dry sticky caps can be stored at RT in a vacuum (with desiccant) for few days if more samples are to be collected and pooled for a single RNA extraction

↓

RNA extraction

3.2 cDNA Hybridizations

3.2.1 Proof of Principle

Four experiments were conducted to provide proof of principle for the amplification protocol and the overall methodology, from cell collection to cDNA hybridization, to be used in our cDNA microarray expression profiling study. Isolation of mRNA, millionfold amplification and labelling of the resulting cDNA with Cy3-dCTP and Cy5-dCTP (PerkinElmer) were performed with the µMACS SuperAmp Kit (Miltenyi Biotec, Bergisch Gladbach, Germany), not yet released on the market, and a thermoMACS Separator (Miltenyi Biotec), according to the recommended protocol. These preliminary results were published as a customer report on Miltenyi's MACS&more newsletter (Vol 12 · 1/2008).

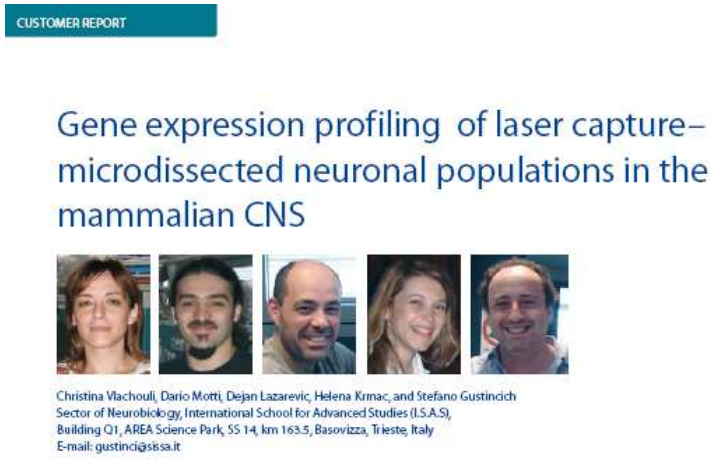

CUSTOMER REPORT

Gene expression profiling of laser capture–microdissected neuronal populations in the mammalian CNS

Christina Vlachouli, Dario Motti, Dejan Lazarevic, Helena Krmac, and Stefano Gustincich
Sector of Neurobiology, International School for Advanced Studies (I.S.A.S),
Building Q1, AREA Science Park, SS 14, km 163.5, Basovizza, Trieste, Italy
E-mail: gustinci@sissa.it

We tested the amplification kit on cultured striatal cells (Trettel et al., 2000) obtained by dilution and on hippocampal and mesencephalic dopaminergic cells collected by LMPC from TH-GFP/31-21 mice. These samples were processed for mRNA extraction and amplification with the µMACS SuperAmp kit (Miltenyi Biotec), which uses magnetic beads to specifically isolate messenger RNA. This RNA was then amplified, labeled with fluorophores and hybridized on home-made microarrays. The arrays used were home-spotted with the FANTOM 2 collection of mouse transcripts (Okazaki, Furuno et al., 2002; FANTOM International Consortium). 14 000 well characterized and non-redundant

transcripts from ~60 000 transcripts in the collection were chosen. Genes were represented in triplicate and the whole collection was printed on two slides, but only one of the two, the SISSA 2 slide bearing 7 246 transcripts, was used for our experiments.

More specifically, the description of experiments used as proof of principle for the overall methodology follows.

A) Experiment A: *300 striatal cells versus 300 mutant striatal cells.*

Striatal cells, derived from cell lines established from wild type and mutant Hdh^{Q111} knock-in mouse embryos (Trettel et al., 2000), were kindly provided to us by Dr Persichetti (Sector of Neurobiology, SISSA, Trieste). Cells were trypsinized, resuspended in DMEM, centrifuged, washed in PBS and dilutions of 300 cells/µl were prepared. The two samples were hybridized against each other on one slide. Amplified cDNA from wild type striatal cells was labeled with Cy3 and cDNA from mutated striatal cells with Cy5. This experiment was performed in order to test the efficiency of the SuperAmp amplification kit on a relatively low quantity (close to the recommended for good reproducibility limit of 100 cells) of unfixed cells of similar identity.

B) Experiment B: *100 mDA cells versus mDA cells.*

Two samples, of 100 mDA cells each, were LCM-isolated from one Zincfix-fixed mesencephalic section and co-hybridized on one microarray slide. With this experiment we tested the kit to its recommended limit. Moreover, we could evaluate the overall methodology, from tissue preparation, to cell isolation, amplification and hybridization on fixed cell samples of similar identity.

C) Experiment C: *100 mDA cells versus 100 granule cells*

One hundred mDA cells and 100 granule cells from the hippocampus were LCM-isolated and their extracted RNA amplified and labeled with Cy3 and Cy5, respectively. The purpose was, as for experiment B, to evaluate the overall methodology, using the kit to its limit, on fixed cell samples of different identity.

D) Experiment D: *Membrane Control*

Pieces of plain PEN membrane were excised and catapulted into a collection cap. This sample, processed exactly as the cell samples, was labeled with Cy3 and was

hybridized on one slide. (See Table 2 for results of amplification and labeling reactions for all four hybridization experiments).

Hybridization experiments	**Cy3 pmol/µl**	**Cy5 pmol/µl**	**ng/µl**	**µg**
Experiment A: WT Striatal cells vs Mutated Striatal cells	1.3	0.7	50	3.0
Experiment B: Midbrain DA cells vs Midbrain DA cells	0.9	0.5	51	3.0
Experiment C: Midbrain DA cells vs Granule cells	0.6	0.5	59	4.2
Experiment D: Membrane Control	1.1	0.8	137	8.2

Table 2. Incorporation rates for dCTP-Cy3 and dCTP-Cy5 and total cDNA quantification performed with the Nanodrop spectrophotometer at the end of the amplification and labeling reactions for each hybridization experiment.

The experimental procedure resulted to be relatively quick, straightforward and, most importantly, reproducible. Considering the very low amount of starting material (ranging from 100 to 300 cells), the cDNA yield at the end of the PCR reaction was good, typically ranging from 30 to 60 ng/ µl in a total volume of 60 µl. As only 200 ng of cDNA were needed for the labeling (Klenow) reaction, there was enough material left over to perform further experiments using the same PCR source. The quantitative yield of paired labeled samples to be co-hybridized on the same slide, after amplification, labeling and purification, ranged in general between 3.0 to 4.0 µg (Table 2), again well over the 2.6 µg needed for hybridization according to our protocol.

We were surprised to see that the membrane control sample resulted in four times the amount of labeled material of the cell samples, especially since each one of the cell samples consisted of two different labeling reactions (Table 2). Despite the high amount of hybridization material, the very few positive spots that appeared on the hybridized slide were mostly due to bacterial genomic DNA present on our cDNA slides as control spots (Figure 17). Presumably, genomic material or RNA species carried over with the enzymes used for amplification and labeling, not being competed by the whole spectrum of cDNAs present for instance in the cell samples, were exponentially amplified, resulting in such a high yield of labeled cDNA. From a technical point of view, the slides were clean and showed a very low background noise (Figure 17).

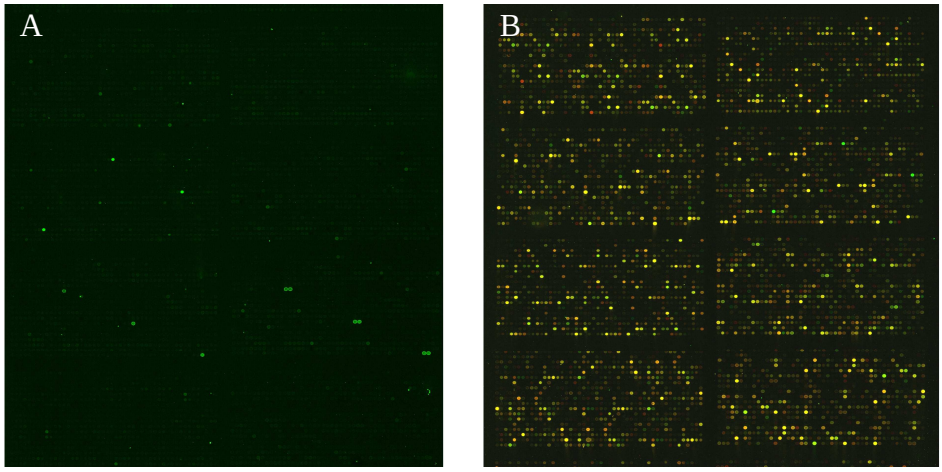

Figura 17. A) Part of the membrane control cDNA microarray slide: the green spots represent bacterial genomic DNA. B) Part of representative cDNA microarray slide probed with labeled cDNA from DA cells (Cy3, green signals) and granule hippocampal cells (Cy5, red signals).

A

Regression correlation	300 WT Striatal cells *	100 midbrain DA cells	100 midbrain DA cells	100 Aceton fixed Jurkat cells**	1000 Aceton fixed Raji cells**
300 Mutated Stiatal cells*	**0.92**				
100 midbrain DA cells		**0.94**			
100 Hippocampal neurons			**0.90**		
100 Aceton Raji cells**				**0.72**	
1000 Aceton fixed Jurkat cells**					**0.88**

B

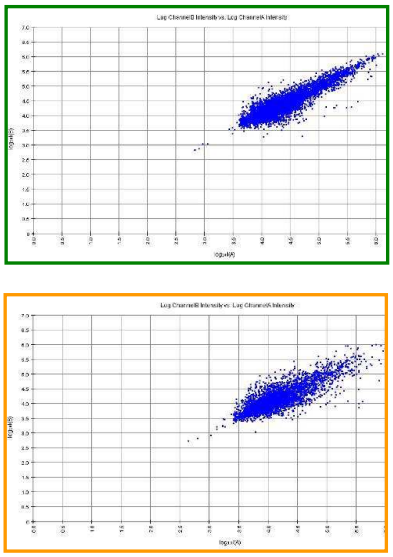

Figure 18. A) Pearson correlation coefficients for gene expression profiles of microdissected cells calculated for the pair-wise hybridizations described in table 2 are in agreement with data communicated by Miltenyi Biotec marked with **. Jurkat and Raji cells were cytospinned, fixed in acetone and microdissected, B) Log Intensity graphs presented for two of the experiments show nice spot distribution along the diagonal and regression correlation coefficients of 0.94 and 0.90 respectively.

Pearson correlation coefficients calculated for co-hybridized samples (Cy3 Intensity against Cy5 Intensity) were high as expected for similar cell populations. Moreover our results were in agreement with results obtained by Miltenyi (see above, Figure 18).

To assess the reproducibility of the method two experiments, experiment 1 featuring mDA cells labeled with Cy3 hybridized against total mesencephalic cells labeled with Cy5 and experiment 2 featuring the same two populations labeled inversely, were performed. These two hybridizations represent a technical replicate as the same pools of cells were used for two independent amplifications followed by cDNA labeling with Cy3 or Cy5 respectively (dye swap). The high linear correlation coefficient of the technical replicate (R=0.93) supports the reproducibility of the experimental approach and the amplification process (Figure 19).

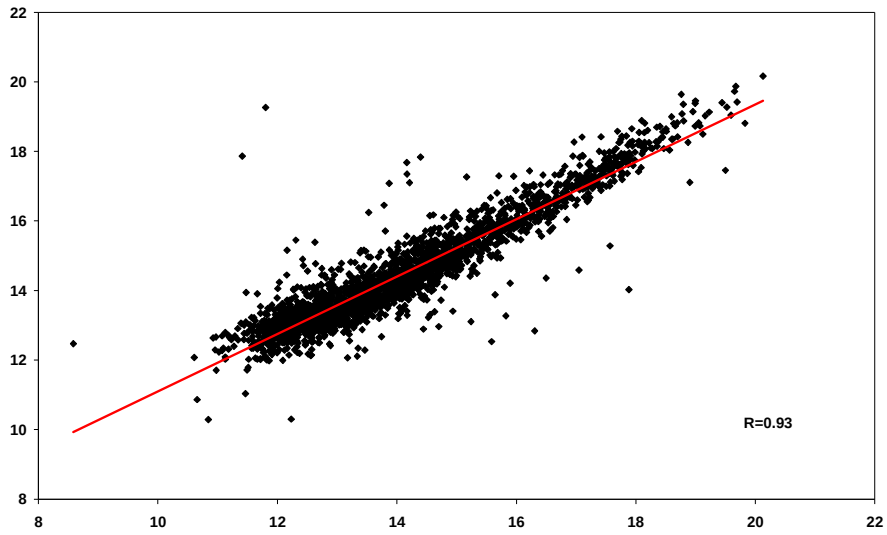

Figure 19. Reproducibility of gene expression profiling experiments, starting from 100 laser-captured cells from the SNc. The plot shows the correlation (R=0.93) of Intensities (I) of a dye-swap experiment. The samples were prepared by two independent amplifications, starting from common pools of cells, followed by cDNA labeling with Cy3 or Cy5, respectively.

3.2.2 Differential expression profiles between A9 and A10 cell population

To reveal molecular differences between A9 and A10 neurons, their gene expression profiles were determined with three different techniques: cDNA

microarrays (presented here) and nanoCAGE sequencing. To this purpose, we took advantage of the TH-GFP/21-31 line of transgenic mice where the majority of mDA neurons can be identified by their GFP labeling while A9 can be distinguished from A10 by their anatomical location. LCM was used to harvest A9 and A10 neurons from Zincfix-fixed tissue sections as described in "Materials and Methods".

For each cDNA microarray experiment 300 GFP-expressing DA cells from the A9 and 300 A10 DA cells were microdissected from mesencephalic sections, their RNA purified, amplified by μMACS amplification kit (Miltenyi Biotec), labeled, and used to monitor the differential gene expression profile between the two populations on custom-made cDNA microarray platform (SISSA arrays) in a direct design experimental mode. mDA cells were hybridized on the SISSA 2 slides which contain 7246 representative full-length cDNA clones of protein encoding genes from the FANTOM2 collection. In the nanoCAGE transcriptome analysis, 2000 mDA cells were isolated from each population and used as template for nanoCAGE, a modification of CAGE (Gustincich et al., 2008). In this technique full length cDNAs are selected and, after cleavage with a class IIS restriction endonuclease, 5' end tags are purified and sequenced. Transcription start sites (TSS) are then identified by mapping tags to the genome (Valen et al., 2008; Kodzius et al., 2006). In nanoCAGE, tags are synthesized from a small quantity of starting material from fixed tissue. The end result is that millions of tags are sequenced without cloning by using second generation sequencers. For our A9 and A10 populations TSS were identified and quantitively determined for coding and non coding expressed RNAs. Analysis from the nanoCAGE data is in progress.

For all transcriptome analysis experiments, I collected A9 DA cells from the rostral to the caudal end of SN, from coronal level 80 (at -2.555 from bregma along the anteroposterior axis) to coronal level 90 (at - 3.68 from bregma along the anteroposterior axis.). A9 cells from SN lateralis (SNl) were excluded from all the transcriptome analysis. A10 cells were collected from the VTA in between the same coordinates (Figure 20).

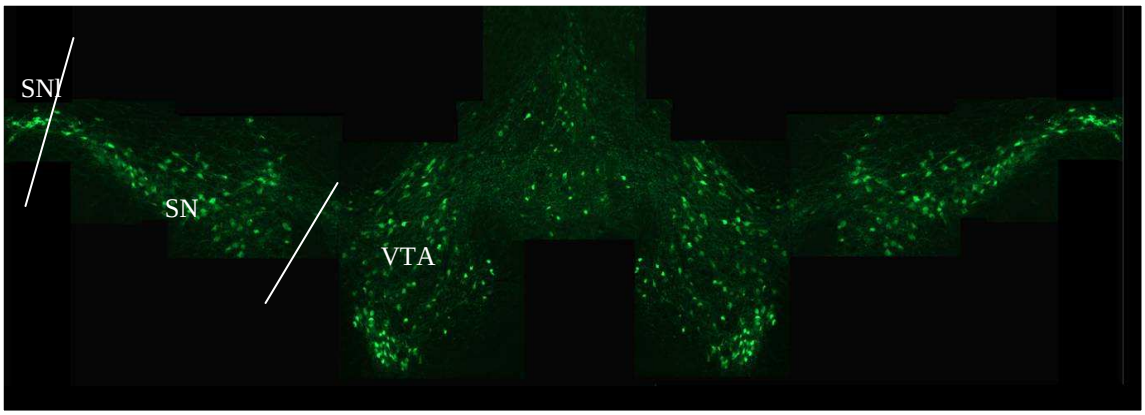

Figure 20. A midbrain section (bregma coordinates: -2.88 mm) from TH-GFP/31-21 mouse showing SN and VTA neurons. A9 cells from the SN and A10 DA cells from the VTA were collected by LMPC according to their GFP expression and topographic localization. A9 from the SNl cells were not included in the analysis.

Three biological replicates were used for hybridization on the cDNA microarray slides, but only two were included in the biostatistical analysis since quality controls showed that omission of one of the three replicates resulted in higher correlation of expressed spots. For each biological replicate there were three technical replicates, each of which with two dye orientations. Amplified material from the same PCR source was inversely labeled with Cy3 and Cy5 in different Klenow reactions. One hybridized slide was not included in the biostatistical analysis since technically did not present at a high standard. Thus, a total of 11 cDNA microarray slides were used to identify differentially expressed genes between the two mDA populations. Data processing was performed in the R computing environment using the LIMMA package from the BioConductor software project as reported in materials and methods. Of the 7246 clones on the microarray slide, 592 were determined to be differentially expressed at a statistical significance level of an adjusted $p \leq 0.01$. Of these 242 showed higher expression in A9 cells and 350 resulted enriched in A10 cells. The entire list of differentially expressed transcripts is available as a “Supplementary Table”.

The mean correlation coefficient relating the different values for signal intensity obtained between all 11 microarrays (2 A9 versus 2 A10 comparisons x three technical replicates x two dye swaps) was 0.94. Scatter plots of VTA signal intensity versus SN signal intensity with their related correlation values for all expressed spots for each slide of the microarray analysis can be seen in figure 20.

Correlations ranging from 0.92 to 0.96 calculated for the technical replicates between signal intensities of VTA versus SN, further supported the reproducibility of the overall methodology. At the same time, correlations ranging from 0.89 to 0.94 for the biological replicates indicated that the level of the majority of transcripts was not different between the two regions.

Differentially expressed transcripts were validated in two ways. First, previously reported gene expression differences between A9 and A10 neurons were verified. Twelve transcripts with higher expression in A9 cells (Grin2c, Cyp4v3, Nrn1, Ksns3, Rab3c, Mpp6, Drd2, Scg2, Ckb, Atp5j, Ldhb, Sri) and ten transcripts with higher expression in A10 neurons (Sdc2, Maoa, Calb1, Tacr3, Ndrg1, Gsbs, Rab3b, Slc7a3, Otx2, Gpr83) were found to be concordant in terms of expression enrichment towards the expected direction (SN and VTA respectively) with previous microarray studies (Greene et al., 2005; Grimm et al.,2004; Chung et al., 2005), in which, independent qPCR validation for some of the transcripts (amongst which, Mpp6, Ldhb Calb1) was also reported. Literature review further validated our microarray results for Calb1, Tacr3, and Drd2 (Hurd et al., 1994; Liang et al., 1996; Massi et al., 2000) (see Table 3). Discrepancies between these results and published data have not emerged with the exception of 4 transcripts from Greene's study. In particular, Arpc1b, Hmgb2, and Gabra4 here enriched in A9 cells, were reported to be enriched in A10 cells in Greene's report, while the inverse was true for the Csrp2 transcript. It is notable that there has been reported no further validation for these genes while the expression of Csrp2 gene in the Allen Brain Atlas showed no significant difference amongst the two subpopulations.

Second, expression of all transcripts that resulted differentially expressed in the A9 and A10 neuron populations from this microarray analysis were verified one by one with the expression data in the Allen Brain Atlas (ABA), which collects the gene expression patterns of over 21,000 genes, derived from high throughput, semi-automated in situ hybridization (ISH) on mouse brain sections.

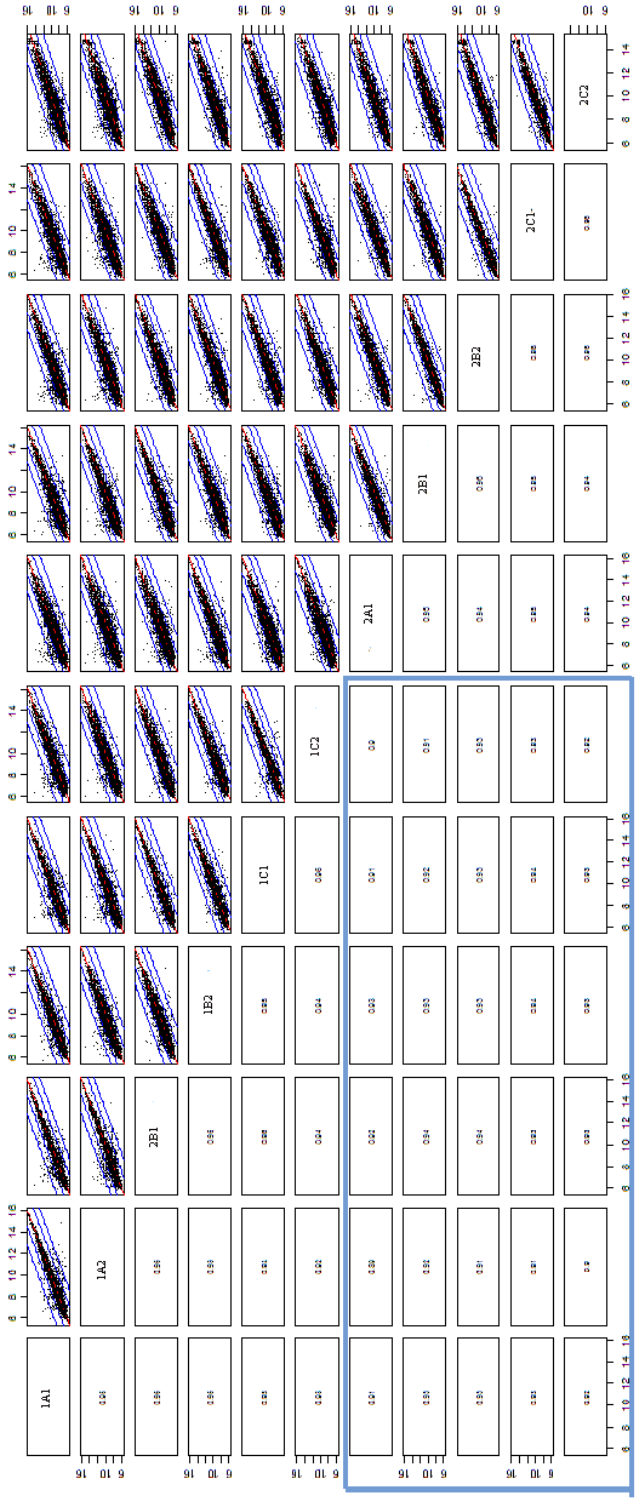

Figure 20. Scatter plots of differential miroarray results plotting fluorescence intensity (FI) of each gene from VTA (x-axis) or SN (y-axis cells). Plots and correlation coefficients highlighted with the blue rectangles refer to comparisons of samples from different biological sources (different mice). The rest of the plots regard the technical replicate samples with their dye orientations. In labels: first number (1 or 2) denote biological replicate, the letters (A, B, or C) technical replicate, and the third number (1 or 2) the dye swap.

Only coronal digital sections from the publicly available Allen's Brain Atlas ISH database at www.brain-map.org/ were used to verify the results as it was difficult to discriminate between the two subpopulations on saggital sections. Of the 242 transcripts resulting enriched in A9 neurons: 35 were not in the Atlas; 134 were represented on the Atlas by saggital sections and were not examined further; 21 were not discernable as to the expression pattern; 17 were ubiquitously expressed or not specific; 2 were expressed in the SNR; 18 transcripts were expressed in both populations. Eleven transcripts resulted enriched in the SN: Grin2c, Cyp4v3, Kcns3 (already reported by previous microarray studies), Hnt, Aurka, Cs, Mif, and Ndfu10 (not previously noted). Rab3c, Mpp6 and Ckb (also mentioned by previous studies) were positively correlated with both populations but with higher expression levels in A9 neurons. Of the 339 A10 enriched transcripts: 41 were not in the Atlas; 103 had only a saggital representation and were not examined further; of 30 transcripts I could not discriminate the expression pattern clearly; 9 transcripts did not seem specifically present in DA cells or showed widespread expression; 3 were present in the expanse of the SNR; 45 transcripts were expressed in both subpopulations. Nine transcripts were expressed only in A10 neurons or showed higher expression in A10 neurons. Amongst those, the already cited transcripts from previous microarray studies (Sdc2, Maoa, Calb1, Tacr3, Scg2) plus 3 transcripts, not described elsewhere (Whrn, Pdia5, Gpx3) (Table 3). In total, differential expression of 19 transcripts among A9 and A10 neurons was *in silico* validated by using the collection of in situ hybridization images from the Allen Brain Atlas.

Moreover, the results of this microarray study were compared with the list of genes compiled by Alavian et al., 2009, which was prepared after combining and comparing the results of the six major gene expression studies conducted on mesencephalic DA cells and verification of each gene in DA neurons with the aid of the Allen Brain Atlas. Forty seven genes (of which 19 described in the above paragraphs) resulted present in that list, which means that they were found expressed in the Allen Brain Atlas above background level in SN/VTA or both regions in saggital and coronal sections (Table 4).

Official Gene Symbol	Expression in Allen Brain Atlas	Confirmation	
		Previous gene expression studies (References)	Literature (References)
A9 DA cells			
Hnt	Yes		
Grin2c	Yes	Chung, Greene	
Cyp4v3	Low	Chung	
Nrn1		Greene	
Aurka	Very Low		
Cs	Yes		
Mif	Yes		
Kcns3	Yes	Greene	
Rab3c	Both populations but higher in A9	Chung	
Mpp6	Both populations but higher in A9	Chung *	
Drd2	BOTH populations	Greene	Hurd et al., 1994
Ckb	Both populations but higher in A9	Greene	
Ndufa10	Yes		
Atp5j		Greene	
Ldhb		Greene*, Chung*	
Sri		Chung	
A10 DA cells			
Sdc2	Yes	Grimm	
Maoa	Yes	Greene	
Whrn	Yes		
Pdia5	Yes – sparse		
Calb1	Yes	Chung*, Greene	Liang et al., 1996
Tacr3	Yes	Chung, Greene	Massi et al., 2000
Gpx3	Sparse, similar to Pdia5		
Scg2	Both	Greene	
Ndrg1		McKenzie	
Gsbs		Chung, Grimm	
Rab3b		Grimm	
Slc7a3		Greene	
Otx2		Chung	
Gpr83		Chung	

*** also validated by Real Time PCR**

Table 3. Differentially expressed genes between A9 and A10 neurons, verified on the Allen Brain Atlas, by previous microarray studies, and by literature search. Blank boxes in the "Expression in Allen Brain Atlas" column mean that the genes seemed expressed in both populations at a comparable level.

Genes espressed in SN/VTA in this gene expression study	Genes espressed in SN/VTA or both according to Allavian et al., 2009
Arl5a	Author not specified
Slc35c2	Author not specified
Tspan6	Author not specified
Cct5	Barret
Morf4l1	Barret
Ube2b	Barret
Ccdc91	Barret
Ssbp2	Barrett
Ndufa10	Barrett
Fdps	Barrett
Scg2	Barrett, Greene
Mpp6	Chung
Cyp4v3	Chung
Sri	Chung
Cs	Chung
Slco1c1	Chung
9130213B05Rik	Chung
Tomm20	Chung
Pdia5	Chung
Idh1	Chung
Otx2	Chung
Gpr83	Chung
Rab3c	Chung
Calb1	Chung, Greene
Grin2c	Chung, Greene
Gsbs	Chung, Grimm
Nrn1	Greene
Drd2	Greene
Atp5j	Greene
Ckb	Greene
Kcns3	Greene
Rgs2	Greene
Maoa	Greene
Slc7a3	Greene
Tacr3	Greene, Chung
Ldhb	Greene, Chung
Serpine2	Grimm
Lmo4	Grimm
Aurka	Grimm
Prmt2	Grimm
Akr1b3	Grimm
Rab3b	Grimm
Slc39a4	Grimm
Gpx3	Grimm
Ndrg1	McKenzie
Slc18a2	Steward
Ran	Thurret

Table 4. List of 47 genes common to our microarray results, to one or more of the six published mDA gene expression studies and to expression data from the Allen Brain Atlas. The genes are expressed either in SN or VTA or both mesencephalic subregions.

Associations of differentially expressed genes with *cellular component*, *molecular function* and *biological process* terms from the Gene Ontology (GO) database were examined by DAVID and clustering association analysis was performed after application of a threshold p-value ≤ 0.05 and a high stringency classification. Enrichment p-values were corrected to control family-wide false discovery rate with the Benjamini correction technique (david.abcc.ncifcrf.gov/; (Dennis et al., 2003; Huang et al., 2009). DAVID returned GO classifications related to one or more of the above terms for 183 out of 242 (75%) A9 enriched transcripts and for 259 out of 350 (74%) A10 enriched transcripts, using the *Mus musculus* database. Of these, for both populations, more than half were related with the *intracellular region* and the *cytoplasmic compartment* categories of the *cellular component* (*CC*) term, and when analyzed for the *biological process* (*BP*) term, more than half the transcripts resulted associated with the *metabolic process* category. Regarding the *molecular function* (*MF*) term, the majority of A9 transcripts (79 transcripts) associated with *catalytic activity*, while the majority of A10 transcripts showed a stronger significant correlation with the *protein binding* category (120 transcripts). Although the number of total microarray spots (7246) was limited for categorical analysis, few concerted gene differences between the two populations emerged. Genes related to the mitochondrion (26 transcripts), the synapse (5 transcripts), and the nucleolus (7 transcripts) were elevated in A9 neurons together with genes associated with generation of precursor metabolites and energy (13 transcripts), organic acid metabolic process (12 transcripts), nervous system development (14 transcripts) and negative regulation of signal transduction (6 transcripts) (Table 5). Similar results were obtained using KEGG pathway classification whereby oxidative phosphorylation, and glutathione metabolism pathways appeared enriched in A9 neurons. These results corroborate well with those of previous studies which noted enriched genes related to energy metabolism, organic acid metabolism, electron transport, mitochondrial proteins.

In A10 cells, genes were found elevated in association to the ribosome (14 transcripts) and the endoplasmic reticulum (23 transcripts), cell redox homeostasis

Enriched gene functional annotations A10

CATEGORY	ASSOCIATED GENES
Ribosome	Rps19, Rps4y2, Rps5, Apex1, Rplp1, BC003885, Rpl6, Rps17, Mrps17, Rps11, Mrpl22, Rps23, Rps12, Mrps11
Endoplasmic reticulum	Ssr2, Plod1, Ergic3, Ero1lb, 0610007P14Rik, Pdia5, Pdia6, Apex1, Upk3a, Sc4mol, Dad1, Srpr, Vwf, Hsd17b10, Txndc11, Tusc3, Gpsn2, Scd2, Agpat2, Dgat1, Dnajc10, Cyp2s1, Stau1
Cell redox homeostasis	Txndc11, Pdia5, Pdia6, Dnajc10, Apex1
Response to stress	Scg2, Asf1a, Idh1, Bax, Alkbh3, Pdia5, Ube2b, Dysf, Fancl, Nono, Apex1, Lta4h, Cd9, Vwf , Rpain, Sfpq, 2410012H22Rik, Gpx3, Hsp110, Dgkk
Lipid biosynthesis	Dctn6, Gpsn2, Scd2, Cyb5r1, Agpat2, 0610007P14Rik, Sc4mol, Lta4h, Fdps
Alcohol metabolism	Pmm2, Ldha, Cyb5r1, 0610007P14Rik, Maoa, Sc4mol, Fdps, Dcxr, Eno2, Pgam1
M phase of mitotic cycle	Ywhah, Trrap, Mad2l2, Wee1, Ndc80, Akap8, Rgs14, Ccnb2
Intracellular protein transport	Ssr2, Ap2a2, Xpo6, Gga3, Tmed1, Rab3b, Ran, Chchd4, Srpr, Rpain, Ywhah, Fndc5, Nxf1, Arl2, Rims2, Tomm20
Protein homotetramerization	Gpx3, Pcbd1, Actn2
Ribosome (KEGG pathway)	Rpl6, Rps17, Rps19, Rps11, Rps23, Rps12, Rps5, Rplp1, BC003885

Enriched gene functional annotations A9

CATEGORY	ASSOCIATED GENES
Mitochondrion	Uqcrc1, Atp5j, Sucla2, Fars2, Ywhaz, Mrpl43, Mfn2, Ndufa10, Ckb, Mrps7, Atp5c1, Atp5a1, Ndufs4, Shmt1, Mrpl2, Mrps5, Bckdha, Gpx4, Sardh, 1700020C11Rik, Scp2, abcb6, Cs, Cox10, Sh3glb1, Hspd1
Nucleolus	Lyar ly1, Rtf1, Ilf2, Nola2, Utp3, Lsm11, Bxdc5
Synapse	Camk2n1, Magee1, Gabra4, Grin3b, Grin2c
Generation of precursor metabolites and energy	Uqcrc1, Atp5j, Sucla2, Mdh1, Cyp4v3, Sardh, Nfia, Cs, Cox10, Atp5c1, Ndufs4, Atp5a1, Pycr2
Organic acid metabolic process	Qk, Scp2, Mdh1, Aldh1l1, Bckdha, Ndufs4, Fars2, Shmt1, Sardh, Pycr2, Sh3glb1, Plp1
Negative regulation of signal transduction	Chrd, Lect1, Chrdl2, Rgs16, Drd2, Socs2
Nervous system development	Chrd, Bzw2, Drd2, Socs2, Lmo4, Cfl1, Ndrg2, Qk, Nrn1, Chat, Utp3, Serpine2, Edg1, Plp1
Oxidative phosphorylation (KEGG pathway)	Uqcrc1, Ndufa10, Atp5j, Cox10, Atp5c1, Ndufs4, Atp5a1
Glutathione metabolism (KEGG pathway)	Ggt1, Gsst1, G6pdx, Gpx4
Citrate cycle (TCA) (KEGG pathway)	Cs, Sucla2, Mdh1
Glycerophospholipid metabolism (KEGG pathway)	Agpat4, Lcat, Chat, Sh3glb1
N-Glycan biosynthesis (KEGG pathway)	Mgat2, St6gal1, Stt3b

Table 5. Categorical differences between A9 and A10 populations using GO annotations and KEGG pathway classification. Some genes fall in more than one category.

(5 transcripts), response to stress (21 transcripts), intracellular protein transport (16 transcripts), lipid biosynthesis (9 transcripts), alcohol metabolism (10 transcripts), M phase of mitotic cycle (8 transcripts), protein homotetramerization (3 transcripts). These results are in accordance with a possibly more stable homeostatic environment of A10 neurons and the capability to respond readily to exogenous and endogenous insults by activating rapidly DNA repair mechanisms, rendering these neurons less vulnerable to disease . A fine control over the cell cycle may corroborate towards the same direction. KEGG analysis has highlighted only the ribosomal pathway (9 transcripts) as enriched in these neurons. For a comprehensive view of the genes see Table 5.

Other differences concerned the number of ion channels, with 5 transcripts (Grin2c, Ttyh3, Grin3b, Gabra4, Kcns3, 1700019N12Rik) found elevated in A9 cells versus one (Fxyd5) present in A10 cells. Selected genes will be discussed.

DISCUSSION

4.1 OVERVIEW

Our knowledge of brain functions and the complex disorders that affect the central nervous system at the molecular level have been hampered by the difficulties that emerge when studying such a complex organ. Amongst those are the high degree of cellular heterogeneity of the brain tissue – which may result in loss of detection of specific gene transcripts or of their enrichment in a cell type, because diluted by the expression profiles of neighboring cells – and the preparation of good quality samples from which to obtain the maximum amount of high quality RNA.

Recent development of the LCM technique, allowing *in situ* isolation of the desired cell type, along with reliable RNA extraction and amplification methods from small samples have made possible the implementation of genome-wide gene expression analysis on brain samples.

In the first part of this study we have optimized a protocol for laser-assisted microdissection of mesencephalic GFP-expressing DA neurons to be used in subsequent microarray profiling, and in the second part we have determined and compared the gene expression profiles of A9 and A10 DA populations with the intent to pick up genes that could underlie their selective vulnerability at a baseline level.

4.2 COMMENTS ON TECHNICAL DEVELOPMENT

Three are the aspects that have been addressed in the optimization of the LCM protocol:

a) tissue fixation in relation to both achieving *i*) clear histological visualization by Nissl staining and/or by retention of the fluorescence in GFP-expressing cells, and *ii*) good RNA recovery and retention of RNA quality,

b) improvement of tissue morphology at inspection, and
c) storage of sections.

We evaluated five fixatives, paraformaldehyde 4% (PFA), Zincfix, acetone, ethanol, and DSP, for two aspects: a) in terms of retention of histological details, by staining cerebellar and hippocampal sections in 1% water-based Nissl stain, and b) in terms of retention of fluorescence in GFP-expressing mesencephalic sections. We found that PFA 4% and Zincfix provided the best results in relation to Nissl-stained sections, and for DA GFP-expressing neurons of TH-GFP/21-31 mouse brain sections. Ethanol and acetone resulted in quenching of the green fluorescent signal.

Evaluation of fixatives in terms of RNA retrieval and integrity with cross-linking agents such as PFA and DSP resulted in poor if any RNA extraction, in agreement with the literature concerning PFA, but in contrast with Xiang et al., 2004, who have reported that DSP fixes soluble antigens and protects RNA in tissue sections. As stated in the "Results" chapter, our failure to extract RNA from DSP-treated tissues could have been due to the omission of a reducing agent such as DTT before RNA extraction that would have released the RNA immobilized by the crosslinking fixative. All precipitating agents – Zincfix, acetone and ethanol – resulted in efficient recovery of good quality RNA, with Zincfix performing best resulting in mRNAs characterized by RINs >7.0. This is in line with reports by several authors (Johansson et al., 2000; Schleidl et al. 2002; and Lykidis et al., 2007) which describe Zincfix as an excellent fixative for preserving RNA integrity for downstream expression profiling experiments. Ethanol is at the centre of a controversy for its effects on RNA quality with some reports claiming degraded RNA following extraction from ethanol-fixed tissues and others like a recent report by Wang et al., 2009 describing RNA profiles obtained by ethanol fixation with RINs >8.0. One other advantage of Zincfix is that tissues are fixed prior to cryosectioning, by immersion, which makes handling of samples easy and quick.

Two slightly different protocols, a standard 1% Nissl stain and a shorter ethanol based 1% Nissl stain, conducted on mouse wild type brain sections fixed in Zincfix, yielded RNA of comparable quality, although staining with the shorter

protocol resulted much weaker, revealing less morphological details, and hence being suitable only for the collection of easily recognizable structures. Reduced aqueous exposure by dipping sections in an ethanol based staining solution should protect from tissue RNases and subsequent RNA degradation. We noted that RNA from such stained sections was associated with higher RINs when compared to RNA deriving from standard stained sections, although this difference was not significant.

In LCM gene profiling studies, it is essential to be able to unequivocally identify and isolate the desired cell type which is in contrast with the methodology of tissue section preparation that requires sections to be used dry and uncovered, resulting in poor morphology. We had difficulties in identifying all fluorescent GFP-expressing cells of TH-GFP/21-31 mice mesencephalic sections because of background fluorescence. We found that visualization of cells is greatly improved by addition of Zincfix drops on the tissue sample to be microdissected. Cells become temporarily visible and can be outlined until the section is damp. Once the section has dried, the excision can take place. We have noted no interference of the dried solution, which acts as "coverslip", with UV laser cutting or catapulting of cell samples into the collector cap. No negative effects have either been noted in RNA quality retention. On the contrary, RNA quality often resulted better preserved in the sections which had been treated with Zincfix drops. We have included this step in our optimized protocol for LMPC and called this step the "post-fixation" step. Drops of ethanol have been used traditionally to ameliorate histological inspection or resins such as the PALM LiquidCover N, which can be thinned with EtOH to reach the desired viscosity, but none of the two have retained GFP fluorescence in the TH-GFP/21-31 mice mesencephalic sections, although they both have worked nicely on Zincfix Nissl-stained sections.

Laser-assisted microdissection can be time consuming, especially if cells need to be collected one by one. It may happen that cell harvesting needs to be continued in the next days, in order to be completed. Although the suggestion is to process slides as close as possible to the time of use of LCM, storage of sections becomes an unavoidable need to be addressed. We have noted that fixed TH-GFP cerebellar sections can be stored with no noticeable RNA degradation in boxes

with dessicant both at -80˚C and under dry conditions, in a vacuum, for up to two months. The two storage modalities are comparable both in terms of retention of GFP fluorescence and RNA integrity.

The successful amplification of cell-specific transcripts from as low as 10 microdissected cells demonstrates the sensitivity of the whole procedure, while the amplification of cell-specific transcripts with fragment sizes of more than 400 bp from 1000 cells or less, with conventional amplification methods, is indicative of the suitability of this LMPC-derived RNA for hybridization on DNA microarrays.

The amplification of GFAP mRNA by both conventional PCR and qPCR from LMPC-captured A9 and A10 cell samples suggests the presence of astrocytes, both when these are collected in groups of 3 or 4 and when they are harvested one at a time, but with contamination being smaller in the latter case. It is of note that the A10 samples showed higher astrocytic contamination than the A9 sample. This might indicate that A10 cells are more strongly associated with astrocytic cells or that, being significantly smaller in size with respect to A9 cells, they are more difficult to be precisely dissected. In fact, although LCM technology has been promoted for its ability to harvest single cells, the technology is best applied for capture of cell clusters and cell regions within a tissue section. Thinner sections and a higher number of collected cells are two ways for reducing contamination. If contamination is small it should be diluted out during the subsequent amplification procedure, assuming that gene expression profiling is intended next. Furthermore, a shorter distance between specimen and cap collector, which implies the use of lower energy both for the excision and cell transfer to the cap, can be another way to reduce contamination due to debris caused by high laser cutting energy. In most studies, LCM is performed on very thin sections (5-12μm). This thickness is considered as a monolayer of cells and will allow good visualization of the tissue. For larger cells, like mesencephalic DA neurons, we have used 14 μm thick sections, a thickness that represents a good compromise between decent optical resolution, good amount of collected material, and a low degree of contamination. As a final comment, we should say

that LCM-collected samples should be considered highly enriched as for the desired cell type rather than pure populations.

As to the slides employed in tissue section preparation for LCM, we have found that the best ones for use with TH-GFP mice mesencephalic sections are plus charged Superfrost slides, as they allow good tissue adherence and low background fluorescence. Moreover, it is easier to dissect cells one at a time from glass slides rather than from membrane-coated slides (PEN or PET for fluorescent structures).

To collect laser-assisted microdissected cells we have opted for PALM adhesive caps (caps coated with a white adhesive inert surface) as they permit visualization of cells at the end of the procedure and provide a dry environment for their short time storage until RNA extraction. Usually, samples were processed for RNA extraction at the end of each session, but if a number of cells was required so that more sessions for their collection were necessary, cells were left in the cap, stored in a box with dessicant, in dry conditions, in a vacuum, for up to a week. We could see no adverse effects on RNA integrity. We have finally noted that, even if the cap collector was brought very closely to the specimen to prevent loss of catapulted material, we could not avoid a 10% loss.

We have observed that 40% to 50% of RNA is lost during fixation, microdissection itself and the RNA extraction process. From 1000 singularly microdissected mDA cells we have extracted RNA quantities that ranged between 2 ng and 3 ng, which is consistent with published data (Schleidl et al., 2002; Wang et al., 2009), with characteristic RNA RINs ranging between 6.1 and 7.5. There are not many reports that use RIN to evaluate their RNA quality (Clément-Ziza et al., 2008; Kerman et al., 2006; Wang et al., 2009). The RINs associated with our LCM-derived RNA (6.1 to 7.5) are lower than, for example, the RINs (all above 8.0) reported by Wang et al., 2009, achieved for their LCM collected cell groups. We have to note though, that they fix their sections briefly in ethanol, while we fix ours for few hours and we cryoprotect the tissue overnight. This, of course, adds to the deterioration of RNA, but, at the same time, ensures better morphological inspection and excellent retention of the GFP fluorescent marker in TH-GFP transgenic mice brain sections, allowing microdissection at the single

cell level. Wang et al., in fact, collect relatively large areas of tissue, which should also result in less damaged RNA as the UV laser comes in contact with less tissue.

For RNA extraction, amplification and target labeling to be used in our cDNA microarray expression profiling study we have used the μMACS SuperAmp Kit (Miltenyi Biotec) that had not been released on the market at the time of this work and for which we have acted as a test site. Our preliminary results, conducted on limited starting material (100 to 300 LCM-isolated cells), resulted in good PCR amplification and efficient Klenow labeling with high Pearson correlation coefficients between signal intensities of co-hybridized samples of similar cell populations. Furthermore, a technical replicate consisting of two independent amplifications from a common pool of cells, labeled inversely, presented with a high linear correlation coefficient, supporting the reproducibility of the amplification process. The strength of this kit lies: a) in the one-step mRNA isolation (by small magnetic beads) and subsequent in column cDNA synthesis procedure, which reduces loss of material due to tube-to-tube transfer; b) the generation of small first-strand cDNA fragments of comparable length, reducing PCR bias in the subsequent amplification procedure which is also avoided by the use of a single-primer global PCR amplification procedure with uniform annealing conditions for all transcripts.

The correlation coefficients calculated for the signal intensities of the technical replicates, ranging from 0.92 to 0.96, and of the biological replicates, ranging from 0.89 to 0.94, for our compared A9 and A10 microdissected samples, further supported the strength of the overall experimental approach and indicated that the level of the majority of transcripts was not different between the two regions. In fact, relative to the total number of cells, the number of differentially expressed transcripts is <8%. Previous microarray gene expression studies comparing these two neuron populations (Grimm et al., 2004; Chung et al., 2005; Greene et al., 2005) are in agreement on an even more conservative figure of less than 5%.

Despite the similarity between the two regions, we have identified 592 out of the 7246 expressed transcripts to be differentially expressed between SN and VTA dopamine neurons at a statistical significance level of a p-value below 0.01.

Of these, 242 transcripts showed higher expression in A9 cells and 350 transcripts resulted enriched in A10 cells. We decided to use the adjusted p-value as the cut off threshold below which genes were to be considered differentially expressed and not the expression fold change. This is for two reasons: a) fold changes in this study are not very high as they range from a maximum of 3 fold to a minimum of 1 fold, but then this should be expected when comparing cells of the CNS; b) moreover, fold changes much depend on the biostatistical tool used and can be vary considerable for the same set of data.

4.3 DIFFERENTIAL GENE EXPRESSION BETWEEN A9 AND A10 NEURONS

Differences in gene expression data may be confirmed by qPCR and/or in situ hybridization. Instead, we verified all differentially expressed genes in silico, with the aid the in situ expression data of the Allen Brain Atlas and by literature review. Validation of transcripts with the Allen Brain Atlas does not constitute definite evidence of expression/absence of a transcript, but rather a strong indication that needs to be further confirmed, since not all images are clear and sections have not always been taken at evenly spaced intervals resulting in areas of interest not well represented and of difficult interpretation. Nonetheless, we have found 30 differentially expressed genes by in situ hybridization, of which 8 not noted by previous microarray hybridization studies.

Comparison of the differentially expressed transcripts herein presented with those found by other microarray gene expression studies has produced a number of genes that are consistent in their expression in terms of direction, A10 rather than A9 population or the inverse. This is important if we consider that these analyses have been conducted on different array platforms and on different species (rat cdna microarrays for Grimm et al., 2004; mouse Affymetrix platform for Chung et al., 2005; rat Affymetrix platform for Greene et al., 2005). Moreover, further validation of transcripts expressed in the mesencephalic DA neurons (SN + VTA) has come from the comparison of the present results with those described in the retrospective study by Alavian et al., 2009, who have compiled a list of transcripts common to all six existing gene expression studies

performed on mesencephalic DA cells and present in either saggital or coronal sections of the Allen Brain Atlas. In addition to the above mentioned 30 genes, other 17 transcripts were identified. None of our differentially expressed genes was in contrast with existing in situ hybridization or validated data. These figures further support the strength of this differential expression study, of its results, and of the overall methodology, from laser-assisted cell isolation to amplification and finally array hybridization.

Eight genes (Mif, Hnt, Ndufa10, Aurka, Cs, enriched in A9 neurons and Pdia5, Whrn, and Gpx3 enriched in A10 neurons), not noted or confirmed as differentially expressed before, emerged from our analysis. The most interesting amongst these A9 expressed neurons are neurotrimin (Hnt) and macrophage migration inhibitory factor (Mif). Hnt is a neuronal adhesion molecule that seems to inhibit axonal outgrowth, which is important in development of CNS and sympathetic nervous system (Gil et al., 1998; Struyk et al., 1995). It is a glycosylphosphatidylinositol (GPI)-anchored protein, expressed in distinct neuronal systems, and regulates the development of neuronal projections via attractive and repulsive mechanisms that are cell type specific and are mediated by homophilic and heterophilic interactions. As an axonal growth inhibitor it may prevent neuronal regeneration or maintenance of synaptic connections in disease states, but at the same time it could be important in repair by helping direct appropriate connections. Mif is a candidate pro-inflammatory cytokine involved in hormonal regulation of inflammation (i.e. estrogen inhibits local inflammatory response by down regulating Mif (Ashcroft et al., 2003). At sites of inflammation, it may have a role in regulating the function of macrophages in host defense. In Alzheimer's disease it has been found associated with amyloid plaques and it has been implicated in MS disease progression. It has a role in the regulation of the cell cycle and thus of normal and malignant cell growth. This corroborates well with the hypothesis that sees neuroinflammation involved in the pathogenesis of PD. Aurora kinase A (Aurka) is a kinase with a control over the cell cycle and a very weak expression in the Atlas. Cells over-expressing Aurka inappropriately enter anaphase despite defective spindle formation. Mitosis is subsequently arrested by failure to complete cytokinesis, resulting in multinucleation. Nadh

dehydrogenase (ubiquinone) 1 alpha subcomplex 10 (Ndufa10) mediates the transfer of electrons from NADH to ubiquinone of the respiratory chain, while citrate synthase (Cs) is the pace-making enzyme in the first step of the citric acid cycle, found in nearly all cells capable of oxidative metabolism. The two latter transcripts are widely expressed, but they appear to be particularly abundant in A9 cells. This is in line with the notion that sees SN neurons under higher metabolic drive and thus highly energy (ATP)-dependent. Amongst the A10 enriched genes, pdia5 is a disulfide-isomerase related protein that catalyzes the rearrangement of -S-S- bonds in proteins. It has been implicated in maintenance of cellular homeostasis, response to stress, and protein folding. Gpx-3 is a gene product that belongs to the glutathione peroxidase family, which functions in the detoxification of hydrogen peroxide. It has been reported that increased Gpx-3 could play a significant role in protecting cardiomyocytes from oxidative stress caused by hyperglycemia (Iwata et al., 2006) while it seems induced in kidney under oxidative stress conditions (Shirota et al., 2006). Pdia5 and Gpx3 show a similar and very particular pattern of expression in the Allen Brain Atlas, with a low and sparse expression. Whirlin (Whrn) encodes a PDZ scaffold protein with expression in both hair cell stereocilia and retinal photoreceptor cells (Eberman et al., 2007). It could be important in linking the cytoskeleton with scaffold transmembrane proteins, having both a structural and signaling role.

It is commonly accepted that the strength of genome wide studies lies in the possibility they offer to identify coordinated gene differences to interpret diverse mechanisms of action, rather than looking at the single gene. Although this work does not represent a complete genome scan, but instead more a large scale survey with only 7246 genes having been enquired, some interesting gene concerted differences have emerged.

Genes related to the mitochondrion, the synapse, the nucleolus were elevated in A9 neurons, together with genes associated with generation of precursor metabolites and energy as well as transcripts implicated in nervous system development. These results are in line with those of previous studies which noted enriched genes related to energy metabolism, organic acid metabolism, electron transport, and mitochondrial proteins. The first categories

that emerge as differentially expressed are mitochondrial transcripts and genes related to generation of energy, which is in agreement with the involvement of complex I dysfunction in human PD pathogenesis (Parker et al., 1989; Schapira et al., 1989, 1990). As discussed earlier, SN cells are thought to be under greater metabolic demand because of higher neuronal activity (Williams et al., 1998). Higher metabolic rates may result in greater levels of oxidative stress, making A9 cells more vulnerable to complex I inhibition. Furthermore, looking in detail at the list of differentially expressed genes, by gene classification, kinase/phospatase related metabolism transcripts emerge as enriched in A9 cells, also reported by Green et al., 2005. Evidence exists for aberrant kinase or phosphatase signaling to be contributing to neurodegeneration in dopamine neurons (Zeevalk et al., 2001). Protein glycosylation and regulation of translation also seem upregulated in A9 cells.

In A10 cells, transcripts were found elevated in association to the ribosome, the endoplasmic reticulum and the *biological process* categories of cell redox homeostasis, response to stress, intracellular protein transport, lipid biosynthesis, alcohol metabolism, M phase of mitotic cycle, protein homo-tetramerization. As mentioned in the “Results” section, these categories are in accordance with a higher compensatory capability of A10 neurons in response to exogenous and endogenous insults. The higher expression of DNA repair associated transcripts in these cells could have a synergistic role in their resistance to neurodegeneration. A finer control over the cell cycle may corroborate towards the same direction.

Other differences concerned the number of ion channels, with 5 transcripts (Grin2c, Ttyh3, Grin3b, Gabra4, Kcns3, 1700019N12Rik) found elevated in A9 cells versus one (Fxyd5) present in A10. A higher presence of ion channels could render cells of the SNc more vulnerable to eventual imbalances of ion fluxes with an effect on membrane excitability and possibly its destabilization. In particular, Grin2c and Grin3b are NMDA receptors of glutamate-gated ion channels, with voltage dependent sensitivity to magnesium and both mediated by glycine. The first with a double channel conductance is characterized by high calcium permeability, the second with a single channel conductance by low calcium

permeability. This finding is in agreement with a possible greater susceptibility of SN neurons to glutamatergic input proposed by Beal in 2000. Kcns3 is a potassium voltage-gated late rectifier channel while Gabra4 is an inhibitory GABA receptor that opens a chloride channel. Both these channels, however, do not show a high fold difference between the two subpopulations. In contrast, Ttyh3, which is a probable large-conductance calcium-activated chloride channel, and the 1700019N12Rik gene or TRAAK, which is an outwardly rectifying potassium channel belonging to K_{2P} channel family, resulted highly enriched in A9 neurons. It has been shown that lipophosphatidic acid (LPA), an abundant cellular lipid, as well as polyunsaturated fatty acids, including arachidonic acid (AA), reversibly open TRAAK channels, directly linking the lipid status to cell electrogenesis (Chemin et al., 2004). TRAAK has been also reported to open upon intracellular alkalosis (Kim Y et al., 2001). Chemin et al., 2004, hypothesize that intracellular LPA sensitizes K_{2P} channels to membrane stretch through a membrane effect of LPA and not through direct binding. They also suggest that this form of ion channel regulation may be involved in normal physiological functions as well as in various disease states, including neurological disorders. The mode of action of these channels through desensitization implies that in the physiological setting, transient stimuli can have large effects without the channels dominating the steady-state background (Chemin et al., 2004).

Tacr3 and Gpr83 are neuropeptide Y receptors with neuroprotective effects and have been extensively reported as enriched in VTA and contributing to the resistance of these neurons to toxins. Amongst the genes enriched in A10, syndecan 2 (Sdc2) has been implicated in synaptic plasticity and G substrare (Gsbs) in learning and long term potentiation. Moreover, expression of glutathione-S-transferase, pi (gstp2) may protect from oxidative damage. All these functions have been traditionally correlated with A10 neurons.

Looking again at single genes that have emerged as differentially expressed between the mDA populations in this study, I would choose to validate the following transcripts.

A) In relation to A9 neurons:

1. Serine (or cysteine) peptidase inhibitor, clade e, member 2 (Serpine2). It is a serine protease inhibitor of thrombin, trypsin, tissue plasminogen activators (tPAs), and urokinase plasminogen activators and a neurite outgrowth promoter. There is evidence that Serpine is inactivated by xanthine oxidase-derived free radicals. It has been suggested that protection of Serpine2 in Alzheimer's or Parkinson's diseases, could be a possible target for a therapeutic function of antioxidants (Bolkenius et al., 1995).

2. Neuritin 1 (Nrn1). It promotes neurite outgrowth and especially branching of neuritic processes in primary hippocampal and cortical cells and it has been suggested that it may take part in an activity-regulated transcriptional program that directs long-term changes in synaptic connections (Fugiino et al., 2003).

3. Single-stranded DNA-binding protein 2 (Ssb2). Since Ssb1 and Ssb2 are believed to promote proper folding of proteins as they are synthesized, their absence or altered function might result in misfolded forms of proteins, which could accumulate in the cell.

B) In relation to A10 neurons:

1. Secretogranin-2 (Scg2) is a neuroendocrine secretory granule protein, which may be the precursor for other biologically active peptides.

2. Sphingomyelin phosphodiesterase 2, neutral (Smpd2). It converts sphingomyelin to ceramide through hydrolysis. It has been reported that various oxidative stress-inducing agents lead to the activation of neutral sphingomyelinase and the production of ceramide. It is interesting to note that antisense knockdown of neutral but not acidic sphingomyelinase ablated oxidative stress-induced apoptosis and cell death in human primary oligodendrocytes (Jana et al., 2007). Moreover, impairment of lysosomal ceramide metabolism has been proposed as a possible pathway leading to Parkinson’s syndromes (Bras et al., 2008).

3. Low density lipoprotein-related protein 1(Lrp1). It is an endocytic receptor. It is suggested that LRP1 mediates anti-apoptotic functions in differentiated neurons by regulating several signaling pathways critical for neuronal survival (Fuentealba et al., 2008).

4. Similar to 1-ACYL-SN-GLYCEROL-3-PHOSPHATE ACYLTRANSFERASE BETA (Agpat2). This gene encodes a member of the 1-acylglycerol-3-phosphate O-acyltransferase family. The protein is located within the endoplasmic reticulum membrane and converts lysophosphatidic acid to phosphatidic acid, the second step in *de novo* phospholipid biosynthesis. Mutations in this gene have been associated with congenital generalized lipodystrophy (CGL), or Berardinelli-Seipsyndrome, a disease characterized by a near absence of adipose tissue and severe insulin resistance.

With this work we have devised a valid methodology for laser-assisted isolation of TH-GFP expressing mesencephalic dopaminergic cells from TH-GFP/21-31 transgenic mice, and the subsequent sample preparation for hybridization on cDNA microarrays. Our results constitute a description of a large mRNA expression analysis from which several interesting genes, to be further confirmed, have emerged. From here, several hypotheses can be advanced towards the susceptibility differences seen in the two populations, namely A9 and A10 neurons, based on concerted or single gene differences that have been detected, but with some limitations. This difference in susceptibility, although it has been largely proposed to be due to intrinsic factors, which can be addressed with these type of studies, is also certainly due to circuitry differences and glial cell associational differences. Finally, we have to keep in mind that post-translational modifications may change relations between mRNA expression and protein function, which makes testing of hypotheses at the protein level a necessary complement.

ACKNOWLEDGEMENTS

I would like to express my gratitude to the people in the lab that have been there for me, in one way or another, during these last four years, and especially:

My supervisor **Stefano** Gustincich for the opportunity he gave me to grow scientifically. Thank you for your encouragement and enthusiasm! **Dejan** Lazarevič for cDNA microarray probe preparation but most of all for his invaluable scientific support, and for looking at things always from the bright side. Thank you for your friendship! **Helena** Krmac for cDNA microarray probe preparation and for our long talks and good company during coffee breaks and lunch times. **Marta** Biagioli for useful discussions and being always so cheerful and willing to help. **Paola** Roncaglia for the microarray data analysis in the R environment. **Tullio** Bigiarini for his technical support. Thank you for making work in the laboratory so much easier. All my colleagues in the group, for making the laboratory environment a nice and friendly place to work in.

I would like to thank Dr Loris De Cecco, Dr Manuela Gariboldi, and Dr Marco Pierotti (IFOM, Milan) for printing of cDNA microarrays; Prof. Kazuto Kobayashi (Fukushima Medical University, Japan) for sending us the TH-GFP/21-31 transgenic line of mice; Dr. Francesca Persichetti for kindly providing to us the striatal cells, derived from wild type and mutant Hdh^{Q111} mouse cell lines; Prof. Giampiero Leanza (Università di Trieste, Italy) for teaching me stereotaxic injection surgery. I would also like to thank Dr. Marco Stebel and Dr. Cristina De Grassi (Università di Trieste, Italy) for their great work at the animal house facility.

Finally, I would like to thank my husband Daniele for all his patience and for his taking care of me when I worked until late at night, and my daughter Eva for cheering me up with her smile. Thanks to all my friends and family that have been there for me during this PhD.

REFERENCES

Aarsland D., Tandberg E., Larsen J.P., Cummings J.L., 1996. Frequency of dementia in Parkinson disease, *Arch Neurol* **53**, 538–542.

Agid Y., 1991. Parkinson's disease pathophysiology. *Lancet* **337**, 1321-1324.

Alavian K.N., Simon H.H., 2009. Linkage of cDNA expression profiles of mesencephalic dopaminergic neurons to a genome-wide in situ hybridization database. *Mol Neurodegener* **4**(6).

Andersson E., Tryggvason U., Deng Q., Friling S., Alekseenko Z., Robert B., Perlmann T., Ericson J.,2006. Identification of intrinsic determinants of midbrain dopamine neurons. *Cell* **124**, 393-405.

Aoyagi K., Tatsuta T., Nishigaki M., Akimoto S., Tanabe C., Omoto Y., Hayashi S., Sakamoto H., Sakamoto M., Yoshida T., Terada M., Sasaki H., 2003. A faithful method for PCR-mediated global mRMA amplification and its integration into microarray analysis of laser captured cells. *Biochem. Biophys. Res. Commun.* **300**, 915-920.

Arlotta P., Molyneaux B.J., Chen J., Inoue J., Kominami R., Macklis J.D., 2005. Neuronal subtype-specific genes that control corticospinal motor neuron development *in vivo*. *Neuron* **45**, 207-221.

Ashcroft G.S., Mills S.J., Lei K., Gibbons L., Jeong M.J., Taniguchi M., Burow M., Horan M.A., Wahl S.M., Nakayama T., 2003. Estrogen modulates cutaneous wound healing by downregulating macrophage migration inhibitory factor. *J Clin Invest* **111**, 1309-1318.

Baldareschi M., Di Carlo A., Vanni P., Ghetti A., CArbonin P., Amaducci L., Inzitari D., 2003. Lifestyle-related risk factors for Parkinson's disease: a population-based study. *Acta Neurol Scand* **108**, 239-244.

Barrett T., Xie T., Piao Y., Dillon-Carter O., Kargul G.J., Lim M.K., Chrest F.J., Wersto R., Rowley D.L., Juhaszova M., Zhou L., Vawter M.P., Becker K.G., Cheadle C., Wood W.H. 3rd, McCann U.D., Freed W.J., Ko M.S., Ricaurte G.A., Donovan D.M., 2001. A murine dopamine neuron-specific cDNA library and microarray/increased COX1 expression during methamphetamine neurotoxicity. *Neurobiol Dis* **8**, 822–833.

Beach T.G., Sue L.I., Walker D.G., Lue L.F., Conner D.J., Cavines J.N., Sabbagh M.N, Alder C.H., 2007. Marked microglial reaction in normal aging human substantia nigra: correlation with extraneuronal neuromelanoin pigment deposits. *Acta Neuropathol* **114**, 419-424.

Beal M.F., 2000. Energetics in the pathogenesis of neurodegenerative diseases. *Trends Neurosci* **23**, 298-304.

Bean B.P., 2007. The action potential in mammalian central neurons. *Nat Rev Neurosci* **8**, 451-465.

Bernheimer H., Birkmeyer W., Hornykiewicz O., Jellinger K., Seitelberger F., 1973. Brain dopamine and the syndromes of Parkinson and Huntington. Clinical, morphological and neurochemical correlations. *J Neurol Sci* **20**, 415-455.

Betarbet R., Sherer T.B., MacKenzie G., Garsia-Osuna M., Panov A.V., Greenamyre J.T., 2000. Chronic systemic pesticide exposure reproduces features of Parkinson's disease. *Nat Neurosci* **3**, 1301-1306.

Bi W.L., Keller-McGandy C., Standaert G. D., Augood S.J., 2002. Identification of nitric oxide synthase neurons for laser capture microdissection and mRNA quantification. *Biotechniques* **33**, 1274-1283.

Björklund A., Lindvall O., 1984. Dopamine-containing systems in the CNS.. In *Handbook of Chemical Neuroanatomy. (Classical Transmitters in the CNS, Part I)* (Vol. 2) (Björklund A. and Höckfelt T., eds), pp. 55-111, Elsevier.

Björklund A., Dunnet S.B., 2007. Dopamine neuron systems in the brain: an update. *Trends Neurosci* **30**, 194-202.

Bjorklund A., Dunnet S.B., Stoessl A.J., Freed C.R., Breeze R.E., Levivier M., Peschanski M., Studer L., Barker R., 2003. Neural transplantation for the treatment of Parkinson's disease. *Lancet Neurol* **2**, 437-445.

Black M.A., Doerge R.W., 2002. Calculation of the minimum number of replicate spots required for detection of significant gene expression fold changes of cDNA microarrays. *Bioinformatics* **18**, 1609-1616.

Blum D., Torch S., Lambeng N., Nissou M., Benabid A.L. Sadoul R., Verna J.M., 2001. Molecular pathways involved in the neurotoxicity of 6-OHDA dopamine and MPTP contribution to the apoptotic theory in Parkinson's disease. *Prog Neurobiol* **65**, 135-72.

Bolkenius F.N., Monard D., 1995. Inactivation of protease nexin-1 by xanthine oxidase-derived free radicals. *Neurochem Int* **26**, 587-592.

Bonaventure P., Guo H., Tian B., Xuejun L., Bittner A., Roland B., Salunga R., Ma X.J., Kamme F., Meurers B., Bakker M., Jurzak M., Leysen J.E., Erlander M.G., 2002. Nuclei and subnuclei gene expression profiling in mammalian brain. *Brain Res* **943**, 38-47.

Bonci A., Bernardi G., Grillner P., Mercuri N.B., 2003. The dopamine-containing neuron: maestro or simple musician in the orchestra of addiction? *Trends Pharmacol Sci* **24**, 172-177.

Bonifati V., Rizzu P., van Baren M.J., Schaap O., Breedveld G.J., Krieger E., Dekker M.C., Squitieri F., Ibanez P., Joosse M., van Dongen J.W., Vanacore N., van Swieten J.C., Brice A., Meco G., van Duijn C.M., Oostra B.A., Heutink P., 2003. Mutations in the *DJ-1* gene associated with autosomal recessive early-onset parkinsonism. *Science* **299**, 256–259.

Bras J., Singleton A., Cookson M.R., Hardy J., 2008. Emerging pathways in genetic Parkinson's disease: potential role of ceramide metabolism in Lewy body disease. *FEBS J* **275,** 5767–5773.

Buchstaller J., Sommer L., Bodmer M., Hoffmann R., Suter U., Mantei N., 2004. Efficient isolation and gene expression profiling of small numbers of neural crest stem cells and developing Schwann cells. *J. Neurosci.* **24**, 2357-2365.

Burbach G.J., Dehn D., Nagel B., Del Turco D., Deller T., 2004. Laser microdissection of immunolabeled astrocytes allows quantification of astrocytic gene expression. *J. Neurosci. Methods* **138**, 141-148.

Burbach G.J., Dehn D., Del Turco D., Deller T., 2003. Quantification of layer-specific gene expression in the hippocampus: Effective use of laser microdissection in combination with quantitative RT-PCR. *J Neurosci Methods* **131**, 83-91.

Burgermeister R., Gangnus R., Haar B., Schutze K., Sauer U., 2003. High quality RNA retrieved from samples obtained by using LMPC (laser microdissection and pressure catapulting) technology. *Pathol Res Pract* **199**, 431-436.

Burns R.S., Chiueh C.C., Markey S.P., Ebert M.H., Jacobowitz D.M., Kopin I.J., 1983. A primate model of parkinsonism: selective destruction of dopaminergic neurons in the pars compacta of the substantia nigra by N-methyl-4-phenyl-1,2,3,6-tetrahydropyridine. *Proc. Natl. Acad. Sci. USA* **80**, 4546-4550.

Calne B., Calne D.M., 2001. Parkinson’s disease: A *syndrome* not a disease. *BC Medical J* **43**, 129-132.

Calne D.B., 1994. Is idiopathic parkinsonism a consequence of an event or a process? *Neurol* **44**, 5-10.

Calne D.B., Lees A.J., 1998. Late progression of post-encephalitic parkinson’s syndrome. *Can J Neurol Sci* **15**, 135-138.

Campbell K.J., Takada M., Hattori T., 1991. Co-localization of tyrosine hydroxylase and glutamate decarboxylase in a subpopulation of single nigrotectal projection neurons. *Brain Res* **558**, 239–244.

Candy J.M., Perry R.H., Perry E.K., Irving D., Blessed G., Fairbairn A.F., Tomlinson B.E., 1983. Pathological changes in the nucleus of Meynert in Alzheimer's and Parkinson's diseases. *J Neurol Sci* **59**, 277-289.

Cao Y., Wilcox K.S., Martin C.E., Rachinsky T.L., Eberwine J., Dichter M.A., 1996. Presence of mRNA for glutamic acid decarboxylase in both excitatory and inhibitory interneurons. *Proc. Natl. Acad. Sci. USA* **93**, 9844-9849.

Carlsson A., Falck B., Hillarp N.A., 1962. Cellular localization of brain monoamines. *Acta Physiol Scan Suppl* **56**, 1-28.

Chan C.S., Guzman J.N., Ilijic E., Mercer J.N., Tkatch T., Meredith G.E., Surmeier D.J., 2007. "Rejuvenation" protects neurons in mouse models of Parkinson's disease. *Nature* **447**, 1081-1086.

Chemin J., Patel A., Duprat F., Zanzouri M., Lazdunski M., Honoré E., 2005. Lysophosphatidic acid-operated K^+ channels. *J Biol Chem* **280**, 4415-4421.

Chen H., Zhang S.M., Herman M.A., Schwarzschild M.A., Willet W.C., Colditz G.A., Speizer F.E., Ascherio A., 2003. Non steroidal antinflammatory drugs and the risk of Parkinson's disease. *Arch Neurol* **60**, 1059-1064.

Chenchik A., Zhu Y.Y., Diatchenko L., Li R., Hill J. Siebert P.D., 1998. Generation and use of high-quality cDNA from small amounts of total RNA by SMART PCR. In *Gene Cloning and Analysis by RT-PCR* (Siebert P.D., Larrick J.W. eds), pp. 305-320, Biotechniques Books.

Chiang M.K., Melton D.A., 2003. Single cell transcript analysis of pancreas development. *Dev. Cell* **4**, 383-393.

Chung C.Y., Hyemyung S., Sonntag K.C., Brooks A., Lin L., Isacson O., 2005. Cell type – specific gene expression of midbrain dopaminergic neurons reveals molecules involved in their vulnerability and protection. *Hum. Mol. Genet.* **14**, 1709-1725.

Cinar H., Cinar H, Keles S, Jin Y., 2005. Expression profiling of GABAergic motorneurons in *Chaenorabditis elegans. Curr. Biol.* **15**, 340-346.

Clark L.N., Ross B.M., Wang Y., Mejia-Santana H., Harris J., Louis E.D., Cote L.J., Andrews H., Fahn S., Waters C., Ford B., Frucht S., Ottman R.,

Marder K., 2007. Mutations in the glucocerebrosidase gene are associated with early-onset Parkinson's disease, *Neurology* **69**, 1270–1277.

Clément-Ziza M., Munnich A., Lyonnet S., Jauber F., Besmond C., 2008. Stabilization of RNA duroing laser capture microdissection by performing experiments under argon atmosphere or using ethanol as a solvent in staining solutions. *RNA* **14**, 2698-2704.

Colosimo M.E., Brown A., Mukhopadhyay S., Gabel C., Lanjuin A.E., Samuel A.D., Sengupta P. 2004. Identification of thermosensory and olfactory neuron-specific genes via expression profiling of single neuron types. *Curr. Biol*. **14**, 2245-2251.

Cotzias G.C., Van Woert M.H., Schiffer L.M., 1967. Aromatic amino acids and modification of parkinsonism. *N Engl J Med* **267**, 347-349.

Crino P.B., Trojanowski J.Q., Dichter M.A., Eberwine J., 1996. Embryonic neuronal markers in tuberous sclerosis: single-cell molecular pathology. *Proc. Natl. Acad. Sci. USA* **93**, 14152-14157.

Dahlström A., Fuxe L., 1964. Evidence for the existence of monoamine-containing neurons in the central nervous systems. I. Demonstration of monoamines in the cell bodies of brain stem neuros. *Acta Physiol Scand Suppl* **232**, 1-55.

Dennis G Jr, Sherman B.T., Hosack D.A., Yang J., Gao W., Lane H.C., Lempicki R.A., 2003. DAVID: Database for Annotation, Visualization, and Integrated Discovery. *Genome Biol* **4**, P3.

DeVries S.H., Baylor D.A., 1997. Mosaic arrangement of ganglion cell receptive fields in rabbit retina. *J Neurophysiol* **78**, 2048-2060.

Di Porzio U., Zuddas A., Cosenza-Murphy D.B., Barker J.L., 1990. Early appearance of tyrosine hydroxylase immunoreactive cells in the mesencephalon of mouse embryos. *Int J Dev Neurosci* **8**, 523-532.

Di Chiara G., Porceddu M.L., Morelli M., Mulas M., Gesa G.L., 1979. Evidence for a GABAergic projection from the substantia nigra to the ventromedial thalamus and to the superior colliculus of the rat. *Brain Res* **176**, 273–284.

Dixon A.K., Richardson P.J., Lee K., Carter N.P., Freeman T.C., 1998. Expression profiling of single cells using 3 prime end amplification (TPEA) PCR. *Nucleic Acids Res.* **26**, 4426-4431.

Duggan D.J., Bittner M., Chen Y., Meltzer P., Trent J.M., 1999. Expression profiling using cDNA microarrays. *Nature Genet.* **21**, 10-14.

Ebermann I., Scholl H.P.N., Charbel Issa P., Becirovic E., Lamprecht J., Jurklies B., Millán J.M., Aller E., Mitter D., Bolz H., 2007. A novel gene for Usher syndrome type 2: mutations in the long isoform of whirlin are associated with retinitis pigmentosa and sensorineural hearing loss. *Human Genet* **121**, 203-211.

Eberwine J., Yeh H., Miyashiro K., Cao Y., Nair S., Finnel R., Zettel M., Coleman P., 1992. Analysis of gene expression in single live neurons. *Proc. Natl. Acad. Sci. USA* **89**, 3010-3014.

Ehringer H., Hornykiewicz O., 1960. Verteilung von Noradrenalin und Dopamin (3-Hydroxytyramin) im Gehirn des Menschen und ihr Verhalten bei Ekrankungen des Extrapyramidalen Systems. *Klin Woschenschr* **38**, 1236-1239.

Falck B., Hillarp N.A., Thieme G., Torp A., 1962. Fluorescence of catecholamines and related compounds condensed with formaldehyde. *J Histochem Cytochem* **10**, 348-354.

Fend F., Emmert-Buck M.R., Chuaqui R., Cole K., Lee J., Liotta L.A., Raffeld M., 1999. Immuno-LCM: laser capture microdissection of immunostained frozen sections for mRNA analysis. *Am J Pathol* **154**, 61-66.

Fink L., Bohle R.M., 2002. Internal standards for laser microdissection. *Methods Enzymol* **356**, 99-113.

Fitzgerald J.C., Plun-Favreau H., 2008. Emerging pathways in genetic Parkinson's disease – a common pathway? *FEBS J* **275**, 5758-5766.

Foss R.D., Guha-Thakurta N., Conran R.M., Gutman P., 1994. Effects of fixative and fixation time on the extraction and polymerase chain reaction amplification from RNA from paraffin-embedded tissue. Comparison of two housekeeping gene mRNA controls. *Diagn Mol Pathol* **3**, 148-155.

Fox R.M., Von Stetina S.E., Barlow S.J., Shaffer C., Olszewski K.L., Moore J.H., Dupuy D., Vidal M., Miller D.M. 3rd, 2005. A gene expression fingerprint of C. *elegans* in embryonic motor neurons. *BMC Genomics* **6**, 42.

Franz O., Liss B., Neu A., Roeper J., 2000. Single-cell mRNA expression of HCN1 correlates with fast gating phenotype of hyperpolarization-activated cyclic nucleotide-gated ion channels (I_h) in central neurons. *Eur J Neurosci* **12**, 2685-2693.

Freeman T.C., Lee K., Richardson P.J., 1999. Analysis of gene expression in single cells. *Curr Opin Biotechnol* **10**, 579-582.

Fuentealba R.A., Bu G., 2008. P4-246: Low density lipoprotein receptor–related protein 1 (LRP1) mediates anti-apoptotic signaling in primary neurons. *Alzheimer's and Dementia* **4**, T743-T744.

Fujimura K., Matduda E., 1989. Autogenous oscillatory potentials in neurons of the guinea pig sub stantia nigra pars compacta in vitro. *Neurosci Lett*, 10453-10457.

Fujino T., Lee W.C., Nedivi E., 2003. Regulation of cpg15 by signaling pathways that mediate synaptic plasticity. *Mol Cell Neurosi* **24**, 538-554.

Galvin J.E., Lee V.M., Trojanowski J.Q., 2001. Synucleinopathies: clinical and pathological implications. *Arch Neurol* **58**, 186-190.

Garris P.A., Wightman R.M., 1994. Different kinetics govern dopaminergic transmission in the amygdale, prefrontal cortex, and striatum: as in vivo voltametric study. *J Neurosci* **14**, 442-450.

Gasser T., 2007. Update on the genetics of Parkinson's disease. *Mov Disord* **22**, S343-S350.

Gates M.A., Torres E.M., White A., Fricker-Gates R.A., Dunnet S.B., 2006. Re-examining the ontogeny of substantia nigra dopamine neurons. *Eur J Neurosci* **23**, 1384-1390.

Gerfen C.R., Herkenham M., Thibault J., 1987. The Neostriatal mosaic II. patch and matrix-directed mesostriatal dopaminergic and non-dopaminergic systems. *J Neurosci* **7**, 3915-3934.

Gerfen C.R., Herkenham M., Tribault J., 1987. The neostriatal mosaic: II. Patch and matrix-directed mesostriatal dopaminergic and non-dopaminergic systems. *J Neurosci* **7**, 3915–3934.

Gerfen C., 2004. The basal ganglia. In *The Rat Nervous System* (Paxinos G., ed), 3rd ed., pp. 445-504, Elsevier.

German D., Manaye K., White III C., Woodward D., McIntire D., Smith W., Kalaria R., Mann D., 1992. Disease-specific patterns of locus coeruleus cell loss. *Ann Neurol* **32**, 667-676.

German D.C., Manaye K.F., 1993. Midbrain dopaminergic neurons (Nuclei A8, A9, and A10): 3-dimentional reconstruction in the rat. *J Comp Neurol* **331**, 297-309.

German D.C., Nelson E.L., Liang C-L., Speciale S.G., Sinton C.M., Sonsalla P.K., 1996. The neurotoxin MPTP causes degeneration of specific nucleus A8, A9 and A10 dopaminergic neurons in the mouse. *Neurodegeneration* **5**, 299-312.

Geschwind D.H., 2000. Mice, microarrays, and the genetic diversity of the brain. *Proc Natl Acad Sci U.S.A.* **97**, 10676-10678.

Gil O.D., Zanazzi G., Struyk A.F., Salzer J.L., 1998. Neurotrimin mediates bifunctional effects on neurite outgrowth via homophilic and heterophilic interactions. *J Neurosci* **18**, 9312-9325.

Gillespie J.W., Best C.J., Bichsel V.E., Cole K.A., Greenhut S.F., Hewitt S.M., Ahram M., Gathright Y.B., Merino M.J., Stausberg R.L., Epstein J.I., Hamilton S.R., Gannot G., Baibakova G.V., Calvert V.S., Flaig M.J., Chuaqui R.F., Herring J.C., Pfeifer J., Petricoin E.F., Linehan W.M., Duray P.H., Bova G.S., Emmert-Buck M.R., 2002. Evaluation of non-fomalin tissue fixation for molecular profiling studies. *Am J Pathol* **160**, 449-457.

Ginsberg S.D., Che S., 2004. Combined histochemical staining, RNA amplification, regional, and single cell analysis within the hippocampus. *Lab Invest* **84**, 952-962 .

Gitler A.D., Chesi A., Geddie M.L., Strathearn K.E., Hamamichi S., Hill K.J., Caldwell K.A., Caldwell G.A., Cooper A.A., Rochet J.C., Lindquist S., 2009. alpha-Synuclein is part of a diverse and highly conserved interaction network that includes PARK9 and manganese toxicity, *Nat Genet* **41**, 308-315.

Godfrey T.E., Kim S.H., Chavira M., Ruff D.W., Warren R.S., Gray J.W., Jensen R.H., 2000. Quantitative mRNA expression analysis from formalin-fixed, paraffin-embedded tissues using 5'nuclease quantitative reverse transcription-polymerase chain reaction. *J Mol Diagn* **2**, 84-91.

Goker-Alpan O., Schiffmann R., LaMarca M.E., Nussbaum R.L., McInerney-Leo A., Sidransky E., 2004. Parkinsonism among Gaucher disease carriers, *J Med Genet* **41**, 937–940.

Goldman J.E., Yen S.H., Chiu F.C., Peress N.S., 1983. Lewy bodies of Parkinson's disease contain neurofilament antigens. *Science* **221**, 1082-1084.

Goldsworthy S.M., Stockton P.S., Trempus C.S., Foley J.F., Maronpot R.R., 1999. Effects of fixation on RNA extraction and amplification from laser capture microdissected tissue. *Mol Carcinog* **25**, 86-91.

Goldworthy S.M., Stockton P.S., Trempus C.S., Foley J.F., Maronpot R.R., 1999. Effects of fixation on RNA extraction and amplification from laser capture microdissected tissue. *Mol Carcinog* **25**, 86-91.

Golovko M.Y., Faergeman N.J., Cole N.B, Castagnet P.I., Nussbaum R.L., Murphy E.J., 2005. Alpha-synuclein gene deletion decreases brain

palmitate uptake and alters the palmitate metabolism in the absence of alpha-synuclein palmitate binding. *Biochemistry* **44,** 8251–8259.

Gonzàlez-Hernàndez T., Barroso-Chinea P., Acevedo A., Salido E. and Rodriguez M., 2001. Colocalization of tyrosine hydroxylase and GAD65 mRNA in mesostriatal neurons. *Europ J Neurosci* **13**, 57-67.

Grace A.A., Bunney B.S., 1984a. The control of firing pattern in nigral dopamine neurons: burst firing. *J Neurosci* **4**, 2877-2890.

Grace A.A., Bunney B.S., 1984b. The control of firing pattern in nigral dopamine neurons: single spike firing. *J Neurosci* **4**, 2866-2876.

Grace A.A., Floresco S.B., Goto Y., Lodge D.J., 2007. Regulation of firing of dopaminergic neurons and control of goal-directed behaviors. *Trends Neurosci* **30**, 220-227.

Grace A.A., Onn S.P., 1989. Morphology and electrophysiological properties of immunocytochemically identified rat dopamine neurons recorded *in vitro*. *J Neurosci* **9**, 3463-3481.

Graham D.G., Tiffany S.M., Bell W.R., Jr., Gutknecht W.F., 1978. Autoxidation versus covalent binding of quinones as the mechanism of toxicity of dopamine, 6-hydroxydopamine, and related compounds towards C1300 neuroblastoma cells in vitro. *Mol Pharmacol* **14**, 644-653.

Graybriel A.M., Ohta K., Roffler-Tarlov S., 1990. Patterns of cell and fiber vulnerability in the mesostriatal system of the mutant mouse weaver. I. Gradients and compartments. *J Neurosci* **10**, 720-733.

Green J.G., Dingledine R., Greenamyre J.T., 2005. Gene expression profiling of rat dopamine neurons: implications for selective vulnerability in parkinsonism. *Neurobiol Dis* **18**, 19-31.

Greenamyre J.T., Sherer T.B., Betarbet R., Panov A.V., 2001. Complex I and Parkinson's disease. *IUBMB Life* **52**, 135-141.

Greene J.G., Dingledine R., Greenamyre J.T., 2005. Gene expression profiling of rat midbrain neurons: implications for selective vulnerability in parkinsonism. *Neurobiol Dis* **18**, 19-31.

Greggio E., Jain S., Kingsbury A., Bandopadhyay R, Lewis P, Kaganovich A., van der Brug M.P., Beilina A., Blackinton J., Thomas K.J., Ahmad R., Miller D.W., Kesavapany S., Singleton A., Lees A., Harvey R.J., Harvey K., Cookson M.R., 2006. Kinase activity is required for the toxic effects of mutant LRRK2/dardarin. *Neurobiol Dis* **23,** 329–341.

Grimm J., Mueller A., Hefti F., Rosenthal A., 2004. Molecular basis for catecholaminergic neuron diversity. *Proc Natl Acad Sci* **101**, 13891-13896.

Gustincich S., Contini M., Gariboldi M., Puopolo M., Kadota K., Bono H., LeMieux J., Walsh P., Carninci P., Hayshizaki Y., Okazaki Y., Raviola E., 2004. Gene discovery in genetically labeled single dopaminergic neurons of the retina. *Proc Natl Acad Sci USA* **101**, 5069-5074.

Gustincich S., Feigenspan A., Wu D.K., Koopman L.J., Raviola E., 1997. Control of dopamine release in the retina: a transgenic approach to neural networks. *Neuron* **18**, 723-736.

Gustincich S., Sandelin A., Plessy C., Katayama S., Simone R., Lazareviĉ D., Hayashizaki Y., Carninci P., 2006. *J Physiol* **575**, 321-332.

Halliwell B., 1992. Reactive oxygen species and the entral nervous system. *J Neurochem* **59**, 1609-1623.

Hardy J., Singleton A., 2007. Reporting and interpretation of genetic variants in cases and controls. *Neurology* **69**, 111–112.

Hardy J., Lewis P., Revesz T., Lees A., Paisan-Ruiz C., 2009. The genetics of Parkinson's syndromes: a critical review. *Curr Opin Genet Dev* **19**, 254-265.

Harris N.C., Webb C., Greenfield S.A., 1989. A possible pacemaker mechanism in pars compacta neurons of the guinea-pig substantia nigrarevealed by various ion channels blocking agents. *Neuroscience* **31**, 355-362.

Harrower T.P., Michell A.W., Barker R.A., 2005. Lewy bodies in Parkinson's disease: protectors or perpetrators? *Exp Neurol* **195**, 1-6.

Hassani O.K., François C., Yelnik J., Féger J., 1997. Evidence for a dopaminergic innervation of the subthalamic nucleus in the rat. *Brain Res* **749**, 88-94.

Hastings T.G., Zigmond M.J., 1994. Identification of catechol-protein conjugates in neostriatal slices incubated with [3H] dopamine: Impact of ascorbic acid and glutathione. *J Neurochem* **63**, 1126-1132.

Hattori T., Takada M., Moriizumi T., Van der Kooy D., 1991 Single dopaminergic nigrostriatal neurons from two chemically distinct synaptic types: possible transmitter segregation within neurons. *J Comp Neurol* **309**, 3910–3401.

Hauser M.A., Li Y.J., Takeuchi S., Walters R., Noureddine M., Maready M., Darden T., Hulette C., Martin E., Hauser E., Xu H, Schmechel D., Stenger J.E., Dietrich F., Vance J., 2003. Genomic convergence: identifying

candidate genes for Parkinson's disease by combining serial analysis of gene expression and genetic linkage. *Hum Mol Genet* **12**, 671-677.

Healy D.G.,Abou-Sleiman P.M., Casas J.P., Ahmadi K.R., Lynch T., Gandhi S., Muqit M.M., Foltynie T., Barker R., Bhatia K.B., Quinn N.P., Lees A.J., Gibson J.M., Holton J.L., Revesz T., Goldstein D.B., Wood N.W., 2006. UCHL-1 is not a Parkinson's disease susceptibility gene. *Ann Neurol* **59**, 627–633.

Healy D.J., Abou-Sleiman P.M., Ahmadi K.R., Gandhi S., Muqit M.M., Bhatia K.P., Quinn N.P., Lees A.J., Holton J.L., Revesz T., Wood N.W., 2006. NR4A2 genetic variation in sporadic Parkinson's disease: a genewide approach, *Mov Disord* **21**, 1960–1963.

Hertzberg M., Sievertzon M., Aspeborg H., Nilsson P., Sandberg G., Lundeberg J., 2001. cDNA microarray analysis of small plant tissue samples using a cDNA tag target amplification protocol. *Plant J* **25**, 585-591.

Herzenberg L.A., Sweet R.G., Herzenberg L.A., 1976. Fluorescence-activated cell sorting. *Sci Am* **234**, 108-117.

Hirasawa H**.,** Puopolo M**.,** Raviola E., 2009. Extrasynaptic release of GABA by retinal dopaminergic neurons. *J Neurophysiol **102***, 146-158**.**

Hirsch E., Graybiel A.M., Agid Y.A., 1988. Melanized dopaminergic neurons are differentially suspectible to degeneration in Parkinson's disease. *Nature* **334**, 345-348.

Höckfelt T., Martensson R., Björklund A., Kleinau S., Goldstein M., 1984. Distributional maps of tyrosine hydroxylase-immunoreactive neurons in the rat brain. In *Handbook of Chemical Neuroanatomy. (Classical Transmitters in the CNS, Part I)* (Vol 2) (Björklund A. and Höckfelt T., eds) pp. 237-379, Elsevier.

Hochberg Y., Benjamini Y., 1990. More powerful procedures for multiple significance testing. *Stat Med* **9**, 811-18.

Hsu L.J., Sagara Y., Arroyo A., Rockenstein E., Sisk A., Mallory M., Wong J., Takenouchi T., Hashimoto M., Masliah E., 2000. Alpha sunuclein promotes mitochondrial deficit and oxidative stress. *Am J Pathol* **157**, 401-410.

Huang D.W., Sherman B.T., Lempicki R.A., 2009. Systematic and integrative analysis of large gene lists using DAVID Bioinformatics Resources. *Nature Protoc* **4**, 44-57.

Huang L.E., Luzzi V., Ehrig T., Holtschlang V., Watson M.A., 2002. Optimized tissue processing and staining for laser capture microdissection and nucleic acid retrieval. *Methods Enzymol* **356**, 49-62.

Hurd Y.L., Pristupa Z.B., Herman M.M, Niznik H.B., Kleinman J.E., 1994. The dopamine transporter and dopamine D2 receptormessenger RNAs are differentially expressed in limbic and motor-related subpopulations of human mesencephalic neurons. *Neuroscience* **63**, 357-362.

Hynes M., Rosenthal A., 1999. Specification of dopaminergic and serotonergic neurons in the vertebrate CNS. *Curr Opin Neurobiol* **9**, 26-36.

Iwata K., Nishinaka T., Matsuno K., Yabe-Nishimura C., 2006. Increased gene expression of glutathione peroxidase-3 in diabetic mouse heart. *Biol Pharm Bull* **29**, 1042-1045.

Ikemoto K., Kitahama K., Nishimura A., Jouvet A., Nishi K., Arai R., Jouvet M., Nagatsu I., 1999. Tyrosine hydroxylase and aromatic L-amino acid decarboxylase do not coexist in neurons in the human anterior cigulate cortex. *Neurosci Lett* **269**, 37-40.

Inaba S., Li C., Shi Y.E., Song D.Q., Jiang J.D., Liu J., 2005. Synuclein gamma inhibits the mitotic checkpoint function and promotes chromosomal instability of breast cancer cells. *Breast Cancer Res Treat* **94**, 25-35.

Iscove N.N., Barbara M., Gu M., Gibson M., Modi C., Winegarden N., 2002. Representation is faithfully preserved in global cDNA amplified exponentially from sub-picogram quantities of mRNA. *Nat Biotechnol* **20**, 940-943.

Jana A., Pahan K., 2007. Oxidative stress kills human primary oligodendrocytes via neutral sphingomyelinase: implications for multiple sclerosis. *J Neuroimmune Pharmacol* **2**, 184-193.

Javitch J.A.., D'Amato R.J., Strittmatter S.M., Snyder S.H., 1985. Parkinsonism-inducing neurotoxin, N-methyl-4-phenyl-1,2,3,6-tetrahydropyridine uptake of the metabolite N-methyl-4-phenylpyridine by dopamine neurons explain selective toxicity. *Proc Natl Acad Sci USA* **82**, 2173-2177.

Ji H., Shepard P.D., 2006. SK Ca^{2+} -activated K^{+} channel ligands alter the firing pattern of dopamine-containg neurons in vivo. *Neuroscience* **140**, 623-633.

Ji W., Zhou W., Gregg K., Lindpaintner K., Davis S., 2004. A method for gene expression analysis by oligonucleotide arrays from minute biological materials. *Anal Biochem* **331**, 329-339.

Jiang Y.H., Davidson L.A., Lupton J.R., Chapkin R.S., 1995. A rapid RT-PCR method for detection of intact RNA in formalin-fixed paraffin-embedded tissues. *Nucleic Acids Res* **23**, 3971-3072.

Johansson M., Jansson T., Powel T.L., 2000. Na(+)-K(+)-ATPase is distributed to microvillous and basal membrane of the syncythiotrophoblast in human placenta. *Am J Physiol* **279**, R287-R294.

Kaelber W.W., Afifi A.K., 1979, Efferent connexions of the pars lateralis of the substantia nigra (SNL). *J Anat* **129**, 405-412.

Kamme F., Salunga R., Yu J., Tran D.T., Zhu J., Luo L., Bittner A., Guo H.Q., Guo N., Miller N., Wan J., Erlander M., 2003. Single-cell microarray analysis in hippocampus CA1: demonstration and validation of cellular heterogeneity. *J Neurosci* **23**, 3607-3615.

Karsten S.L., Van Deerlin V.M., Sabatti C., Gill L.H., Geschwind D.H., 2002. An evaluation of tyramide signal amplification and archived fixed and frozen tissue in microarray gene expression analysis. *Nucleic Acids Res*. **30**, E4.

Kasischke K.A., Vishwasrao H.D., Fisher P.J., Zipfel W.R., Webb W.W., 2004. Neural activity triggers neuronal oxidative metabolism followed by astrocytic glycolysis. *Science* **305**, 99–103.

Katayama S., Tomaru Y., Kasukawa T., Waki K., Nakanishi M., Nakamura M., Nishida H., Yap C.C., Suzuki M., Kawai J., Suzuki H., Carninci P., Hayashizaki Y., Wells C., Frith M., Ravasi T., Pang K.C., Hallinan J., Mattick J., Hume D.A., Lipovich L., Batalov S., Engström P.G., Mizuno Y., Faghihi M.A., Sandelin A., Chalk A.M., Mottagui-Tabar S., Liang Z., Lenhard B., Wahlestedt C.; RIKEN Genome Exploration Research Group; Genome Science Group (Genome Network Project Core Group); FANTOM Consortium, 2005. Antisense transcription in the mammalian transcriptome. *Science* **309,** 1564-1566.

Kawaguchi Y., Kubota Y., 1997. GABAergic cell subtypes and their synaptic connections in rat frontal cortex. *Cereb Cortex* **7**, 476-486.

Kawano H., Ohyama K., Kawamura K., Nagatsu I., 1995. Migration of dopaminergic neurons in embryonic mesencephalon of mice. *Dev Brain Res* **86**, 101-113.

Kenzelmann M., Klaren R., Hergenhahn M., Bonrouhi M., Groni H.J., Schmidt W., Schutz G., 2004. High-accuracy amplification of nanogram total RNA amounts for gene profiling. *Genomics* **83**, 550-558.

Kerman I.A., Buck B.J., Evans S.J., Akil H., Watson S.J., 2006. Combining laser capture microdissection with quantitative real-time PCR: effects of tissue

manipulation on RNA quality and gene expression. *J Neurosci Methods* **153**, 71-85.

Kerr M.K., Churchill G.A., 2001. Experimental design for gene expression microarrays. *Biostatistics* **2**, 183-201.

Kim Y., Bang H., Gnatenco C., Kim D., 2001. Synergistic interaction and the role of C-terminus in the activation of TRAAK K^+ channels by pressure, free fatty acids and alkali. *Pflugers Arch* **442**, 64- 72.

Kitada T., Asakawa S., Hattori N., Matsumine H., Yamamura Y., Minoshima S., Yokochi M., Mizuno Y., Shimizu N., 1998. Mutations in the parkin gene cause autosomal recessive juvenile parkinsonism. *Nature* **392**, 605-608.

Kitai S.T., Shepard P.D., Callaway J.C., Scroggs R., 1999. Afferent modulation of dopamine neuron firing patterns. *Curr Opin Neurobiol* **9**, 690-697.

Klur S., Toy K., Williams M.P., Certa U., 2004. Evaluation of procedures for amplification of small-size samples for hybridization on microarrays. *Genomics* **83**, 508-517.

Kodzius R., Kojima M., Nishiyori H., Nakamura M., Fukuda S., Tagami M., Sasaki D., Imamura K., Kai C., Harbers M., Hayashizaki Y., Carninci P., 2006. CAGE: cap analysis of gene expression. *Nat Methods* **3**, 211-222.

Kress G.J., Reynolds I.J., 2005. Dopaminergic neurotoxins require excitotoxic stimulation in organotypic cultures. *Neurobiol Dis* **20**, 639-645.

Kumar R., Lonzano A.M., Kim Y.J., Hutchison W.D., Sime E., Halket E., Lang A.E., 1998a. Double-blind evaluation of subthalamic nucleus deep brain stimulation in advanced Parkinson's disease. *Neurology* **51**, 850-855.

Kumar R., Lonzano A.M., Montgomery E., Lang A.E., 1998b. Pallidotomy and deep brain stimulation of the pallidum and subthalamic nucleus in advanced Parkinson's disease. *Mov Disord* **13**, S73-S82.

Laman H., 2006. Fbxo7 gets proactive with cyclin D/cdk6. *Cell Cycle* **5**, 279-282.

Lammel S., Hetzel A., Häckel O., Jones I., Liss B., Roeper J., 2008. Unique properties of mesoprefrontal neurons within a dual mesocorticolimbic dopamin system. *Neuron* **57**, 760-773.

Lang A.E., Lozano A.M., 1998a. Parkinson's disease. First of two parts. *New Engl J Med* **339**, 1044-1053.

Lang A.E., Lozano A.M. 1998b. Parkinson's disease. Second of two parts. *New Engl J Med* **339**, 1030-1043.

Langston J.W., Ballard P., Tetrud J.W. Irwin I., 1983. Chronic Parkinsonism in humans due to a product of meperidine-analog synthesis. *Science*, **219**, 5411-5417.

Langston J.W., Forno L.S., Tetrud J., 1999. Evidence of active nerve cell de generation in the sub stantia nigra of humans years after 1-methyl-4-phenyl-1,2,3,6-tetrahydropyridine exposure. *Ann Neurol* **46**, 598-605.

Le W.D., Xu P., Jankovic J. , Jiang H., Appel S.H., Smith R.G., and Vassilatis D.K., 2003. Mutations in NR4A2 associated with familial Parkinson's disease. *Nat Genet* **33,** 85-89.

Lee M.T., Kuo F.C., Whitmore G.A., Skiar J., 2000. Importance of replication in microarray gene expression studies: statistical methods and evidence from repetitive cDNA hybridizations. *Proc Natl Acad Sci USA* **97**, 9834-9839.

Leroy E., Boyer R., Auburger G., Leube B., Ulm G., Mezey E., Harta G., Brownstein M.J., Jonnalagada S., Chernova T., Dehejia A., Lavedan C., Gasser T., Steinbach P.J., Wilkinson K.D., Polymeropoulos M.H., 1998. The ubiquitin pathway in Parkinson's disease. *Nature* **395**, 451-452.

Lewis D.A., Sesack S.R., Levey A.I., Rosenberg D.R., 1998. Dopamine axons in primate prefrontal cortex: specificity of distribution, synaptic targets, and development. *Adv Pharmacol* **42**, 703-706.

Lewis F., Maughan N.J., Smith V., Hillan K., Quirke P., 2001. Unlocking the archive gene expression in paraffin – embedded tissue. *J. Pathol*. **195**, 66-71.

Liang C.L., Sinton C.M., Sonsalla P.K., German D.C., 1996. Midbrain dopaminergic neurons in the mouse that contain calbindin-D28k exhibit reduced vulnerabilità to MPTP-induced neurodegeneration. *Neurodegeneration* **5**, 313-318.

Lindvall O., Björklund A., 1974. The glyoxylic acid fluorescence histochemical method: A detailed account of methodology fort he vizualization of central catecholamine neurons. *Histochemistry* **39**, 97-127.

Linvall O., Björklund A., 1979. Dopaminergic innervation of the globus pallidus by collaterals from the nigrostriatal pathway. *Brain Res* **172**, 169-173.

Liss B., Franz O., Sewing S., Bruns R., Neuhoff H., Roeper J., 2001. Tuning pacemaker frequency of individual dopaminergic neurons by Kv4.3L and KChip3.1 transcription. *EMBO J* **20**, 5715-5724.

Liss B., Haeckel O., Wildmann J., Miki T., Seino S., Roeper J., 2005. K-ATP channels promote the differnetial degeneration of dopaminergic midbrain neurons. *Nat Neurosci* **8**, 1742-1751.

Liss B., Roeper J., 2008. Individual dopamine midbrain neurons: Functional diversity and flexibility in health and disease. *Brain Res Rev* **58**, 314-321.

Liu Y., Fallon L., Lashuel H.A., Liu Z., Lansbury P.T., 2002. The UCHL-1 gene encodes two opposing enzymatic activities that affect a-synuclein degradation and Parkinson's disease susceptibility. *Cell* **111**, 209-218.

Lockhart D.J., Dong H., Byrne M.C., Follettie M.T., Gallo M.V., Chee M.S., Mittmann M., Wang C., Kobayashi M., Horton H., Brown E.L., 1996. Expression monitoring by hybridization to high-density oligonucleotide arrays. *Nat Biotechnol* **14**, 1675-1680.

Loy R., Koziell D.A., Lindsey J.D., Moore R.Y., 1980. Noradrenergic innervation of the adult hippocampal formation. *J Comp Neutrol* **189**, 699-710.

Lukyanov K., Diatchenko L., Chenchik. A., Nanisetti A., Siebert P., Usman N., Matz M., Lukyanov S., 1997. Construction of cDNA libraries from small amounts of total RNA using the suppression PCR effect. *Biochem Biophys Res Commun* **230**, 285-288.

Luo L., Salunga R.C., Guo H., Bittner A., Joy K.C., Galindo J.E., Xiao H., Rogers K.E., Wan J.S., Jackson M.R., Erlander M.G., 1999. Gene expression profiles of laser-captured adjacent neuronal subtypes. *Nat Med* **5**, 117-122.

Luzzi V., Mahadevappa M., Raja R., Warrington J.A., Watson M.A., 2003. Accurate and reproducible gene expression profiles from Laser Capture Microdissection, transcript amplification, and high density oligonucleotide microarray analysis. *J Mol Diagn* **5**, 9-14.

Lyons P.A., Koukoulaki M., Hatton A., Doggett K., Woffendin H.B., Chaudhry A.N., Smith K.G.C., 2007. Microarray analysis of human leucocyte subsets: the advantages of positive selection and rapid purification. *BMC Genomics* **8**, 64.

MacNeil M.A., Masland R.H., 1998. Extreme diversity among amacrine cells: implications for function. *Neuron* **20**, 971-982.

Madison R.D., Robinson G.A., 1998. lambda RNA internal standards quantify sensitivity and amplification efficiency of mammalian gene expression profiling. *Biotechniques* **25**, 504-508.

Markey S.P., Johannessen J.P., Chiueh C.C., Burns R.S., Herkenham M.A., 1984. Intraneuronal generation of pyridinium metabolite may cause drug-induced parkinsonism. *Nature* **311**, 464-467.

Markram H., Toledo-Rodriguez M., Wang Y., Gupta A., Silberberg G., Wu C., 2004. Interneurons of the neocortical inhibitory system. *Nat. Rev Neurosci* **5**, 793-807.

Marten P., Smidt P., Burbach P.H., 2007. Hoe to make a mesodiencephalic dopaminergic neuron. *Nature Neurosci* **8**, 21-32.

Martinat C., Bacci J.J., Leete T., Kim J., Vanti W.B., Newman A.H., Cha J.H., Gether U., Wang H., Abeliovich A., 2006. Cooperative transcription activation by Nurr1 and Pitx3 induces embryonic stem cell maturation to the midbrain dopamine neuron phenotype. *Proc Natl Acad Sci USA* **103**, 2874-2879.

Marx F.P., Holzmann C., Strauss K.M., Li L., Eberhardt O., Gerhardt E., Cookson M.R., Hernandez D., Farrer M.J., Kachergus J., Engelender S., Ross C.A., Berger K., Schöls L., Schulz J.B., Riess O., Krüger R., 2003. Identification and functional characterization of a novel R621C mutation in the *synphilin-1* gene in Parkinson's disease. *Hum Mol Genet* **12**, 1223-1231.

Masland R.H., 2004. Neuronal cell types. *Curr Biol* **14**, R497-R500.

Massi M., Panocka I., de Caro G., 2000. The psychopharmacology of tachynin NK-3 receptors in laboratory animals. *Peptides* **21**, 1597-1609.

Matsushita N., Okada H., Yasoshima Y., Takahashi K., Ciuchi K., Kobayashi K., 2002. Dynamics of tyrosine hydroxylase promoter activity during midbrain dopaminergic neuron development. *J Neurochem* **82**, 295-304.

Matus A., 2005. MARCKS for maintainance in dendritic spines. *Neuron* **48**, 4-5.

McNaught K.S., Perl D.P., Brownell A.L., Olanow C.W., 2004. Systemic exposure to proteasome inhibitors causes a progressive model of Parkinson's disease. *Ann Neurol* **56**, 149-162.

Méndez-Alvarez E., Soto-Otero R., Hermida-Ameijeiras A., López-Martín M.E., Labandeira-García J.L., 2001. Effect of iron and manganese on hydroxyl radical production by 6-hydroxydopamine: mediation of antioxidants. *Free Radic Biol Med* **31**, 986-998.

Mercuri N.B., Bonci A., Calabresi P., Stefani A., Bernardi G., 1995. Properties of the hyperpolarization-activated cation curent Ih in rat midbrain dopaminergic neurons. *Eur J Neurosci* **7**, 462-469.

Meyer-Lindenberg A., Miletich R.S., Kohn P.D., Esposito G., Carson R.E., Quantarelli M., Weinberger D.R., Berman K.F., 2002. Prefrontal Cortex Activity Predicts Exaggerated Striatal Dopaminergic Function in Schizophrenia. *Nat Neurosci* **5**, 267-271.

Mikulowska-Mennis A., Taylor T.B., Vishnu P., Michie S.A., Raja R., Horner N., Kunitake S.T., 2002. High-quality RNA from cells isolated by laser capture microdissection. *BioTechniques* **33**, 176-179.

Mirnics K., Middleton F.A., Marquez A., Lewis D.A., Levitt P., 2000. Molecular characterization of schizophrenia viewed by microarray analysis of gene expression in prefrontal cortex. *Neuron* **28**, 53-67.

Mojsilovic-Petrovic J., Nesic M., Pen A., Zhand W., Stanimirovic D., 2004. Development of rapid staining protocols for laser-capture microdissection of brain vessels from human and rat coupled to gene expression analysis. *J Neurosci* **133**, 39-48.

Monyer H., Markram H., 2004. Interneuron diversity series: Molecular and genetic tools to study GABAergic interneuron diversity and function. *Trends Neurosci* **27**, 90-97.

Mora J., Akram M., Gerald W.L., 2002. Comparison of normal and tumor cells by laser capture microdissection. *Methods Enzymol* **356**, 240-247.

Morgan N.V., Westaway S.K., Morton J.E., Gregory A., Gissen P., Sonek S., Cangul H., Coryell J., Canham N., Nardocci N., Zorzi G., Pasha S., Rodriguez D., Desguerre I., Mubaidin A., Bertini E., Trembath R.C., Simonati A., Schanen C., Johnson C.A., Levinson B., Woods C.G., Wilmot B., Kramer P., Gitschier J., Maher E.R., Hayflick S.J., 2006. PLA2G6, encoding a phospholipase A2, is mutated in neurodegenerative disorders with high brain iron, *Nat Genet* **38**, 752-754.

Moriizumi T., Leduc-Cross B., Wu J.Y., Hattori T., 1992. Separate neuronal populations of the rat substantia nigra pars lateralis with distinct projection sites and transmitter phenotypes. *Neurosci* **46**, 711-720.

Mott D.D., Dingledine R., 2003. Interneuron Diversity series: Interneuron research – challenges and strategies. *Trends Neurosci* **26**, 484-488.

Nakagawa T., Schwartz J.P., 2004. Gene expression profiles of reactive astrocytes in dopamine-depleted striatum. *Brain pathol* **14**, 275-280.

Nauta W.J.H., Smith G.P., Faull R.L.M., Domesick V.B., 1978. Efferent connections and nigral afferents of the nuceus accumbens septi in the rat. *Neurosci* **3**, 385-401.

Nelson E.L, Liang C.L., Sinton C.M., German D.C., 1996. Midbrain dopaminergic neurons in the mouse: computer-assisted mapping. *J Comp Neurol* **369**, 361-371.

Nestler E.J., Carlezon W.A. Jr., 2006. The mesolimbic dopamine renard circuit in depression. *Biol Psychiatry* **12**, 1151-1159.

Neuhoff H., Neu A., Liss B., Roeper J., 2002. I(h) channels contribute to the different functional properties of identified dopaminergic subpopulations in the midbrain. *J Neurosci* **22**, 1290-1302.

Ng D.S., Maguire G.F., Wylie J., Ravandi A., Xuan W., Ahmed Z., Eskardarian M., Kuksis A., Connelly P.W., 2002. Oxidative stress is markedly elevated in lecithin:cholesterol acyltransferase-deficient mice and is parodoxically reversed in the apolipoprotein E knockout background in association with a reduction in atherosclerosis. *J Biol Chem* **277**, 11715-11720.

Niyaz Y., Stich M., Sagmuller B., Burgemeister R., Freidemann G., Sauer U., Gangnus R., Schutze K., 2005. Noncontact laser microdissection and pressure catapulting: sample preparation for genomic, transcriptomic, and proteomic analysis. *Methods Mol Med* **114**, 1-24.

Nunes I., Tovmasian L.T., Silva R.M., Burke R.E., Goff S.P., 2003. Pitx3 is required for the development of substantia nigra dopaminergic neurons. *Proc Natl Acad Sci USA* **100**, 4245-4250.

Nygaard V., Hovig E., 2006. Options available for profiling small tissue samples: a review of sample amplification technology when combined with microarray profiling. *Nucleic Acids Res* **34**, 996-1014.

Nygaard V., Løland A., Holden M., Langaas M., Rue H., Liu F., Myklebost O., Fodstad Ø., Hovig E., Smith-Sørensen B., 2003. Effects of mRNA amplification on gene expression ratios in cDNA experiments estimated by analysis of gene variance. *BMC Genomics* **4**, 11.

Ohstuka S., Iwase K., Kato M., Seki N., Shimizu-Yabe A., Miyauchi O., Sakao E., Kanazawa M., Yamamoto S., Kohno Y., Takiguchi M., 2004. An mRNA amplification procedure with directional cDNA-cloning and strand specific cRNA synthesis for comprehensive gene expression analysis. *Genomics* **84**, 715-729.

Okazaki Y., Furuno M., Kasukawa T. et al., 2002. Analysis of the mouse transcriptome basedon functional annotation of 60,770 full-length cDNAs. *Nature* **420**, 563-573.

Olanow C.W., Tatton W.G., 1999. Etiology and pathogenesis of Parkinson's disease. *Annu Rev Neurosci* **22**, 123-144.

Olanow C.W., Goetz C.G., Kordower J.H., Stoessl A.J., Sossi V., Brin M.F., Shannon K.M., Nauert G.M., Perl D.P., Godbold J., Freeman T.B., 2003. A double-blind controlled trial of bilateral fetal nigral transplantation in Parkinson's disease. *Ann Neurol* **54**, 403-14.

Oleskevich S., Descarries L.,Lacaille J-C., 1989. Quantified distribution of the noradrenaline innervation in the hippocampus of adult rat. *The J Neurosci* **9**, 3803-3815.

Osaka H., Wang Y.L., Takada K., Takizawa S., Setsuie R., Li H., Sato Y., Nishikawa K., Sun Y.J., Sakurai M., Harada T., Hara Y., Kimura I., Chiba S., Namikawa K., Kiyama H., Noda M., Aoki S., Wada K., 2003. Ubiquitin carboxy-terminal hydrolase L1 binds to and stabilizes monoubiquitin in neuron. *Hum Mol Genet* **12**, 1945-1958.

Paisán-Rui'z C., Jain S., Evans E.W., Gilks W.P., Simón J., van der Brug M., López de Munain A., Aparicio S., Gil A.M., Khan N., Johnson J., Martinez J.R., Nicholl D., Carrera I.M., Pena A.S., de Silva R., Lees A., Martí-Massó J.F., Pérez-Tur J., Wood N.W., Singleton A.B., 2004. Cloning of the gene containing mutations that cause *PARK8*-linked Parkinson's disease. *Neuron* **18**, 595-600.

Palacino J.J., SAgi D., Goldberg M.S., Krauss S., Motz C., Wacker M., Klose J., Shen J., 2004. Mitochondial dysfunction and oxidative damage in parkin-deficient mice. *J Bioc Chem* **279**, 18614-18622.

Paradis E., Clement S., Julien P., Ven Murthy M.R., 2003. Lipoprotein lipase affects the survival and differentiation of neural cellsexposed to very low density lipoprotein. *J Biol Chem* **278**, 9698-9705.

Parker W.D. Jr., Boyson S.J., Parks J.K., 1989. Abnormalities of the electron transport chain in idiopathic Parkinson's disease. *Ann Neurol* **26**, 719-723.

Parlato R., Rosica R., Cuccurullo V., Mansi L., Macchia P., Owens J.D., Mushinski J.F., De Felice M., Bonner R.F., Di Lauro R., 2002. A preservetion method that allows recovery of intact RNA from tissues dissected by laser capture microdissection. *Anal Biochem* **300**, 139-145.

Parra P., Gulyás A. I., Miles R., 1998. How many subtypes of inhibitory cells in the hippocampus? *Neuron* **20**, 983-993.

Paxinos G., 2004. *The Rat Nervous System*, 3rd ed , Elsevier.

Paxinos G., Franklin K.B.J., 2001. *The Mouse Brain in Stereotaxic Coordinates*, 3rd ed., Elsevier.

Pellerin L., Magistretti P.J., 2004. Neuroscience Let there be (NADH) light. *Science* **305**, 50-52.

Petalidis L., Bhattacharyya S., Morris G.A., Collins V.P., Freeman T.C., Lyons P.A., 2003. Global amplification of mRNA by template-switching PCR:

linearity and application to microarray analysis. *Nucleic Acids Res* **31**, e142.

Poirier G.M., Pyati J., Wan J.S., Erlander M.G., 1997. Screening differentially expressed cDNA clones obtained by differential display using amplified RNA. *Nucleic Acids Res* **25**, 913-914.

Polymeropoulos M.H., Lavedan C., Leroy, E., Ide S.E., Dehejia A., Dutra A., Pike B., Root H., Rubenstein J., Boyer R., Stenroos E.S., Chandrasekharappa S., Athanassiadou A., Papapetropoulos T., Johnson W.G., Lazzarini A.M., Duvoisin R.C., Di Iorio G., Golbe L.I., Nussbaum R.L., 1997. Mutation in the α-*synuclein* gene identified in families with Parkinson's disease. *Science* **276**, 2045-2047.

Prensa L., Parent A., 2001. The nigrostriatal pathway in the rat: a single-axon study of the relationship between dorsal and ventral tier nigral neuronsand the striosome/matrix striatal compartments. *J Neurosci* **21**, 7247-7260.

Puoppolo M., Raviola E., Bean B.C., 2007. Roles of subthreshold calcium and sodium current in spontaneous firing of mouse midbrain neurons. *J Neurosci* **27**, 645-656.

Purba J.S., Hofman M.A., Swaab D.F., 1994. Decreased number of oxytocin-immunoreactive neurons in the paraventricular nucleus of the hypothalamus in Parkinson's disease. *Neurology* **44**, 84-89.

Puskás L.G., Zvara A., Hackler L. Jr., Van Hummelen P., 2002. RNA amplification results in reproducible microarray data with slight ratio bias. *Biotechniques* **32**, 1330-1334.

Putzke J.D., Wharen R.E.,, Wszolek Z.K., Turk M.F., Strongosky A.J., Uitti R.J., 2003. Thalamic deep brain stimulation fro tremor-predominant Parkinson's disease. *Parkinsonism Relat Disord* **10**, 81-88.

Quackenbush J., 2001. Computational analysis of microarray data. *Nat Rev Genet* **2**, 418-427.

Rajput A.H., Uitty R.J., Sudhakar S., Rozdilsky B., 1989. Parkinsonism and neurofibrillary tangle pathology in pigmented nuclei. *Ann Neurol* **26**, 602-606.

Ramirez A., Heimbach A., Gründemann J., Stiller B., Hampshire D., Cid L.P., Goebel I., Mubaidin A.F., Wriekat A.L., Roeper J., Al-Din A., Hillmer A.M., Karsak M., Liss B., Woods C.G., Behrens M.I., Kubisch C., 2006. Hereditary parkinsonism with dementia is caused by mutations in ATP13A2, encoding a lysosomal type 5 P-type ATPase. *Nat Genet* **38**, 1184-1191.

Ramón y Cajal S., 1888. Sobre las fibras nerviosas de la capa molecular del cerebelo. *Revista trimestral de Histología Normal y Patológica* **2**, 33-49.

Redgrave P., Marrow L., Dean P., 1992. Topographical organization of the nigrotectal projection in rat: Evidence for segregated channels. *Neurosci* **50**, 571-595.

Reglodi D., Lubics A., Tamas A., Szalontay L., Lengvari I., 2004. Pituitary adenylate cyclase-activating polypeptide protects dopaminergic neurons and improves behavioural deficits in a rat model of Parkinson's disease. *Behav Brain Res* **151**, 303-312.

Rehman H.U., 2000. Progressive supranuclear palsy. *Postgrad Med J* **76**, 333-336.

Rodriguez M., Barroso-Chinea P., Abdala P., Obeso J., Gonzalez-Hernandez T., 2001. Dopamine cell de generation induced by intraventricular administration of 6-hydroxydopamine in the rat: similarities with cell loss in Parkinson's disease. *Exp Neurol* **169**, 163-181.

Rommelfanger K.S., Edwards G.L., Freeman K.G., Liles L.C., Iller G.W., Weinshenker D., 2007. Norepinephrine loss produces more profound motor deficits than MPTP treatment in mice. *Proc Natl Acad Sci* **104**, 13804-13809.

Salunga R.C., Guo H., Luo L., Bittner A., Joy K.C., Chambers J., Wan J., Jackson Erlander M.G., 1999. Gene expression analysis via cDNA microarrays of laser capture microdissected cells from fixed tissue. In *DNA Microarrays: A Practical Approach* (M. Schena, ed), pp. 121-137, Oxford Univ. Press.

Sanberg R., Yasuda R., Pankratz D.G., Carter T.A., Del Rio J.A., Wodicka L., Mayford M., Lockhart D.J., Barlow C., 2000. Regional and strain-specific gene expression mapping in the adult mouse brain. *Proc Natl Acad Sci U.S.A.* **97**, 11038-11043.

Saper C.B., 1999. 'Like a thief in the night': the selectivity of degeneration in Parkinson's disease. *Brain* **122**, 1401-1402.

Sawamoto K., Nakao N., Kobayashi K., Matsushita N., Takahashi H., Kakishita K., Yamamoto A., Yoshizaki T., Terashima T., Muratami F., Itakura T., Okano H., 2001. Visualization, diret isolation, and transplantation of midbrain dopaminergic neurons. *Proc Natl Acad Sci* **98**, 6423-6428.

Schapira A.H., Cooper J.M., Dexter D., Jenner P., Clark J.B., Marsden C.D., 1989. Mitochondrial complex I deficiency in Parkinson's disease. *Lancet* **1**, 1269.

Schena M., Shalon D., Davis R.W., Brown P.O., 1995. Quantitative monitoring of gene expression patterns with a complementary DNA microarray. *Science* **270**, 467-470.

Schleidl S.J., Nilsson S., Kalén M., Hellström M., Takemoto M., Håkansson, Lindahl P., 2002. mRNA expression profiling of laser microbeam microdissected cells from slender embryonic structures. *Am J Pathol* **160**, 801-813.

Schutze K., Becker B., Bernsen M., Björnsen T., Broksch D., Bush C., Clement-Sengewald A., et al., 2003. Tissue microdissection, laser pressure catapulting. In *DNA Microarrays: A Molecular Cloning Manual* (Bowtell D., Sambrook J., eds), pp. 331-356, Cold Spring Harbor Laboratory Press.

Schutze K., Lahr G., 1998. Identification of espresse genes by laser-mediated manipulation of single cells. *Nat Biotechnol* **16**, 737-742.

Seamans J.K., Yang C.R., 2004. The principal features and mechanisms of dopamine modulation in the prefrontal cortex. *Prog Neurobiol* **74**, 1-58.

See J., Mamontov P., Ahn K., Wine-Lee L., Crenshaw E.B. 3rd, Grinspan J.B., 2007. BMP signalling mutant mice exhibit glial cell maturation defects. *Mol Cell Neurosci* **35**, 171-182.

Seiger A., Olson L., 1973. Late prenatal ontogeny of central monoamine neurons in the rat: Fluorescence histochemical observations. *Z Anat Entwicklungsgesch* **140**, 281-318.

Selby G., 1984. The Graeme Robertson memorial lecture. 1983. The long-term prognosis of Parkinson's disease. *Clin Exp Neurol* **20**, 1-25.

Seth D., Gorrell M.D., McGuinness P.H., Leo M.A., Lieber C.S., McGaughan G.W., Haber P.S., 2003. SMART amplification maintains representation of relative gene expression: quantitative validation by real time PCR and application to studies of alcoholic liver disease in primates. *J. Biochem Biophys Methods* **55**, 53-66.

Sgadò P., Albéri L., Gherbassi D., Galasso S.L., Ramakers G.M., Alavian K.N., Smidt M.P., Dyck R.H., Simon H.H., 2006. Slow progressive degeneration of nigral dopaminergic neurons in postnatal Engrailed mutant mice. *Proc Natl Acad Sci USA* **103**, 15242-15247.

Shapira A.H., Cooper J.M., Dexter D., Clark J.B., Jenner P., Marsden C.D., 1990. Mitochondrial complex I deficiency in Parkinson's Disease. *J Neurochem* **54**, 823-827.

Shiraki T., Kondo S., Katayama S., Waki K., Kasukawa T., KAwaji H., Kodzius R., Watahiki A., Nakamura M., Arakawa T., Fukuda S., Sasaki D.,

Podhajska A., Harbers M., Kawai J., Carninci P., and Hayashizaki Y., 2003. Cap analysis gene expression of high-throughput analysis of transcriptional starting point and identification of promoter usage. *Proc Natl Acad Sci USA* **100**, 15776-15781.

Shirota S., Yoshida T., Sakai M., Kim J.I., Sugiura H., Oishi T., Nitta K., Tsuchiva K., 2006. Correlation between the expression level of c-maf and glutathione peroxidase-3 in c-maf -/- mice kidney and c-maf overexpressed renal tubular cells. *Bichem Biophys Res Commun* **348**, 501-506.

Sillitoe R.V., Vogel M.W., 2008. Desire, disease, and the origins of the dopaminergic system. *Schizof Bull* **34**, 212-219.

Simon H., Sauressig H., Wurst W., Goulding M., O'Leary D., 2001. Fate of midbrain dopaminergic neurons controlled by the engrailed genes. *J Neurosci* **21**, 3126-3134.

Simone N.L., Bonner R.F., Gillespie J.W., Emmert-Buck M.R., Liotta R.A., 1998. Laser-capture microdissection: opening the microscopic frontier to molecular analysis. *Trends Genet* **14**, 272-276.

Simón-Sánchez J., Singleton A.B., 2008. Sequencing analysis of OMI/HTRA2 shows previously reported pathogenic mutations in neurologically normal controls. *Hum Mol Genet* **17,** 1988-1993.

Smidt M.P., van Schaick H.S., Lancot C., Tremblay J.J., Cox J.J., van der Kleij A.A., Wolterink G., Drouin J., Burbach J.P., 1997. A homedomain gene Pitx3 has higly restricted brain expression in mesencephalic dopaminergic neurons. *Proc Natl Acad Sci USA* **94**, 13305-13310.

Smidt M.P., Asbreuk C.H., Cox J.J., Chen H., Johnson R.L., Burbach J.P., 2000. A second independent pathway for development of mesencephalic dopaminergic neurons requires Lmx1b. *Nature Neurosci* **3**, 337-341.

Smyth G. K., 2004. Linear models and empirical Bayes methods for assessing differential expression in microarray experiments. *Statistical Applications in Genetics and Molecular Biology*, Vol. 3, No. 1, Article 3.

Soverchia L., Ubaldi M., Leopardi-Essmann F., Ciccocioppo R., Hardiman G., 2005. Microarrays – The challenge of preparing brain tissue samples. *Addict Biol* **10**, 5-13.

Spillantini M.G., Schmidt M.L., Lee V.M., Trojanowski J.Q., Jakes R., Goedert M., 1997. Alpha-synuclein in Lewy bodies. *Nature* **388**, 839-840.

Srinivasan J., Schmidt W., 2004. Behavioral and neurochemical effects of noradrenergic depletions with N-(2-cloroethyl-)-N-ethyl-2-

bromobenzylamine in 6-hydroxydopamine-induced rat model of Parkinson's disease. *Behav Brain Res* **151**, 191-199.

Srinivasan R., 1996. Ablation of polymers and biological tissue by ultraviolet lasers. *Science* **234**, 559-565.

Stears R. L., Getts R. C., Gullans S.R., 2000. A novel, sensitive detection system for high – density microarrays using dendrimer technology. *Physiol Genomics* **3**, 93-99.

Stenman J., Lintula S., rissansen O., Finne P., Hedstrom J., Palotie A., Orpana A., 2003. Quanitative detection of low-copy-number mRNAs differing at single nucleotide positions. *Biotechniques* **34**, 172-177.

Stevens C.F., 1998. Neuronal diversity: too many cell types for confort? *Curr. Biol.* **8**, R708-R710.

Stewart G.J., Savioz A., Davies R.W., 1997. Sequence analysis of 497 mouse brain ESTs expressed in the substantia nigra. *Genomics* **39**, 147-153.

Storch A., Sabolek M., Milosevic J., Schwarz S.C., Schwarz J., 2004. Midbrain-derived neural stem cells: From basic science to therapeutic approaches. *Cell Tissue Res* **318**, 15-22.

Stoyanova R., Upson J.J., Patriotis C., Ross E.A., Henske E.P., Datta K., Boman B., Clapper M.L., Knudson A.G., Bellacosa A., 2004. Use of RNA amplification in the optimal characterization of global gene expression using cDNA microarrays. *J Cell Physiol* **201**, 359-365.

Strauss K.M., Martins L.M., Plun-Favreau H., Marx F.P., Kautzmann S., Berg D., Gasser T., Wszolek Z., Müller T., Bornemann A., Wolburg H., Downward J., Riess O., Schulz J.B., Krüger R., 2005. Loss of function mutations in the gene encoding Omi/HtrA2 in Parkinson's disease. *Hum Mol Genet* **14**, 2099-2111.

Struyk A.F., Canoll P.D., Wolfgang M.J., Rosen C.L., D'Eustachio P., Salzer J.L., 1995. Cloning of neurotrimin defines a new subfamily of differentially expressed neural cell adhesion molecules. *J Neurosci* **15**, 2141-2156.

Sugino K., Hempel C.M., Miller M.N., Hattox A.M., Shapiro P., Wu C., Huang Z.J., Nelson S.B., 2006. Molecular taxonomy of major neuronal classes in the adult mouse forebrain. *Nat Neurosci* **9**, 99-107.

Swanson L.W., 1982. The projections of the ventral tegmental area and adjacent regions: a combined fluorescent retrograde tracer and immunofluorescence study in the rat. *Brain Res Bull* **9**, 321-353.

Takei N., Scoglosa Y., Lindholm D., 1998. Neurotrophic and neuroprotective effect of pituitary adenylate cyclase-activating polypeptide (PACAP) on mesencephalic dopaminergic neurons. *J Neurosci Res* **54**, 698-706.

Tanner C.M., Ottman R., Goldman S.M., Ellenberg J., Chan P., Mayeux R., Langston J.W., 1999. Parkinson disease in twins: an etiologic study. *JAMA* **281**, 341-346.

Thuret S., Bhatt L., O'Leary D.D., Simon H.H., 2004. Identification and developmental analysis of genes expressed by dopaminergic neurons of the substantia nigra pars compacta. *Mol Cell Neurosci* **25,** 394-405.

Thurret S., Bhatt L., O'Leary D.D.M., Simon H.H., 2004. Identification and developmental analysis of genes expressed by dopaminergic neurons of the substantia nigra pars compacta. *Mol Cell Neurosci* **25**, 394-405.

Tietjen I., Rihel J.M., Cao Y., Koentges G., Zakhary L., Dulac C., 2003. Single-cell transcriptional analysis of neuronal progenitors. *Neuron* **38**, 161-175.

Torres – Muñoz J.E., Van Waveren C., Keegan M. G., Bookman R.J., Petito C.K., 2004. Gene expression profiles in microdissected neurons from human hippocampal subregions. *Mol Brain Res* **127**, 105-114.

Trettel F., Rigamonti D., Hilditch-Maguire P., Wheeler V.C., Sharp A.H., Persichetti F., Cattaneo E., MacDonald M.E., 2000. Dominant phenotypes produced by the *HD* mutation in ST*Hdh*^{Q111} striatal cells. *Hum Mol Genet* **9**, 2799-2809

Trodaec J-D., Marien M., Darios F., Hartmann A., Ruberg M., Colpaert F.C., Michel P.P., 2001. Noradrenaline provides long term protection to dopaminergic neurons by reducing oxidative stress. *J Neurochem* **79**, 200-210.

Valen E., Pascarella G., Chalk A., Maeda N., Kojima M., Kawazu C., Murata M., Mishiyori H., Lazareviĉ D., Motti D., Marstrand T.T., Tang M.H., Zhao X., Krogh A., Winther O., Arakawa T., Kawai J., Wells C., Daub C., Harbers M., Hayashizaki Y., Gustincich S., Sandelin A., Carninci P., 2009. Genome-wide detection and analysis of hippocampus core promoters using DeepCAGE. *Genome Res* **19**, 255-265.

Valente E.M., Abou-Sleiman P.M., Caputo V., Muqit M.M., Harvey K., Gispert S., Ali Z., Del Turco D., Bentivoglio A.R., Healy D.G., Albanese A., Nussbaum R., González-Maldonado R., Deller T., Salvi S., Cortelli P., Gilks W.P., Latchman D.S., Harvey R.J., Dallapiccola B., Auburger G., Wood NW., 2004. Hereditary early onset Parkinson's disease is caused by mutations in *PINK1*. *Science* **304**, 1158-1160.

Valverde F., 1970. A pool for comparative structural analyses. In *Contemporary Research Methods in Neuroanatomy* (Nauta W.J.H., Ebbesson S.O.E., eds),, pp. 12-31, Sprimger.

Van Deerlin V.M., Gill L.H., Nelson P.T., 2002- Optimizing gene expression analysis in archival brain tissue. *Neurochem Res* **27**, 993-1003.

Van der Kooy D., Coscina D.V., Hattori T., 1981. Is there a non-dopaminergic nigrostriatal pathway? *Neurosci* **6**, 345–357.

Van Gelder R.N., von Zastrow M.E., Yool A., Dement W.C., Barchas J.D., Eberwine J.H., 1990. Amplified RNA synthesized from limited quantities of heterogeneous cDNA. *Proc Natl Acad Sci* **8**, 1663-1667.

Varastet M., Richie D., Maziere M., Hantraye P., 1994. Chronic MPTP treatment reproduces in baboons the differential vulnerability of mesencephalic dopaminergic neurons observed in Parkinson's disease. *Neuroscience* **63**, 47-56.

Vaudry D., Gonzalez B.J., Basille M., Yon M., Fournier A., Vaudry H., 2000. Pituitary adenylate cyclase-activating polypeptide and its receptors : from structure to functions. *Pharmacol Rev* **52**, 269-324.

Velculescu V.E., Zhang L., Vogelstein B., Kinzler K.W., 2005. Serial analysis of gene expression. *Science* **270**, 484-487.

Viggiano D., Vallone D., Ruocco L.A., Sadile A.G., 2003. Behavioural, pharmacological, morpho-functional molecular studies reveal a hyperfunctioning mesocortical dopamine system in an animal model of attention deficit and hyperactivity disorder. *Neurosci Biobehav Rev* **27**, 683-689.

Vincek V., Nassiri M., Nadji M., Morales A.R., 2003. A tissue fixative that protects macromolecules (DNA, RNA, and Protein) and histomorphology in clinical samples. *Lab Invest* **83**, 1427-1436.

Vingerhoets F.J.G., Snow B.J., Tetrud J.W., 1994. Positron emission tomography evidene for progression of human MPTP-induced dopaminergic lesions. *Ann Neurol* **36**, 765-770.

Vlachouli C., Motti D., Lazarevic̆ D., Krmac H., Gustincich S., 2008. Gene expression profiling of laser capture-microdissected neuronal population in the mammalian CNS. *MACS&more*, costumer report, vol. 12, 2-4; www.miltenyibiotec.com

Vogel A., Venugopalan V., 2003. Mechanisms of pulsed laser ablation of biological tissues. *Chem Rev* **103**, 577-644.

Wang E., Miller L.D., Ohnmacht G.A., Liu E.T., Marincola F.M., 2000. High-fidelity mRNA amplification for gene profiling. *Nat Biotechnol* **18**, 457-459.

Wang W.Z., Oeschger F.M., Lee S., Molnar Z., 2009. High quality RNA from multiple brain regions simultaneously acquired by laser capture microdissection. *BMC Mol Biol* **10**, 69.

Wässle H., Peichl L., Boycott B. B., 1981. Denditic territories of of cat retinal ganglion cells. *Nature* **292**, 344-345.

Weihe E., Depboylu C., Schütz B., Schäfer M.K., Eiden L.E., 2006. Three types of tyrosine hydroxylase-positive CNS neurons distinguished by DOPA-decarboxylase and VMAT2 co-expression. *Cell Mol Neurobiol* **26**, 659-678.

Weldeyer-Hartz H.W.G., 1891. Űber eirige neuere Forschungen im Gebiete der Anatomie des Contrahervenoyotoms. Deutsch Med Wohnsohr 17, 1213-1216, 1244-1246, 1267-1269, 1297-1299, 1331-1332, 1352-1356.

Williams J.M., Thompson V.L., Mason-Parker S.E., Abraham W.C., Tate W.P., 1998. Synaptic activity-dependent modulation of mitochondrial gene expression in the hippocampus. *Brain Res Mol Brain Res* **60**, 50-56.

Williams S.M., Goldman-Rakic P.S., 1998. Widespread origin of the primate mesofrontal dopamine system. *Cereb Cortex* **8**, 321-345.

Willingham S., Outeiro T.F., DeVit M.J., Lindquist S.L., Muchowski P.J., 2003. Yeast genes that enhance the toxicity of a mutant huntingtin fragment or alpha-synuclein. *Science* **302**, 1769-1772.

Wirdefeldt L., Gatz M., Schalling M., Pedersen N.L., 2004. No evidence for heritability of Parkinson's disease in Swedish twins. *Neurol* **63**, 305-311.

Wodicka L., Dong H., Mittmann M., Ho M.H., Lockhart D.J., 1997. Genome-wide expression monitoring in *Saccharomyces cervisiae. Nature Biotechnol* **15**, 1359-1367.

Wolfart J., Neuhoff H., Franz O., Roeper J., 2001. Differential expression of the small-conductance, calcium-activated potassium channel SK3 is critical for pacemaker control in dopaminergic midbrain neurons. *J Neurosci* **21**, 3443-3456.

Wurmbach E., Gonzales-Maeso J., Yuen T., Ebersole B.J., Maistaitis J.W., Mobbs C.V., Sealfon S.C., 2002. Validated genomic approach to study differentially expressed genes in complex tissues. *Neurochem Res* **27**, 1027-1033.

Xiang C.C., Mezey E., Chen M., Key S., Ma L., Brownstein M.J., 2004. Using DSP, a reversible cross-linker, to fix tissue section for immunostaining, microdissection and expression profiling. *Nucleic Acids Res* **32**, e185.

Xie T., Tong L., Barrett T., Yuan J., Hatzidimitriou G., McCann U.D., Becker K.G., Donovan D.M., Ricaurte G.A., 2002. Changes in gene expression linked to methamphetamine-induced dopaminergic neurotoxicity. *J Neurosci* **22**, 274-283.

Yang Y.H.,Speed T.P., 2002. Design issues for cDNA microarrays experiments. *Nat Rev Genet* **3**, 579-588.

Yao F., Yu F., Gong L., Taube D., Rao D.D., MacKenzie R.G., 2005. Microarray analysis of fluoro-gold labeled rat dopamine neurons harvested by laser capture microdissection. *J Neurosci Methods* **143**, 95-106.

Yavich L., Forsberg M.M., Karayiorgou M., Gogos J.A., Mannisto P.T., 2007. Site-specific role of catechol-O-methyltransferase in dopamine overflow within prefrontal cortex and dorsal striatum. *J Neurosci* **27**, 10196-10209.

Ye W., Shimamura K., Rubenstein J.L., Hynes M.A., Rosenthal A., 1998. FGF and Shh signals control dopaminergic and serotonergic cell fate in the anterior neural plate. *Cell* **93**, 755-766.

Zarranz J.J., Alegre J., Gómez-Esteban J.C, Lezcano E, Ros R, Ampuero I., Vidal L., Hoenicka J., Rodriguez O., Atarés B., Llorens V., Gomez Tortosa E., del Ser T., Muñoz D.G., de Yebenes J.G., 2004. The new mutation, E46K, of alpha-synuclein causes Parkinson and Lewy body dementia. *Ann Neurol* **55**, 164-173.

Zeevalk G.D., Bernard L.P., Manzino L., Sonsalla P.K., 2001. Differential sensitivity of mesencephalic neurons to inhibition of phosphatase 2A. *J Pharmacol Exp Ther* 298, 925-933.

Zetterstrom R.H., Solomin L., Jansson L., Hoffer B.J., Olson L., Perlmann T., 1997. Dopamine neuron agenesis in Nurr1-deficient mice. *Science* **276**, 248-250.

Zhang Y., Ma C., Delohary T., Nasipak B., Foat B.C., Bounoutas A., Bussemaker H. J., Kim S.K., Chalfie M., 2002. Identification of genes expressed in *C. elegans* touch receptor neurons. *Nature* **418**, 331-335.

Zhao H., Hastie T., Whitfield M.L., Børresen-Dale A.L., Jeffrey S.S., 2002. Optimization and evaluation of T7 based RNA linear amplification protocols for cDNA microarray analysis. *BMC Genomics* **3**, 31.

Zhao X., Lein E.S., He A., Smith S.C., Aston C., Gage F.H., 2001. Transcriptional profiling reveals strict boundaries between hippocampal subregions. *J Comp Neurol* **441**, 187-196.

Zhou B., Westaway S.K., Levinson B., Johnson M.A., Gitschier J., and Hayflick S.J., 2001. A novel pantothenate kinase gene (PANK2) is defective in Hallervorden–Spatz syndrome, *Nat Genet* **28**, 345-349.

Zimprich A., Biskup S., Leitner P., Lichtner P., Farrer M., Lincoln S., Kachergus J., Hulihan M., Uitti R.J., Calne D.B., Stoessl A.J., Pfeiffer R.F., Patenge N., Carbajal I.C., Vieregge P., Asmus F., Müller-Myhsok B., Dickson D.W., Meitinger T., Strom T.M., Wszolek Z.K., Gasser T., 2004. Mutations in LRRK2 cause autosomal-dominant parkinsonism with pleomorphic pathology. *Neuron* **18**, 601-607.

Zirlinger M., Anderson D., 2003. Molecular dissection of the amygdale and its relevance to autism. *Genes Brain Behav* **2**, 282-294.

SUPPLEMENTARY TABLE

Differentially expressed genes between A9 cells from SN and A10 cells from VTA

Gene description	Gene name	logFC	AveExpr	adj.P.Val
More expressed in A9				
GLIA DERIVED NEXIN PRECURSOR (GDN)	Serpine2	1.6	11.87	5.34E-17
membrane protein. palmitoylated 3 (MAGUK p55 subfamily member 6)	Mpp6	1.19	9.78	9.54E-12
NEUROTRIMIN PRECURSOR (GP65) homolog [Rattus norvegicus]	Hnt	1.14	10.15	4.92E-18
Similar to 10-formyltetrahydrofolate dehydrogenase	Aldh1l1	0.97	9.51	2.19E-15
RAB3C. member RAS oncogene family	Rab3c	0.95	9.55	4.99E-07
Grin2c	Grin2c	0.93	10.53	2.56E-11
Similar to LIM and cysteine-rich domains 1	Lmcd1	0.91	7.5	7.77E-07
UXT PROTEIN (UBIQUITOUSLY EXPRESSED TRANSCRIPT PROTEIN)	Uxt	0.89	9.21	3.27E-10
PLASMA KALLIKREIN PRECURSOR (EC 3.4.21.34)	Cyp4v3	0.85	8.11	1.22E-08
1-acylglycerol-3-phosphate O-acyltransferase 1	Agpat4	0.84	12.49	2.56E-11
PHOSPHATIDYLCHOLINE-STEROL ACYLTRANSFERASE PRECURSOR (EC 2.3.1.43)	Lcat	0.82	7.91	1.16E-08
L-LACTATE DEHYDROGENASE B CHAIN (EC 1.1.1.27)	Ldhb	0.81	14.33	1.81E-10
hypothetical Cytochrome c family heme-binding site containing protein	Mtmr15	0.81	8.48	1.10E-06
hypothetical protein	Sft2d3	0.81	11.46	1.81E-07
Neuritin	Nrn1	0.79	10.09	5.05E-13
single-stranded DNA binding protein 2	Ssbp2	0.77	10.23	2.22E-07
hypothetical protein	Ttyh3	0.74	9.72	6.51E-07
transducin-like enhancer of split 6. homolog of Drosophila E(spl)	Tle6	0.73	8.15	0.003785
LIM DOMAIN TRANSCRIPTION FACTOR LMO4	Lmo4	0.72	10.59	8.37E-09
SH3-domain GRB2-like B1 (endophilin)	Sh3glb1	0.71	8.8	0.00025
similar to THYRO1001033 PROTEIN [Homo sapiens]	Ttc12	0.7	8.26	1.45E-06
Esau protein		0.69	9.76	5.09E-07
RIKEN cDNA 2210417O06	Sri	0.67	10.25	8.37E-09
CHONDROMODULIN-I PRECURSOR (CHM-I)	Lect1	0.67	8.85	8.37E-09
Similar to phenylalanine-tRNA synthetase	Fars2	0.67	8.4	2.15E-05
hypothetical protein	2810432D09Rik	0.67	8.97	0.000216

RIKEN cDNA 2410015N17	2410015N17Rik	0.66	9.06	7.27E-06
unknown EST		0.64	9.2	6.17E-05
PREFOLDIN SUBUNIT 6 (PROTEIN KE2)	H2-Ke2	0.63	11.85	3.45E-07
mitchondrial ribosomal protein S7	Mrps7	0.6	10.53	1.14E-06
GLUTATHIONE S-TRANSFERASE THETA 1 (EC 2.5.1.18)	Gstt1	0.6	8.51	0.001452
RIKEN cDNA 1700019N12	1700019N12Rik	0.59	7.83	0.000176
Similar to RIKEN cDNA 2700094L05 gene	Ccdc12	0.58	9.89	7.29E-09
hypothetical Kelch repeat containing protein	Klhl30	0.58	12.89	8.76E-08
RNA PROCESSING FACTOR 1 homolog [Homo sapiens]	Bxdc5	0.57	7.85	3.91E-05
serine/threonine kinase 6	Aurka	0.56	8.4	0.000356
RIKEN cDNA 2410130M07	Nola2	0.55	10.64	1.53E-06
hypothetical P-loop containing nucleotide triphosphate hydrolases structure containing	4922503N01Rik	0.55	7.93	0.008411
ubiquitin conjugating enzyme 6	Ube2j2	0.55	9.84	4.81E-05
RIKEN cDNA 2010001H09 gene	2410081M15Rik	0.55	8.77	9.70E-05
ubiquinol-cytochrome c reductase core protein 1	Uqcrc1	0.54	11.77	0.000784
2-OXOISOVALERATE DEHYDROGENASE ALPHA SUBUNIT	Bckdha	0.54	9.03	0.000796
Unknown (protein for IMAGE:3990036)	1810048J11Rik	0.53	8.02	0.000645
RIKEN cDNA 2810036K01	Srfbp1	0.52	8	3.74E-05
mouse fat 1 cadherin	Fat1	0.52	7.78	0.002313
hypothetical protein	Camk2n1	0.52	11.88	2.05E-09
CHORDIN PRECURSOR	Chrd	0.51	8.27	0.001441
hypothetical protein	1300010M03Rik	0.51	9.58	5.96E-07
ADP.ATP CARRIER PROTEIN. FIBROBLAST ISOFORM (ADP/ATP TRANSLOCASE 2)	EG433923	0.5	11.06	4.62E-06
magnesium-dependent phosphatase-1	1810034K20Rik	0.5	10.65	0.000148
RIKEN cDNA 2400007P05		0.5	9.94	0.002306
hypothetical Microbodies C-terminal targeting signal containing protein	Tmem177	0.5	7.81	0.000512
damage specific DNA binding protein 1 (127 kDa)	Ddb1	0.5	12.57	3.81E-09
TRANSCRIPTION FACTOR S-II-RELATED PROTEIN 4 (FRAGMENT)	Tcea3	0.5	8.71	0.002154
tumor-suppressing subchromosomal transferable fragment 4	Tssc4	0.5	9.06	3.29E-05
ARP2/3 COMPLEX 41 KDA SUBUNIT (P41-ARC)	Arpc1b	0.5	8.29	0.001094
Similar to hypothetical protein FLJ12949	Kri1	0.49	8.62	0.002967

disrupter of silencing SAS10	Utp3	0.49	10.1	1.07E-10
TAF15 RNA polymerase II. TATA box binding protein (TBP)-associated factor. 68 kDa	Taf15	0.49	11.14	1.61E-05
N-ACETYLLACTOSAMINIDE BETA-1.6-N-ACETYLGLUCOSAMINYLTRANSFERASE (EC 2.4.1.150)	Gcnt2	0.49	7.69	0.000221
citrate synthase	Cs	0.48	8.54	0.00088
hypothetical Src homology 3 (SH3) domain profile	Fchsd1	0.48	8.31	0.003046
RIKEN cDNA 2310005G07	D10Ertd641e	0.48	8.76	0.005221
histocompatibility 47	H47	0.48	10.22	5.95E-06
melanoma antigen. family E. 1	Magee1	0.47	9.68	0.000119
E430004M18	G6pdx	0.47	10.15	0.004429
v-ral simian leukemia viral oncogene homolog B (ras related)	Ralb	0.47	8.28	0.000293
similar to PUTATIVE LAG1-INTERACTING PROTEIN (FRAGMENT) [Homo sapiens]	BC003331	0.47	9.05	0.003092
HYPOTHETICAL 23.9 KDA PROTEIN (CDNA FLJ31142 FIS. CLONE IMR322001317	Dusp26	0.47	9.31	0.000149
weakly similar to RIBONUCLEASE III (EC 3.1.26.3) (RNASE III) (P241) [Homo sapiens]	Rnasen	0.47	7.54	0.000148
hypothetical COMPLETE PROTEOME BOLA/YRBA FAMILY REGULATION	Bola1	0.47	7.82	0.003266
similar to PROTOHEME IX FARNESYLTRANSFERASE [Homo sapiens]	Cox10	0.47	8.29	0.009928
ARYLAMINE N-ACETYLTRANSFERASE 2 (EC 2.3.1.5) (ARYLAMIDE ACETYLASE 2)	Nat2	0.47	9.78	2.84E-06
CALCIPRESSIN 2 (DOWN SYNDROME CANDIDATE REGION 1-LIKE PROTEIN 1)	Rcan2	0.47	8.84	1.25E-07
expressed sequence C78613	Med10	0.46	9.44	0.002505
hypothetical protein	Lrrc27	0.46	8.1	0.000269
CORONIN 1B (CORONIN 2)	Coro1b	0.46	9.82	0.003532
RIKEN cDNA 2010003O14		0.46	13.1	0.001891
hypothetical protein	Nfic	0.46	9.16	0.001414
E430004M18	G6pdx	0.46	9.22	0.001533
Similar to fusion. derived from t(12:16) malignant liposarcoma	Fus	0.45	7.84	0.00273
succinate-Coenzyme A ligase. ADP-forming. beta subunit	Sucla2	0.45	10.53	1.28E-05
MITOCHONDRIAL IMPORT INNER MEMBRANE TRANSLOCASE SUBUNIT TIM23		0.45	11.34	0.005981
weakly similar to KRAB ZINC FINGER PROTEIN [Mus musculus]	2810487A22Rik	0.45	9.24	0.001329
weakly similar to HYPOTHETICAL 66.8 KDA PROTEIN (FRAGMENT) [Homo sapiens]	RP23-336F11.32	0.45	7.72	0.00309
Drd2	Drd2	0.45	13.05	2.29E-07
embryonic ectoderm development	Eed	0.44	11.36	0.001919
RIKEN cDNA 1110001I24	Bzw2	0.44	10.41	1.07E-05

SPERM SURFACE PROTEIN SP17 (SPERM AUTOANTIGENIC PROTEIN 17)	Spa17	0.44	9.26	7.75E-06
HYPOTHETICAL 43.8 KDA PROTEIN homolog [Homo sapiens]	Kif26b	0.44	8.04	1.17E-05
SERINE/THREONINE-PROTEIN KINASE PRP4 HOMOLOG (EC 2.7.1.37)	Prpf4b	0.44	8.08	0.000916
sialyltransferase 8 (alpha 2. 8 sialytransferase) E	St8sia5	0.44	7.92	3.06E-06
RIKEN cDNA 1810018M05	Pycr2	0.44	11.09	0.000953
von Ebner minor salivary gland protein	U46068	0.44	11.01	0.000203
RIKEN cDNA 1500019L24	Osgep	0.43	9.34	7.94E-05
CDNA FLJ14883 FIS. CLONE PLACE1003596	Stt3b	0.43	9.16	0.000216
ATP SYNTHASE COUPLING FACTOR 6. MITOCHONDRIAL PRECURSOR (EC 3.6.3.14) (F6)	Atp5j	0.43	11.26	0.000177
Rhotekin	Rtkn	0.43	10.15	0.000418
RIKEN cDNA 2310003F16	2310003F16Rik	0.43	12.12	6.64E-05
Grin3b	Grin3b	0.43	9.68	9.12E-05
expressed sequence tag mouse EST 12	X83328	0.43	8.81	0.000418
weakly similar to SIMILAR TO ZINC FINGER PROTEIN 254 [Homo sapiens]	1700049G17Rik	0.42	7.08	0.009306
hypothetical protein	5031410I06Rik	0.42	11.29	0.000312
sterol regulatory element binding protein 2	Srebf2	0.42	7.86	0.003266
proteasome (prosome. macropain) 26S subunit. non-ATPase. 11	Psmd11	0.42	9.74	0.000986
hypothetical protein	1700058G18Rik	0.42	8	0.002955
RIKEN cDNA 0610007P06	l7Rn6	0.42	8.65	0.001297
GENERAL TRANSCRIPTION FACTOR II-I (GTFII-I) (TFII-I)(BTK-ASSOCIATED PROTEIN-135) (BAP-135)		0.42	11.2	9.59E-08
DNA segment. human D6S2654E	D0H6S2654E	0.42	9.5	0.005257
ring finger protein 11	4732491K20Rik	0.41	8.43	0.004346
desmoglein 2	Dsg2	0.41	8.62	0.000813
CELL GROWTH REGULATING NUCLEOLAR PROTEIN	Lyar	0.41	8.78	0.000435
hypothetical protein	Rtf1	0.41	9.84	1.56E-07
NICOTINAMIDE N-METHYLTRANSFERASE (EC 2.1.1.1)	Nnmt	0.41	7.57	0.009306
hypothetical D111/G-patch domain containing protein	2310002B06Rik	0.4	8.46	0.000668
CREATINE KINASE. B CHAIN (EC 2.7.3.2) (B-CK)	Ckb	0.4	13.79	0.00155
HETEROGENEOUS NUCLEAR RIBONUCLEOPROTEIN K (HNRNP K) (65 KDA PHOSPHOPROTEIN)	Hnrpk	0.4	9.63	0.000216
mitochondrial ribosomal protein S5	Mrps5	0.4	8.86	0.008982
HYPOTHETICAL 67.2 KDA PROTEIN homolog [Homo sapiens]	Zfp653	0.4	8.98	0.002598

Unknown (protein for IMAGE:4948318)	Hmgb2l1	0.4	8.44	0.00408
mitochondrial ribosomal protein L43	Mrpl43	0.39	10.78	0.001037
unknown EST	Socs2	0.39	7.78	0.002374
nudix (nucleoside diphosphate linked moiety X)-type motif 7	Nudt7	0.39	8.95	0.003637
DA59H18.2 (NOVEL PROTEIN SIMILAR TO HUMAN	Cerk	0.39	8.66	0.000213
cofilin 1. non-muscle	Cfl1	0.38	12.59	4.41E-05
hypothetical PH domain-like structure containing protein	1700003H04Rik	0.38	9.37	0.000505
testis specific gene A2	Rsph1	0.38	8.32	0.001223
ACYLPHOSPHATASE. MUSCLE TYPE ISOZYME (EC 3.6.1.7)	Acyp2	0.38	7.7	0.005178
Unknown (protein for MGC:37173)	Mgat2	0.37	10.44	0.001106
hypothetical Zinc finger. C2H2 type containing protein	Zfp512	0.37	9.3	0.001879
PROTEASOME SUBUNIT ALPHA TYPE 7 (EC 3.4.25.1) (PROTEASOME SUBUNIT RC6-1)	Psma7	0.37	11.77	0.004414
CHOLINE O-ACETYLTRANSFERASE (EC 2.3.1.6) (CHOACTASE) (CHOLINE ACETYLASE) (CHAT)	Chat	0.37	7.45	0.002232
hypothetical Glutamine-rich region containing protein	1700090G07Rik	0.36	6.27	0.006413
2310009C03RIK PROTEIN homolog [Mus musculus]	Wdr5b	0.36	7.42	0.0028
heparan sulfate (glucosamine) 3-O-sulfotransferase 1	Hs3st1	0.36	7.65	0.000524
HISTIDINE TRIAD NUCLEOTIDE-BINDING PROTEIN (PROTEIN KINASE C INHIBITOR 1)	Hint1	0.36	13.46	0.00189
NUCLEAR FACTOR 1 A-TYPE (NUCLEAR FACTOR 1/A) (NF1-A) (NFI-A) (NF-I/A)	Nfia	0.36	12.44	6.69E-05
RIKEN cDNA 2810405O22	Med29	0.36	10.35	0.00746
CARNITINE DEFICIENCY-ASSOCIATED PROTEIN EXPRESSED IN VENTRICLE 1 (CDV-1 PROTEIN)	Ift81	0.36	11.32	0.000372
lymphocyte antigen 6 complex. locus A	Ly6a	0.36	10.65	0.00114
ADENYLATE CYCLASE. TYPE VII (EC 4.6.1.1) (ATP PYROPHOSPHATE-LYASE)	Adcy7	0.36	8.86	0.000988
hypothetical protein	Purb	0.36	10.7	9.26E-06
CHITINASE-3 LIKE PROTEIN 1 PRECURSOR (CARTILAGE GLYCOPROTEIN-39) (GP-39)	Chi3l1	0.36	8.17	0.005439
proline rich protein expressed in brain	Dazap2	0.36	9.69	0.004418
hypothetical protein	5730437N04Rik	0.36	10.49	0.000133
SPARC PRECURSOR (SECRETED PROTEIN ACIDIC AND RICH IN CYSTEINE) (OSTEONECTIN)	Sparc	0.36	12.6	0.000692
DNA-DIRECTED RNA POLYMERASES I. II. AND III 7.0 KDA POLYPEPTIDE (EC 2.7.7.6)	Polr2k	0.35	9.77	8.49E-05
nudix (nucleoside diphosphate linked moiety X)-type motif 5	Nudt5	0.35	7.96	0.004649
hypothetical protein	2310046A06Rik	0.35	7.68	0.001734
KETOHEXOKINASE (EC 2.7.1.3) (HEPATIC FRUCTOKINASE)	Khk	0.35	9.82	0.008317

similar to Cell division control protein 2 homolog (P34 protein kinase)	Pdik1l	0.35	7.72	0.009619
RAS-RELATED PROTEIN RAB-5B	LOC433464	0.35	7.41	0.004205
ribosomal protein. mitochondrial. L14	Mrpl2	0.34	10.33	7.67E-06
tripartite motif protein	Trim12	0.34	7.51	0.000348
Similar to protein phosphatase methylesterase-1	Ppme1	0.34	9.36	0.000393
interleukin enhancer binding factor 2	Ilf2	0.34	9.29	0.002407
WEAKLY SIMILAR TO RIBOSOMAL LARGE SUBUNIT PSEUDOURIDINE SYNTHASE C[Homo sapiens]	Rpusd4	0.34	8.56	0.004788
SERINE HYDROXYMETHYLTRANSFERASE. CYTOSOLIC (EC 2.1.2.1) (SERINE METHYLASE)	Shmt1	0.33	10.3	0.002232
COP9 (constitutive photomorphogenic). subunit 3 (Arabidopsis)	Cops3	0.33	7.52	0.0058
HIGH MOBILITY GROUP PROTEIN 2 (HMG-2)	Hmgb2	0.33	10.05	4.48E-05
similar to NICE-1 PROTEIN [Homo sapiens]	Crct1	0.33	12.24	0.008911
unknown EST	BB031773	0.33	7.63	0.000339
reserpine-sensitive vesicular monoamine transporter homolog [Rattus norvegicus]	Slc18a2	0.33	11.01	0.005355
RIKEN cDNA 1810022C01	Chrdl2	0.33	9.98	3.12E-05
SIMILAR TO HYPOTHETICAL PROTEIN FLJ12806 homolog [Mus musculus]	2610208M17Rik	0.33	8.7	0.004456
GALACTOSYLTRANSFERASE ASSOCIATED PROTEIN KINASE P58/GTA (EC 2.7.1.-)	Cdc2l1	0.32	11.09	0.000119
MY022 PROTEIN homolog [Homo sapiens]	1700020C11Rik	0.32	9.43	0.002889
ATP-binding cassette. sub-family B (MDR/TAP). member 6	1700020C11Rik, abcb6	0.32	8.47	0.003424
hypothetical Pseudouridine synthase I structure containing protein		0.32	9.3	0.0028
PROBABLE PYRROLIDONE-CARBOXYLATE PEPTIDASE (EC 3.4.19.3)	Pgpep1	0.32	7.95	0.009671
syntaxin 8	Stx8	0.32	10.93	0.00015
Similar to RIKEN cDNA 3110009E18 gene	3110009E18Rik	0.32	7.52	0.004598
hypothetical S-adenosyl-L-methionine-dependent methyltransferases structure containing protein	2410127L17Rik	0.32	10.38	0.001172
MICROTUBULE-ASSOCIATED PROTEIN EMAP homolog [Rattus norvegicus]	Eml2	0.32	11.6	0.002169
RIKEN cDNA 2900053E13	Ndufa10	0.31	12.84	0.005249
Cd27 binding protein (Hindu God of destruction)	Siva1	0.31	8.64	0.002072
GAMMA-GLUTAMYLTRANSPEPTIDASE PRECURSOR (EC 2.3.2.2)	Ggt1	0.31	7.54	0.000418
hypothetical Eukaryotic protein of unknown function. DUF279 containing protein	Chmp2b	0.31	8.74	0.004094
KINESIN HEAVY CHAIN (UBIQUITOUS KINESIN HEAVY CHAIN) (UKHC)	Kif5b	0.31	7.36	0.004414
MYELIN PROTEOLIPID PROTEIN (PLP) (LIPOPHILIN) [CONTAINS: MYELIN PROTEIN DM-20]	Plp1	0.3	11.77	0.001167

PEPTIDYLPROLYL ISOMERASE MATRIN CYP (EC 5.2.1.8)	Ppig	0.3	8.2	0.006922
STOMATIN RELATED PROTEIN homolog [Homo sapiens]	Stoml1	0.3	10.24	0.000595
ovary-specific MOB-like protein	2700078K21Rik	0.3	10.79	0.005766
hypothetical Small nuclear ribonucleoprotein (Sm protein) containing protein	Lsm11	0.3	10.59	0.002146
hypothetical LysM motif containing protein	Lysmd2	0.3	8.83	1.64E-05
weakly similar to GH13975P [Drosophila melanogaster]	Mon2	0.3	11.23	5.99E-05
hypothetical GroEL-like chaperone. apical domain/GroEL-like chaperones	Bbs10	0.3	7.82	0.001879
hypertension related protein 1	Mfn2	0.3	8.69	0.003592
similar to SIMILAR TO NUCLEOLAR PHOSPHOPROTEIN P130 [Mus musculus]	LOC331392	0.29	10.41	0.001497
CMP-N-ACETYLNEURAMINATE-BETA-GALACTOSAMIDE-ALPHA-2.6-SIALYLTRANSFERASE	St6gal1	0.29	7.73	0.0028
DNA MISMATCH REPAIR PROTEIN MSH6 (MUTS-ALPHA 160 KDA SUBUNIT)	Msh6	0.29	8.99	0.004711
RIKEN cDNA 2810403H05 gene		0.29	8.95	0.004287
ADP-RIBOSYLATION FACTOR-LIKE PROTEIN 5 homolog [Rattus norvegicus]	Arl5a	0.29	10.4	0.00227
14-3-3 PROTEIN ZETA/DELTA (PROTEIN KINASE C INHIBITOR PROTEIN-1) (KCIP-1)	Ywhaz	0.29	9.67	0.005249
phospholipase C. delta 4	Zfp142	0.29	8.7	0.005028
allograft inflammatory factor 1	Aif1	0.29	7.49	0.002598
ATP synthase. H+ transporting. mitochondrial F1 complex. gamma polypeptide 1	Atp5c1	0.29	12.1	0.000402
PROBABLE G PROTEIN-COUPLED RECEPTOR EDG-1	Edg1	0.28	7.51	0.006616
TRANSLOCATIONAL PROTEIN-1 (SIMILAR TO TRANSLOCATION PROTEIN 1) homolog [Homo sapiens]	Tloc1	0.28	10.84	0.002482
transferrin receptor	Tfrc	0.28	6.45	0.003393
hypothetical protein MGC6279	Sardh	0.28	7.52	0.001533
RIKEN cDNA 1810009J06	1810009J06Rik	0.28	11.35	0.001262
expressed sequence AA617265	Ciapin1	0.28	10.97	0.001069
similar to ETHANOLAMINE KINASE-LIKE PROTEIN EKI2 (FLJ10761) [Homo sapiens]	Etnk2	0.27	9.15	0.000216
REGULATOR OF G-PROTEIN SIGNALING 16 (RGS16)	Rgs16	0.27	7.72	0.009671
unknown EST	EG328451	0.27	11.88	0.005773
NONSPECIFIC LIPID-TRANSFER PROTEIN. MITOCHONDRIAL PRECURSOR (NSL-TP)	Scp2	0.27	9.25	0.003126
PHOSPHOLIPID HYDROPEROXIDE GLUTATHIONE PEROXIDASE	Gpx4	0.27	13.33	0.003322
U2 small nuclear ribonucleoprotein polypeptide A'	Snrpa1	0.27	9.43	0.002769
hypothetical IQ calmodulin-binding motif/Leucine-rich repeat containing protein	Lrriq2	0.27	7.66	0.009902
GAMMA-AMINOBUTYRIC-ACID RECEPTOR ALPHA-4 SUBUNIT PRECURSOR (GABA(A) RECEPTOR)	Gabra4	0.27	12.4	0.004042

beta-transducin repeat containing protein	Btrc	0.26	7.29	0.00954
MACROPHAGE MIGRATION INHIBITORY FACTOR (MIF) (PHENYLPYRUVATE TAUTOMERASE)	Mif	0.26	14.07	0.00055
solute carrier family 21 (organic anion transporter). member 14	Slco1c1	0.26	7.33	0.004665
METHIONINE AMINOPEPTIDASE 2 (EC 3.4.11.18) (METAP 2) (PEPTIDASE M 2)	Metap2	0.26	10.11	0.006469
T-COMPLEX PROTEIN 1. EPSILON SUBUNIT (TCP-1-EPSILON) (CCT-EPSILON)	Cct5	0.26	10.27	0.00746
RIKEN cDNA 3110043J09 gene	3110043J09Rik	0.25	7.51	0.003669
RAC-GAMMA SERINE/THREONINE PROTEIN KINASE (EC 2.7.1.-) (RAC-PK-GAMMA)	Akt3	0.25	8.81	0.004251
hypothetical protein	1810013L24Rik	0.25	11.3	0.000389
inferred: thyroid hormone receptor-associated protein complex component TRAP240 {Homo sapiens}	LOC432586	0.25	11.45	0.000418
NDRG2 PROTEIN (NDR2 PROTEIN)	Ndrg2	0.25	13.02	0.007678
TRANSLATION INITIATIONFACTOR EIF-4GAMMA (FRAGMENT) homolog [Homo sapiens]	Eif4g3	0.24	10.06	0.004114
ATP SYNTHASE ALPHA CHAIN. MITOCHONDRIAL PRECURSOR (EC 3.6.3.14)	Atp5a1	0.24	12.81	0.003058
COATOMER BETA' SUBUNIT (BETA'-COAT PROTEIN) (BETA'-COP) (P102)	Copb2	0.24	9.52	0.006673
RIKEN cDNA 2310050K10	Paip2	0.24	11.72	0.001289
60 KDA HEAT SHOCK PROTEIN. MITOCHONDRIAL PRECURSOR (HSP60) (60 KDA CHAPERONIN)	Hspd1	0.24	11.1	0.003202
RIKEN cDNA 2900072D10	Ncaph2	0.23	10.44	0.0058
ADP-RIBOSYLATION FACTOR-LIKE PROTEIN 3	Arl3	0.23	11.77	0.002154
SECRETOGRANIN I PRECURSOR (SGI) (CHROMOGRANIN B) (CGB)	Chgb	0.22	12.28	0.001734
RAPAMYCIN-SELECTIVE 25 KDA IMMUNOPHILIN (FKBP25)	Fkbp3	0.22	11.74	0.002062
PIPPIN PROTEIN (FRAGMENT) homolog [Rattus norvegicus]	Csdc2	0.22	10.52	0.004373
MALATE DEHYDROGENASE. CYTOPLASMIC (EC 1.1.1.37)	Mdh1	0.22	13.39	0.002928
quaking protein	Qk	0.21	11.23	0.003455
steroid receptor RNA activator 1	Sra1	0.21	10.28	0.004598
eukaryotic translation initiation factor 4E binding protein 1	Eif4ebp1	0.21	10.82	0.002407
tubulin cofactor a	Tbca	0.2	11.87	0.006886
MORF-related gene 15	Morf4l1	0.2	11.88	0.004406
gamma-aminobutyric acid reseptor associated protein	Gabarap	0.2	12.51	0.008731
proprotein convertase subtilisin/kexin type 1 inhibitor	Pcsk1n	0.2	12.51	0.008122
voltage-gated potassium channel alpha chain Kv9.3 homolog [Rattus norvegicus]	Kcns3	0.19	7.18	0.006222
PROTEASOME SUBUNIT ALPHA TYPE 2 (EC 3.4.25.1) (PROTEASOME COMPONENT C3)	Psma2	0.19	11.46	0.004418
NADH dehydrogenase (ubiquinone) 1 alpha subcomplex. 7 (14.5kD. B14.5a)	Ndufs4	0.17	11.45	0.007889

More expressed in A10				
14-3-3 PROTEIN ETA (PROTEIN KINASE C INHIBITOR PROTEIN-1) (KCIP-1)	Ywhah	-0.18	12.93	0.005104
hypothetical HMG-I and HMG-Y DNA-binding domain (A+T-hook)	Ube2o	-0.19	10.71	0.005696
hypothetical protein	Rexo1	-0.2	10.6	0.005012
RIKEN cDNA 4733401H14	Dnase1l2	-0.21	7.77	0.009468
Similar to chromosome 11 open reading frame 23	Saps3	-0.21	10.24	0.004414
RANBP20	Xpo6	-0.21	9.15	0.005766
protein phosphatase 1. regulatory (inhibitor) subunit 11	Ppp1r11	-0.22	11.74	0.00837
UBIQUITIN-CONJUGATING ENZYME E2 B (EC 6.3.2.19) (UBIQUITIN-PROTEIN LIGASE B)	Ube2b	-0.22	11.6	0.006217
ADP-ribosylation-like 2	Arl2	-0.22	12.71	0.005823
RIKEN cDNA 2310061B02	Tmbim1	-0.22	8.04	0.00537
similar to CICK0721Q.5 (POLYPEPTIDE FROM PATENTED CDNA EMBL:E06811) [Homo sapiens]	Cuta	-0.22	11.82	0.00334
similar to ALPHA-INTERFERON INDUCIBLE PROTEIN (FRAGMENT) [Mesocricetus auratus]		-0.22	12.36	0.002374
DNA segment. human DXS9928E	D0HXS9928E	-0.22	12.64	0.001533
dynactin 6	Dctn6	-0.22	10.78	0.007691
RIKEN cDNA 3010026O09	3010026O09Rik	-0.23	12.03	0.004649
40S RIBOSOMAL PROTEIN S23	Rps23	-0.23	13.68	0.001607
hypothetical protein	AI662250	-0.24	7.87	0.006222
HAIRY/ENHANCER-OF-SPLIT RELATED WITH YRPW MOTIF 1	Hey1	-0.24	9.75	0.0028
ribosomal protein S19	Rps19	-0.24	12.1	0.00241
ribosomal protein L6	EG620213, Rpl6	-0.24	13.79	0.000321
RAN. member RAS oncogene family	Ran	-0.24	12.26	0.006408
hypothetical protein	2610003J06Rik	-0.25	12.32	0.008846
similar to BA122O1.2 [Homo sapiens]	Actr5	-0.25	9.69	0.004456
expressed sequence C78013	Praf2	-0.25	12.15	0.000799
putative GTP binding protein	Gtpbp6	-0.25	9.96	0.003761
40S RIBOSOMAL PROTEIN S11	Rps11	-0.25	13.37	0.0058
mitochondrial ribosomal protein S11	Mrps11	-0.25	10.54	0.001494
hypothetical protein	Camsap1l1	-0.25	9.15	0.001869
similar to A DISINTEGRIN-LIKE AND METALLOPROTEASE DOMAIN [Homo sapiens]	Adamts3	-0.25	7.62	0.00746

28S RIBOSOMAL PROTEIN S17. MITOCHONDRIAL PRECURSOR (MRP-S17)	Mrps17	-0.25	10.42	0.000798
NICE-3	4933434E20Rik	-0.26	9.35	0.00309
polyglutamine binding protein 1	Pqbp1		11.33	0.002032
HEAT-SHOCK PROTEIN 105 KDA (HEAT SHOCK-RELATED 100 KDA PROTEIN E7I) (HSP-E7I)	Hsp110	-0.26	12.04	0.000723
histone 4 protein	Hist1h4h	-0.26	9.37	0.001532
similar to APOPTOSIS RELATED PROTEIN APR-3 [Homo sapiens]	0610007C21Rik	-0.26	11.51	0.001219
periodic tryptophan protein 1 homolog	Pwp1	-0.26	7.96	0.002539
hypothetical Ypt/Rab-GAP domain of gyp1p structure containing protein	Tbc1d7	-0.26	10.04	0.00825
PTERIN-4-ALPHA-CARBINOLAMINE DEHYDRATASE	Pcbd1	-0.26	11.39	0.007908
arsenate resistance protein 2	Ars2	-0.27	11.08	0.002619
RIKEN cDNA 1810060J02	Ccdc91	-0.27	11.59	0.002288
glyoxylate reductase/hydroxypyruvate reductase	Grhpr	-0.27	10.34	0.001387
AQUAPORIN-CHIP (WATER CHANNEL PROTEIN FOR RED BLOOD CELLS)	Aqp1	-0.27	7.29	0.004815
WEE1-LIKE PROTEIN KINASE (EC 2.7.1.112)	Wee1	-0.27	10.76	0.004028
DERMATAN/CHONDROITIN SULFATE 2-SULFOTRANSFERASE homolog [Homo sapiens]	Ust	-0.27	6.87	0.003399
U4/U6 SMALL NUCLEAR RIBONUCLEOPROTEIN HPRP3 homolog [Homo sapiens]	Prpf3	-0.27	10.46	0.003996
40S RIBOSOMAL PROTEIN S5	Rps5	-0.27	13.74	0.000873
NUCLEOLAR GTP-BINDING PROTEIN 1 (CHRONIC RENAL FAILURE GENE PROTEIN)	Gtpbp4	-0.27	9.07	0.005028
similar to VON WILLEBRAND FACTOR PRECURSOR (VWF) [Canis familiaris]	Vwf	-0.27	7.59	0.001586
RIKEN cDNA 1810014G04	Coq5	-0.27	11.08	0.005561
similar to CDNA FLJ30600 FIS. CLONE BRAWH2009360 [Homo sapiens]	2610301B20Rik	-0.27	9.71	0.004418
homeo box C5	Hoxc5	-0.27	9.03	0.003411
SIGNAL RECOGNITION PARTICLE RECEPTOR ('DOCKING PROTEIN') homolog [Homo sapiens]	Srpr	-0.28	9.41	0.004499
hypothetical LIM domain. Villin headpiece domain containing protein	Ablim2	-0.28	7.78	0.00334
ATAXIN-1 (SPINOCEREBELLAR ATAXIA TYPE 1 PROTEIN)	2900016G23Rik	-0.28	7.71	0.004415
similar to DELTEX 2 (FRAGMENT) [Gallus gallus]	Dtx4	-0.28	7.49	0.002686
hypothetical protein	Tmem71	-0.28	8.59	0.001346
cyclin L	Ccnl1	-0.28	8.13	0.007942
protein arginine N-methyltransferase 2	Prmt2	-0.28	12.4	0.004373
hypothetical BRCT domain containing protein		-0.28	8.66	0.003759
hypothetical protein	2410012H22Rik	-0.29	10.05	0.0028

non-POU-domain-containing. octamer binding protein	Nono	-0.29	10.1	0.00089
similar to THYROID RECEPTOR INTERACTING PROTEIN 3 (TRIP-3) (FRAGMENT) [Homo sapiens]	Myo19	-0.29	8.48	0.003669
DIACYLGLYCEROL O-ACYLTRANSFERASE 1 (EC 2.3.1.20) (DIGLYCERIDE ACYLTRANSFERASE)	Dgat1	-0.29	9.98	0.000572
RIKEN cDNA 4930511N13	Btbd14b	-0.29	9.43	0.007993
DNA (CYTOSINE-5)-METHYLTRANSFERASE 1 (EC 2.1.1.37) (DNMT1)	Dnmt1	-0.29	7.63	0.000557
engulfment and cell motility 2. ced-12 homolog (C. elegans)	Elmo2	-0.29	8.43	0.006363
ribosomal protein S12	Rps12	-0.29	13.22	0.000648
ribosomal protein S17	Rps17	-0.29	13.58	0.000269
hypothetical Zn-finger CCHC type containing protein	Zcchc12	-0.29	11.39	0.000202
HIPPOCALCIN-LIKE PROTEIN 4 (HYPOTHETICAL 22.2 KDA PROTEIN) homolog [Homo sapiens]	Hpcal4	-0.29	10.36	0.003329
hypothetical protein	Zfyve9	-0.29	8.31	0.006707
GAMMA ENOLASE (EC 4.2.1.11) (2-PHOSPHO-D-GLYCERATE HYDRO-LYASE) (NEURAL ENOLASE)	Eno2	-0.29	9.82	0.001672
methionyl aminopeptidase 1	Metap1	-0.3	8.57	0.001106
PHOSPHORYLASE B KINASE GAMMA CATALYTIC CHAIN. TESTIS/LIVER ISOFORM	Gm166	-0.3	10.95	0.001701
ubiquitin specific protease 20	Usp20	-0.3	10.04	0.007447
P37 TRAP/SMCC/PC2 SUBUNIT homolog [Homo sapiens]	Med27	-0.3	9.31	0.000723
PHOSPHOMANNOMUTASE 2 (EC 5.4.2.8) (PMM 2)	Pmm2	-0.3	8.43	0.001375
unclassifiable		-0.3	10.64	1.07E-05
DNA-(APURINIC OR APYRIMIDINIC SITE) LYASE (EC 4.2.99.18) (AP ENDONUCLEASE 1)	Apex1	-0.31	10.75	0.000866
expressed sequence AI481500	Trrap	-0.31	9.76	0.001447
hypothetical protein	1110014N23Rik	-0.31	8.75	0.0058
hypothetical Zinc finger. C2H2 type containing protein	Zfp618	-0.31	11.21	0.001069
EDAR (ectodysplasin-A receptor)-associated death domain	Edaradd	-0.31	10.22	0.001743
MICROSOMAL SIGNAL PEPTIDASE 21 KDA SUBUNIT (EC 3.4.-.-) (SPASE 21 KDA SUBUNIT) (SPC21)		-0.31	11.18	0.000144
PRKC. apoptosis. WT1. regulator	Pawr	-0.31	8.59	0.0028
hypothetical protein	LOC432471	-0.31	8.59	0.003892
similar to NITZIN (FRAGMENT) [Rattus norvegicus]	Frmd4a	-0.31	10.31	2.49E-05
hypothetical protein		-0.31	9.62	0.004787
Rab3 interacting protein 1	Rims2	-0.31	7.92	0.00347
RIKEN cDNA 1500041N16	1500041N16Rik	-0.32	10.57	0.009027
HEC protein	Ndc80	-0.32	7.44	0.000924

methyltransferase Cyt19	As3mt	-0.32	8.89	0.002769
Unknown (protein for MGC:6627)	Plekhf1	-0.32	10.45	0.004193
SHORT CHAIN 3-HYDROXYACYL-COA DEHYDROGENASE. MITOCHONDRIAL PRECURSOR (HCDH)		-0.32	7.93	0.007644
hypothetical N-terminal nucleophile aminohydrolases (Ntn hydrolases) structure containing protein	Tmem41b	-0.32	9.49	0.001046
hypothetical protein		-0.32	9.4	0.002865
hypothetical Ribosomal protein S4E containing protein	Rps4y2	-0.32	8.89	0.002928
SIMILAR TO PROTEIN DISULFIDE ISOMERASE-RELATED PROTEIN homolog [Mus musculus]	Pdia6	-0.32	10.19	1.66E-05
ENDOSOMAL PROTEIN homolog [Homo sapiens]	Eea1	-0.32	7.98	0.000448
Similar to phosphoinositol 3-phosphate-binding protein-2	Plekha5	-0.32	9.5	0.006616
hypothetical Cysteine-rich region containing protein		-0.32	8.63	9.62E-05
3-HYDROXYACYL-COA DEHYDROGENASE TYPE II (EC 1.1.1.35) (TYPE II HADH)	Hsd17b10	-0.32	9.96	0.000997
hypothetical protein. MNCb-0385	Nap1l5	-0.32	12.16	1.45E-05
similar to COPINE-LIKE PROTEIN KIAA1599 [Homo sapiens]	Cpne8	-0.32	8.33	0.001538
Notch-regulated ankyrin repeat protein	Nrarp	-0.32	9.13	0.003616
open reading frame 11	0610007P14Rik	-0.32	9.61	0.002032
RIKEN cDNA 2410018C20	2410018C20Rik	-0.33	8.38	0.009671
open reading frame 18	Tmem59	-0.33	11.51	0.000406
cytokine receptor-like factor 1	Crlf1	-0.33	10.76	0.000411
AD-017 PROTEIN (GLYCOSYLTRANSFERASE) homolog [Homo sapiens]	Glt8d1	-0.33	9.44	0.001223
ADAPTOR-RELATED PROTEIN COMPLEX 2 ALPHA 2 SUBUNIT (ALPHA-ADAPTIN C)	Ap2a2	-0.33	12.4	0.002232
GALECTIN-8 (LGALS-8)	Lgals8	-0.33	8.93	0.00344
2410007J07	LOC100041511	-0.33	13.18	0.000345
similar to PROTEASOME INHIBITOR PI31 SUBUNIT (HPI31) [Homo sapiens]	Psmf1	-0.33	9.55	0.000799
RIKEN cDNA 2610005A10 gene	Adck1	-0.33	8.43	0.00072
hypothetical Aminotransferases class-II containing protein	Lhfpl2	-0.33	7.38	0.000576
RIKEN cDNA 2410012P20 gene	Chchd4	-0.33	11.28	3.06E-06
Unknown (protein for IMAGE:5345342)	Bptf	-0.33	9.8	4.85E-05
hypothetical Crystallin/RING finger containing protein	Mgrn1	-0.33	10.08	4.91E-05
NUCLEOSIDE DIPHOSPHATE KINASE. MITOCHONDRIAL PRECURSOR (EC 2.7.4.6)	Nme4	-0.33	9.54	0.001323
RIKEN cDNA 2410004B18	2410004B18Rik	-0.33	10.77	0.007538
SWI/SNF related. matrix associated. actin dependent regulator of chromatin. subfamily f. member 1	Arid1a	-0.33	8.28	0.007993

hypothetical protein	1700027J05Rik	-0.34	10.73	1.32E-05
expressed sequence AI428195	B230342M21Rik	-0.34	9.41	0.00334
CHROMOBOX PROTEIN HOMOLOG 1 (HETEROCHROMATIN PROTEIN 1 HOMOLOG BETA)	Cbx1	-0.34	8.53	0.008911
Similar to DKFZP564O0823 protein	9130213B05Rik	-0.34	8.03	0.001192
MAX-INTERACTING TRANSCRIPTIONAL REPRESSOR MAD4 (MAX-ASSOCIATED PROTEIN 4)	Mxd4	-0.34	11.18	0.005766
2310050F24	Pgam1	-0.34	9.3	0.004787
SIMILAR TO PURITY OF ESSENCE (FRAGMENT) homolog [Homo sapiens]	Ubr4	-0.34	10.76	4.85E-05
CTLA-2-BETA PROTEIN PRECURSOR (FRAGMENT)	Ctla2a	-0.34	7.47	0.00334
SIMILAR TO HYPOTHETICAL PROTEIN MGC4707 homolog [Homo sapiens]	1110051M20Rik	-0.34	10.67	0.000148
NADH dehydrogenase (ubiquinone) 1 alpha subcomplex. 7 (14.5kD. B14.5a)	Ndufa7	-0.35	12.37	0.000613
UBIQUITIN FUSION DEGRADATION PROTEIN 1 HOMOLOG (UB FUSION PROTEIN 1)	Ufd1l	-0.35	9.99	0.000418
weakly similar to KIAA0542 PROTEIN (FRAGMENT) [Homo sapiens]	Sfi1	-0.35	8.2	0.001027
TFIIIC2 SUBUNIT homolog [Homo sapiens]	Gtf3c2	-0.35	8.49	0.002421
hypothetical TPR repeat containing protein	Ttc32	-0.35	7.63	0.000439
APOPTOSIS REGULATOR BAX. MEMBRANE ISOFORM ALPHA	Bax	-0.35	10.25	0.009671
RPB5-mediating protein	C80913	-0.35	8.95	0.002154
unknown EST		-0.35	7.74	0.001194
ganglioside-induced differentiation-associated-protein 2	Gdap2	-0.35	8.99	0.00067
60S ACIDIC RIBOSOMAL PROTEIN P1	Rplp1	-0.35	14.09	0.00019
RIKEN cDNA 1810037K07	Mmachc	-0.35	9.34	0.004418
G2/MITOTIC-SPECIFIC CYCLIN B2	Ccnb2	-0.36	7.1	0.000182
KAIA2372 PROTEIN homolog [Homo sapiens]	AW124722	-0.36	10.73	0.002598
Unknown (protein for MGC:29167)	Angel1	-0.36	8.99	0.003591
similar to HCDI PROTEIN [Homo sapiens]	2310014G06Rik	-0.36	10.56	1.39E-05
REGULATOR OF G-PROTEIN SIGNALING 2 (RGS2)	Rgs2	-0.36	10.39	0.00021
small nuclear ribonucleoprotein polypeptide A	Snrpa	-0.36	10.23	7.14E-05
hypothetical protein. MGC:6989	Tusc3	-0.37	9.6	0.000594
RIKEN cDNA 2610510L01		-0.37	9.4	0.003848
LEUKOTRIENE A-4 HYDROLASE (LTA-4 HYDROLASE) (LEUKOTRIENE A(4) HYDROLASE)	Lta4h	-0.37	9.57	0.000123
SIMILAR TO SEVEN TRANSMEMBRANE DOMAIN PROTEIN homolog [Homo sapiens]	Tmem147	-0.37	12.08	6.35E-07
CARBONYL REDUCTASE (EC 1.1.1.184) (CARBONYL REDUCTASE 3) homolog [Cricetulus griseus]	Cbr3	-0.37	7.6	0.001164

organic cationic transporter-like 2	Slc22a18	-0.37	7.51	0.001586
SERINE PROTEASE HTRA2. MITOCHONDRIAL PRECURSOR (EC 3.4.21.-)	Htra2	-0.37	8.09	0.004711
hypothetical protein		-0.37	8.15	0.001215
cysteine-rich protein 2	Csrp2	-0.37	11.1	2.15E-05
MAP/microtubule affinity-regulating kinase 3	Mark3	-0.37	9.71	0.005883
hypothetical RING finger domain. C3HC4 structure containing protein	March5	-0.37	8.56	0.002598
hypothetical Immunoglobulin and major histocompatibility complex domain	Vstm2a	-0.37	7.7	0.002757
interferon-stimulated protein (20 kDa)	Isg20	-0.37	8.21	0.001223
GERANYLGERANYL TRANSFERASE TYPE II BETA SUBUNIT (EC 2.5.1.-)	Rabggtb	-0.37	9.44	0.007364
expressed sequence AI427833	Txndc11	-0.38	10.25	9.62E-05
signaling intermediate in Toll pathway-evolutionarily conserved	Ecsit	-0.38	9.11	0.000229
hypothetical protein	Map3k14	-0.38	8.65	0.004251
hypothetical protein	Sfi1	-0.38	8.08	0.001533
SOLUTE CARRIER FAMILY 2. FACILITATED GLUCOSE TRANSPORTER. MEMBER 3	Slc2a3	-0.38	10.27	1.06E-05
DOUBLE-STRANDED RNA-BINDING PROTEIN STAUFEN HOMOLOG	Stau1	-0.38	9.46	0.000594
MITOTIC SPINDLE ASSEMBLY CHECKPOINT PROTEIN MAD2B (MAD2-LIKE 2) [Homo sapiens]	Mad2l2	-0.38	9.04	0.001888
protocadherin gamma subfamily C. 5	Pcdhga12	-0.38	10.4	0.000798
prenylated Rab acceptor	Rabac1	-0.38	13.03	0.000164
MARCKS-RELATED PROTEIN	Marcksl1	-0.39	7.6	0.000701
CALCIUM-BINDING PROTEIN P22 (CALCIUM-BINDING PROTEIN CHP)	1500003O03Rik	-0.39	10.11	5.41E-05
hypothetical protein		-0.39	6.95	0.004028
recombination activating gene 1 gene activation	Rag1ap1	-0.39	10.07	0.000312
phosphoserine/threonine/tyrosine interaction protein	Styx	-0.39	8.07	0.009462
ALPHA-1 CATENIN (102 KDA CADHERIN-ASSOCIATED PROTEIN) (CAP102) (ALPHA E-CATENIN)	Ctnna1	-0.39	10.62	2.81E-06
RIKEN cDNA 1300013B24	Ero1lb	-0.39	8.06	0.001205
spermatid specific RING zinc finger 1	Znrf4	-0.39	9.08	0.005249
SYNDECAN-2 PRECURSOR (FIBROGLYCAN)	Sdc2	-0.39	12.22	4.42E-07
SERINE/THREONINE-PROTEIN KINASE RECEPTOR R3 PRECURSOR (EC 2.7.1.37) (SKR3)	Kcnn3	-0.39	9.64	0.001637
general transcription factor II I repeat domain-containing 1	Gtf2ird1	-0.39	8.17	0.006154
ADAM33 alpha	Adam33	-0.4	7.94	0.000123
WEAKLY SIMILAR TO SPLICEOSOME ASSOCIATED PROTEIN 49 [Homo sapiens]	BC038822	-0.4	7.74	0.006513

hypothetical protein	Rpain	-0.4	9.42	0.001632
NUANCE (FRAGMENT) homolog [Mus musculus]	Syne2	-0.4	11.88	1.06E-06
Unknown (protein for MGC:6908)	Dhrs7b	-0.4	9.13	0.00199
similar to ADP-RIBOSYLATION FACTOR BINDING PROTEIN GGA3 (GOLGI-LOCALIZED)	Gga3	-0.4	8.97	0.000663
Unknown (protein for MGC:25689)	Ccdc115	-0.4	9.36	0.001533
ALPHA-AMYLASE. PANCREATIC PRECURSOR (1.4-ALPHA-D-GLUCAN GLUCANOHYDROLASE)		-0.41	8.03	0.000677
unknown EST	Larp1	-0.41	9.25	0.005766
similar to deoxyhypusine synthase (EC 2.5.1.46) [Homo sapiens]	Dhps	-0.41	9.45	0.001387
CALCIUM/CALMODULIN-DEPENDENT 3'.5'-CYCLIC NUCLEOTIDE PHOSPHODIESTERASE 1B	Pde1b	-0.41	11.18	1.55E-06
DYNAMIN 2 (EC 3.6.1.50) (DYNAMIN UDNM)	Tmed1	-0.41	9.13	0.004469
hypothetical Esterase/acetylhydrolase structure containing protein		-0.41	8.72	0.003791
CDNA FLJ20594 (SIMILAR TO MITOCHONDRIAL RIBOSOMAL PROTEIN L22) homolog [Homo sapiens]	Mrpl22	-0.41	8.08	0.009902
ENVOPLAKIN (P210) (210 KDA CORNIFIED ENVELOPE PRECURSOR)	Evpl	-0.41	7.78	0.000393
serologically defined breast cancer antigen 84	Ergic3	-0.42	12.27	0.000643
INTEGRIN BETA-1 BINDING PROTEIN 1 (BODENIN)	Itgb1bp1	-0.42	9.42	0.006217
hypothetical SET-domain of transcriptional regulators (TRX. EZ. ASH1 etc)	Wbp7	-0.42	9.85	0.004222
HYPOTHETICAL 72.4 KDA PROTEIN homolog [Macaca fascicularis]	Ccdc128	-0.42	9.59	0.001719
weakly similar to PERQ1 [Mus musculus]	Tnrc15	-0.42	11.75	2.21E-06
RIKEN cDNA 1100001H23	1100001H23Rik	-0.42	7.4	0.002002
RIKEN cDNA 1500032E05	Ssr2	-0.42	11.17	5.96E-07
low density lipoprotein receptor-related protein 1	Lrp1	-0.42	10.52	8.90E-09
HEPATIC LEUKEMIA FACTOR homolog [Rattus norvegicus]	Hlf	-0.42	8.05	0.000921
similar to C316G12.2 (NOVEL PROTEIN SIMILAR TO PREDICTED YEAST	0610007P22Rik	-0.43	11.21	0.00746
sterol-C4-methyl oxidase-like	Sc4mol	-0.43	10.13	6.55E-08
expressed sequence AA959601	Dock9	-0.43	7.68	0.000813
PUTATIVE PROTEIN DJ747H23.2 homolog [Homo sapiens]	Rwdd2a	-0.43	8.53	1.07E-05
latent transforming growth factor beta binding protein 3	Ltbp3	-0.43	10.41	0.001069
hypothetical protein	Mitd1	-0.44	8.09	0.000596
ankyrin repeat and BTB (POZ) domain containing 1	Abtb1	-0.44	9.15	0.001223
hypothetical AAA ATPase superfamily containing protein	Katnal2	-0.44	9.59	0.004575
similar to PROTEIN DISULFIDE ISOMERASE PDIP [Homo sapiens]	Pdia2	-0.44	11.75	6.73E-05

hypothetical Rhodopsin-like GPCR superfamily containing protein	C130060K24Rik	-0.44	7.73	9.67E-06
RAS GTPASE-ACTIVATING PROTEIN 3 (GAP1(IP4BP)) (INS P4-BINDING PROTEIN) (GAPIII)	Rasa3	-0.44	9.03	0.006363
hypothetical Cytochrome c family heme-binding site containing protein	1700024G10Rik	-0.44	7.82	0.002018
hypothetical protein	Tmem130	-0.44	12.69	4.42E-07
N-myc downstream regulated 1	Ndrg1	-0.45	9.16	0.009452
CARBONIC ANHYDRASE-RELATED PROTEIN (CARP) (CA-VIII)	Car8	-0.45	7.79	3.29E-05
INTERFERON-INDUCED GTP-BINDING PROTEIN MX1 (INFLUENZA RESISTANCE PROTEIN)	Mx1	-0.45	7.95	0.006619
BAG-FAMILY MOLECULAR CHAPERONE REGULATOR-3 (BCL-2 BINDING ATHANOGENE- 3) (BAG-3)	Bag3	-0.45	8.53	0.005692
hypothetical Zinc-containing alcohol dehydrogenase superfamily containing protein	AI427515	-0.45	7.86	2.69E-05
COMPLEMENT C1Q SUBCOMPONENT. B CHAIN PRECURSOR	C1qb	-0.46	10.27	9.45E-08
PROCOLLAGEN C-TERMINAL PROTEINASE ENHANCER PROTEIN homolog [Homo sapiens]	Pcolce2	-0.46	8.51	0.00368
Lutheran blood group (Auberger b antigen included)	Bcam	-0.46	8.41	0.001586
hypothetical Quinoprotein alcohol dehydrogenase structure containing protein	Itfg3	-0.46	8.79	0.000186
AMINE OXIDASE [FLAVIN-CONTAINING] A (EC 1.4.3.4) (MONOAMINE OXIDASE) (MAO-A)	Maoa	-0.46	8.86	4.06E-05
HYPOTHETICAL 38.5 KDA PROTEIN homolog [Macaca fascicularis]	6430550H21Rik	-0.46	9.34	0.001215
glutathione S-transferase. pi 2	Gstp2	-0.46	12.93	1.20E-07
EUKARYOTIC TRANSLATION INITIATION FACTOR 4E (EIF-4E) (EIF4E) (MRNA CAP-BINDING PROTEIN)	Eif4e	-0.46	10.93	0.000195
hypothetical protein	Zfp553	-0.46	8.56	5.90E-05
Pxmp4	Pxmp4	-0.46	9.28	0.004989
Unknown (protein for MGC:18664)	Slc35c2	-0.46	9.98	7.08E-06
REGULATOR OF G-PROTEIN SIGNALING 14 (RGS14) (RAP1/RAP2 INTERACTING PROTEIN)	Rgs14	-0.46	10.14	1.36E-08
RIKEN cDNA 1210002B07	Tspan6	-0.47	9.61	6.90E-10
RIKEN cDNA 2810437E14	Zkscan14	-0.47	8.45	0.004566
microtubule-associated protein 6	Mtap6	-0.47	7.73	0.006426
PHOSPHOLYSINE PHOSPHOHISTIDINE INORGANIC PYROPHOSPHATE PHOSPHATASE homolog	2310007H09Rik	-0.47	8.01	0.006217
protein kinase C and casein kinase substrate in neurons 2	Pacsin2	-0.47	8.99	3.88E-06
RIKEN cDNA 2010322C19	Fancl	-0.47	8.28	3.91E-05
neural-salient serine/arginine-rich	Fusip1	-0.47	7.82	6.73E-05
RIKEN cDNA 5830412B09	Sfpq	-0.48	7.83	0.000817
weakly similar to PROSTATE CANCER ANTIGEN-1 [Homo sapiens]	Alkbh3	-0.48	9.77	0.001086

AMP DEAMINASE 2 (EC 3.5.4.6) (AMP DEAMINASE ISOFORM L) homolog [Homo sapiens]	Ampd2	-0.48	8.33	0.002103
DEFENDER AGAINST CELL DEATH 1 (DAD-1)	Dad1	-0.48	13.29	9.21E-07
hypothetical protein	2510039O18Rik	-0.49	8.67	0.004373
RIKEN cDNA 1500015G18	Tmem9	-0.49	10.29	2.15E-05
RIKEN cDNA 1110068E11 gene	Maf1	-0.49	10.04	0.00114
ALDOSE REDUCTASE (EC 1.1.1.21) (AR) (ALDEHYDE REDUCTASE)	Akr1b3	-0.49	11.79	1.17E-05
GLUTATHIONE S-TRANSFERASE YC (EC 2.5.1.18) (GST CLASS-ALPHA)	Gsta3	-0.49	7.95	0.001037
SORTING NEXIN 3 (SDP3 PROTEIN)	Snx3	-0.49	9.27	7.72E-05
INTEGRAL PLASMA MEMBRANE PROTEIN	2310001A20Rik	-0.49	9.1	0.003856
hypothetical protein	Sacs	-0.5	7.26	0.000312
similar to HEPARAN SULFATE D-GLUCOSAMINYL 3-O-SULFOTRANSFERASE-4 [Homo sapiens]	Hs3st2	-0.5	7.4	1.66E-05
hypothetical Fibronectin type III domain containing protein	Fndc5	-0.5	10.03	1.39E-05
MYOSIN REGULATORY LIGHT CHAIN 2. SMOOTH MUSCLE ISOFORM homolog [Homo sapiens]	Myl9	-0.51	9.33	0.000784
LAMININ BETA-1 CHAIN PRECURSOR (LAMININ B1 CHAIN)	Lamb1-1	-0.51	8.97	0.000789
synaptotagmin 4	Traf7	-0.51	8.02	0.002977
RIKEN cDNA 2310046N15	Fbxo31	-0.52	8.4	0.001854
ACYL-COA DESATURASE 2 (EC 1.14.99.5) (STEAROYL-COA DESATURASE 2)	Scd2	-0.52	8.29	6.07E-08
A kinase anchor protein 8	Akap8	-0.52	9.31	0.001054
MITOCHONDRIAL IMPORT RECEPTOR SUBUNIT TOM20 HOMOLOG [Homo sapiens]	Tomm20	-0.53	13.24	2.69E-05
RIKEN cDNA 1110003B01	Pdlim7	-0.53	10.45	1.03E-08
RAB3B. member RAS oncogene family	Rab3b	-0.53	9.18	5.80E-11
PROTEIN KINASE C-BINDING PROTEIN NELL1 PRECURSOR homolog [Rattus norvegicus]	Nell1	-0.53	8	7.65E-08
NADH-CYTOCHROME B5 REDUCTASE ISOFORM homolog [Homo sapiens]	Cyb5r1	-0.53	9.2	8.10E-05
procollagen-lysine. 2-oxoglutarate 5-dioxygenase 1	Plod1	-0.53	8.34	0.000692
RIKEN cDNA 2410012H02 gene	Xrcc6bp1	-0.53	7.37	0.000159
hypothetical Thioredoxin-like structure containing protein	Dnajc10	-0.53	9	0.003729
L-LACTATE DEHYDROGENASE A CHAIN (EC 1.1.1.27) (LDH-A) (LDH MUSCLE SUBUNIT) (LDH-M)	Ldha	-0.53	11.48	1.36E-07
nucleosome assembly protein 1-like 1	Nap1l1	-0.53	10.1	0.00019
Unknown (protein for MGC:28451)	Osbpl2	-0.54	7.77	0.002154
MYB binding protein (P160) 1a	Mybbp1a	-0.54	8.49	0.002676
similar to CDNA FLJ32338 FIS. MODERATELY SIMILAR TO HUMAN BREAST CANCER	Slc39a4	-0.54	8.87	2.43E-08

SECRETOGRANIN II PRECURSOR (SGII) (CHROMOGRANIN C)	Scg2	-0.55	10.11	0.000363
weakly similar to SNAP190 [Homo sapiens]	Snapc4	-0.55	8.95	6.94E-05
Similar to 60S ribosomal protein L30 isolog	BC003885	-0.55	8.79	0.001264
Similar to tetratricopeptide repeat domain 4	Ttc4	-0.55	9.96	1.26E-06
proteasome (prosome. macropain) 28 subunit. beta	Psme2b-ps	-0.56	10.55	0.000197
CADHERIN-16 PRECURSOR (KIDNEY-SPECIFIC CADHERIN) (KSP-CADHERIN)	Cdh16	-0.56	9.77	3.32E-05
hypothetical protein	Obsl1	-0.56	8.31	7.21E-05
binder of Rho GTPase 4	Cdc42ep4	-0.56	8.28	0.004094
RAN-SPECIFIC GTPASE-ACTIVATING PROTEIN (RAN BINDING PROTEIN 1) (RANBP1)	Ranbp1	-0.56	11.81	3.27E-10
weakly similar to GOLGI MEMBRANE PROTEIN GP73 [Homo sapiens]	Golm1	-0.57	7.11	0.000162
hypothetical Collagen triple helix repeat containing protein	Cthrc1	-0.57	7.96	2.11E-05
SIMILAR TO CACTIN (FRAGMENT) homolog [Homo sapiens]	2510012J08Rik	-0.58	9.76	0.000246
unclassifiable		-0.59	8.63	1.63E-07
BRF1 homolog. subunit of RNA polymerase III transcription initiation factor IIIB (S. cerevisiae)	Brf1	-0.6	9.15	0.000997
RIKEN cDNA 1520402O14	Leprotl1	-0.6	8.78	0.000123
HEREDITARY HAEMOCHROMATOSIS PROTEIN HOMOLOG PRECURSOR		-0.6	7.59	3.79E-06
sphingomyelin phosphodiesterase 2. neutral	Smpd2	-0.6	8.46	0.003411
RIKEN cDNA 6720485C15	Dcakd	-0.6	9.21	0.000115
cDNA sequence AF134346	Tdh	-0.6	7.51	8.45E-08
DIAPHANOUS PROTEIN HOMOLOG 2 (DIAPHANOUS-RELATED FORMIN 2) (DRF2) (MDIA3)	Diap2	-0.61	8.82	0.00155
similar to FALSE P73 TARGET PROTEIN [Homo sapiens]	Mett11d1	-0.61	8.77	0.001088
Similar to transmembrane 6 superfamily member 2	Tm6sf2	-0.62	10.03	3.44E-07
FARNESYL PYROPHOSPHATE SYNTHASE (EC 2.5.1.10) homolog [Mus musculus]	Fdps	-0.62	12.32	2.33E-11
fucosyltransferase 8	Fut8	-0.62	8.83	5.41E-05
iroquois related homeobox 5 (Drosophila)	Irx5	-0.63	9.45	8.82E-09
hypothetical protein D15Wsu59e	Tars	-0.64	11.69	9.03E-09
synaptic glycoprotein SC2	Gpsn2	-0.64	14.07	7.17E-05
unknown EST	Whrn	-0.65	10.19	1.76E-09
LYSOSOMAL ALPHA-GLUCOSIDASE PRECURSOR (EC 3.2.1.20) (ACID MALTASE)	Gaa	-0.65	8.79	7.77E-10
hypothetical protein	Dgkk	-0.66	7.82	0.000751
RIKEN cDNA 2310079C17	Asf1a	-0.67	9.91	2.60E-05

diacetyl/L-xylulose reductase	Dcxr	-0.68	8.32	0.007653
Similar to for protein disulfide isomerase-related	Pdia5	-0.68	8.71	6.69E-05
G substrate	Gsbs	-0.69	7.84	3.91E-06
LATENT TRANSFORMING GROWTH FACTOR-BETA BINDING PROTEIN 4 homolog [Homo sapiens]	Ltbp4	-0.7	9.21	8.19E-06
hypothetical protein	1700001L19Rik	-0.7	9.03	3.82E-06
seryl-aminoacyl-tRNA synthetase 2	Sars2	-0.71	9.2	0.002154
Dysferlin	Dysf	-0.72	8.17	0.00016
unknown EST	2310030N02Rik	-0.72	8.05	0.000148
TRAF-interacting protein	Traip	-0.72	8.21	2.74E-06
solute carrier family 7 (cationic amino acid transporter. y+ system). member 3	Slc7a3+B32	-0.73	9.63	1.16E-08
Mex 67 homolog (S. cerevisiae)	Nxf1	-0.73	10.04	6.08E-09
CD9 ANTIGEN	Cd9	-0.73	8.15	2.86E-05
hypothetical protein	1700040L02Rik	-0.74	7.94	8.04E-08
similar to 1-ACYL-SN-GLYCEROL-3-PHOSPHATE ACYLTRANSFERASE BETA (EC 2.3.1.51)	Agpat2	-0.75	13.38	2.56E-11
angiopoietin-like 1	Angptl1	-0.77	8.26	2.84E-06
similar to CYTOCHROME P450 2S1 [Homo sapiens]	Cyp2s1	-0.77	8.41	1.57E-06
ATPase. H+/K+ transporting. alpha polypeptide	Atp4a	-0.77	7.61	0.000159
ISOCITRATE DEHYDROGENASE [NADP] CYTOPLASMIC (EC 1.1.1.42)	Idh1	-0.78	8.8	1.82E-09
thymus LIM protein	Crip3	-0.79	8.64	8.24E-05
FXYD DOMAIN-CONTAINING ION TRANSPORT REGULATOR 5 PRECURSOR	Fxyd5	-0.81	8.49	7.87E-07
hypothetical protein	3100002J23Rik	-0.81	9.5	4.38E-08
UROPLAKIN III PRECURSOR (UPIII)	Upk3a	-0.81	7.35	0.000126
similar to TRANSMEMBRANE 4 SUPERFAMILY. MEMBER 5 [Homo sapiens]	Tm4sf5	-0.88	8.18	3.51E-06
INTERFERON-INDUCED 35 KDA PROTEIN HOMOLOG (IFP 35)	Ifi35	-0.9	8.11	2.47E-06
hypothetical protein		-0.92	8.21	2.40E-07
RIKEN cDNA 2510006M18	Asl	-0.93	9.1	4.51E-07
ALPHA-ACTININ 2 (ALPHA ACTININ SKELETAL MUSCLE ISOFORM 2)	Actn2	-1.04	8.02	1.07E-08
BONE MORPHOGENETIC PROTEIN 1 PRECURSOR (EC 3.4.24.19) (BMP-1)	Bmp1	-1.04	8.2	6.98E-05
RIKEN cDNA 1700027N10 gene	1700027N10Rik	-1.08	9.16	1.55E-10
LYMPHOCYTE ANTIGEN LY-6E PRECURSOR (THYMIC SHARED ANTIGEN-1) (TSA-1)	Ly6e	-1.13	11.89	4.47E-15
carbohydrate (N-acetylgalactosamine 4-0) sulfotransferase 8	Chst8	-1.16	7.86	6.91E-10

HOMEOBOX PROTEIN OTX2	Otx2	-1.16	7.68	5.74E-10
PROBABLE G PROTEIN-COUPLED RECEPTOR GPR72 PRECURSOR	Gpr83	-1.26	7.72	3.75E-09
CALBINDIN (VITAMIN D-DEPENDENT CALCIUM-BINDING PROTEIN. AVIAN-TYPE) (CALBINDIN D28)	Calb1	-1.27	8.22	1.92E-13
NEUROMEDIN K RECEPTOR (NKR) (NEUROKININ B RECEPTOR) (NK-3 RECEPTOR) (NK-3R)	Tacr3	-1.5	9.31	3.73E-12
PLASMA GLUTATHIONE PEROXIDASE PRECURSOR (EC 1.11.1.9) (GSHPX-P)	Gpx3	-1.75	9.38	3.49E-23

APPENDIX

BACKGROUND

A very interesting subpopulation of mDA cells is constituted by the SNl, situated laterally to the SNc. This subregion is considered to be the source the projections of the nigra to the inferior collilculus (IC) (Björklund and Lindvall, 1984, in *Handbook of Chemical Neuroanatomy*). Besides this projection, the SNl is also known to give rise to axonal projections that reach the striatum, the amygdala and superior colliculus (SC) (Kaebler et al., 1979; Björklund and Lindvall, 1984, in *Handbook of Chemical Neuroanatomy*). It seems that the *pars lateralis* pathway to the IC utilizes GABA as a neurotransmitter, whereas the cells projecting to the striatum and SC utilize dopamine and GABA as neurotransmitters (Moriizumi et al., 1992). Moreover, Moriizumi reports that cells projecting to these distinct regions are well partitioned in the expanse of the SNl; with cells projecting to the IC, lacking TH immunoreactivity, positioned dorsolaterally, and cells projecting to the amygdala and striatum, positive for TH immunoreactivity, situated ventromedially.

Always Moriizumi suggests that the SNl-IC cells may constitute a unique neuronal population in the basal ganglia, influencing auditory associated movement, since the major target of the IC projection seems to be the pericentral region surrounding the central nucleus, which is speculated to be a centre associated with acousticomotor behavior rather than pure auditory function.

With regards to neurodegeneration, it has been reported that in MPTP treated animals that recapitulate the pattern of nigral loss seen in Parkinson's disease, cells in the SNl are spared (Figure 1) (German et al., 1996). These cells have also been found to be calbindin positive (Thompson et al., 2005). Finally, it is interesting to note that one of the genes that has emerged as enriched in A10 neurons from our analysis, Pdia5 (a protein disulfide isomerase-related protein), seems also expressed in the SNl according to the in situ hybridization data of the Allen Brain Atlas.

For all the above reasons and for the facts that this circuit is well defined, underlies a specific task, is constituted by more cell types, and there is 15 year gap surrounding its study make this region an excellent candidate for informative gene expression profiling.

By combining fluorescent retrograde labeling with the use of the transgenic TH-GFP/21-31 line of mice, in which GFP is expressed in all catecholaminergic cells, double labeled cells of interest could be collected by LCM and their expression profiles determined and compared to those of other DA and GABA cell populations of the same region. This part of the project was not taken further from preliminary tests but it would be interesting to take it in consideration for future completion of the expression profiles of DA cells belonging to the SN.

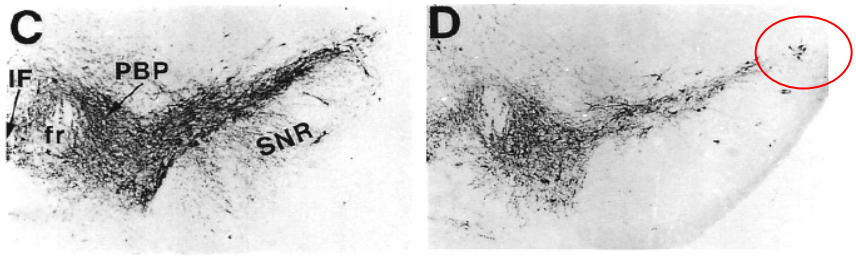

Figure1. Coronal sections through the rostral midbrain, immunostained for TH, of MPTP-treated C57BL/6 mice. Neurodegeneration can be noted at the ventrolateral region of the SNc while VTA, medial SNc and SNl (highlighted by the red circle) are relatively spared (Figure from German et al., 1996).

MATERIALS AND METHODS

Stereotaxic delivery in the mouse brain

Briefly. Two months old adult C57BL/6J mice were used for the retrograde labeling experiments. Mice were anesthesized with a mixture of ketamine and xylazine at a dose of 80-100 mg ketamine and 10 mg xylazine per kilogram body weight, given intraperitoneally. When deeply anesthetized, the fur

of the skull was shaved and animals were placed in a stereotaxic apparatus (Stoelting Inc.).

Surgical area had been prepared by disinfection with 70% EtOH while tools had been sterilized by autoclaving. A dissection microscope was used to visualize the top of the skull, which was disinfected with 70% EtOH before making a small midline incision with a small scalpel. The subcutaneous and muscle tissue was separated and held open with the aid of forceps. The bregma and lamba areas were gently cleaned with a small brain scraper. The head was leveled so that bregma and lambda were flat and on the same horizontal plane. To avoid drying of the skull and eyes, drops of PBS were applied throughout the surgery. The position of the x and y coordinates of bregma were taken and the coordinates of the target injection area were calculated (by subtraction), as determined by the stereotaxic brain atlas (Paxinos and Franlin, 2003). The skull over the target area was thinned with a motor drill until the dura madre became visible. At this point the injection of the retrograde tracer was performed through a glass capillary adapted to the tip of a 2μl Hamilton syringe. The tip of the glass capillary, loaded with 1 μl of the fluorescent tracer (Lumafluor, green fluorescent beads; Lumafluor Laboratories, Naples, USA), was brought to the correct position, over the target area, and lowered until it touched the dura. Its sharp edge easily penerated the brain and the capillary was lowered gently at the desired depth. The tracer was released very slowly. We waited for 5 minutes before withdrawing the glass capillary to avoid backflow of the solution. The injection site was cleaned with cotton swabs and the skin was sutured. Lidocaine was injected subcutaneously near the wound for local anesthesia. The animal was kept warm under a heat lamp until it recovered and returned to a clean cage. Injections were performed in the striatum, at the following coordinates with respect to bregma: a) anteroposterior: -0.8, b) mediolateral: -2.8, c) dorsoventral: -3.2.
At least seven days were allowed before assessing success of sterotaxic delivery.

Immunofluorescence

Operated mice were deeply anesthetized and intensively perfused

transcardially with PBS followed by 4% paraformaldehyde diluted in PBS. Brains were removed and post-fixed in 4% paraformaldehyde for 1h at room temperature and cryoprotected overnight in 30% sucrose at 4˚C. The midbrain was isolated, embedded in O.C.T medium, snap-frozen on a liquid nitrogen-cooled isopentane layer (Sigma, St Louis, MO, USA), and 10 μm sections cut at -21˚C in a cryostat (Microm International, Walldorf, Germany). Sections were blocked with PBS, 10% NGS, 1% BSA, 1% Fish gelatin (filtered) for 1h at RT, the primary and secondary antibodies were diluted in PBS, 1% BSA, 0.1% Fish gelatin, 0.3% tritonX- 100. Incubation with primary antibodies was performed for 2 hours at RT; incubation with secondary antibodies was performed for 1 hour at RT. Slides were mounted with Vectashield (Vector Lab) for inspection at the confocal microscope (LEICA TCS SP2). For detection, Alexa Fluor 488, and 594 (Invitrogen) were used at a 1:250 dilutions. Primary antibodies used were a monoclonal anti-TH (DiaSorin) at 1:1000 dilution and an anti-calbindin polyclonal (Sigma) at 1:1000 dilution.

PRELIMINARY RESULTS AND COMMENTS

Immunofluorescence

Double immunofluorescence on mesencephalic sections for TH and calbindin resulted, as expected from literature, with small calbindin+/TH+ cells distributed within the VTA and larger TH+/calbindin– situated in the expansion of the SNc with the exception of the lateral population that constitutes the SN *pars lateralis* where cells belonged predominantly to the calbindin/TH subtype (Figure 2).

Retrograde labeling

Injections of green fluorescent beads were centered in the rostral striatum (see figure 3 for a representative injection site). Retrograde labeling was detected

in the VTA, SNc, and the SNl (Figure 3). The same sections were processed for TH immunofluorescence. Intense red fluorescence could be noted in the expanse

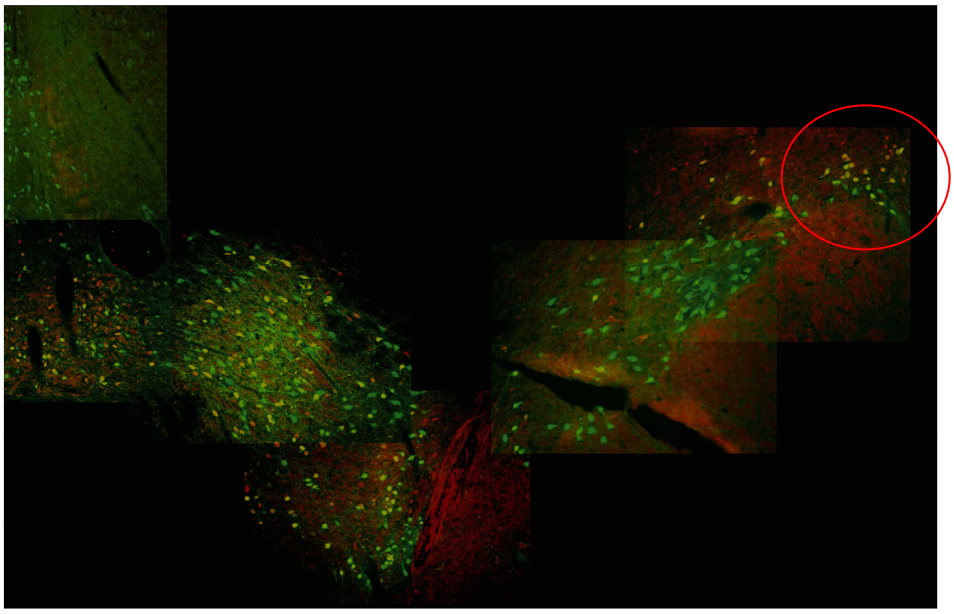

Figure 2. Double immunofluorescence for TH-GFP (green) and calbindin (red). As expected from literature, small calbindin+/TH+ (here appear yellow by the overlay of green and red) are distributed within the VTA, whereas SN neurons are TH+/calbindin–, with the exception of the SN *pars lateralis* (highlighted by the red circle), where cells are predominantly of the calbindin/TH subtype.

of the dopaminergic ventral midbrain. Tracer beads inside dopaminegic cells appeared yellow because of the color overlay. It is of note that green fluorescent beads appeared also in cells that were negative for TH immunofluorescence but presumably projected to the same striatal region. These cells might be GABAergic projection neurons, but this is simple speculation.

Retrograde labeling of cells worked very nicely and it held promise for future application in the context of gene expression profiling.

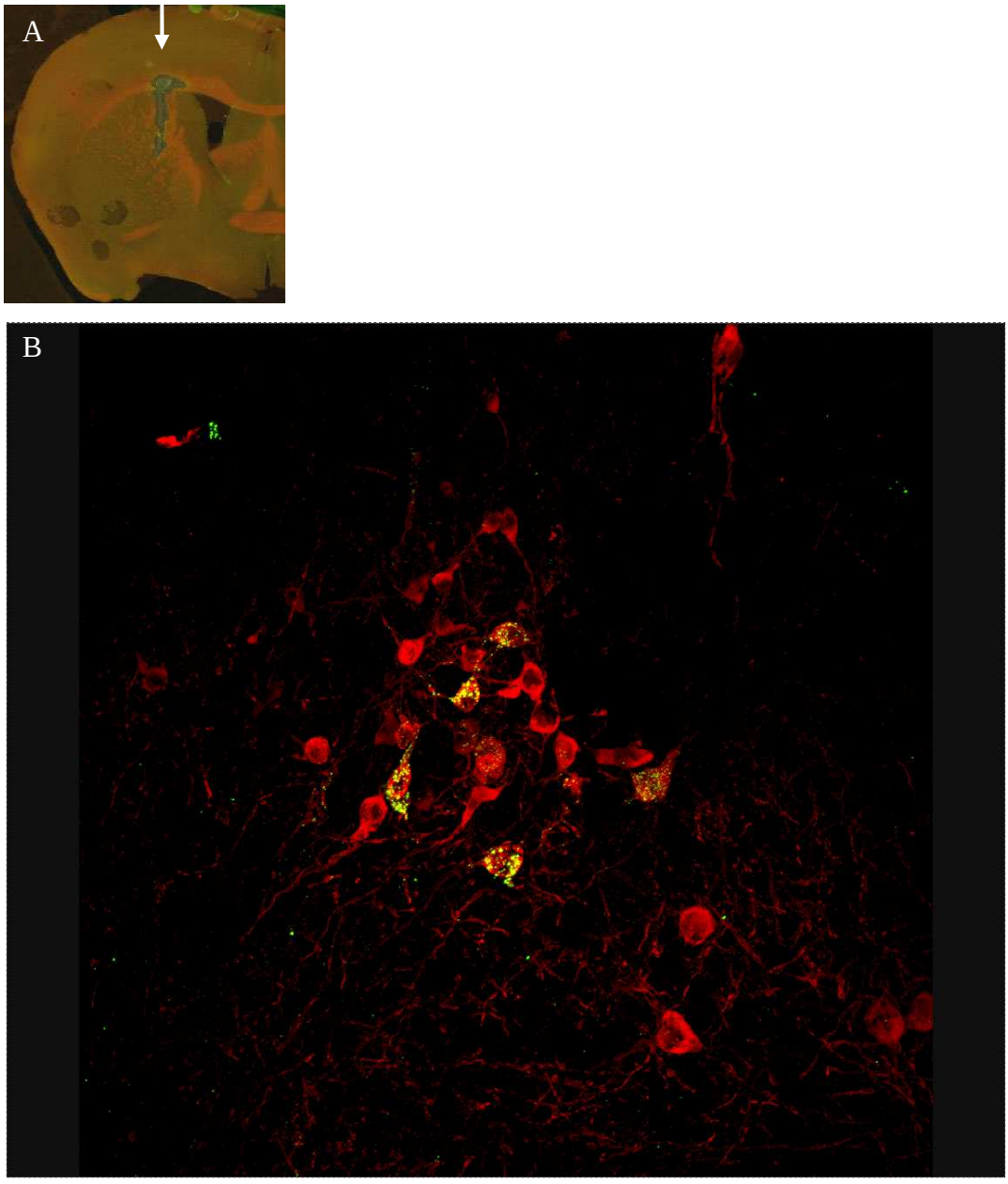

Figure 3. A) Green beads injected in the striatum, B) DA cells in the SN *pars lateralis*, retrogradely lebeled by green fluorescent beads (here appearing yellow due to the green and red color overlay). DA cells in red are revealed with anti-TH immunofluorescence. As it can be noted ghosts of cells can be guessed by the green bead filing, which means that cells immunonegative for TH were also retrogradely labeled.